The role of cellular morphogenesis in the pathogenicity of the rice blast fungus *Magnaporthe oryzae*

Submitted by Yasin Fatih Dagdas

to the University of Exeter for the degree of Doctor of Philosophy, in Biological Sciences.

March 2013.

I certify that all material in this thesis which is not my own work has been identified and that no material has been previously submitted and approved for the award of a degree by this or any other University.

Yasin F. Dagdas

Abstract

Appressorium-mediated plant infection is a common strategy used by many plant pathogenic fungi. Understanding the underlying genetic network that controls cellular differentiation of appressorium is therefore pivotal to design durable resistance strategies for these devastating pathogens. This thesis describes four published studies, which investigate the role of septin GTPases in infection and the role of secretion during plant tissue invasion by the rice blast pathogen *Magnaporthe oryzae*.

Appressorium development involves a series of morphogenetic changes that are tightly regulated by cell cycle checkpoints. Entry into mitosis allows differentiation of an appressorium, while penetration peg emergence appears to require progression through subsequent cell cycle checkpoints and cytokinesis. The studies presented here show that symmetry-breaking events that occur during appressorium differentiation are mediated by scaffold proteins, named septins. Septin GTPases recruit actomyosin ring components during septation and define the site of cytokinesis. They also recruit a toroidal cortical F-actin network to the appressorium pore that provides cortical rigidity to facilitate plant infection. Septins act as diffusion barriers for proteins that mediate membrane curvature necessary for penetration peg formation. Repolarization of the F-actin cytoskeleton at the appressorium pore is essential for plant penetration and is controlled by cell polarity regulators, such as Cdc42 and Chm1. Septin-mediated plant infection is regulated by NADPH oxidase (Nox) dependent generation of reactive oxygen species (ROS). The Nox2/NoxR complex is essential for septin organization at the appressorium pore. Septins are therefore key determinants of appressorium repolarization. I also report an investigation of fungal secretory processes during tissue invasion and present evidence that distinct pathways are involved in effector secretion

by *Magnaporthe oryzae*. A BrefeldinA-sensitive pathway is necessary for secretion of apoplastic effectors, such as Bas4 and Slp1, while a BrefeldinA-insensitive pathway is necessary for secretion of effectors destined for delivery to rice cells.

Table of contents

Acknowledgements

First of all I would like to thank my supervisor Nick Talbot, for not only being a great supervisor but also for being an inspirational scientist. He always showed great interest in my projects and motivated me all the time during my PhD. He also showed me the importance of self-respect and self-confidence to achieve my goals. Thanks very much for everything Nick!

Sincere regards to Claire and Les Halpin for providing the support for my PhD. Without their support, none of these would have been possible.

Thanks very much to the Alzwiy family, Ibrahim, Fouzeah, Teyimah, Inas, Wiyam, Abdul and Lamar for being a family for us.

Many thanks to Muhammad Badaruddin, Muhammad Islam and Termizi Yosouf who helped me to settle in UK.

A big “thank you” to the Halpin Scholars Muhammad Islam and Yogesh Gupta with whom I enjoyed sharing many things in and out of the lab.

Special thanks to Diane Saunders, Martin Egan, Muhammad Badaruddin, Michael Kershaw and Romain Huguet and Ana-Lilia Martinez-Rocha who helped me to establish myself in the lab.

Thanks to everyone whom I collaborated and currently collaborating for the papers, especially Lauren Ryder, George Littlejohn, Miriam Oses-Ruiz, Kae Yoshino, Ewa Bielska and Gero Steinberg.

Special thanks to Barbara Valent and Martha Giraldo with whom we made the effector paper and Zhongua Wang and Jisheng Cheng with whom we will make the septation paper.

I would also like to thank all the past and current members of the Halpin Lab, including Nick Tongue, Barbara Saddler, Tina Penn, Magdelana Martin Urdiroz, Magdalena

Basciewicz, Termizi Yosouf, Darren Soanes, Min He, Tom Mentlak, Antonio Nhani, Rita Galhano, Angus Dawe, Apratim Chakrabarti, Xia Yan and Wasin Sakulkoo.

Finally biggest thanks to my wife Gulay, who has shown tremendous patience with the demanding lab life and always stood next to me when I needed. Life in the lab would have been unbearable without your companionship!!! Although she may not understand at the moment, I would also like to thank my daughter Emine, who has been the joy of our life since she is born.

Dedicated to Les Halpin,

Whose dedication and vision is a true inspiration for me.

Chapter 1

Illuminating the infection headquarters of a cereal killer: Checkpoints controlling infection related development of the rice blast fungus.

To ensure global food security there is an urgent need to reduce the damage caused by plant pathogenic fungi (1). Until now fungicides were not very effective on controlling the diseases and many of them had adverse effects on environment. To devise translational cures for plant infecting fungi we need a better understanding of the underlying infection process. This may result in discovery of molecular targeted fungicides.

The most devastating plant pathogenic fungus is an ascomycete called *Magnaporthe oryzae* (2). It causes blast disease on many of the staple food sources such as rice, wheat, and finger millet. Neither chemical treatments nor resistance gene breeding are effective to control the disease (3). The Infection cycle of the fungus starts when a three-celled conidium lands on the plant surface. Upon recognition of plant signals, a polarized germ tube emerges from the conidium. The germ tube then starts swelling and forms the melanised infection cell called appressorium (4). This cell accumulates glycerol to generate enormous amount of turgor pressure (5). The turgor pressure is then used to drill through the cuticle for penetration hyphae formation and fungal colonization. 5-days after infection the fungus produce spores and the infection cycle starts again (Figure1). Appressorium is not unique to *Magnaporthe oryzae*, many other plant infecting fungi such as *Ustilago maydis*, *Fusarium spp.*, *Colletotrichum spp.*, mildews and rusts also use appressorium to infect their hosts(6). So, understanding the underlying genetic elements leading to appressorium development is pivotal for designing smart disease management agents.

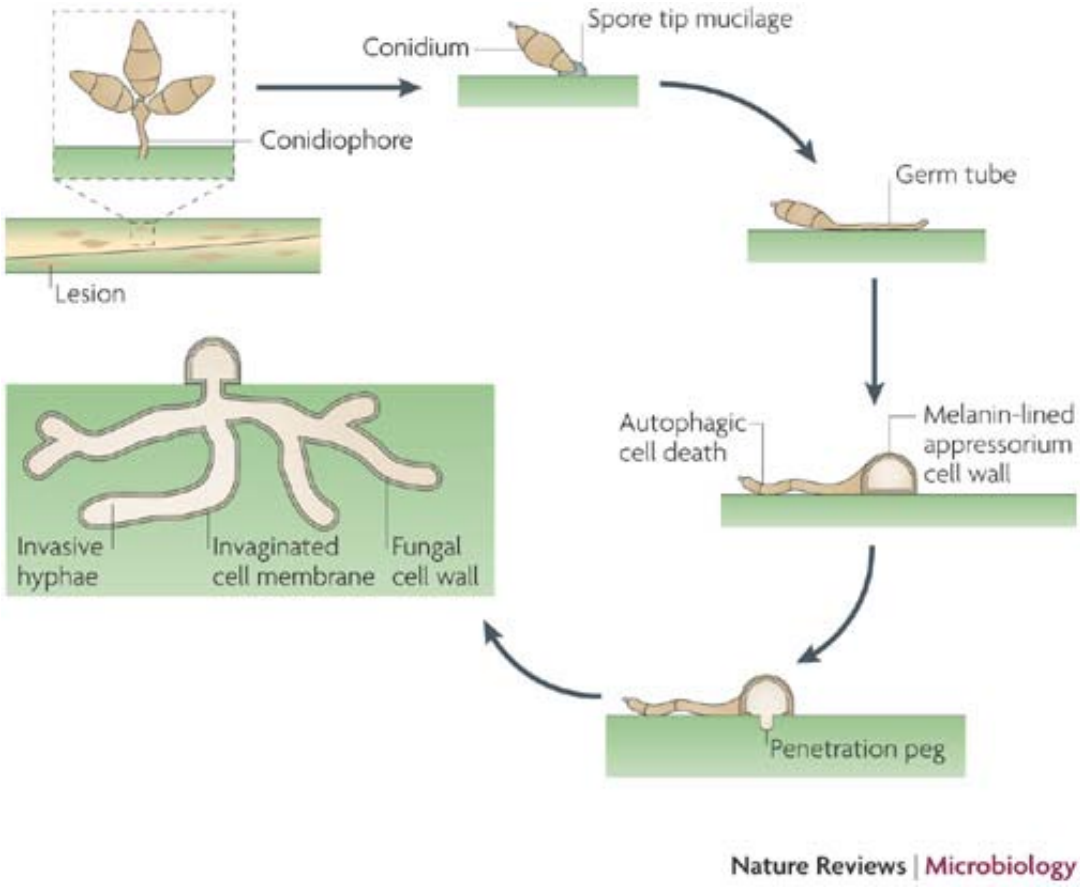

Figure 1: The life cycle of *Magnaporthe oryzae* (Taken from Wilson and Talbot, *Nature Reviews Microbiology* 7, 185-195 (March 2009)).

Evolutionary fitness of *M. oryzae* largely depends on formation of a functional appressorium, which is able to penetrate the plant cuticle. Recent discoveries have shown that appressorium development requires a very complex genetic network and is very tightly regulated by developmental and cell cycle regulated checkpoints that ensure development of a functional appressorium. As in nearly all biological systems the network is composed of sensors, signals, and effectors (7). In this review, we will discuss the checkpoints controlling appressorium development of *M. oryzae*. Since appressorium is broadly utilized by plant pathogens, defining the checkpoints indispensable for plant infection will significantly improve our tools for designing durable resistance approaches.

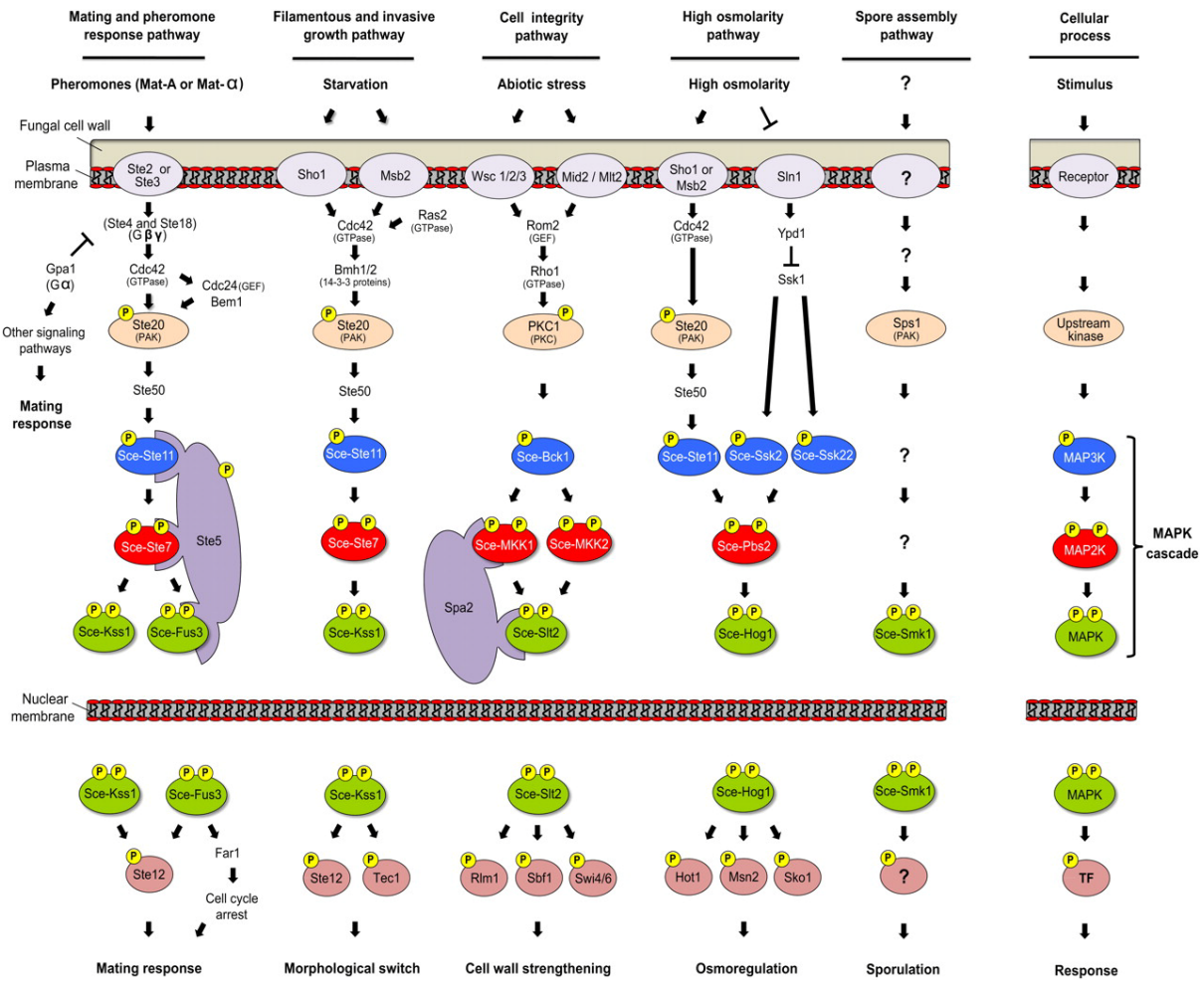

Figure2: Conserved MAPK pathways in fungi (Taken from Hamel L et al. Plant cell 2012;24:1327-1351).

Surface recognition checkpoint

M. oryzae spores are carried on rain drops. Immediately after landing on the plant surface, the fungus recognizes the inductive plant surface and starts the processes that will result an appressorium. If spores land on non-inductive surfaces germ tubes cannot differentiate into appressorium. Surface recognition and downstream signalling processes have been studied extensively (8, 9). Fungal spores sense surface hydrophobicity and hardness. Cutin monomers, primary alcohols and leaf waxes induce appressorium formation even on hydrophilic surfaces (10). Till now three surface sensors have been characterized: (1) *CBP1*, a novel chitin binding protein which was suggested to recognize physical cues on plant surfaces. Null mutants of *CBP1* were unable to form appressoria on artificial surfaces, whereas they formed appressorium on

plant leaves (11). (2) *PTH11*, a CFEM domain containing G-protein coupled receptor (GPCR) localized to plasma membrane. GPCRs transmit environmental signals to heterotrimeric G-proteins which activate secondary messengers and regulate gene expression. *PTH11* mutants were able to hook, which is a sign of surface recognition, but could not differentiate into an appressorium. This suggests *PTH11* might respond to chemical cues on plant surface (12). (3) *MSB2* and *SHO1*, surface receptors suggested to recognize hydrophobicity and cutin monomers, and leaf waxes, respectively. *Δmsb2-sho1* double mutants could rarely form appressorium on inductive hydrophobic surfaces and significantly reduced in virulence (13) (Figure 2).

One of the transducers that transmit the signal from surface receptors to effectors seems to be cAMP for *M. oryzae* infection related development. G-proteins activating cAMP synthesis (MagB) (14), Adenylate cyclase synthesizing cAMP (Mac1) (15), cAMP responsive kinases (cPKA) (16) were shown to be important regulators of appressorium morphogenesis (reviewed in (17)). Recently, regulators of G-proteins (Rgs) were also shown to be important for surface recognition and thigmotropism. 8 of these proteins were functionally characterized and shown to play roles in regulating Gα subunit MagB and cAMP levels during appressorium morphogenesis(18, 19). Also a novel component of the signalling pathway, MoRic8 was shown to interact with MagB in yeast two hybrid assays and targeted gene replacement of MoRic8 impaired appressorium differentiation (20). Moreover phosphodiesterases that degrade cAMP (PdeL and PdeH) were also important for virulence and disruption of PdeH partially restored mutant phenotype of ΔmagB and Δpka (21). Effectors of cAMP signalling were identified by protein pull down and insertional mutagenesis studies. In vivo pull down experiments identified Cap1 as an interactor of adenylate cyclase Mac1. Functional characterization of Cap1 revealed the link between cAMP signalling and cytoskeleton. Cap1 had a similar localization pattern to actin during appressorium development and *Δcap1* mutants had defects in germ tube growth (22). Transcription factors downstream of cAMP signalling were identified by insertional mutagenesis. MoSom1 has shown to interact with cPKA in yeast two hybrid studies (23). Moreover MoSom1 interacts with two other transcription factors MoStu1 and MoCdtf1. All three transcription factors were shown to be important for appressorium morphogenesis (23).

Another MAP kinase that links surface recognition to appressorium morphogenesis is Pmk1. Pmk1 is orthologous to budding yeast MAP kinase Fus3/Kss1. Germ tubes of *pmk1* mutants are unable to differentiate and form appressoria (24). Pmk1 is an effector

for Msb2 surface receptor and is regulated by several other proteins such as adaptor protein Mst50, MEKK Mst11 and MEK MSt7 (13, 25). Pmk1 pathway has been shown to interact with the small GTPase Cdc42 via the Mst50 adaptor protein (26). Cdc42 has a central role in establishing polarity and this might explain why *pmk1* mutants cannot initiate the switch from polarized growth to isotropic swelling of germ tubes (Figure3).

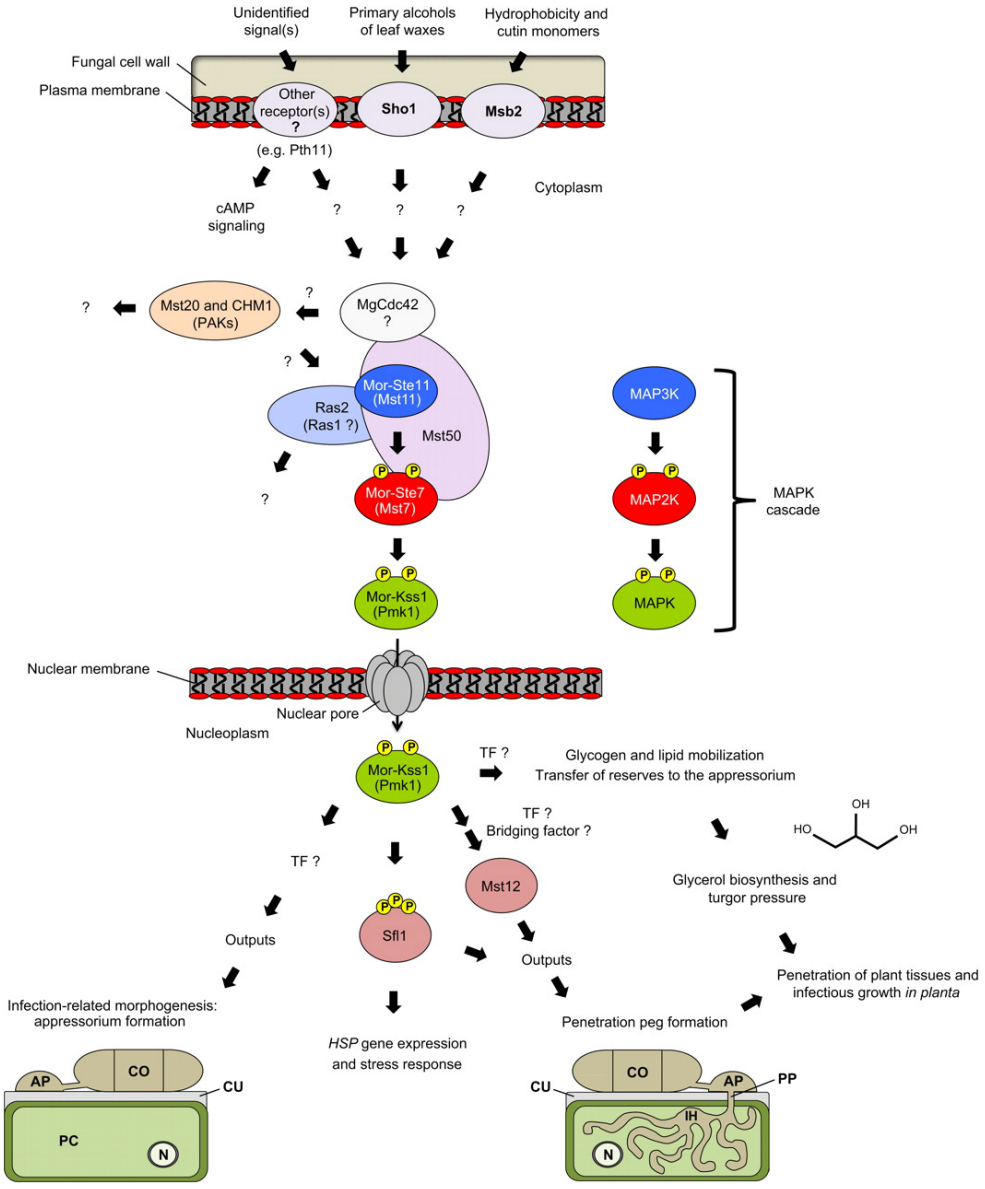

Figure3: *Magnaporthe oryzae* MAPK pathway responsible for host recognition and infection related development **(**Taken from Hamel L et al. Plantcell 2012;24:1327-1351**).**

Cell cycle checkpoints

Appressorium morphogenesis starts with a polarized germ tube. On an inductive surface the tip of the germ tube starts growing isotropically and forms an initial appressorium. Turgor generation and melanisation matures the appressorium and a penetration hyphae emerges after reorienting the axis of polarity. These kinds of symmetry breaking events have been shown to be tightly linked with cell cycle progression in filamentous fungi and budding yeast (27-29).

Cell cycle is generally categorized into four main phases (G_0-S-G_2-M) and each phase depends on completion of the previous one(30). Checkpoints, discovered by L. Hartwell, P. Nurse and T. Hunt, ensure each phase is completed accurately and the cell is ready to divide. Malfunctioning in checkpoint controls may result in uncontrolled cell division as in cancer cells or may induce cell death as a protection mechanism. There are three main checkpoints: (1) G_1 checkpoint makes sure that the cell has an appropriate size and metabolic state for division. (2) G_2 checkpoint controls the accuracy of DNA replication. (3) Spindle assembly checkpoint ensures correct alignment of chromosomes on metaphase plate (31). Using filamentous fungus *Aspergillus nidulans* as a model organism, Ron Morris identified components of the mitotic machinery by using forward genetics approach, nearly at the same time with L. Hartwell and others (32). These studies have shown that a conserved set of cyclins and cyclin dependant kinases (CDKs) regulate the onset of mitotic events.

Differentiating a functional appressorium is pivotal for evolutionary success of *M. oryzae*, and it requires a complete re-programming of cellular metabolism and morphogenesis. The first line of evidence suggesting a cell cycle regulation of appressorium development was obtained by live cell imaging of nuclear division. Using Histone-GFP fusions as a marker for nucleus, our lab has shown only the nucleus at the germ tube forming cell divides and mitosis always precedes appressorium development. When appressorium matures, the other nuclei left in the conidia are degraded in an autophagic cell death mechanism as shown by targeted gene replacements of *MoATG8 (33)*. Functional characterization of autophagy related genes (ATG) in *M. oryzae* has shown that degradation of nuclei happens in a macroautophagic process and all the genes involved in macroautophagy are important for virulence (34).

Time-lapse analysis has shown that nuclear division takes place 3-4 hours after germination of spores. Addition of drugs which inhibit DNA synthesis (hydroxyurea)

inhibited appressorium formation in a time dependant manner. When hydroxyurea was applied 0-3 hours post inoculation (hpi) of spores, germ tubes could not swell and form appressoria, however if it was applied 6-8 hpi, appressorium morphogenesis was not affected. This suggests mitotic checkpoints may regulate appressorium development. The genetic evidence was obtained when an analogous thermosensitive allele of NimA (*never in mitosis*) kinase (MonimA^{E37G}) was generated. NimA is a Serine/Threonine kinase that has been shown to regulate entry into mitosis. *nimA* thermosensitive mutants are arrested in G_2 when shifted to restrictive temperatures(35). When MonimA^{E37G} was shifted to restrictive temperatures at early stages of appressorium development (0-3 hpi), nuclear division and appressorium formation was inhibited. Blocking entry into mitosis also inhibited autophagic cell death. However if temperature shift was done 6 hpi there was no significant difference in appressorium development (33).

Systematic analysis of cell cycle checkpoints was performed by Saunders et. al, 2010. Results of hydroxyurea treatments suggested completion of DNA replication is a prerequisite for appressorium formation. In budding yeast initiation of DNA replication is controlled by Cdc7-Dbf4 complex. Cdc7 physically interacts and controls firing at replication origins. Dbf4 controls activity of Cdc7 in an analogous way to cyclins controlling CDKs (36, 37). Dbf4 homolog in A. nidulans is called NimO, and conditional mutants of nimO is unable to replicate DNA under restrictive temperatures (38). An analogous thermosensitive allele of NimO called nim1^{I327E} behaved same as hydroxyurea treated cells under restrictive temperatures. Germ tubes could not swell and differentiate into appressorium. These results confirmed that G_1 checkpoint, which ensures the cell is ready to divide, is necessary for the symmetry breaking process that will induce the switch from polarized growth to isotropic swelling.

Targeted deletion of surface recognition receptors such as Pth11 or downstream kinases such as Pmk1 prevented initiation of appressorium development. This suggests (i) surface recognition checkpoint operates at a very early stage of appressorium morphogenesis (ii) when considered together with the observation that swelling of germ tube happens before the completion of mitosis, surface recognition receptors act on G1 checkpoint to initiate DNA replication, which will be followed by nuclear division. This is consistent with the data obtained in budding yeast. A cyclin dependant kinase inhibitor Far1 is able to arrest cell cycle by inhibiting a G_1 cyclin Cln2 upon recognition of the mating pheromone. Far1 is activated by Fus3 phosphorylation and is able to form a complex with Cdc42 to induce polarized growth required for mating (39, 40).

As explained above blocking entry into mitosis by preventing NimA kinase activity resulted in appressoria which are not melanised and hence unable to infect plants. This suggests G_2 checkpoint oversees the commitment step in appressorium formation, once the cell has entered mitosis, there is no turning back. Further evidence showing mitotic entry is necessary and sufficient for appressorium formation was obtained by preventing mitotic exit either by disrupting the function of Anaphase promoting complex (APC) or preventing degradation of B-type cyclins. Anaphase promoting complex is a conserved E3 Ubiquitin ligase, required for transition from metaphase to anaphase. By marking mitotic cyclins for degration, APC induces mitotic exit(41). *In A. nidulans* BimE encodes for the large subunit of APC complex and bimE7 mutant is arrested in a pre-anaphase stage under restrictive temperatures (42). An orthologous mutation in *M. oryzae* (*bim1*^{F1763*}), also prevented mitotic exit and caused nuclear migration defects. Although *bim1*^{F1763*} mutants developed melanised appressoria, they were unable to cause plant infection. B type cyclins interact with CDK1 (or Cdc28 in yeast) to induce progression through M phase. B type cyclins have a destruction box at their N-termini that is necessary for their ubiquitin mediated degradation. The level of B type cyclins increase as the cell progress through M phase and upon mitotic exit they are targeted for degradation by 26S proteasome. Expression of stabilized B type cyclins in *M. oryzae*, which were generated by deletion of destruction boxes, prevented mitotic exit and caused nuclear migration defects (43).

Appressorium development involves a unique septation event

A rather unexpected discovery was made when cell cycle progression during appressorium development was observed upto septum formation stage by imaging actomyosin ring formation using Tropomyosin-GFP. In other filamentous fungi or budding yeast the site of septation is determined pre-mitotically and depends on the site of mitotic nucleus. Upon completion of mitosis an actomyosin ring forms in the middle of the two recently divided nuclei. Constriction of actomyosin ring is followed by deposition of chitin which will result in formation of the septum (44, 45). During appressorium development cytokinesis is spatially uncoupled from mitosis; mitosis happens at the germ tube, whereas actomyosin ring is laid down at the neck of appressorium (46). When actomyosin ring formation was observed in mutants defective in appressorium morphogenesis such as *Δpmk1* or *ΔcpkA*, it was similar to the pattern

observed in other fungi, the ring formed in the middle of the division plane. Furthermore mitosis was coupled to cytokinesis in vegetative hypae of *M. oryze* as well, suggesting a unique uncoupling mechanism for infection related development of *M. oryzae*. This is consistent with surface recognition checkpoint controlling appressorium morphogenesis via cell cycle regulation.

Septation is controlled by a conserved signalling cascade called Mitotic Exit Network in *S. cerevisiae* and Septation Initiation Network in *S. pombe*. MEN/SIN coordinates mitosis with initiation of cytokinesis and makes sure that mitosis has finished before cytokinesis starts(47). A Ser/Thr kinase called Cdc7 in *S. pombe* or SepH in *A. nidulans* is a component of septation initiation network and controls septum formation (48). A temperature sensitive allele of Cdc7 homolog ($sep1^{G849R}$) affected infection associated cytokinesis in M. oryzae and rendered the fungus non-pathogenic.

Septin mediated symmetry breaking events are key to appressorium morphogenesis

Oriented growth requires establishment of cellular asymmetry. Symmetry breaking processes are generally induced upon changes in environment (for example chemical attractants or morphogen gradients) and require dynamic re-arrangements of cytoskeleton and morphogenetic elements (28). One of the best studied examples of asymmetric growth is budding in *S. cerevisiae*. New buds are always formed adjacent to the previous cell separation site also known as “bud scar”. Asymmetric localization of Cdc42 leads to a Turing type autocatalytic process that activates the PAK kinase Cla4p (49). Cla4p phosphorylates and recruits septins to the bud site. By localizing to the future bud site, septins act as a scaffold to recruit proteins required for Cortical actomyosin ring (CAR) formation such as myosinII, formins Bni1p and Bnr1p, and F-bar protein Hof1. A primary septum forms followed by CAR constriction and the daughter cell with a new scar gets seperated from the mother cell after hydrolysis of the septum (50) (Figure 4).

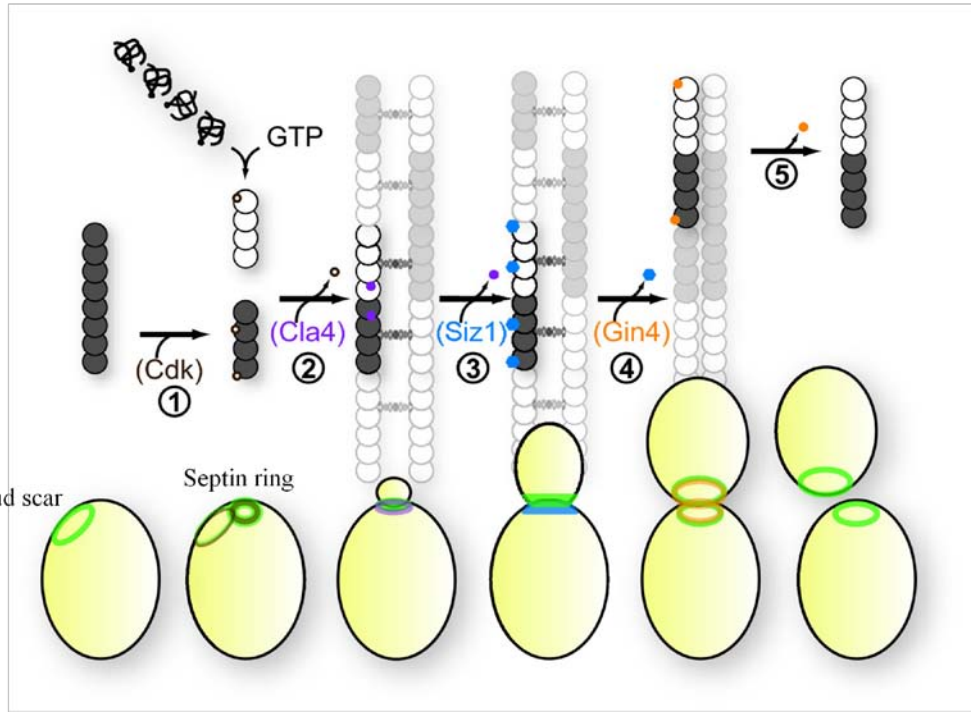

Figure 4: Septin ring splitting during *S. cerevisiae* budding (Modified from McMurray and Thorner *Cell Division* 2009 **4**:18).

Similar to yeast, appressorium development involves three changes in the axis of polarity: (1) initial polarized growth forms the germ tube, (2) a switch from polarized to isotropic growth leads to swelling and appressorium formation, and (3) re-polarization of mature appressorium results in penetration peg emergence. As explained above, the whole process is tightly regulated by cell cycle and surface recognition checkpoints.

Like budding yeast, septins play critical roles in appressorium morphogenesis of *M. oryzae*. Septins are conserved small GTPases that are able to form hetero-oligomeric structures (Figure 5). They are very well conserved from yeast to humans but not found in plants (Figure 6 and 7). They control various morphogenetic events such as polarized growth and secretion, cytokinesis, septum formation (51). Septins act by two main ways: (i) they act as subcellular scaffolds and encourage specific protein-protein interactions, and (ii) they act as diffusion barriers to help compartmentalization of the cell. The best characterized example for a septin scaffold is the dynamic hourglass shaped septin collars at yeast mother-bud neck. Here septins scaffold proteins around 100 proteins required for actomyosin ring formation, asymmetric localization of Chitin synthase-3 on mother side, and cortical landmark proteins on the bud site (52). The first demonstration of septins acting as a diffusion barrier for compartmentalization of cells

was done by localizing Ash1p mRNA in budding yeast. It was shown that Ash1p is maintained at the daughter cell with a septin mediated diffusion barrier at mother-bud neck (53). Later on septin-mediated diffusion barriers were shown at the base of primary cilia, sperm annulus and dendritic cells. Although still not completely clear, there is increasing evidence that septin-mediated diffusion barriers help to generate polarized membrane domains within plasma membrane, ER membrane and nuclear envelope (54, 55).

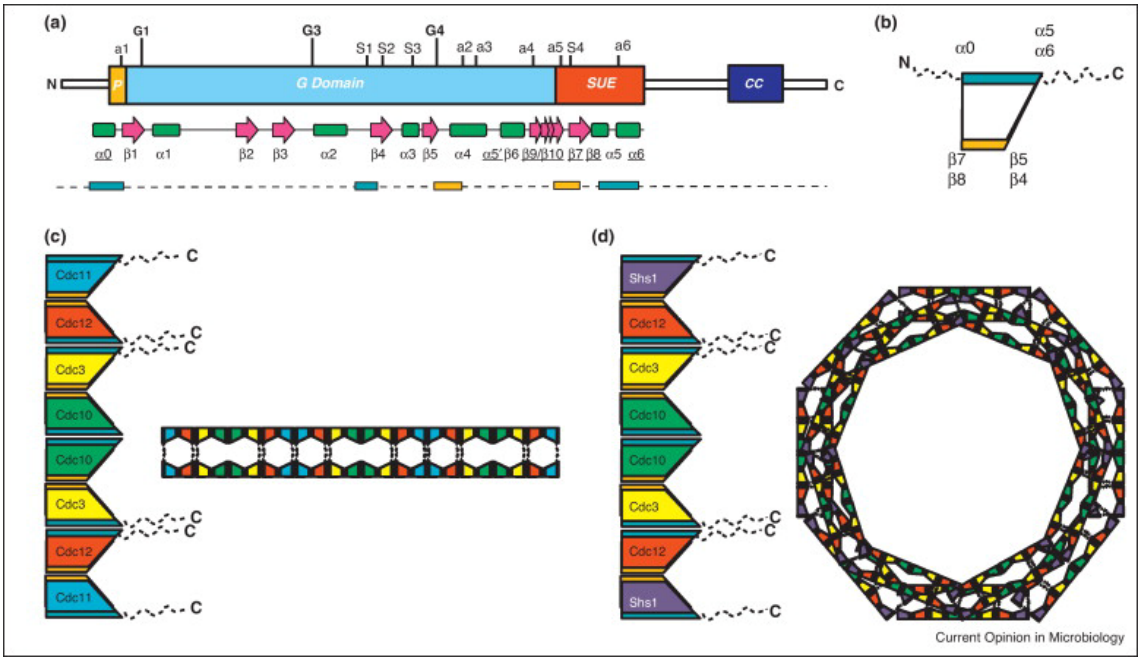

Figure 5: Septin heterooligomers (Taken from Hernandez-Rodriguez and Momany Current Opinion in Microbiology 2012, **15**:660–668)

One of the key functions of septin in appressorium development is determining the site of septation. Sep4 and Sep5 form a ring at the neck of appressorium, where the first symmetry breaking event takes place, before the onset of mitosis (56). They scaffold the actomyosin ring components necessary for septation. In the absence of septins, mitotic division cannot be controlled and asynchronous nuclear divisions are observed. Conidial nuclei which normally do not undergo nuclear division also starts to divide in septin mutants, suggesting septin-mediated morphogenetic checkpoints control cell cycle arrest during appressorium development (57).

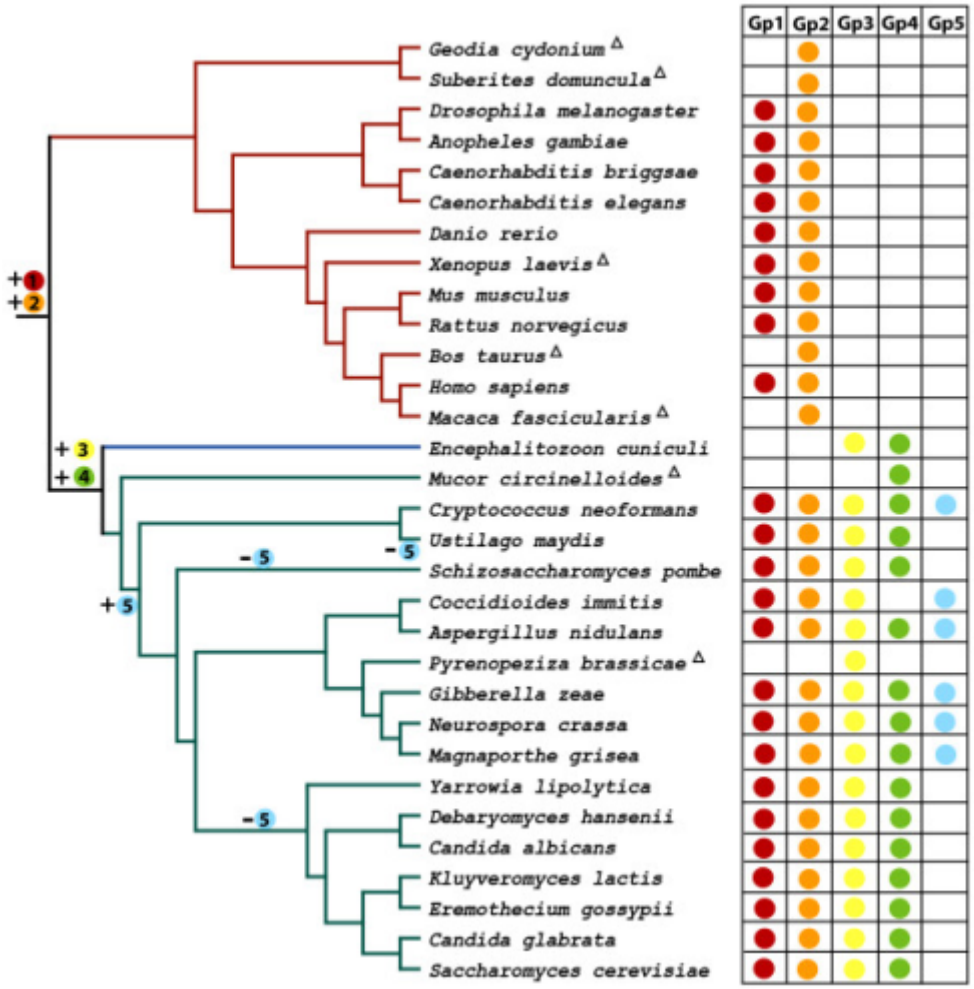

Figure 6: Pylogenetic tree summarizing septin evolution (Taken from Pan F, Malmberg RL, Momany M - BMC Evol. Biol. (2007))

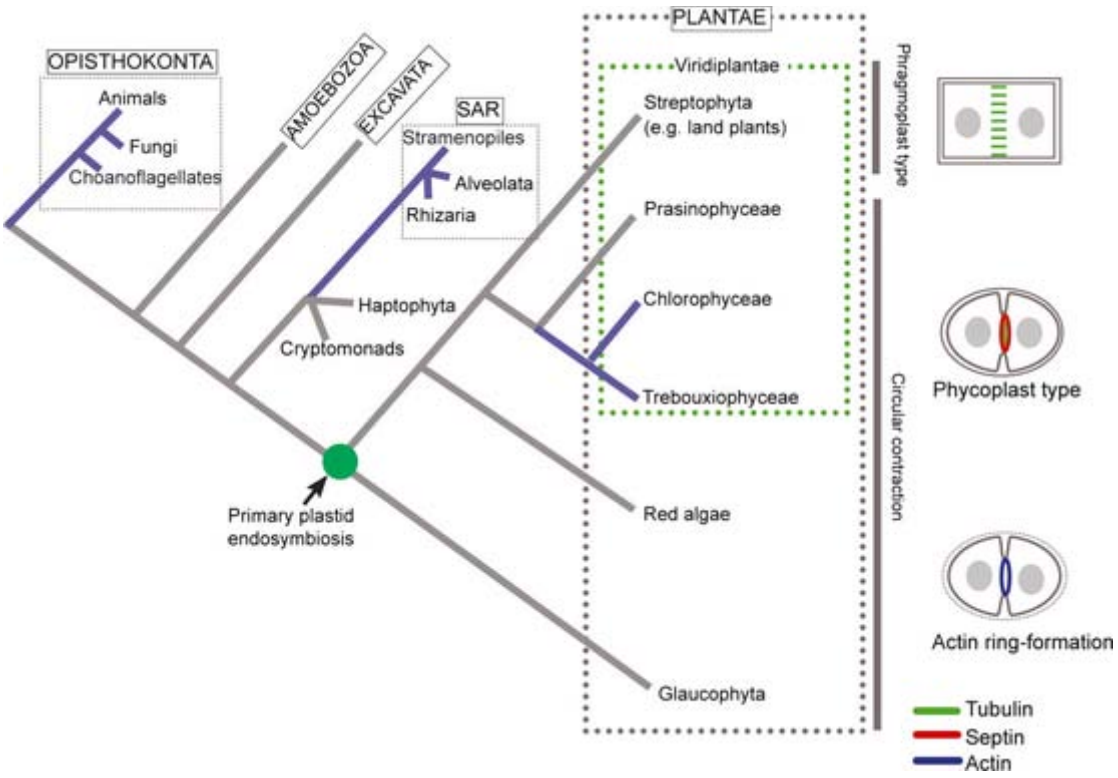

Figure 7: Tree showing septin distribution in eukaryotic supergroups (Taken from Yamazaki et. al., Plant Journal 2013).

All four septins (Sep3-Sep4-Sep5-Sep6) also form a heterooligomeric ring at the base of appressorium where it is in contact with the plant surface. This site marks the second symmetry breaking process during appressorium development since it will lead to a polarized penetration peg. Here septins recruit a toroidal actin network linked to the plasma membrane with ERM protein Tea1 (57). Early electron microscopy studies have demonstrated that the appressorium pore does not have a cell wall or melanin layer (58). Having a septin mediated actin network would provide cortical rigidity to the plasma membrane. This is vital for maintaining the integrity of the cell under enormous turgor pressure. It is also shown that septin diffusion barriers concentrate proteins which will induce membrane curvature such as N-WASP protein homolog Las17 (57). An initial evagination in the pore plasma membrane will channel turgor pressure to initiate penetration peg emergence. This is consistent with septin mutants being non-pathogenic and unable to produce a penetration peg (57).

References

1. Fisher MC*, et al.* (2012) Emerging fungal threats to animal, plant and ecosystem health. *Nature* 484(7393):186-194.
2. Dean R*, et al.* (2012) The Top 10 fungal pathogens in molecular plant pathology. *Mol Plant Pathol*.
3. Skamnioti P & Gurr SJ (2009) Against the grain: safeguarding rice from rice blast disease. *Trends Biotechnol* 27(3):141-150.
4. Wilson RA & Talbot NJ (2009) Under pressure: investigating the biology of plant infection by Magnaporthe oryzae. *Nat Rev Microbiol* 7(3):185-195.
5. de Jong JC, McCormack BJ, Smirnoff N, & Talbot NJ (1997) Glycerol generates turgor in rice blast. *Nature* 389(6648):244-244.
6. Deising HB, Werner S, & Wernitz M (2000) The role of fungal appressoria in plant infection. *Microbes Infect* 2(13):1631-1641.
7. Deamer D (2009) On the origin of systems. Systems biology, synthetic biology and the origin of life. *EMBO Rep* 10 Suppl 1:S1-4.
8. Li G, Zhou X, & Xu JR (2012) Genetic control of infection-related development in Magnaporthe oryzae. *Curr Opin Microbiol*.
9. Xu JR (2000) Map kinases in fungal pathogens. *Fungal Genet Biol* 31(3):137-152 .
10. Gilbert RD, Johnson AM, & Dean RA (1996) Chemical signals responsible for appressorium formation in the rice blast fungus Magnaporthe grisea. *Physiol Mol Plant P* 48(5):335-346.
11. Kamakura T, Yamaguchi S, Saitoh K, Teraoka T, & Yamaguchi I (2002) A novel gene, CBP1, encoding a putative extracellular chitin-binding protein, may play an important role in the hydrophobic surface sensing of Magnaporthe grisea during appressorium differentiation. *Mol Plant Microbe Interact* 15(5):437-444 .
12. DeZwaan TM, Carroll AM, Valent B, & Sweigard JA (1999) Magnaporthe grisea pth11p is a novel plasma membrane protein that mediates appressorium differentiation in response to inductive substrate cues. *Plant Cell* 11(10):2013-2030 .
13. Liu W*, et al.* (2011) Multiple plant surface signals are sensed by different mechanisms in the rice blast fungus for appressorium formation. *PLoS Pathog* 7(1):e1001261 .
14. Fang EG & Dean RA (2000) Site-directed mutagenesis of the magB gene affects growth and development in Magnaporthe grisea. *Mol Plant Microbe Interact* 13(11):1214-1227 .
15. Choi W & Dean RA (1997) The adenylate cyclase gene MAC1 of Magnaporthe grisea controls appressorium formation and other aspects of growth and development. *Plant Cell* 9(11):1973-1983 .
16. Mitchell TK & Dean RA (1995) The cAMP-dependent protein kinase catalytic subunit is required for appressorium formation and pathogenesis by the rice blast pathogen Magnaporthe grisea. *Plant Cell* 7(11):1869-1878 .
17. Lee N, D'Souza CA, & Kronstad JW (2003) Of smuts, blasts, mildews, and blights: cAMP signaling in phytopathogenic fungi. *Annu Rev Phytopathol* 41:399-427 .
18. Liu H*, et al.* (2007) Rgs1 regulates multiple Galpha subunits in Magnaporthe pathogenesis, asexual growth and thigmotropism. *Embo J* 26(3):690-700 .

19. Zhang H*, et al.* (2011) Eight RGS and RGS-like proteins orchestrate growth, differentiation, and pathogenicity of Magnaporthe oryzae. *PLoS Pathog* 7(12):e1002450 .
20. Li Y*, et al.* (MoRic8 Is a novel component of G-protein signaling during plant infection by the rice blast fungus Magnaporthe oryzae. *Mol Plant Microbe Interact* 23(3):317-331 .
21. Zhang H*, et al.* (2011) Two phosphodiesterase genes, PDEL and PDEH, regulate development and pathogenicity by modulating intracellular cyclic AMP levels in Magnaporthe oryzae. *PLoS One* 6(2):e17241 .
22. Zhou X, Zhang H, Li G, Shaw B, & Xu JR (2012) The Cyclase-associated protein Cap1 is important for proper regulation of infection-related morphogenesis in Magnaporthe oryzae. *PLoS Pathog* 8(9):e1002911 .
23. Yan X*, et al.* (2011) Two novel transcriptional regulators are essential for infection-related morphogenesis and pathogenicity of the rice blast fungus Magnaporthe oryzae. *PLoS Pathog* 7(12):e1002385 .
24. Xu JR & Hamer JE (1996) MAP kinase and cAMP signaling regulate infection structure formation and pathogenic growth in the rice blast fungus Magnaporthe grisea. *Genes Dev* 10(21):2696-2706 .
25. Xu JR, Peng YL, Dickman MB, & Sharon A (2006) The dawn of fungal pathogen genomics. *Annu Rev Phytopathol* 44:337-366 .
26. Park G*, et al.* (2006) Multiple upstream signals converge on the adaptor protein Mst50 in Magnaporthe grisea. *Plant Cell* 18(10):2822-2835 .
27. Slaughter BD, Smith SE, & Li R (2009) Symmetry breaking in the life cycle of the budding yeast. *Cold Spring Harb Perspect Biol* 1(3):a003384 .
28. Johnson JM, Jin M, & Lew DJ (2011) Symmetry breaking and the establishment of cell polarity in budding yeast. *Curr Opin Genet Dev* 21(6):740-746 .
29. Arkowitz RA & Bassilana M (2011) Polarized growth in fungi: symmetry breaking and hyphal formation. *Semin Cell Dev Biol* 22(8):806-815 .
30. Hartwell LH, Culotti J, Pringle JR, & Reid BJ (1974) Genetic control of the cell division cycle in yeast. *Science* 183(4120):46-51 .
31. Murray A (1994) Cell cycle checkpoints. *Curr Opin Cell Biol* 6(6):872-876 .
32. Morris NR (1975) Mitotic mutants of Aspergillus nidulans. *Genet Res* 26(3):237-254 .
33. Veneault-Fourrey C, Barooah M, Egan M, Wakley G, & Talbot NJ (2006) Autophagic fungal cell death is necessary for infection by the rice blast fungus. *Science* 312(5773):580-583 .
34. Kershaw MJ & Talbot NJ (2009) Genome-wide functional analysis reveals that infection-associated fungal autophagy is necessary for rice blast disease. *Proc Natl Acad Sci U S A* 106(37):15967-15972 .
35. Oakley BR & Morris NR (1983) A mutation in Aspergillus nidulans that blocks the transition from interphase to prophase. *J Cell Biol* 96(4):1155-1158 .
36. Bousset K & Diffley JF (1998) The Cdc7 protein kinase is required for origin firing during S phase. *Genes Dev* 12(4):480-490 .
37. Donaldson AD, Fangman WL, & Brewer BJ (1998) Cdc7 is required throughout the yeast S phase to activate replication origins. *Genes Dev* 12(4):491-501 .
38. James SW*, et al.* (1999) nimO, an Aspergillus gene related to budding yeast Dbf4, is required for DNA synthesis and mitotic checkpoint control. *J Cell Sci* 112 (Pt 9):1313-1324 .

39. Shimada Y, Gulli MP, & Peter M (2000) Nuclear sequestration of the exchange factor Cdc24 by Far1 regulates cell polarity during yeast mating. *Nat Cell Biol* 2(2):117-124 .
40. Yu L, Qi M, Sheff MA, & Elion EA (2008) Counteractive control of polarized morphogenesis during mating by mitogen-activated protein kinase Fus3 and G1 cyclin-dependent kinase. *Mol Biol Cell* 19(4):1739-1752 .
41. King RW, Deshaies RJ, Peters JM, & Kirschner MW (1996) How proteolysis drives the cell cycle. *Science* 274(5293):1652-1659 .
42. James SW, Mirabito PM, Scacheri PC, & Morris NR (1995) The Aspergillus nidulans bimE (blocked-in-mitosis) gene encodes multiple cell cycle functions involved in mitotic checkpoint control and mitosis. *J Cell Sci* 108 (Pt 11):3485-3499 .
43. Saunders DG, Aves SJ, & Talbot NJ (Cell cycle-mediated regulation of plant infection by the rice blast fungus. *Plant Cell* 22(2):497-507 .
44. Gladfelter A & Berman J (2009) Dancing genomes: fungal nuclear positioning. *Nat Rev Microbiol* 7(12):875-886 .
45. Harris SD (2001) Septum formation in Aspergillus nidulans. *Curr Opin Microbiol* 4(6):736-739.
46. Saunders DG, Dagdas YF, & Talbot NJ (Spatial uncoupling of mitosis and cytokinesis during appressorium-mediated plant infection by the rice blast fungus Magnaporthe oryzae. *Plant Cell* 22(7):2417-2428 .
47. Simanis V (2003) Events at the end of mitosis in the budding and fission yeasts. *J Cell Sci* 116(Pt 21):4263-4275 .
48. Bruno KS, Morrell JL, Hamer JE, & Staiger CJ (2001) SEPH, a Cdc7p orthologue from Aspergillus nidulans, functions upstream of actin ring formation during cytokinesis. *Mol Microbiol* 42(1):3-12 .
49. Howell AS*, et al.* (2012) Negative feedback enhances robustness in the yeast polarity establishment circuit. *Cell* 149(2):322-333 .
50. Oh Y & Bi E (Septin structure and function in yeast and beyond. *Trends Cell Biol* 21(3):141-148 .
51. Douglas LM, Alvarez FJ, McCreary C, & Konopka JB (2005) Septin function in yeast model systems and pathogenic fungi. *Eukaryot Cell* 4(9):1503-1512.
52. Wloka C*, et al.* (Evidence that a septin diffusion barrier is dispensable for cytokinesis in budding yeast. *Biol Chem* 392(8-9):813-829 .
53. Takizawa PA, DeRisi JL, Wilhelm JE, & Vale RD (2000) Plasma membrane compartmentalization in yeast by messenger RNA transport and a septin diffusion barrier. *Science* 290(5490):341-344.
54. Caudron F & Barral Y (2009) Septins and the Lateral Compartmentalization of Eukaryotic Membranes. *Dev Cell* 16(4):493-506.
55. Mostowy S & Cossart P (2012) Septins: the fourth component of the cytoskeleton. *Nat Rev Mol Cell Biol* 13(3):183-194 .
56. Saunders DG, Dagdas YF, & Talbot NJ (2010) Spatial uncoupling of mitosis and cytokinesis during appressorium-mediated plant infection by the rice blast fungus Magnaporthe oryzae. *Plant Cell* 22(7):2417-2428 .
57. Dagdas YF*, et al.* (2012) Septin-mediated plant cell invasion by the rice blast fungus, Magnaporthe oryzae. *Science* 336(6088):1590-1595 .

58. Howard RJ, Ferrari MA, Roach DH, & Money NP (1991) Penetration of hard substrates by a fungus employing enormous turgor pressures. *Proc Natl Acad Sci U S A* 88(24):11281-11284 .

Introduction to the Current Study

The main focus of this thesis is the investigation and characterization of the molecular processes necessary for allowing plant infection by the devastating rice blast pathogen *Magnaporthe oryzae*. This thesis is submitted for examination for the award of a PhD by publication at the University of Exeter. As such, much of its content has already appeared as individual research publications. These are briefly described below.

In Chapter 2, I present data for a series of experiments which provide evidence that nuclear division and cytokinesis are spatially uncoupled during appressorium development. In contrast to the hyphae of most filamentous fungi where the site of nuclear division defines the site of cytokinesis, these processes are spatially and temporally separated during appressorium development. I show how the septation site is defined by a family of septin GTPase proteins, prior to nuclear division. Septation in *M. oryzae* is controlled by the yeast Cdc15 homolog Sep1. Perturbation of Sep1 function renders the fungus non-pathogenic, confirming the importance of timely septation for the development of a functional appressorium. This chapter was published in *The Plant Cell* (Saunders, D.G., Dagdas, Y.F., Talbot, N.J. (2010),)[1]. Part of this work previously appeared in PhD thesis of Diane Saunders. My specific contribution was to define the septin GTPase family, clone the corresponding genes, characterize them and define their roles in cytokinesis.

In Chapter 3, I present further characterization of the septin GTPase family in *M. oryzae*. Septins form hetero-oligomeric structures during appressorium development, the most striking of which is a large ring around the appressorium pore, the point at which the penetration peg subsequently emerges. I first present evidence that septins control cell cycle progression and actomyosin ring formation during septation. I also show that septins recruit a toroidal F-actin network to the appressorium pore which is necessary for penetration peg emergence. Septins also act as diffusion barriers for proteins that initiate penetration peg formation by inducing negative membrane curvature. The signalling pathways regulating septin polymerization are also discussed. This chapter was published in *Science* (Dagdas et. al., 2012)[2]. The principal finding of the published study is that septins play a hitherto unrecognized function in regulating cell shape changes associated with microbial pathogenesis.

In Chapter 4, I present evidence that defines a new role for NADPH oxidases during rice blast infection. Previously, reactive oxygen species (ROS) generation by NADPH oxidase (Nox) enzymes has been shown to be necessary for plant infection[3]. In this thesis I present data, which suggests that ROS generation is required for re-modelling of F-actin and septin accumulation around the appressorium pore. The Nox2-NoxR complex is necessary for septin ring formation at the pore, whereas Nox1 is required for actin polymerization necessary for penetration hypha elongation. Strikingly, the inhibitory effect of LatrunculinA on F-actin polymerization can be competitively inhibited by exposure to hydrogen peroxide. Moreover, a ROS-regulated actin binding protein, gelsolin, also forms a ring at the pore and accumulation of gelsolin is sensitive to the ROS scavenger Ascorbic acid and the Nox inhibitor diphenylene iodonium (DPI). Furthermore, gelsolin localisation at the appressorium pore requires Nox2-NoxR complex. This work was published in *Proceedings of the National Academy of Sciences USA* (Ryder et. al., 2013)[4]. My contribution was to define the role of Nox2 in septin assembly and to distinguish the two roles of the NADPH oxidase complexes with regard to septin dynamics.

In Chapter 5, I present the results of a series of experiments to investigate the post-invasion strategies of *M. oryzae*. I present data which shows that the biotrophic interfacial complex (BIC) is mainly composed of plant cellular membranes and is an active site of fungal secretion. This study showed that the SNARE protein, Snc1 and Spitzenkörper component, Myosin light chain kinase 1 (Mlc1) are re-located from the hyphal tip to the BIC-associated cell during invasive hyphae differentiation. I also present data which suggests that apoplastic and symplastic effectors are translocated via different secretion systems. Apoplastic effector secretion requires the ER-Golgi pathway and is sensitive to BrefeldinA, whereas symplastic effectors are secreted via a BrefeldinA-insensitive pathway which involves the exocyst components Sec5 and Exo70 and SNARE protein Sso1. This study is under review, following revision, by *Nature Communications*. I am joint first author and was responsible for designing the experiments and defining the nature of invasive hyphae using exocyst and polarisome components. The transgenic rice lines used in the study were generated by Tom Mentlak and appeared in his PhD thesis of the University of Exeter.

References

1. Saunders, D.G., Dagdas, Y.F. & Talbot, N.J. Spatial uncoupling of mitosis and cytokinesis during appressorium-mediated plant infection by the rice blast fungus *Magnaporthe oryzae*. *The Plant Cell* **22**, 2417-28 (2010).

2. Dagdas, Y.F. et al. Septin-mediated plant cell invasion by the rice blast fungus, *Magnaporthe oryzae*. *Science* **336**, 1590-5 (2012).

3. Egan, M.J., Wang, Z.Y., Jones, M.A., Smirnoff, N. & Talbot, N.J. Generation of reactive oxygen species by fungal NADPH oxidases is required for rice blast disease. *Proc Natl Acad Sci U S A* **104**, 11772-7 (2007).

4. Ryder, L.S., Dagdas, Y.F. et al. NADPH oxidases regulate septin-mediated cytoskeletal remodeling during plant infection by the rice blast fungus. *Proceedings of the National Academy of Sciences of the United States of America* **110**, 3179-84 (2013).

5. Martha C. Giraldo[1,5], Yasin F. Dagdas[2,5], Yogesh K. Gupta[2,6], Thomas A. Mentlak[2,4,6], Mihwa Yi[1], Hiromasa Saitoh[3], Ryohei Terauchi[3], Nicholas J. Talbot[2,7], Barbara Valent[1,7] ([5,6,7]Contributed equally), under review for publication at *Nature Communications*

"It is not easy to convey, unless one has experienced it, the dramatic feeling of sudden enlightenment that floods the mind when the right idea finally clicks into place. One immediately sees how many previously puzzling facts are neatly explained by the new hypothesis. One could kick oneself for not having the idea earlier, it now seems so obvious. Yet before, everything was in a fog."

Francis Crick

Chapter2

Spatial uncoupling of mitosis and cytokinesis during appressorium-mediated plant infection by the rice blast fungus *Magnaporthe oryzae*

Diane G. O. Saunders[1], Yasin F. Dagdas and Nicholas J. Talbot[2]

School of Biosciences, University of Exeter, Geoffrey Pope Building, Stocker Road, Exeter EX4 4QD, United Kingdom

Short title: Cytokinesis in Magnaporthe

[1]Current Address; The Sainsbury Laboratory, Norwich Research Park, Colney Lane, Norwich NR47UH, United Kingdom.

[2]Author Correspondence to n.j.talbot@exeter.ac.uk

Final Accepted Manuscript: Saunders, D.G., Dagdas, Y.F. & Talbot, N.J. Spatial uncoupling of mitosis and cytokinesis during appressorium-mediated plant infection by the rice blast fungus Magnaporthe oryzae. *The Plant Cell* **22**, 2417-28 (2010)

SYNOPSIS

This study examines the relationship between nuclear division and cytokinesis during formation of appressoria by a plant pathogenic fungus. It also identifies a key spatial regulator of cytokinesis and nuclear division and shows that it is required for the fungus to cause disease.

ABSTRACT

To infect plants, many pathogenic fungi develop specialised infection structures called appressoria. Here, we report that appressorium development in the rice blast fungus *Magnaporthe oryzae* involves an unusual cell division, in which nuclear division is spatially uncoupled from the site of cytokinesis and septum formation. The position of the appressorium septum is defined prior to mitosis by formation of a heteromeric septin ring complex, which was visualised by spatial localisation of Septin4:GFP and Septin5:GFP fusion proteins. Mitosis in the fungal germ tube is followed by long distance nuclear migration and rapid formation of an actomyosin contractile ring in the neck of the developing appressorium, at a position previously marked by the septin complex. By contrast, mutants impaired in appressorium development, such as *Δpmk1* and *ΔcpkA* regulatory mutants, undergo coupled mitosis and cytokinesis within the germ tube. Perturbation of the spatial control of septation, by conditional mutation of the *SEPTATION-ASSOCIATED 1* gene of *M. oryzae*, prevented the fungus from causing rice blast disease. Over-expression of *SEP1* did not affect septation during appressorium formation, but instead led to de-coupling of nuclear division and cytokinesis in non-germinated conidial cells. When considered together, these results indicate that *SEP1* is essential for determining the position and frequency of cell division

sites in *M. oryzae* and demonstrate that differentiation of appressoria requires a cytokinetic event that is distinct from cell divisions within hyphae.

INTRODUCTION

The position and orientation of cell division is pivotal in the development of multi-cellular organisms (Oliferenko et al., 2009). Although cell division can often lead to daughter cells of equal size, in many instances cells of unequal size and fate are generated. The differentiation of new cell types, tissues and organs, for example, requires distinct patterns of cell division in which the machinery that physically divides a cell is subject to precisely synchronized genetic regulation (Oliferenko et al., 2009). In pathogenic fungi, which are responsible for some of the most serious plant diseases, the ability to cause disease relies on the ability to form specialised cells, such as spores and infection structures (Tucker and Talbot, 2001). The genetic regulation of cell division in these organisms is, however, not well understood, especially during infection-associated development (Tucker and Talbot, 2001; Gladfelter and Berman, 2009).

In this report, we have investigated the control of cell division during plant infection by the rice blast fungus *Magnaporthe oryzae*. Rice blast destroys 10-30 % of the annual rice harvest and represents a considerable threat to global food security (Wilson and Talbot, 2009). The disease is initiated when *M. oryzae* forms specialised dome-shaped infection cells called appressoria, which are distinct, in both shape and cellular organisation, from the cylindrical hyphae by which fungi normally grow (Wilson and Talbot, 2009; Dean, 1997). Appressoria develop enormous turgor of up to 8.0 MPa, and this pressure is translated into physical force to rupture the rice (*Oryza sativa*) leaf cuticle, allowing invasion of plant tissue (Dean, 1997). Previously, we showed that mitosis is a pre-requisite for appressorium development in *M. oryzae* (Veneault-Fourrey et al., 2006). A single round of nuclear division occurs shortly after

spore germination on the rice leaf surface. One of the daughter nuclei migrates to the germ tube tip where the appressorium is formed, while the other nucleus migrates back into the conidial cell from which its mother nucleus originated (Veneault-Fourrey et al., 2006). Following mitosis and nuclear migration, an appressorium is formed and the conidium undergoes autophagic, programmed cell death during which its nuclei are degraded (Veneault-Fourrey et al., 2006; Kershaw and Talbot, 2009). A DNA replication-associated checkpoint is necessary for initiation of appressorium formation, whereas entry into mitosis is essential for differentiation of functional appressoria (Saunders et al., 2010). The checkpoints that regulate appressorium differentiation are therefore responsible for a precisely choreographed developmental programme leading to plant infection, in which the single nucleus in the appressorium is the source for all subsequent genetic material in the fungus as it invades host plant tissue (Veneault-Fourrey et al., 2006; Saunders et al., 2010).

In this study, we set out to investigate the position, orientation and timing of infection-associated cell division in *M. oryzae*. We report here that appressorium development in *M. oryzae* involves spatial uncoupling of mitosis and cytokinesis. The cell division that leads to appressorium differentiation is defined initially by formation of a heteromeric septin ring complex before the onset of mitosis. Nuclear division is then followed by long distance nuclear migration, which triggers development of an actomyosin contractile ring at the base of the nascent appressorium. We also demonstrate that conditional mutation of Sep1, a key spatial regulator of cytokinesis and nuclear division, is sufficient to prevent rice blast disease.

RESULTS

Live cell imaging of mitosis during appressorium morphogenesis in *M. oryzae*

To investigate spatial regulation of cell division in *M. oryzae*, we first visualized the relative positions of nuclear division and subsequent cytokinesis, by determining the position of the actomyosin contractile ring involved in septum formation (Bi, 2001; Bi et al., 1998; Harris, 2001). We introduced a Tropomyosin:*eGFP* gene fusion (Pearson et al., 2004) into a wild type strain of *M. oryzae*, Guy11 (Leung et al., 1988), expressing a histone H1:RFP gene fusion (Saunders et al., 2010) and carried out live cell imaging of mitosis and cytokinesis. In hyphae of *M. oryzae* we found that actomyosin ring formation was consistently associated with the position of the pre-mitotic nucleus and the medial position of the spindle during nuclear division, as shown in Figure 1A. This occurred during both hyphal branching and sub-apical nuclear division within growing hyphae. To determine the spatial pattern of mitosis during appressorium formation, we incubated a conidial suspension of the *M. oryzae* H1:RFP strain on a hydrophobic glass surface and observed mitosis 4-6 hours later (Figure 1B). Nuclear division always occurred in the germ tube, close to the site of germ tube emergence, 4-6 hours after germination (Figure 1B; Supplemental Movie 1 online). Staining with the lipophilic dye 3,3'-dihexyloxacarbocyanine iodide ($DiOC_6$) highlighted the nuclear envelope (Koning et al., 1993), as well as extensive endoplasmic reticulum throughout the germ tube. The nuclear envelope appeared to remain intact throughout nuclear division, consistent with a closed, or partially closed, mitosis occurring in *M. oryzae* as in other filamentous ascomycetes (Gladfelter and Berman, 2009; Ukil et al., 2009). Migration of a daughter nucleus into the incipient appressorium was, however, immediately followed by intense localisation of tpmA:eGFP at the neck of the appressorium, perpendicular to the longitudinal axis of the germ tube (Figure 1C and Supplemental Movie 2 online). Actomyosin ring formation at the site of cytokinesis was typically completed within 6

min of the preceding mitosis, whereas ring formation during septation in vegetative hyphae was observed to take 30 min (Figure 1). Actin then accumulated within the appressorium during its maturation, prior to formation of the penetration hypha which the fungus uses to rupture the plant cuticle, as shown in Supplemental Figure 1.

To test whether spatial uncoupling of nuclear division and cytokinesis is specific to appressorium development, we introduced *H1:eRFP* and *tpmA:eGFP* gene fusions into mutants defective in appressorium morphogenesis. The *M. oryzae Δpmk1* mutant is unable to differentiate appressoria, due to absence of the pathogenicity-associated mitogen-actived protein kinase (MAPK), and instead produces undifferentiated germ tubes (Xu and Hamer, 1996). Strikingly, we found that *Δpmk1* mutants underwent numerous rounds of nuclear division within the germ tube in which actomyosin ring formation always occurred at the medial position between daughter nuclei, rather than at the hyphal apex, as shown in Figure 1D and Supplemental Figure 2. Similarly in *ΔcpkA* mutants, which form aberrant non-functional appressoria (Mitchell and Dean, 1995; Xu et al., 1997), cytokinesis also occurred predominantly at the mid-point between daughter nuclei (Figure 1D and Supplemental Figure 1). *CPKA* encodes the cAMP-dependent protein kinase A (PKA) catalytic subunit and is essential for appressorium function (Mitchell and Dean, 1995; Xu et al., 1997). By contrast, developmental mutants that form morphologically normal appressoria, such as Δ*mst12*, a transcription factor mutant unable to form penetration hyphae (Park et al., 2002), showed clear separation of mitosis and cell division with actomyosin ring formation at the neck of the incipient appressorium (Figure 1D; Supplemental Figure 2). We conclude that spatial uncoupling of mitosis and cytokinesis is specifically associated with the morphogenetic programme for appressorium differentiation in *M. oryzae*.

Septin ring formation precedes mitosis during appressorium morphogenesis by *M. oryzae*

To investigate the relationship between mitosis and septation during appressorium development, we decided to determine the positions and times at which septin complexes form during conidial germination and appressorium formation. Septins are conserved cytoskeletal GTPases that were first described in the budding yeast *Saccharomyces cerevisiae* and fulfil diverse functions, forming heteromeric complexes that assemble as filaments, gauzes or ring structures. They interact with membranes, actin and microtubules and serve as organisational markers during cell division and polarised growth, in addition to being components of the morphogenesis and spindle position checkpoints (Lew, 2003; Douglas et al., 2005; Gladfelter and Berman, 2009). At a prospective bud site, the core septins Cdc3, Cdc10, Cdc11 and Cdc12 form a ring, which then develops into an hourglass-shaped collar at the mother-bud neck, before splitting into two rings during cytokinesis (Gladfelter et al., 2001; Gladfelter et al., 2005). In filamentous fungi, septins assemble into a wider variety of complexes that form at growing hyphal tips, hyphal branch points, the bases of cellular protrusions and, importantly, at sites of future septum formation. In *Aspergillus nidulans*, four of the five septins, AspA, AspB, AspC and AspD form a heteropolymeric complex, which appears as a ring or collar at the base of an emerging germ tube shortly after conidial germination. This septin ring is formed post-mitotically and provides the first positional cue for the subsequent site of septation (Westfall and Momany, 2002; Lindsey et al., 2010). We therefore identified a family of six putative septin-encoding genes from the *M. oryzae* genome. We characterized two of these genes; *SEP4*, which shows 55% identity and 76% similarity to Cdc10 from *Saccharomyces cerevisiae* and *SEP5*, which is 44% identical and 64% similar to Cdc11 (See Supplemental Figure 3). *SEP4* and *SEP5* gene fusions with GFP were constructed and expressed under their native

promoters in a *M. oryzae* strain expressing H1:RFP (Saunders et al., 2010), to investigate the relationship between nuclear division and septin ring formation. We observed that a septin ring was formed at the base of the germ tube, proximal to the conidium, within 2 h of germination and a second septin ring developed at the neck of the developing appressorium, 4 h after germination, as shown in Figure 2. Interestingly, septin ring formation at the future site of septum formation always occurred before the onset of mitosis (Figure 2B). Septin rings dispersed, or were degraded, soon afterwards and only very small numbers of germlings had clear septin rings after 8h, during appressorium maturation. We conclude that the appressorium septation site is defined at an early stage following spore germination by formation of a heteromeric septin ring complex, which precedes mitosis in the germ tube.

Genetic analysis of the role of cytokinesis and septation during infection-related morphogenesis

To test the biological relevance of the observed pattern of cytokinesis, we investigated the genetic control of septation. In the fission yeast, *Schizosaccharomyces pombe*, the septation initiation network (SIN) consists of a suite of proteins that monitors mitotic progression and co-ordinately initiates cytokinesis (Bardin and Amon, 2001). The *S. pombe* Cdc7 SIN protein is a serine-threonine kinase necessary for septum formation (Fankhauser and Simanis, 1994). Cdc7 shows 42% identity to *A. nidulans* SepH (Bruno et al., 2001), which is required for septum development in the filamentous fungus, suggesting that this is a conserved regulatory function (Harris, 2001; Bruno et al., 2001). We reasoned that perturbation of Cdc7 function in *M. oryzae* would provide a test of the functional significance of infection-associated cytokinesis. We identified a putative Cdc7 homologue, Sep1, with 52 % amino acid identity to *A. nidulans* SepH, as shown in Supplemental Figure 4. Sep1 has a protein kinase domain at its N-terminus

(residues 59-313) and a highly conserved region with 73% identity to the *A. nidulans* SepH kinase domain. We introduced *M. oryzae SEP1* into a temperature-sensitive *A. nidulans sepH1* mutant, and this restored its ability to form septa when vegetative hyphae were incubated at the non-permissive temperature, as shown in Figure 3A, indicating that the proteins are functionally related.

To test the role of Sep1 in *M. oryzae*, we generated a temperature-sensitive allele of the gene analogous to the *A. nidulans sepH1* temperature-sensitive mutation, which has a glycine to arginine substitution at codon 793 (Bruno et al., 2001). The mutation was generated in *M. oryzae SEP1* (Figure 3B) and the resulting allele introduced into the fungus by targeted allelic replacement. We generated 24 *sep1*^{G849R} transformants that displayed a hyphal growth defect at 32ºC, but which could be partially restored by subsequent incubation at 24ºC (Figure 3C). DNA gel blot analysis and genomic DNA sequencing allowed selection of two transformants (76 and 169) containing single homologous insertions of the *sep1*^{G849R} allele. One of these transformants, 76, was subjected to a second transformation to introduce the *H1:eRFP* gene fusion enabling us to assess the effect of the *sep1*^{G849R} mutation on nuclear division.

We quantified septum formation and nuclear number in *sep1*^{G849R} mutants, compared to the isogenic H1:RFP strain of *M. oryzae*. Conidial suspensions were incubated in a moist chamber at 24°C or, after 1 h, transferred to a semi-restrictive temperature of 29ºC, which does not interfere with appressorium formation (Veneault-Fourrey et al., 2006). Surprisingly, calcofluor white staining revealed an increased frequency of septation in the germ tube during appressorium development of the *M. oryzae sep1*^{G849R} mutant, as shown in Figure 3D (see also Supplemental Figure 5). This suggests that, in contrast to *A. nidulans* SepH (Bruno et al., 2001), Sep1 may act as a negative-regulator of cytokinesis in *M. oryzae*. However, we also observed multiple septa in two wild type strains that expressed a copy of the *sep1*^{G849R} allele (as well as a

functional copy of *SEP1*), when these were incubated at 29°C (Supplemental Figure 6). This suggests that the *sep1*^{G849R} allele might have a dominant effect on the regulation of septation. Consistent with this idea the *SEP1 sep1*^{G849R} strains showed reduced growth in culture compared to the isogenic wild type Guy11 (Supplemental Figure 7), but did not show the severe temperature sensitive phenotype of *sep1*^{G849R} mutants (Figure 3). Interestingly, we observed that the cell-cycle arrest of nuclei in non-germinating cells of the three-celled conidium of the *sep1*^{G849R} mutant was alleviated, because nuclear number increased rapidly, as shown in Figure 3E-F and Supplemental Figure 8. In spite of the mis-regulation of germ-tube morphology and nuclear division in *sep1*^{G849R} mutants, the frequency of appressorium development was indistinguishable from that of the wild type Guy-11 (Figure 4A), although germ tubes were elongated and branched (Figure 4B).

To test the ability of *sep1*^{G849R} appressoria to cause rice blast disease, we inoculated the blast-susceptible rice cultivar CO-39. The density of disease lesions on rice leaves inoculated with the *sep1*^{G849R} strain was significantly reduced at the semi-restrictive temperature of 29ºC, as shown in Figure 4C (two sample *t*-test assuming equal variances, $t = 9.35$, df = 10, $P < 0.05$), although no reduction was observed at the permissive temperature of 24ºC compared to Guy-11, (Figure 4C; two sample *t*-test assuming equal variances, $t = 1.41$, df = 16, $P > 0.05$). When considered together, these results suggest that spatial control of septation is necessary for development of infection-competent appressoria by the rice blast fungus.

SEP1 is a dose-dependent regulator of nuclear division

A conditional mutation in *SEP1* increased septation and nuclear division during appressorium morphogenesis. We therefore hypothesized that over-expression of *SEP1* might, conversely, prevent cytokinesis and enable us to investigate the requirement for

cytokinesis during appressorium development. To test this, we placed *SEP1* under control of the isocitrate lyase gene promoter ($ICL1_{(p)}$) to enable induction of gene expression by acetate (Wang et al., 2003) and introduced the *ICL1(p):SEP1* gene fusion into the *M. oryzae* H1:RFP strain. Two putative *ICL1(p):SEP1* transformants were identified carrying either single, or multiple insertions of the fusion construct. The two transformants, SEP1-1 and SEP1-9, grew normally in culture in the presence or absence of acetate, as shown in Figure 5A. During conidial germination and appressorium development, inducible over-expression of *SEP1* increased nuclear number rapidly as a consequence of alleviating the cell-cycle arrest of nuclei within non-germinating conidial cells (Figure 5B-C; Supplemental Figure 9). When considered with analysis of the $sep1^{G849R}$ mutant, these results are consistent with requirement for a steady-state level of Sep1 protein to maintain the inherent cell-cycle arrest phenotype in non-germinated conidial cells during infection-related development. Inducible over-expression of *SEP1* did not, however, affect septation (Figure 5D; Supplemental Figure 10). We conclude that normal Sep1 function, which is adversely affected by the $sep1^{G849R}$ allele even in a heterozygous state, is necessary to co-ordinate the spatial control of septation in *M. oryzae*, regardless of its abundance. The frequency of appressorium development in SEP1-1 and SEP1-9 was, however, identical to that of the wild type as shown in Figure 5E, with no associated germ tube-specific morphological defect (Figure 5F). Correct *SEP1* function is therefore necessary for spatial control of septation but also for maintaining the cell cycle arrested state of nuclei in non-germinating cells of *M. oryzae* spores. The septation-associated role of *SEP1* is necessary for appressorium-mediated plant infection by the rice blast fungus.

DISCUSSION

In this study, we aimed to determine the relationship between nuclear division and cytokinesis during formation of appressoria by a plant pathogenic fungus. Previous analysis have shown that development of appressoria in the rice blast fungus requires a morphogenetic programme regulated by the cAMP response pathway and the Pmk1 MAP kinase cascade in response to the hard, hydrophobic rice leaf surface and absence of exogenous nutrients (Wilson and Talbot, 2009; Dean, 1997). In response to these signals, a germinating conidium undergoes a single round of mitosis, which is a necessary pre-requisite for appressorium differentiation as evidenced by the fact that a conditional *nimA* mutant, blocked at mitotic entry, fails to differentiate functional infection cells (Veneault-Fourrey et al., 2006; Saunders et al., 2010).

Our first conclusion from this study is that in *M. oryzae,* spatial uncoupling of nuclear division and septation occurs during appressorium development, distinguishing it from cytokinesis during hyphal growth of the fungus. In hyphae of *M. oryzae,* the position of cell division coincides with the medial position of the preceding mitosis, defining the position of the subsequent septum and leading to an even distribution of cellular compartments along the hypha with relatively uniform intercalary length and an even distribution of nuclei. During appressorium differentiation, nuclear division and cytokinesis are, instead, spatially separated and transit of the nucleus to the swollen hyphal tip always precedes differentiation and cytokinesis of the appressorium (Supplemental Movie 2 online). By contrast, germ tubes of Δ*pmk1* and Δ*cpkA* mutants, which do not differentiate functional appressoria (Xu and Hamer, 1996; Mitchell and Dean, 1995), undergo coupled mitosis and cytokinesis, which is identical to the pattern observed in hyphae. When these results are considered together, this suggests that the spatial relationship between mitosis and cytokinesis is a component of the morphogenetic programme leading to appressorium formation.

The site of cell division in fungi is normally determined early in the cell cycle (Oliferenko et al., 2009; Gladfelter and Berman, 2009). In *S. cerevisiae*, for instance, cells divide by budding and the site of bud assembly is determined in G1 by landmark proteins, such as Bud3p, Bud4p, Bud10p and Axl1p (Casamayor and Snyder, 2002). These proteins recruit the GTPase Bud1p, which in turn recruits the guanine nucleotide exchange factor protein Cdc24p, that acts on Cdc42p-GTPase, ultimately leading to assembly of septins (Cdc3, Cdc10, Cdc11, Cdc12, and Shs1) at the future site of cytokinesis (Park et al., 1997; Barral et al., 2000; Schuyler and Pellman, 2001). Budding yeast then has a mechanism to ensure that the mitotic spindle is correctly oriented across the mother-bud neck so one daughter nucleus successfully migrates into the bud before cell division. This process involves microtubule-associated proteins, Kar9 and Bim1, and a dynein Dyn1p, which has a key role in nuclear positioning, providing the main force which pulls the nucleus via astral microtubules (Schuyler and Pellman, 2001; Yeh et al., 2000; see model in Figure 6). If the spindle is not correctly oriented across the mother-daughter cell junction, this delays activation of the mitotic exit network, which prevents cytokinesis from occurring (Schuyler and Pellman, 2001; Yeh et al., 2000; Lew, 2003). Cytokinesis is therefore dependent on the correct positioning of nuclear division. In the fission yeast, *S. pombe*, the cell division site is determined late in G2 by position of the pre-mitotic nucleus, leading to fission of the cell across its equatorial plane and generation of two equally-sized daughter cells (Bähler and Pringle, 1998; Bähler et al., 1998). In the filamentous fungus *A. nidulans* during spore germination, asymmetric division delimits the extending germ-tube from the spore, coincident with completion of the third nuclear division (Harris, 2001; Kaminskyi, 2000). The septum in *A. nidulans*, however, assembles at a point equi-distant from each daughter nucleus in response to signals that appear to originate from the mitotic spindle during nuclear division (Wolkow et al., 1996). Spatial separation of nuclear division and

cytokinesis in *M. oryzae* is therefore very unusual indeed (see Figure 6), with very few previous examples reported (Straube et al., 2005; Gladfelter et al., 2006).

It was particularly significant that deposition of the septin ring, which provides the first organisation cue for cytokinesis, defines the position of the appressorium septum, prior to mitosis in the germ tube. This is consistent with the spatially separate position of cell division being identified at a very early stage in the cell cycle (Gladfelter and Berman, 2009). Recently, we demonstrated that the initiation of appressorium formation in *M. oryzae* requires pre-mitotic DNA replication to have occurred because treatment of germlings with hydroxyurea, which inhibits DNA replication and causes G1 arrest, prevents differentiation of germ tube tips (Saunders et al., 2010). Moreover, a *nim1* temperature-sensitive mutant that prematurely enters mitosis in the absence of DNA replication is unable to initiate appressorium development (Saunders et al., 2010). The temporal pattern of septin ring formation that we observed in this study is therefore consistent with septin regulation by the DNA replication checkpoint that initiates appressorium morphogenesis in *M. oryzae*. The pre-mitotic control of septin ring formation following conidial germination contrasts with previous observations in *A. nidulans* where the AspB septin has been shown, for instance, to contribute to ring formation under post-mitotic control (Westfall and Momany, 2002), although pre-mitotic control of septin complex formation does occur during hyphal branching (Westfall and Momany, 2002; Lindsey et al., 2010). Further investigation of the septin gene family in *M. oryzae* may prove to be very valuable in view of their diverse roles in cell division control, polarised growth, cell surface organisation, exocytosis and vesicle fusion, all of which are likely to be necessary virulence-associated functions in the fungus. Consistent with this idea, septins have found to be important for virulence of a number of fungal species (Boyce et al., 2005; Douglas et al., 2005; Gonzales-Novo et al., 2006; Kozubowski and Heitman, 2010).

To test whether control of appressorium septation might be significant in the developmental programme for plant infection, we perturbed the spatial regulation of cytokinesis and showed that this prevents *M. oryzae* from carrying out plant infection. The *M. oryzae sep1*^{G849R} mutant was predicted to impair cytokinesis based on previous analysis in *A. nidulans* (Bruno et al., 2001), but the equivalent *M. oryzae* mutant displayed enhanced septation at the restrictive temperature, perhaps due to a dominant negative effect of the temperature-sensitive allele. Cell-cycle arrest of non-germinating conidial cells was also alleviated, resulting in multiple nuclei being present in spores of the *sep1*^{G849R} mutant. Interestingly, in spite of undergoing nuclear division, these conidial cells did not germinate, showing that dormancy was not affected. The *A. nidulans* mutant *sepH1* has no such effect on nuclear division at its restrictive temperature (Bruno et al., 2001), suggesting a divergence in function in *M. oryzae*. Significantly, we observed that appressoria of the *sep1*^{G849R} mutant could not cause plant disease at a semi-restrictive temperature. Therefore, it is apparent that co-ordination of either nuclear or cellular division, or indeed both, is essential in preserving the functional competency of *M. oryzae* appressoria. Recently, we showed that the pivotal checkpoints that regulate appressorium morphogenesis occur prior to mitosis at S-phase and at mitotic entry (Saunders et al., 2010). By contrast, we found that arresting mitotic exit does not affect the frequency of appressorium formation, but does affect the ability of infection cells to re-polarise and cause plant infection. In this study, we have shown that septation initiation, which is linked to mitotic exit, is also not a pre-requisite for appressorium morphogenesis, but is essential for penetration peg formation and subsequent plant infection. The formation of a septum to separate the differentiated appressorium from the germ tube is likely to be essential for generation of the enormous turgor that is built up during cuticle penetration (de Jong et al., 1997; Thines et al., 2000). It is also possible that septation is a necessary pre-requisite for cell wall

differentiation and melanisation that are necessary for appressorium function (Chumley and Valent, 1990; Tucker et al., 2004)

Our final conclusion is that Sep1 has a dual function in co-ordinating cytokinesis, which is independent of Sep1 abundance, and also nuclear division, but here in a Sep1 dose-dependent manner. Over-expression of Sep1, for instance, did not affect septation, but instead led to release of the cell cycle arrest of nuclei in non-germinating conidial cells. Alleviation of such a cell-cycle arrest phenotype has not previously been observed in *sepH/cdc7* mutants (Fankhauser and Simanis, 1994). In *S. pombe*, for example, deletion of *cdc7* which is a component of the septation initiation network, produces highly elongated, multinucleate cells as a consequence of the inability to form septa, rather than resulting from a direct effect of Cdc7 on nuclear division (Fankhauser and Simanis, 1994). In addition, over-expression of Cdc7 initiated a multiple-septa phenotype (Fankhauser and Simanis, 1994). Similarly in *S. cerevisiae*, deletion or over-expression of the Sep1 homologue CDC15, a component of the mitotic exit network, inhibited or disrupted actin ring formation, blocking subsequent septum formation with a consequent cell-cycle arrest phenotype (Cenamor et al., 1999). Therefore, dose-dependent cell-cycle regulation by Sep1 in *M. oryzae* represents a previously unknown signalling mechanism for co-ordination of cell-cycle progression during spore germination, infection structure formation and plant infection.

METHODS

Fungal strains, growth conditions, pathogenicity and infection-related development assays

Isolates of *Magnaporthe oryzae* (Couch and Kohn, 2002; formerly *M. grisea*) used in this study are stored in the laboratory of NJT (University of Exeter, UK). Previously described strains are listed in Supplemental Table 1 online, and those generated in this

study are in Supplemental Table 2 online. All strains were routinely maintained on complete medium (Talbot et al., 1993). DNA-mediated transformation, genomic DNA extractions and plant infection assays were carried out as described previously (Talbot et al., 1993). Conidial germination and development of appressoria were monitored on hydrophobic borosilicate glass coverslips (Hamer et al., 1988). A conidial suspension of 5 x 10^4 conidia mL^{-1} was placed onto the surface of glass coverslips, then incubated in a moist chamber at 24°C.

Microscopy methods

All images acquired during hyphal growth, germination and appressorium development were recorded using a Zeiss LSM510 Meta confocal-light scanning microscope (CLSM) system. Slides were prepared by sealing the coverslip with adhered conidia, with Vaseline Petroleum Jelly (Vaseline, Unilever UK Limited). Blue diode (405nm), Argon (458, 477, 488, 504nm), Helium-Neon (He-Ne) 543nm and He-Ne 633nm lasers were used to excite the various fluorochromes and all images recorded following examination under the 63 x oil objective. Offline image analysis was carried out using the LSM image browser (Zeiss) or MetaMorph 7.5 (Molecular Devices). The CLSM multi-track setting was used to enable synchronised image acquisition.

The lipophilic stain 3,3'-dihexyloxacarbocyanine iodide ($DiOC_6$; AnaSpec) was used to stain the nuclear envelope (Koning et al., 1993). A conidial suspension of 5 x 10^4 conidia mL^{-1} from the *M. oryzae* H1:RFP strain was applied to coverslips in a moist chamber at 24°C. A 10 mM stock solution of $DiOC_6$ was prepared in DMSO and a 10µM $DiOC_6$ aliquot added to the conidial suspension.

***tpmA :eGFP* fusion plasmid construction**

The 2.8 kb modified *M. oryzae ILV1* allele, conferring resistance to sulfonylurea, was amplified, with primers 5SU and 3SU, from pCB1532 (Sweigard et al., 1997;). Sequences of all primers are shown in Supplemental Table 3 online. The resulting 2.8 kb amplicon was introduced into the *tpmA:eGFP* gene fusion vector pCP32 (Pearson et al., 2004), kindly provided by Dr Steven Harris (University of Nebraska, Lincoln, NE, USA) and introduced into a *H1:eRFP*-expressing Guy-11 strain of *M. oryzae* (Saunders et al., in press). The *tpmA:eGFP* vector was also introduced into *ΔcpkA, Δmst12 and Δpmk1* mutants of *M. oryzae*, all in the same isogenic strain background, Guy-11. All transformants were assessed by DNA gel blot analysis and observations confirmed with at least two independent transformants.

Generation of *Sep4:eGFP* and *Sep5:eGFP* gene fusions

The *SEP4* and *SEP5* genes were identified from the *M. oryzae* genome sequence database and amplified from genomic DNA of strain Guy11 with primers SEP4-F/SEP4-R and SEP5-F/SEP5-R (See Supplemental Table 3 online) and transformed with *HindIII*-digested pYSGFP-1 into *S. cerevisiae*. Gene fusions were constructed by yeast gap repair cloning, based on homologous recombination in yeast (Oldenburg et al., 1997). Resulting plasmids were introduced in *M.oryzae* strain Guy11 expressing H1:eRFP, and assessed by DNA gel blot analysis. All experimental observations were confirmed with at least two independent transformants.

***SEP1* genomic cloning, plasmid construction and complementation**

A 7.2 kb gene fragment spanning the *SEP1* locus was amplified from genomic DNA with primers 5SepH-ts1-KpnI and 3SepH-KpnI. The *SEP1* fragment was ligated into

the *Kpn* I site of pCB1004 (Carroll et al., 1994) and the resulting vector, pDS100, used to transform the *A. nidulans sepH1* mutant (Bruno et al., 2001).

Five putative *A. nidulans sepH1* transformants were selected and assessed for insertion of a single copy of *SEP1* by DNA gel blot. Each transformant was then analysed for restoration of septation at 42ºC. Septa were visualised with 0.4 μg mL^{-1} Calcofluor solution as previously described (Veneault-Fourrey et al., 2006).

The *Mosep1*^{G849R} gene replacement vector

In order to generate the *Mosep1*^{G849R} gene replacement vector, a genomic clone spanning *SEP1* (pDS100) was amplified, using primers 5SepH-ts1-KpnI and 3SepH-ts1-NotI. The *ILV1* selectable marker was amplified, with primers 5SU-ts-NotI and 3SU-ts-NotI, and inserted downstream of the 3'UTR of *SEP1*. A 2.6 kb fragment of *SEP1* was amplified from a unique *Nde* I site within *SEP1* to the end of the *SEP1* 0.5 kb 3'UTR fragment, with primers 5SepH-ts2-NotI and 3SepH-ts2-XbaI. The resulting 2.6 kb amplicon was gel-purified and ligated to pGEM-T (Promega). The 2.6 kb fragment was subject to site-directed mutagenesis (Invitrogen), with primers 5SepH-ts3-NdeI and 3SepH-ts1-NotI, to introduce two single base substitutions; nucleotide 3175 was changed from guanine to cytosine in order to bring about a glycine to arginine substitution and a second silent mutation at nucleotide 3177 substituted thymine with adenine to generate a unique *Sal* I site to enable rapid screening of the resulting mutation. The mutagenesis procedure was carried out according to the manufacturer's protocol (Invitrogen). Positive clones were identified by digestion with *Sal* I and the G849R mutation confirmed by DNA sequence analysis.

A 2.0 kb region adjacent and downstream of *SEP1* was introduced into pCR®2.1-TOPO containing the 7.2 kb *sep1*^{G849R} gene replacement fragment. The 2.6 kb *sep1*^{G849R} region was excised from pGEM-T and ligated into pCR®2.1-TOPO containing

the 7.2 kb *SEP1* gene replacement fragment and the 2.0 kb region adjacent and downstream of *SEP1*, to create pDS101. The 2.8 kb modified *ILV1* cassette was introduced into pDS101 and the resulting vector, pDS102, digested with *Kpn* I and *Xba* I, gel-purified and introduced into Guy-11. Potential $sep1^{G849R}$ transformants were selected by DNA gel blot and sequence analysis. Two transformants were selected and transformed with the *grg(p):H1:eRFP* gene fusion to allow visualisation of nuclei.

Regulated expression of the *M. oryzae SEP1* gene

A 1.5 kb *ICL1* promoter fragment, *ICL1(p)*, which drives expression of the isocitrate lyase-encoding gene, was amplified, with primers 5ICL1P-NotI and 3ICL1P-SepH, from a *ICL1(p):sGFP* fusion construct (Wang et al., 2003). A 5.7 kb gene fragment including the 5.2 kb ORF of *M. oryzae SEP1* and 0.5 kb of 3'UTR was amplified from genomic DNA, with primers 5SepH-ICL1P and 3SepH-NotI. The 1.5 kb *ICL1(p)* and 5.7 kb *SEP1* amplicons were joined by fusion PCR. The 7.2 kb *ICL1(p):SEP1* region was ligated to pCB1532 (Sweigard et al., 1997) and subsequently used for fungal transformation of *M. oryzae* H1:eRFP (tdTomato). In *M. oryzae* strains expressing *SEP1* under the control of the *ICL1* promoter, hyphal growth and appressorium development were assessed in the presence or absence of 50 mM sodium acetate.

Accession Numbers

Sequence data from this article can be found in the Genbank/EMBL databases under the following accession numbers: *M. oryzae SEP1* (MGG04100), *M. oryzae SEP4* (MGG06726), *M. oryzae SEP5* (MGG03087), *M. oryzae ILV1* AF013601, *S. cerevisiae CDC10* (YCR002C), *S. cerevisiae CDC11* (YJR076C), *A. nidulans SepH* (XM360771).

Supplemental Data

The following materials are available in the online version of this article.

Supplemental Figure 1. Live cell imaging of nuclear dynamics and actomyosin ring formation in the *M. oryzae* strains Guy-11 and *ΔcpkA*.

Supplemental Figure 2. Live cell imaging of nuclear dynamics and actomyosin ring formation in the *M. oryzae* strains *Δpmk1* and *Δmst12*.

Supplemental Figure 3. Alignment of the predicted *M. oryzae* Sep4 and Sep5 amino acid sequences with Cdc10 and Cdc11 from *S. cerevisiae*.

Supplemental Figure 4. Alignment of the predicted *M. oryzae* Sep1 amino acid sequence with *A. nidulans* SepH.

Supplemental Figure 5. A temperature-sensitive mutation in *M. oryzae SEP1* increases septation frequency during appressorium formation.

Supplemental Figure 6. The $sep1^{G849R}$ allele increases the frequency of septation during appressorium development even in the presence of a wild type copy of *SEP1*.

Supplemental Figure 7. The $sep1^{G849R}$ allele reduces hyphal growth but has no effect on appressorium development even in the presence of a wild type copy of *SEP1*.

Supplemental Figure 8. A temperature-sensitive mutation in *M. oryzae SEP1* alleviates the cell cycle arrest phenotype of non-germinating conidial cells during appressorium development.

Supplemental Figure 9. Inducible over-expression of *M. oryzae SEP1* alleviates the cell cycle arrest phenotype of non-germinating conidial cells during appressorium development.

Supplemental Figure 10. Inducible over-expression of *M. oryzae SEP1* has no effect on septation frequency during appressorium development**.**

Supplemental Table 1. *Magnaporthe oryzae* strains used in this study

Supplemental Table 2. *Magnaporthe oryzae* strains generated in this study

Supplemental Table 3. Detailed information of the primers used in this study

Supplemental Movie 1. Live cell imaging of closed mitosis during appressorium development in *M. oryzae*.

Supplemental Movie 2. Live cell imaging of actomyosin ring formation during the asymmetric cellular division associated with appressorium development in *M. oryzae*.

Acknowledgements

This work was supported by a grant to N.J.T. from the Biotechnology and Biological Sciences Research Council, a graduate fellowship to D.G.O.S. from the University of Exeter, and a Halpin Studentship in Rice Blast Research to Y.F.D. We acknowledge Steve Harris (University of Nebraska, Lincoln, NE) for providing tpmA:eGFP, *Aspergillus* mutants, and for valuable discussions, Gero Steinberg (University of Exeter, UK) for help with figures and movie preparation, and Richard Wilson (University of Nebraska, Lincoln, NE) for helpful discussions.

Figures

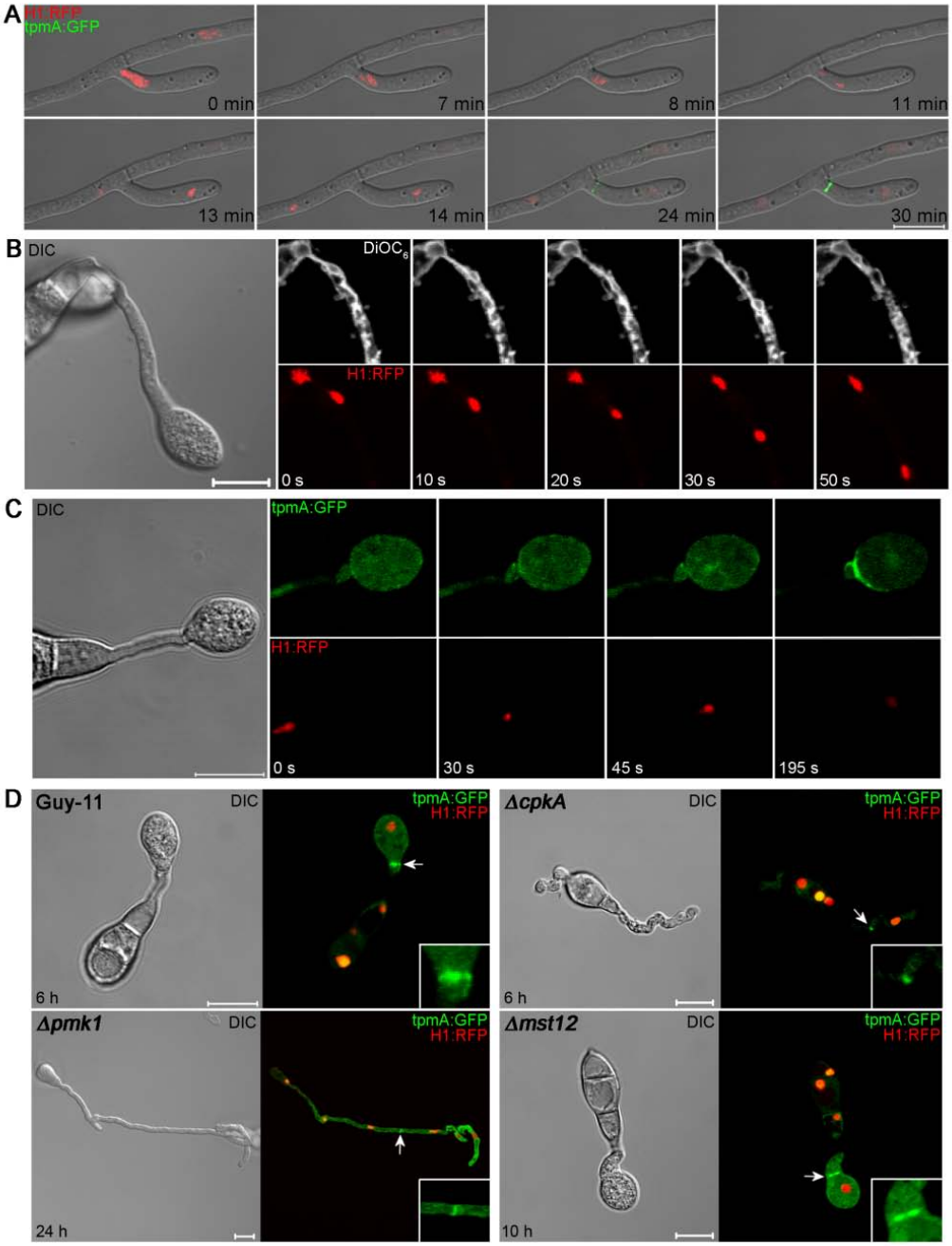
A
H1:RFP
tpmA:GFP
0 min
7 min
8 min
11 min
13 min
14 min
24 min
30 min
B
DIC
DiOC6
H1:RFP
0 s
10 s
20 s
30 s
50 s
C
DIC
tpmA:GFP
H1:RFP
0 s
30 s
45 s
195 s
D
Guy-11
DIC
tpmA:GFP
H1:RFP
6 h
ΔcpkA
DIC
tpmA:GFP
H1:RFP
6 h
Δpmk1
DIC
tpmA:GFP
H1:RFP
24 h
Δmst12
DIC
tpmA:GFP
H1:RFP
10 h

Figure 1. Spatial uncoupling of mitosis and cytokinesis during infection-related development in the rice blast fungus *M. oryzae*.

A. Laser confocal micrographs of a time series to show actomyosin ring formation in *M. oryzae* expressing tpmA:GFP and Histone H1:RFP during vegetative hyphal growth. The site of septation in a hyphal branch occurs at the medial position of the preceding nuclear division. **B**. Time series of micrographs showing mitosis occurring during appressorium development by *M. oryzae*. Conidial suspensions of the *M. oryzae* H1:RFP strain were prepared and the lipophilic stain 3,3'-dihexyloxacarbocyanine iodide ($DiOC_6$) used to stain the nuclear envelope. A differential interference contrast (DIC) image of the whole germ tube and developing appressorium is shown in the left panel. **C.** Time series to show actomyosin contractile ring formation during differentiation of the appressorium in *M. oryzae* tpmA:GFP-Histone H1:RFP strain. Left panel shows DIC image of the nascent appressorium. Right panels show TpmA:GFP and H1:RFP signals, respectively. **D.** Micrographs of *M. oryzae* strain Guy-11, Δ*cpkA*, Δ*pmk1* and Δ*mst12* mutants expressing H1:RFP and tpmA:GFP gene fusions, incubated on coverslips to allow appressorium development. Septation was spatially separated from the site of nuclear division only in Guy11 and the *Δmst12* strains, which are competent in appressorium formation. All images were recorded using a Zeiss LSM510 Meta laser confocal-light scanning microscope system. min, minutes; h, hours; Scale bars represent 10 μm.

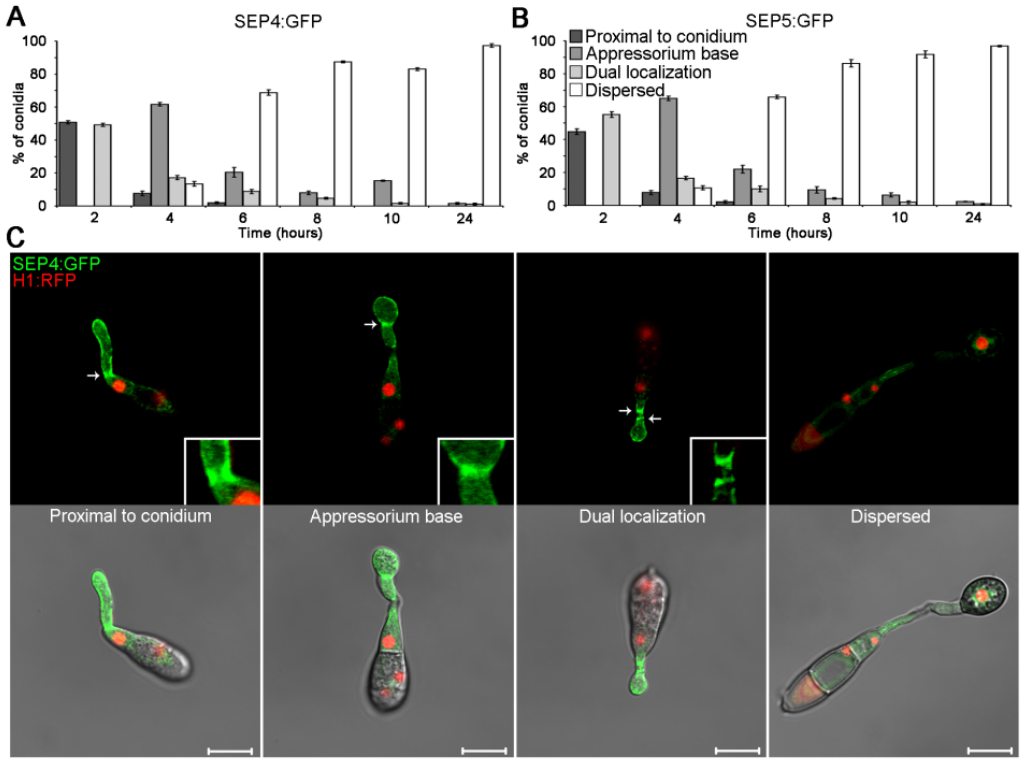
A
SEP4:GFP
% of conidia
Time (hours)
B
SEP5:GFP
Proximal to conidium
Appressorium base
Dual localization
Dispersed
C
SEP4:GFP
H1:RFP
Proximal to conidium
Appressorium base
Dual localization
Dispersed

Figure 2. Septin ring formation occurs prior to mitosis during appressorium development by *M. oryzae*

Nuclear division and septin ring formation were visualized in *M. oryzae* by constructing *SEP4:GFP* and *SEP5:GFP* gene fusions and expressing these in a *H1:RFP* expressing strain of Guy11. **(A, B)** Bar charts to show the frequency of septin complex formation by SEP4:GFP **(A)** or SEP5:GFP **(B)** during a time course of appressorium development. Values represent the mean and the error bars represent 1 standard error. **(C)** Laser confocal microscopy to show septin ring formation at the base of the germ tube proximal to the conidium, at the base of incipient appressoria, dual localization to both of these positions, and the dispersal of septin complexes during appressorium maturation. Arrows indicate the positions of septin ring structures. All images were recorded using a Zeiss LSM510. Scale bars for all panels represent 10□m.

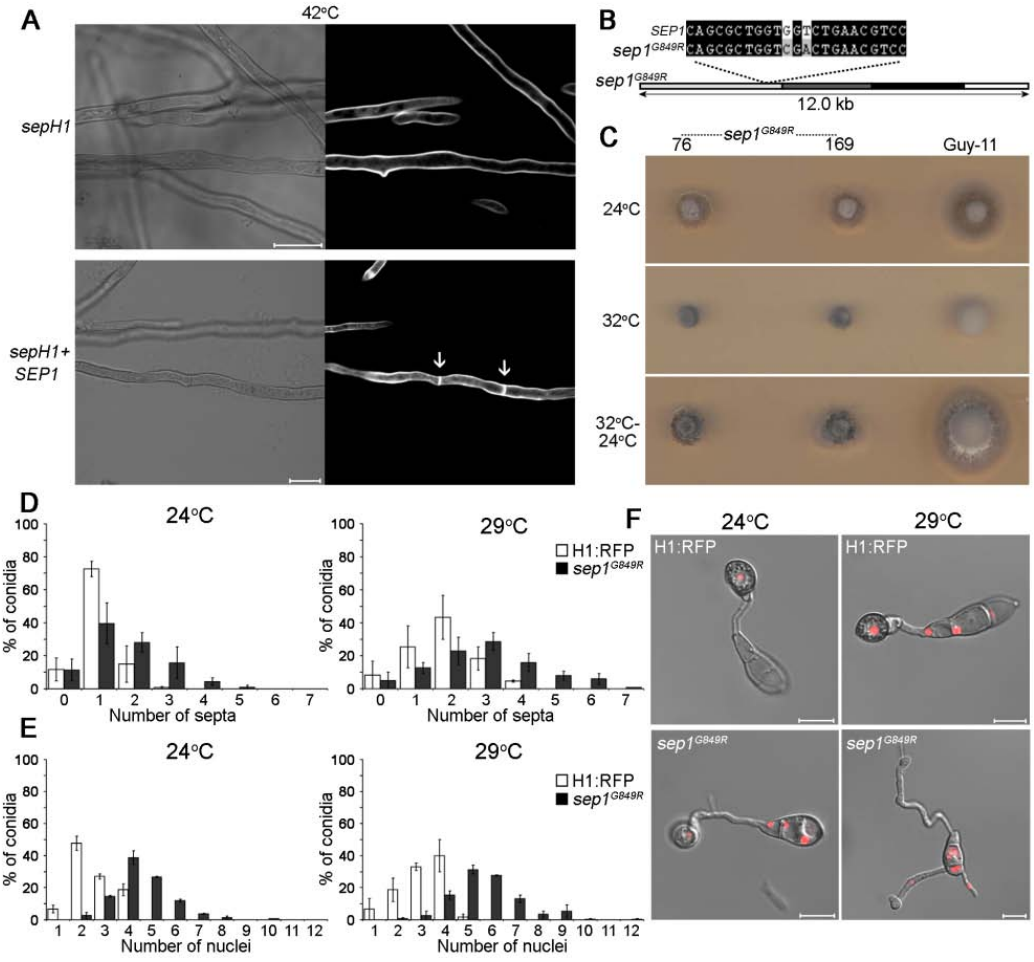
A
42°C
sepH1
sepH1+
SEP1
B
SEP1 CAGCGCTGGTGGTCTGAACGTCC
sep1G849R CAGCGCTGGTCGACTGAACGTCC
sep1G849R
12.0 kb
C
76
sep1G849R
169
Guy-11
24°C
32°C
32°C-
24°C
D
24°C
29°C
H1:RFP
sep1G849R
% of conidia
Number of septa
E
24°C
29°C
H1:RFP
sep1G849R
% of conidia
Number of nuclei
F
24°C
29°C
H1:RFP
H1:RFP
sep1G849R
sep1G849R

Figure 3. *SEP1* is a spatial regulator of cytokinesis in *M. oryzae*

A. *M. oryzae SEP1* is a functional homologue of the *A. nidulans sepH* septation gene. The *M. oryzae SEP1* gene was expressed in a *A. nidulans sepH1* thermo-sensitive mutant under the native SepH promoter and restored its ability to form septa at 42ºC, as shown by calcofluor white staining (right panels, light micrographs are on the left). **B.** Schematic representation of the $sep1^{G849R}$ allele, which was introduced into *M. oryzae* Guy-11 by homologous recombination. **C.** Thermo-sensitivity of the $sep1^{G849R}$ mutant of *M. oryzae*. Plugs of mycelium (5 mm diameter) from putative $sep1^{G849R}$ transformants, and Guy-11, were incubated at 24ºC or 32ºC for 4 days. Restoration of hyphal growth was assessed by incubation for a further 3 days at 24ºC. **D.** Quantitative analysis of infection-associated septation in $sep1^{G849R}$ mutants. The *grg(p):H1:eRFP* vector was introduced into the *M. oryzae* $sep1^{G849R}$ strain. Conidial suspensions were then prepared from the *M. oryzae* H1:RFP and $sep1^{G849R}$ strains and allowed to form appressoria at 24ºC or 29ºC. After 10 hours the number of septa was recorded following calcofluor white staining. **E.** Quantitative analysis of nuclear number in $sep1^{G849R}$. Conidial suspensions were allowed to form appressoria at 24ºC or 29ºC and nuclear number was recorded after 10 hours. **F.** Representative images of nuclear distribution during appressorium morphogenesis of $sep1^{G849R}$. Bars = 10 μm; error bars are 1 standard error.

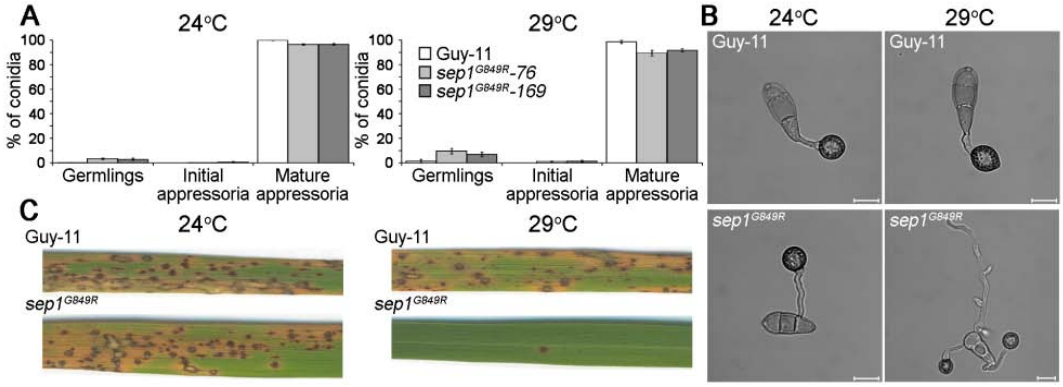
A
24°C
29°C
% of conidia
100
80
60
40
20
0
Germlings
Initial appressoria
Mature appressoria
Guy-11
sep1G849R-76
sep1G849R-169
B
24°C
29°C
Guy-11
Guy-11
sep1G849R
sep1G849R
C
24°C
29°C
Guy-11
Guy-11
sep1G849R
sep1G849R

Figure 4. *SEP1* is required for appressorium-mediated plant infection by *M. oryzae*.

(A) Bar charts to show the frequency of appressorium development in *M. oryzae* *sep1*^{G849R} temperature-sensitive mutants. Error bars are 1 standard error. **(B)** Conidial suspensions of two independent *M. oryzae* *sep1*^{G849R} transformants were incubated in conditions to allow appressorium development which was recorded after 24 hours. Bar = 10 μm. **(C)** *M. oryzae* *sep1*^{G849R} mutants were unable to cause rice blast disease. Leaves from the dwarf Indica rice (*Oryza sativa*) cultivar, CO-39 following inoculation with 5 x 10^4 spores mL^{-1} of a *sep1*^{G849R} mutant and Guy 11. Following inoculation, rice plants were incubated initially for 24 hours at either the permissive temperature of 24°C, or a semi-restrictive temperature of 29ºC. All plants were then transferred to 24°C and leaves harvested 5 days later.

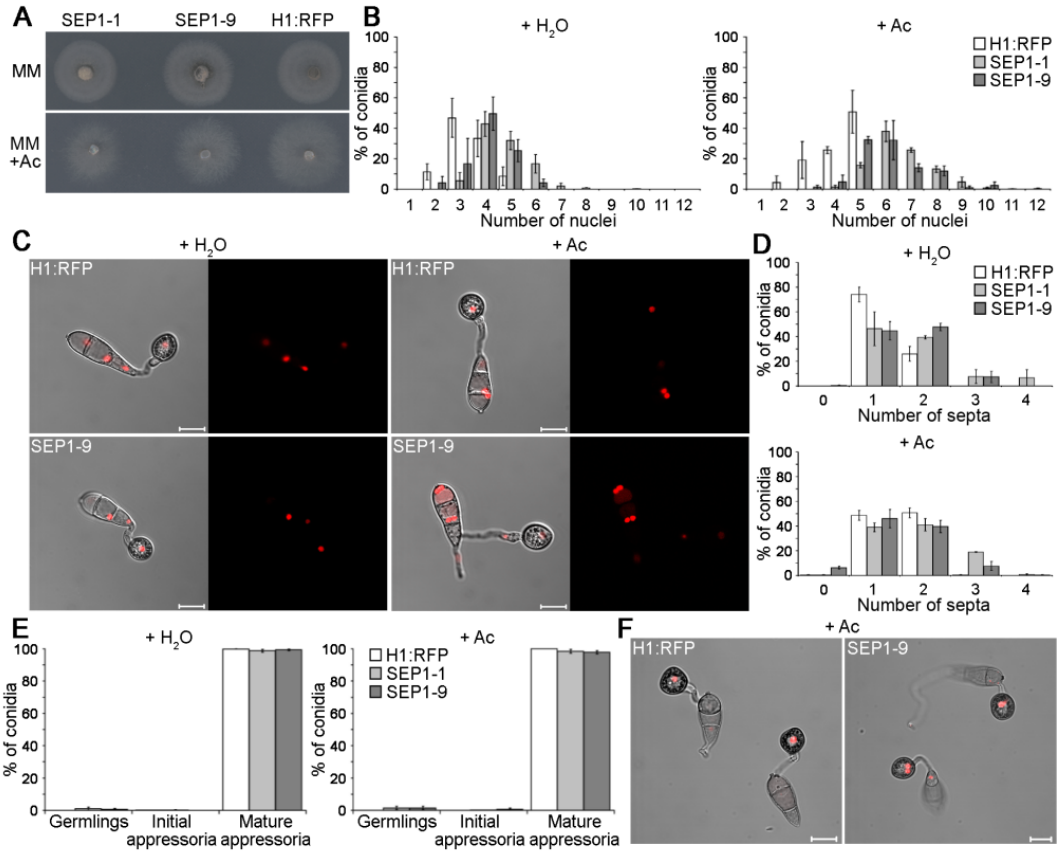
A
SEP1-1
SEP1-9
H1:RFP
MM
MM +Ac
B
+ H2O
+ Ac
% of conidia
Number of nuclei
H1:RFP
SEP1-1
SEP1-9
C
+ H2O
+ Ac
H1:RFP
SEP1-9
D
+ H2O
+ Ac
% of conidia
Number of septa
H1:RFP
SEP1-1
SEP1-9
E
+ H2O
+ Ac
% of conidia
Germlings
Initial appressoria
Mature appressoria
H1:RFP
SEP1-1
SEP1-9
F
+ Ac
H1:RFP
SEP1-9

Figure 5. Inducible over-expression of *SEP1* in *M. oryzae* leads to aberrant nuclear division.

SEP1 was placed under control of the isocitrate lyase gene promoter sequence to enable induction of gene expression by acetate. Two transformants were isolated, one containing multiple insertions of the *ICL1(p):SEP1* construct, SEP1-1, and one containing a single insertion of the transgene, SEP1-9. (**A)** Vegetative growth of SEP1-1 and SEP1-9 transformants. Plugs of mycelium (5 mm diameter) from the SEP1-1 and SEP1-9 strains and the isogenic H1:RFP strain were used to inoculate minimal medium (MM) with or without 50 mM sodium acetate. Hyphal growth was assessed 4 days later. (**B)** Quantitative analysis of nuclear number in H1:RFP, SEP1-1 and SEP1-9. Conidial suspensions were prepared and incubated to allow appressorium development in the presence or absence of acetate. Nuclear number was recorded 10 hours later. **(C)** Representative images to show nuclear distribution during appressorium morphogenesis. **(D)** Quantitative analysis of septum formation during appressorium morphogenesis. Conidial suspensions were stained with calcofluor white after 10 hours and the number of septa recorded. **(E)** Bar charts to show the frequency of appressorium development in the presence or absence of acetate. Appressorium development was recorded 24 hours pi. **(F)** Representative images of appressorium formation. Ac; sodium acetate; scale bars =10 μm; error bars are 1 standard error.

Magnaporthe oryzae

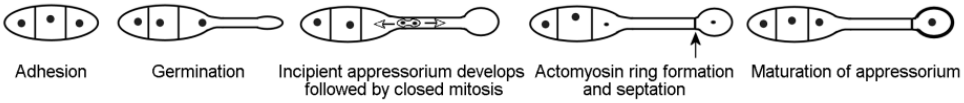

Aspergillus nidulans

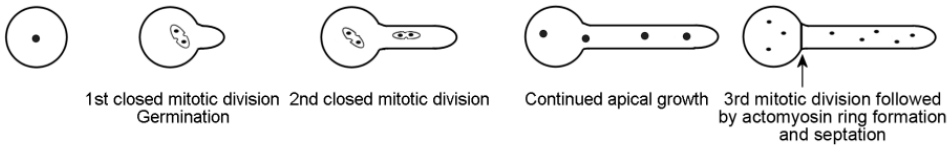

Saccharomyces cerevisiae

Schizosaccharomyces pombe

Figure 6. Spatial uncoupling of mitosis and cytokinesis is associated with appressorium formation in the rice blast fungus *M. oryzae*.

Schematic diagram to show the position and organisation of septum formation in *M. oryzae* during appressorium development. The site of septation is spatially separated from the previous nuclear division. This contrasts with common patterns of septation in fungi, in which nuclear division is associated with the subsequent site of cytokinesis and septation. This occurs during spore germination in *A. nidulans*, budding of *S. cerevisiae* and fission of *S. pombe*. Closed arrows indicate position of actomyosin ring formation; open arrows indicate direction of nuclear movement; nuclei are represented by closed circles.

Supplemental Movie 1. Live cell imaging of closed mitosis during appressorium development in *M. oryzae*.

Movie of nuclear division occurring during appressorium development. A conidial suspension was prepared from the *M. oryzae* H1:eRFP strain and incubated in conditions to allow appressorium development. A 10 μM aliquot of 3,3'-dihexyloxacarbocyanine iodide ($DiOC_6$) was added 4-6 hours post-inoculation and images acquired at 10 second intervals with sequential excitation at the two wavelengths.

Supplemental Movie 2. Live cell imaging of actomyosin ring formation during the asymmetric cellular division associated with appressorium development in *M. oryzae*.

Movie to show position and formation of the actomyosin contractile ring and septum during appressorium development. A conidial suspension was prepared from the *M. oryzae* tpmA:GFP strain and the suspension was incubated to allow appressorium development. Actomyosin ring formation was observed 4-6 hours post-inoculation and images were acquired at 15 second intervals.

Supplemental Figures

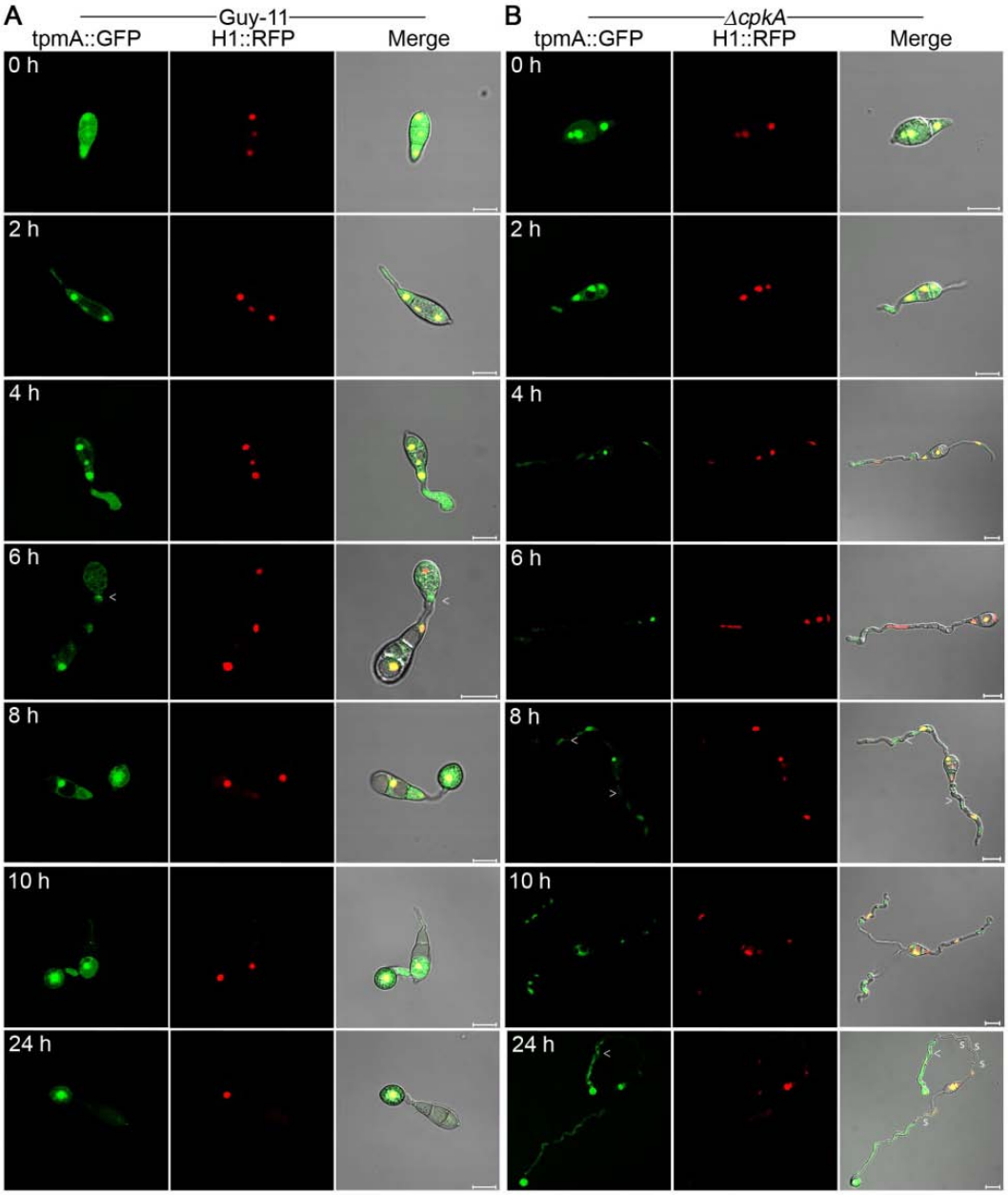

Supplemental Figure 1. Live cell imaging of nuclear dynamics and actomyosin ring formation in the *M. oryzae* strains Guy-11 and *ΔcpkA*.

Time series of micrographs to show nuclear division and cytokinesis during appressorium formation. Conidial suspensions were prepared from the *M. oryzae* Guy-11 (**A**) and a *ΔcpkA* mutant (**B**), expressing *H1:eRFP* and *tpmA:sGFP*. The suspensions were incubated in conditions to allow appressorium formation and representative images recorded at seven time points during germination and appressorium formation. Septa are highlighted by arrowheads. Scale bars represent 10 μm.

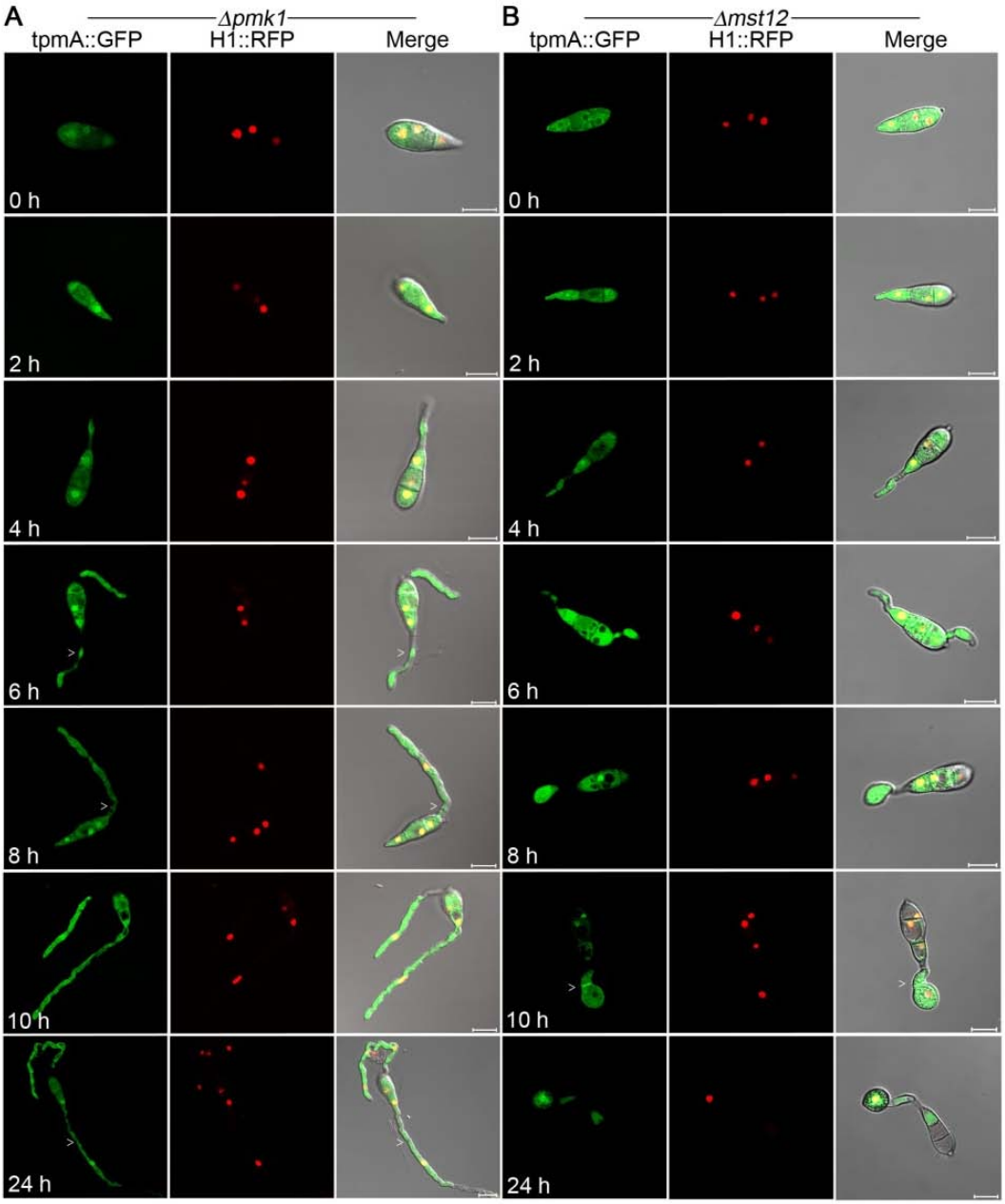
A
Δpmk1
tpmA::GFP
H1::RFP
Merge
B
Δmst12
tpmA::GFP
H1::RFP
Merge
0 h
2 h
4 h
6 h
8 h
10 h
24 h

Supplemental Figure 2. Live cell imaging of nuclear dynamics and actomyosin ring formation in the *M. oryzae* strains *Δpmk1* and *Δmst12*.

Time series of micrographs to show nuclear division and cytokinesis during appressorium formation. Conidial suspensions were prepared from the *M. oryzae Δpmk1* (**A**) and *Δmst12* (**B**) mutants, expressing *H1:eRFP* and *tpmA:sGFP*. The suspensions were incubated to allow appressorium formation and representative images recorded at seven time points during germination and appressorium formation. Septa are highlighted with arrowheads. Scale bars represent 10 μm.

A

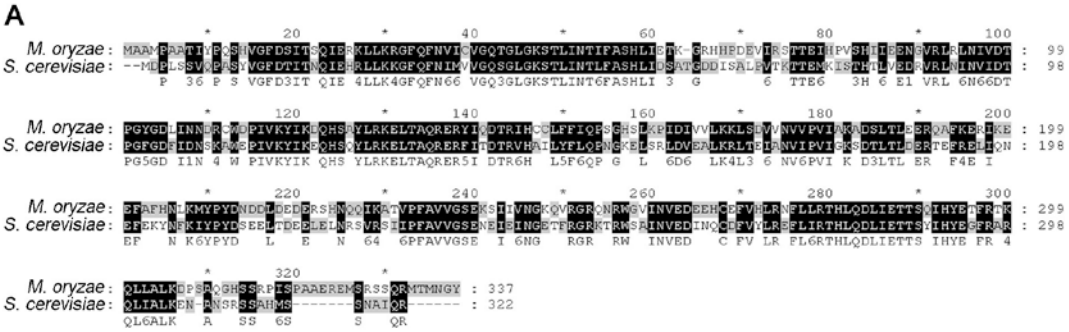

B

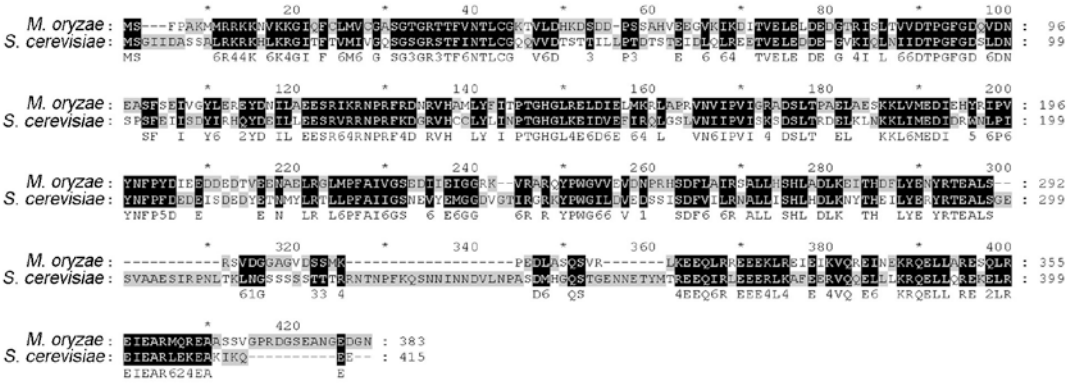

Supplemental Figure 3. Alignment of the predicted *M. oryzae* Sep4 and Sep5 amino acid sequences with Cdc10 and Cdc11 from *S. cerevisiae*.

The alignment was generated using ClustalW and shaded using Boxshade v 2.01. Numbers on the right indicate amino acid residue positions. Residues within a black background, dark grey background and light grey background represent 100%, 80% and 60% amino acid conservation.

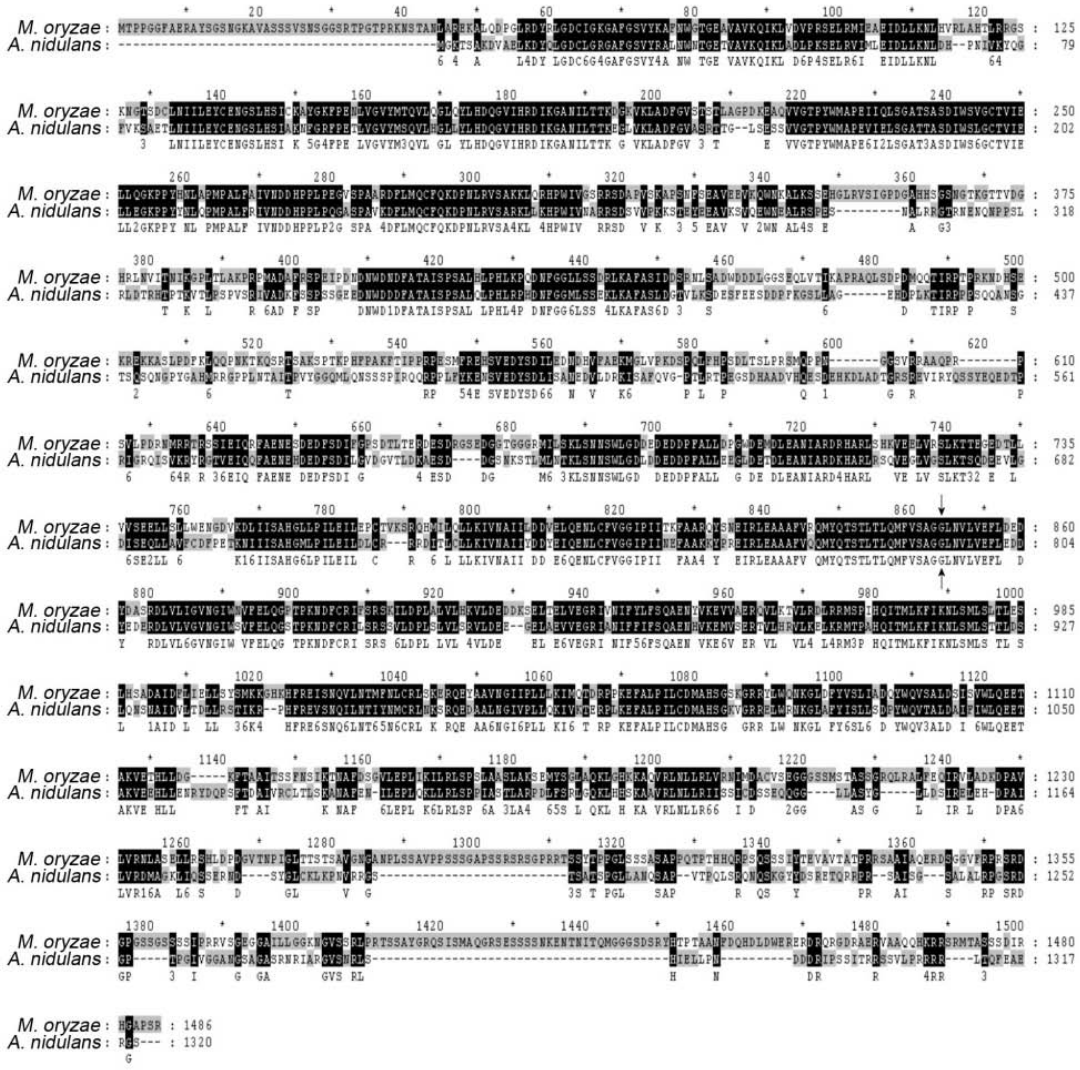
M. oryzae
A. nidulans

Supplemental Figure 4. Alignment of the predicted *M. oryzae* Sep1 amino acid sequence with *A. nidulans* SepH.

The alignment was generated using ClustalW and shaded using Boxshade v 2.01. Numbers on the right indicate amino acid residue positions. Residues within a black background, dark grey background and light grey background represent 100%, 80% and 60% amino acid conservation. Arrow indicates position of nucleotide substitution.

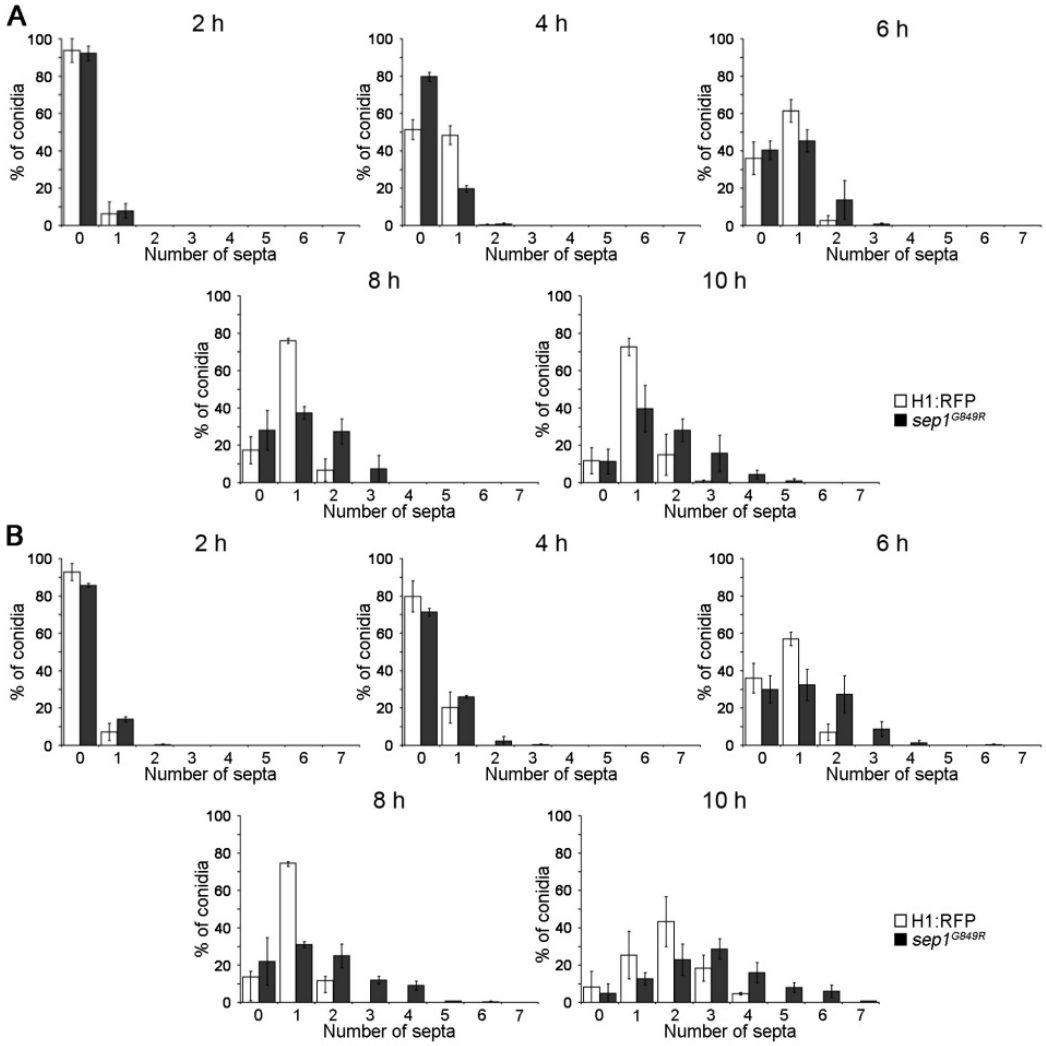
A
2 h
4 h
6 h
8 h
10 h
% of conidia
Number of septa
H1:RFP
sep1GB49R
B
2 h
4 h
6 h
8 h
10 h
% of conidia
Number of septa
H1:RFP
sep1GB49R

Supplemental Figure 5. A temperature-sensitive mutation in *M. oryzae SEP1* increases septation frequency during appressorium formation.

Quantitative analysis of septum formation during appressorium formation in *sep1*^{G849R}. Conidial suspensions were prepared from the *M. oryzae sep1*^{G849R} and *H1:eRFP* strains and incubated in conditions to allow appressorium development at a permissive temperature of 24ºC (**A**) or after an initial incubation for 1 hour at 24ºC germinating conidia were transferred to the semi-restrictive temperature of 29ºC (**B**). The number of septa within the germ tube was determined by calcofluor white staining and epifluorescence microscopy. Error bars are 1 standard error.

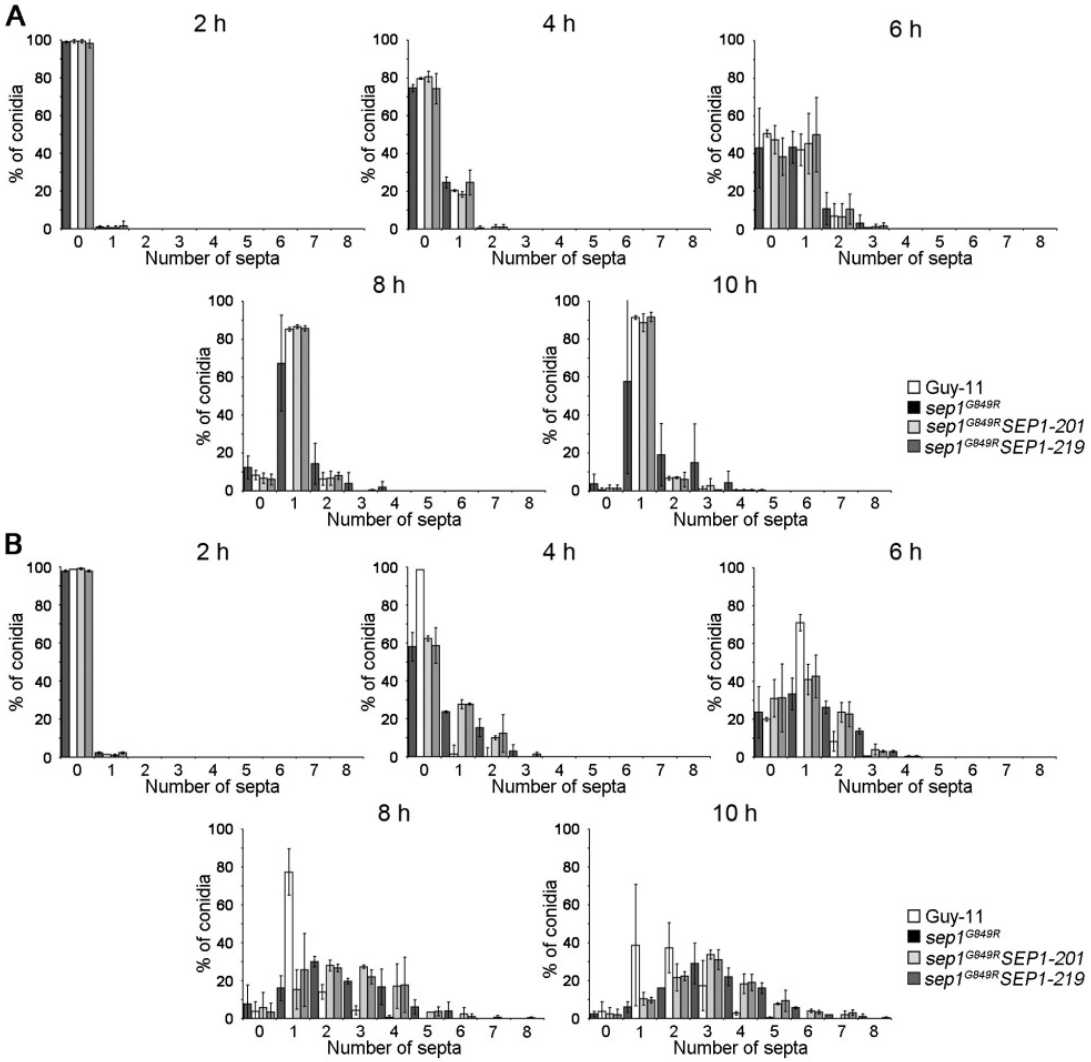
A
2 h
4 h
6 h
8 h
10 h
% of conidia
Number of septa
Guy-11
sep1G849R
sep1G849RSEP1-201
sep1G849RSEP1-219
B
2 h
4 h
6 h
8 h
10 h
% of conidia
Number of septa
Guy-11
sep1G849R
sep1G849RSEP1-201
sep1G849RSEP1-219

Supplemental Figure 6. The *sep1*^{G849R} allele increases the frequency of septation during appressorium development even in the presence of a wild type copy of *SEP1*.

Bar charts to show number of septa present during appressorium development of *M. oryzae*. Conidial suspensions were prepared from two transformants carrying both a wild type copy of *SEP1* and the temperature-sensitive *sep1*^{G849R} allele -strains *sep1*^{G849R} *SEP1*-201, *sep1*$^{;G849R}$*SEP1*-219, as well as a *sep1*^{G849R} mutant and the wild type H1:eRFP strain of Guy11. Each *M. oryzae* strain was incubated on hydrophobic borosilicate glass surfaces inductive for appressorium development. The conidial suspensions were incubated at a permissive temperature of 24ºC (**A**) or after an initial incubation for 1 hour at 24ºC germinating conidia were transferred to the semi-restrictive temperature of 29ºC (**B**). The number of septa within the germ tube was determined through calcofluor white staining and epifluorescence microscopy. Error bars are 1 standard error.

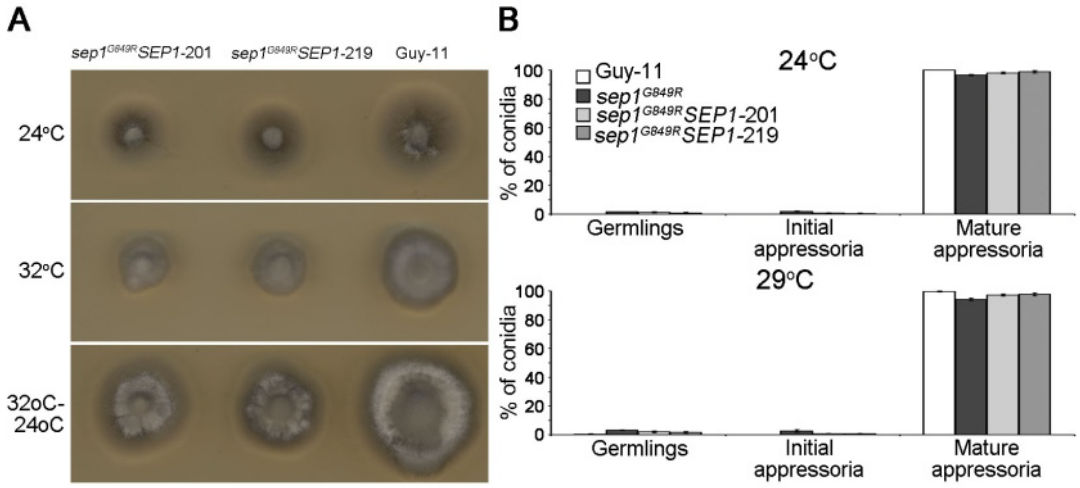
A
sep1G849RSEP1-201
sep1G849RSEP1-219
Guy-11
24ºC
32ºC
32oC-
24oC
B
24ºC
Guy-11
sep1G849R
sep1G849RSEP1-201
sep1G849RSEP1-219
% of conidia
100
80
60
40
20
0
Germlings
Initial appressoria
Mature appressoria
29ºC
% of conidia
100
80
60
40
20
0
Germlings
Initial appressoria
Mature appressoria

Supplemental Figure 7. The *sep1*^{G849R} allele reduces hyphal growth but has no effect on appressorium development even in the presence of a wild type copy of *SEP1*.

A. Plugs of mycelium (5 mm diameter) from *sep1*^{G849R} *SEP1*-201, *sep1*$^{;G849R}$*SEP1*-219, alongside Guy-11, were used to inoculate complete medium agar plates incubated at a permissive temperature of 24ºC or a semi-restrictive temperature of 32ºC for 4 days. Reversion of any hyphal growth defects was then assessed by transferring plates to the permissive temperature, of 24ºC, followed by incubation for a further 3 days. **B.** Bar charts to show frequency of appressorium development. Conidial suspensions of the two independent *M. oryzae sep1*$^{;G849R}$*SEP1* transformants, alongside Guy-11 and *sep1*^{G849R}, were prepared and incubated on hydrophobic borosilicate glass slides inductive for appressorium development at either 24ºC or 29ºC. Appressorium development was recorded 24 hours post-inoculation (pi).

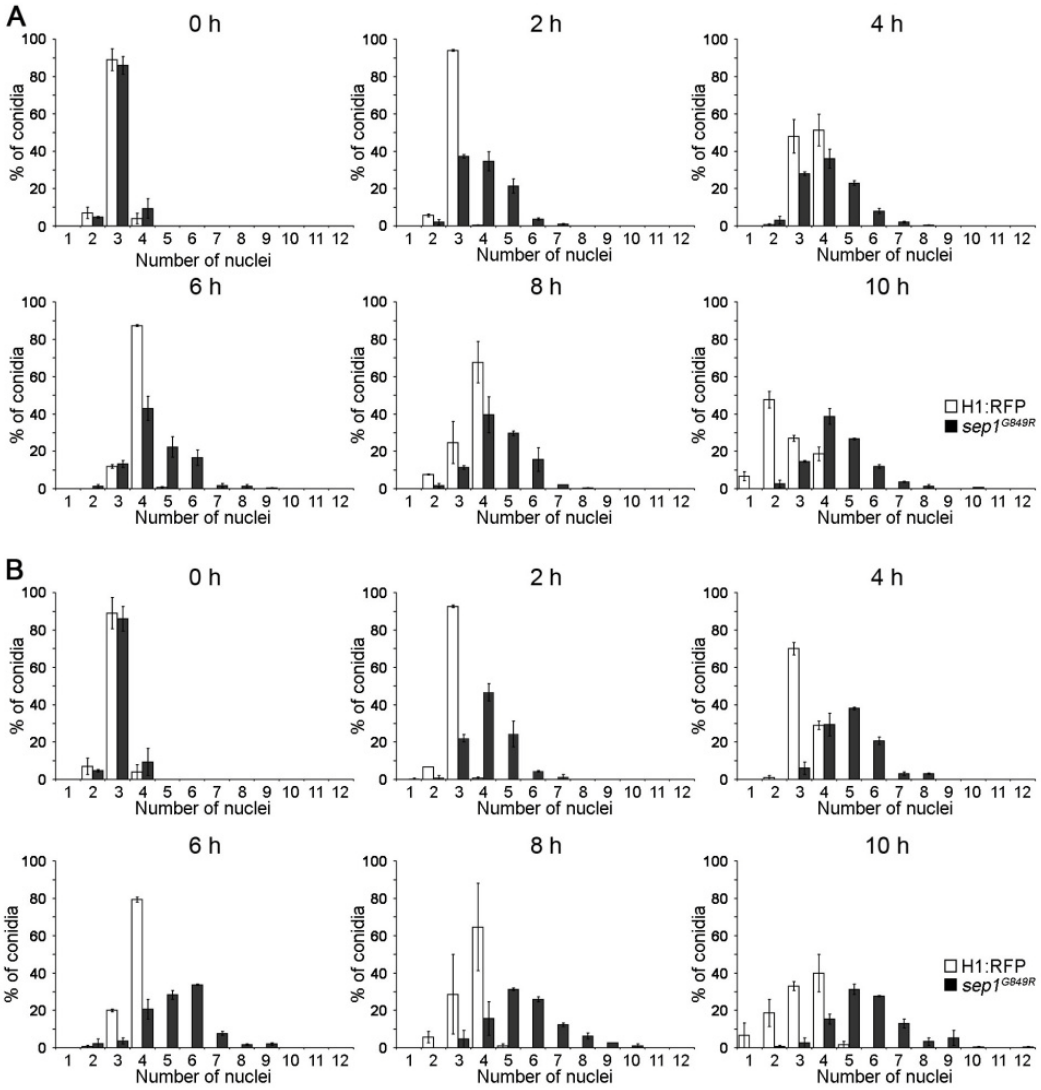
A
0 h
2 h
4 h
6 h
8 h
10 h
% of conidia
Number of nuclei
H1:RFP
sep1G849R
B
0 h
2 h
4 h
6 h
8 h
10 h
% of conidia
Number of nuclei
H1:RFP
sep1G849R

Supplemental Figure 8. A temperature-sensitive mutation in *M. oryzae SEP1* alleviates the cell cycle arrest phenotype of non-germinating conidial cells during appressorium development.

Bar charts to show number of nuclei present during a time course of appressorium development in *sep1*^{G849R} and H1:eRFP. Conidial suspensions were prepared from *sep1*^{G849R} and H1:eRFP strains and incubated to allow appressorium development. The conidial suspensions were incubated at a permissive temperature of 24ºC (**A**) or after an initial incubation for 1 hour at 24ºC germinating conidia were transferred to the semi-restrictive temperature of 29ºC (**B**). The number of nuclei was determined through epifluorescence microscopy. Error bars are 1 standard error.

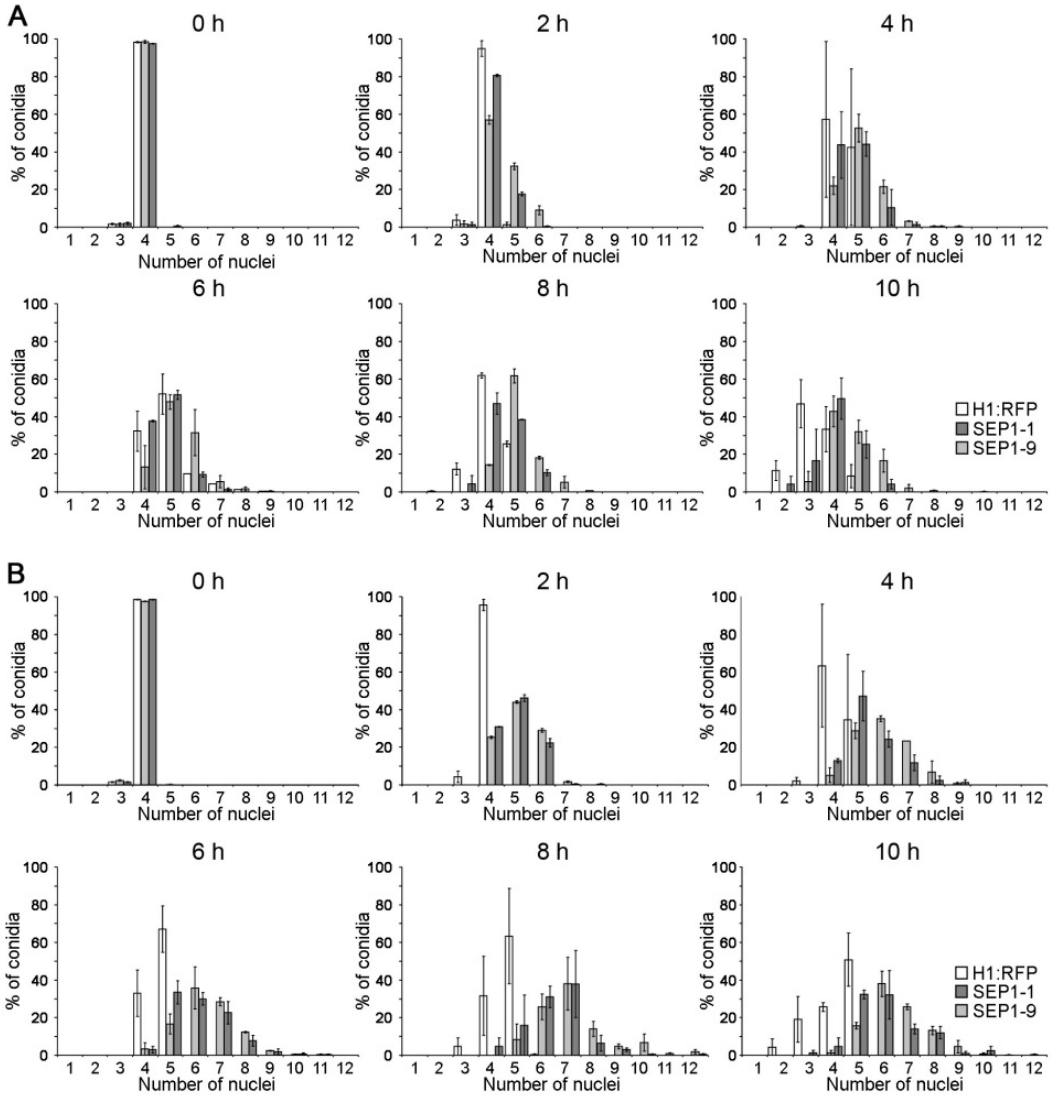
A
0 h
2 h
4 h
6 h
8 h
10 h
% of conidia
Number of nuclei
H1:RFP
SEP1-1
SEP1-9
B
0 h
2 h
4 h
6 h
8 h
10 h
% of conidia
Number of nuclei
H1:RFP
SEP1-1
SEP1-9

Supplemental Figure 9. Inducible over-expression of *M. oryzae SEP1* alleviates the cell cycle arrest phenotype of non-germinating conidial cells during appressorium development.

Bar charts to show the number of nuclei present during a time course of appressorium development in the presence or absence of acetate. Conidial suspensions were prepared from the *M. oryzae* SEP1-1, SEP1-9 and H1:RFP strains and incubated in conditions inductive for appressorium development. The conidial suspensions were incubated in the absence (**A**) or presence (**B**) of sodium acetate and the number of nuclei was determined through epifluorescence microscopy at various time points during germination and appressorium morphogenesis. Error bars are 1 standard error.

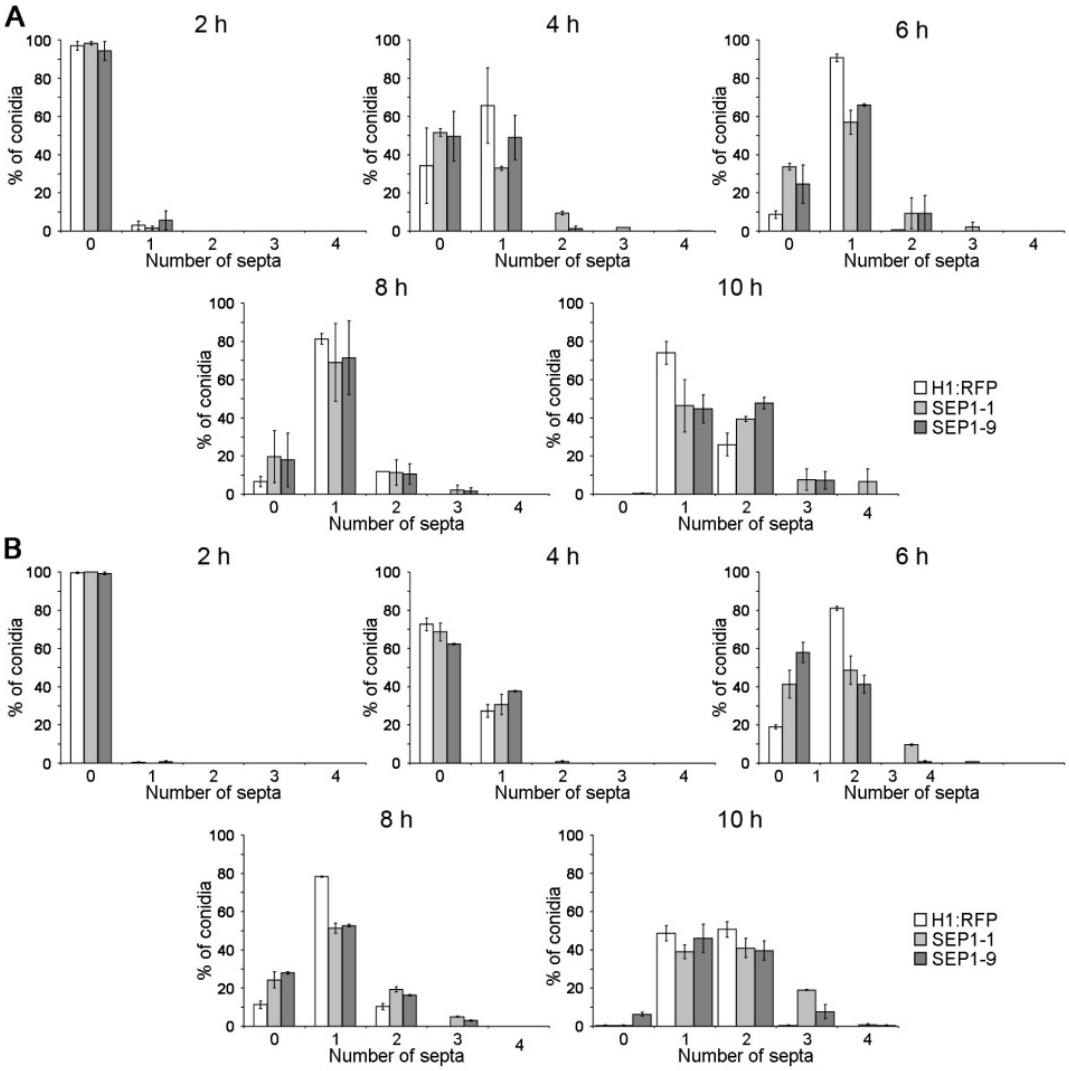
A
2 h
4 h
6 h
8 h
10 h
% of conidia
Number of septa
H1:RFP
SEP1-1
SEP1-9
B
2 h
4 h
6 h
8 h
10 h
% of conidia
Number of septa
H1:RFP
SEP1-1
SEP1-9

Supplemental Figure 10. Inducible over-expression of *M. oryzae SEP1* has no effect on septation frequency during appressorium development**.**

Quantitative analysis of septum formation during a time course of appressorium development. Conidial suspensions were prepared from the *M. oryzae* SEP1-1, SEP1-9 and H1:RFP strains and incubated in conditions inductive for appressorium development in the absence (**A**) or presence (**B**) of sodium acetate. The number of septa that formed in the germ tube was determined through calcofluor white staining and epifluorescence microscopy at various time points during germination and appressorium morphogenesis. Error bars are 1 standard error.

Supplemental Table 1 *Magnaporthe oryzae* strains used in this study.

Strain	Genotype	Reference
H1:eRFP	*grg(p):H1:eRFP*	Saunders et al., 2010
Guy-11		Leung et al., 1988
DF51	*Δcpk A*	Xu et al., 1997
MK23	*Δmst12*	Park et al., 2002
nn95	*Δpmk1*	Xu and Hamer, 1996

Supplemental Table 2 *Magnaporthe oryzae* strains generated in this study.

Strain background	Generated strains	Description
H1:eRFP	*tpmA:eGFP*	H1:RFP strain expressing *tpmA:eGFP* fusion protein; *tpmA* from *Aspergillus nidulans* (strain denoted tpmA:GFP)
H1:eRFP	*SEP4:eGFP*	H1:RFP strain expressing SEP4:eGFP fusion protein (strain denoted SEP4:GFP).
H1:eRFP	*SEP5:eGFP*	H1:RFP strain expressing SEP5:eGFP fusion protein (strain denoted SEP5:GFP).
DF51	*ΔcpkA; H1:RFP; tpmA:eGFP*	*ΔcpkA* strain expressing H1:RFP and tpmA:eGFP fusion proteins; *H1* from *N. crassa* and *tpmA* from *A. nidulans*
MK23	*Δmst12; H1:RFP; tpmA:eGFP*	*Δmst12 s*train expressing H1:RFP and tpmA:eGFP fusion proteins; *H1* from *N. crassa* and *tpmA* from *A. nidulans*
Δpmk1	*Δpmk1; H1:RFP; tpmA:eGFP*	*Δpmk1 s*train expressing H1:RFP and tpmA:eGFP fusion proteins; *H1* from *N. crassa* and *tpmA* from *A. nidulans*
Guy-11	*sep1*^{G849R} +/- *H1:RFP*	Strain expressing the *Mosep1*^{G849R} temperature sensitive allele; the H1:RFP fusion protein was added post-transformation
H1:eRFP	*H1:RFP; ICL1(p): sep1*	H1:RFP strain expressing *SEP1* under acetate inducible expression (strain denoted SEP1)

Supplemental Table 3. Detailed information of the primers used in this study.

Primer name	Primer sequence[1]	Strand	Annealing Temp. (°C)	Template
5SU	5'T CGA CGT GCC AAC GCC ACA G3'	+	62	pCB1532 (Sweigard et al., 1997)
3SU	5'T CGA CGT GAG AGC ATG CAA TTC3'	-	62	pCB1532
SEP4-F	**5'GATTATTGCACGGGAATTGCATGC TCTCACCTAGTTACTGGACTAGCCTA GACG3'**	+	62	Guy-11 genomic DNA
SEP4-R	5'GGTGAACAGCTCCTCGCCCTTGCTCA CCATGTAGCCATTCATAGTCATCCTTTG 3'	-	62	Guy-11 genomic DNA
SEP5-F	5'**GATTATTGCACGGGAATTGCATGC TCTCAC**CGGTCTGCGCACCAGCGTTAC CAG3'	+	62	Guy-11 genomic DNA
SEP5-R	5'GGTGAACAGCTCCTCGCCCTTGCTCA CCATGTTGCCGTCTTCCCCGTTTGCCTC 3'	-	62	Guy-11 genomic DNA
5SepH-ts1-KpnI	5'AAg gta ccA TGA CAC CCC CGG GAG GCT TTG3'	+	65	Guy-11 genomic DNA
3SepH-KpnI	5'AAg gta ccG TGG AGT CGA AAG GAT TGC C3'	-	65	Guy-11 genomic DNA
3SepH-ts1-NotI	5'AAg cgg ccg cGT GGA GTC GAA AGG ATT GCC3'	-	65	Guy-11 genomic DNA
5SU-ts-NotI	5'AAg cgg ccg cGT CGA CGT GCC AAC GCC ACA G3'	+	65	pCB1532
3SU-ts-NotI	5'AAg cgg ccg cGT CGA CGT GAG AGC ATG CAA TTC3'	-	65	pCB1532
5SepH-ts2-NotI	5'AAg cgg ccg cTT TAG CGG GAA ATA	+	65	Guy-11

	GCT CCG3'			genomic DNA
3SepH-ts2-XbaI	5'AAt cta gaC GGA CAT GGA GAG CGT CCA GG3'	-	65	Guy-11 genomic DNA
5SepH-ts3-NdeI	5'AAc ata tgA TCT TGC AGC TGC TC3'	+	65	Guy-11 genomic DNA
5SepH-mutant	5'GTT CGT CAG CGC TGG T**C**G **A**CT GAA CGT CCT TG3'	+	-	Guy-11 genomic DNA
5ICL1P-NotI	5'AAg cgg ccg cGA ATT CGT CCA GTA ATC AAA G3'	+	65	*ICL1(p):sGFP* gene fusion (Wang et al., 2003)
3ICL1P-SepH	5'CAA AGC CTC CCG GGG GTG TCA TCT CGG GAA TAT GGT TCT TAC G3'	-	65	*ICL1(p):sGFP*
5SepH-ICL1P	5'CGT AAG AAC CAT ATT CCC GAG ATG ACA CCC CCG GGA GGC TTT G3'	+	62	Guy-11 genomic DNA
3SepH-NotI	5'AAg cgg ccg cTC CTC ATC TAC CCC AGA ATT C3'	-	62	Guy-11 genomic DNA

[1]Lowercase denotes restriction endonuclease recognition sequences and bold font signifies nucleotide substitutions.

REFERENCES

Bähler, J., and Pringle, J.R. (1998). Pom1p, a fission yeast protein kinase that provides positional information for both polarized growth and cytokinesis. Genes Dev. **12**: 1356-1370.

Bähler, J., Steever, A.B., Wheatley, S., Wang, Y.L., Pringle, J.R., Gould, K.G., McCollum, D. (1998). Role of polo kinase and Mid1p in determining the site of cell division in fission yeast. J. Cell Biol. **143**: 1603-1616.

Bardin, A.J., and Amon, A. (2001). MEN and SIN: What's the difference? Nature Rev. Mol. Cell Biol. **2**: 815-826.

Barral, Y., Mermall, V., Mooseker, M.S., and Snyder, M. (2000). Compartmentalization of the cell cortex by septins is required for maintenance of cell polarity in yeast. Mol. Cell **5**: 841-851.

Bi, E., Maddox, P., Lew, D.J., Salmon, E.D., McMillan, J.N., Yeh, E., and Pringle, J.R. (1998). Involvement of an actomyosin contractile ring in *Saccharomyces cerevisiae* cytokinesis. J. Cell Biol. **142**: 1301-1312.

Bi, E. (2001). Cytokinesis in budding yeast: the relationship between actomyosin ring formation and septum formation. Cell Struct. Funct. **26**: 529-537.

Boyce, K.J., Chang, H., D'Souza, C.A., and Kronstad, J.W. (2005) A Ustilago maydis septin is required for filamentous growth in culture and for full symptom development on maize. Eukaryot. Cell **4:** 2044-2056.

Bruno, K.S., Morrell, J.L., Hamer, J.E., and Staiger, C.J. (2001). SEPH, a Cdc7p orthologue from *Aspergillus nidulans*, functions upstream of actin ring formation during cytokinesis. Mol. Microbiol. **42**: 3-12.

Carroll, A.M., Sweigard, J.A., and Valent, B. (1994). Improved vectors for selecting resistance to hygromycin. Fungal Genet. Newsl. **41**: 22.

Casamayor, A., and Snyder, M. (2002). Bud-site selection and cell polarity in budding yeast. Curr. Opin. Microbiol. **5**: 179-186.

Cenamor, R., Jimenez, J., Cid, V.J., Mobela, C., and Sanchez, M. (1999). The budding yeast Cdc15 localizes to the spindle pole body in a cell-cycle-dependent manner. Molec. Cell Biol. Res. Commun. **2**: 178-184.

Chumley, F.G., and Valent, B. (1990) Genetic analysis of melanin-deficient, nonpathogenic mutants of *Magnaporthe grisea* Molec. Plant Microbe Interact. **3:** 135-143.

Couch, B.C. and Kohn, L.M. (2002). A multilocus gene genealogy concordant with host preference indicates segregation of a new species, *Magnaporthe oryzae*, from *M. grisea*. Mycologia **94**: 683-693.

Dean, R.A. (1997). Signal pathways and appressorium morphogenesis. Annu. Rev. Phytopathol. **35**: 211-234.

de Jong, J.C., McCormack, B.J., Smirnoff, N. and Talbot, N.J. (1997) Glycerol generates turgor in rice blast. Nature **389:** 471 - 483

Douglas,L.M., Alvarez, F.J., McCreary, C., and Konopka, J.B. (2005) Septin function in yeast model systems and pathogenic fungi. Eukaryot. Cell **7:** 1503-1512.

Fankhauser, C., and Simanis, V. (1994). The *cdc7* protein kinase is a dosage dependent regulator of septum formation in fission yeast. The EMBO J. **13**: 3011-3019.

Gladfelter, A.S., Kozubowski, L., Zyla, T.R., and Lew, D.J. (2005) Interplay between septin organization, cell cycle and cell shape in yeast. J. Cell Sci **118:** 1617-1628.

Gladfelter, A.S., Hungerbuehler, A.K., and Phillipsen, P. (2006). Asynchronous nuclear division cycles in multinucleated cells. J. Cell Biol. **172**: 347-362

Gladfelter, A., and Berman, J. (2009). Dancing genomes: fungal nuclear positioning. Nat. Rev. Microbiol. **7**: 875-886

Gonzalez-Novo, A., Labrador, L., Jimenez, A., Sanchez-Perez, M., and Jimenez, J. (2006) Role of septin Cdc10 in the virulence of Candida albicans. Microbiol. Immunol. 50: 499-511.

Hamer, J.E., Howard, R.J., Chumley, F.G., and Valent, B. (1988). A mechanism for surface attachment in spores of a plant pathogenic fungus. Science **239**: 288-290.

Harris, S.D. (2001). Septum formation in *Aspergillus nidulans*. Curr. Opin. Microbiol. **4**: 736-739.

Kaminskyj, S.G.W. (2000). Septum position is marked at the tip of *Aspergillus nidulans* hyphae. *Fungal Genet. Biol.* **31**: 105-113.

Kershaw, M.J., and Talbot, N.J. (2009). Genome-wide functional analysis reveals that infection-assciated fungal autophagy is essential for rice blast disease. Proc. Natl. Acad. Sci. USA **106**: 15967-72

Koning, A.J., Lum, P.Y., Williams, J.M., and Wright, R. (1993). $DiOC_6$ staining reveals organelle structure and dynamics in living yeast cells. Cell Motil. Cytoskeleton **25**: 111-128.

Kozubowski, L. and Heitman, J. (2010) Septins enforce morphogenetic events during sexual reproduction and contribute to virulence of *Cryptococcus neoformans.* Molec. Microbiol. **75:** 658-675.

Leung, H., Borromeo, E.S., Bernardo, M.A., and Notteghem, J.L. (1988). Genetic analysis of virulence in the rice blast fungus *Magnaporthe grisea*. Genetics **78**: 1227-1233.

Lew, D.J. (2003). The morphogenesis checkpoint: how yeast cells watch their figures. Curr. Opin. Cell Biol. **15**: 648-653.

Lindsey, R., Cowden, S., Hernandez-Rodriguez, Y., and Momany, M. (2010). Septins AspA and AspC are important for normal development and limit the emergence of new growth foci in the multicellular fungus *Aspergillus nidulans*. Eukaryot. Cell **9:** 155-163.

Mitchell, T.K., and Dean, R.A. (1995). The cAMP-dependent protein kinase catalytic subunit is required for appressorium formation and pathogenesis by the rice blast pathogen *Magnaporthe grisea*. Plant Cell **7**: 1869-1878.

Oldenburg, K.R., Vo, K.T., Michaelis, S., and Paddon, C. (1997) Recombination-mediated PCR-directed plasmid construction in vivo in yeast. Nucleic Acids Res **25:** 451–452

Oliferenko, S., Chew, T.G., and Balasubramanian, M.K. (2009). Positioning cytokinesis. Genes Dev. **23**: 660-674.

Park, H.O., Bi, E., Pringle, J.R., and Herskowitz, I. (1997). Two active states of the Ras-related Bud1/Rsr1 protein bind to different effectors to determine yeast polarity. Proc. Natl., Acad. Sci USA **94**: 4463-4468.

Park, G., Xue, C., Zheng, L., Lam, S., and Xu, J. (2002). *MST12* regulates infectious growth but not appressorium formation in the rice blast fungus *Magnaporthe grisea*. Mol. Plant Microbe Interact. **15**: 183-192.

Pearson, C.L., Xu, K., Sharpless, K.E., and Harris, S.D. (2004). MesA, a novel fungal protein required for the stabilisation of polarity axes in *Aspergillus nidulans*. Mol. Biol. Cell **15**: 3658-3672.

Saunders, D.G.O., Aves, S.J., and Talbot, N.J. (2010) Cell cycle-mediated regulation of plant infection by the rice blast fungus *Magnaporthe oryzae* The Plant Cell **22:**2417

Schuyler, S.C., and Pellman, D. (2001). Search, capture and signal: games microtubules and centrosomes play. J. Cell Sci. **114**: 247-255.

Straube, A., Weber, I., and Steinberg, G. (2005). A novel mechanism of nuclear envelope break-down in a fungus: nuclear migration strips off the envelope. EMBO J. **24**: 1674-1685.

Sweigard, J.A., Carroll, A.M., Farrall, L., and Valent, B. (1997). A series of vectors for fungal transformation. Fungal Genet. Newsl. **44**: 52-53.

Talbot, N.J., Ebbole, D.J., and Hamer, J.E. (1993). Identification and characterization of *MPG1*, a gene involved in pathogenicity from the rice blast fungus *Magnaporthe grisea*. Plant Cell **5**: 1575-1590.

Thines, E., Weber, R.W.S. and Talbot, N. J. (2000) MAP kinase and protein kinase A-dependent mobilisation of triacylglycerol and glycogen during appressorium turgor generation by *Magnaporthe grisea.* Plant Cell **12:** 1703 - 1718

Tucker, S.L., and Talbot, N.J. (2001). Surface attachment and pre-penetration stage development by plant pathogenic fungi. Annu Rev Phytopathology **39**: 385-417.

Tucker, S.L. Thornton, C.R., Tasker, K., Jacob, C., Giles, G., Egan, M. and Talbot, N.J. (2004) A fungal metallothionein is required for pathogenicity of *Magnaporthe grisea* Plant Cell **16:** 1575-88.

Ukil, L., De Souza, C.P., Lui, H.L., and Osmani, S.A. (2009). Nucleolar separation from chromosomes during *Aspergillus nidulans* mitosis can occur without spindle forces. Molec. Biol. Cell **20**: 2132-2145

Veneault-Fourrey, C., Barooah, M., Egan, M., Wakley, G., and Talbot, N.J. (2006). Cell cycle-regulated autophagic cell death is necessary for plant infection by the rice blast fungus. Science **312**: 580 - 583.

Wang, Z., Thornton, C.R., Kershaw, M.J., Debao, L., and Talbot, N.J. (2003). The glyoxylate cycle is required for temporal regulation of virulence by the plant pathogenic fungus *Magnaporthe grisea*. Mol. Microbiol. **47**: 1601–1612.

Westfall, P.J. and Momany, M. (2002) *Aspergillus nidulans* septin AspB plays pre- and postmitotic roles in septum, branch, and conidiophore development. Molec. Biol. Cell **13:**110-118.

Wilson, R.A., and Talbot, N.J. (2009). Under pressure: investigating the biology of plant infection by *Magnaporthe oryzae*. Nat. Rev. Microbiol. **7**: 185-195.

Wolkow, T.D., Harris, S.D., and Hamer, J.E. (1996). Cytokinesis in *Aspergillus nidulans* is controlled by cell size, nuclear positioning and mitosis. J. Cell Sci. **109**: 2179-2188.

Xu, J.R., and Hamer, J.E. (1996). MAP kinase and cAMP signaling regulate infection structure formation and pathogenic growth in the rice blast fungus *Magnaporthe grisea*. Genes Dev. **10**: 2696-2706.

Xu, J.R., Urban, M., Sweigard, J.A., and Hamer, J.E. (1997). The *CPKA* gene of *Magnaporthe grisea* is essential for appressorial penetration. Mol. Plant Microbe Interact. **10**: 187-194.

Yeh, E., Yang, C., Chin, E., Maddox, P., Salmon, E.D., Lew, D.J., and Bloom, K. (2000). Dynamic positioning of mitotic spindles in yeast: Role of microtubule motors and cortical determinants. Molec. Biol. Cell **11**: 3949-3961.

Chapter3

Septin-mediated plant cell invasion by the rice blast fungus *Magnaporthe oryzae*

Authors: Yasin Fatih Dagdas[1], Kae Yoshino[1,2], Gulay Dagdas[1], Lauren S. Ryder[1], Ewa Bielska[1], Gero Steinberg[1] and Nicholas J. Talbot[1*]

Affiliations: [1]School of Biosciences, University of Exeter, Geoffrey Pope Building, EX4 4QG, United Kingdom. [2] Division of Applied Biosciences, Graduate School of Agriculture, Kyoto University, Sakyo-ku, Kyoto 606-8502, Japan

* To whom correspondence should be addressed. E-mail: n.j.talbot@exeter.ac.uk

Final Accepted Manuscript: Dagdas, Y.F. et al. Septin-mediated plant cell invasion by the rice blast fungus, *Magnaporthe oryzae*. *Science* **336**, 1590-5 (2012)

Abstract:

To cause rice blast disease, the fungus *Magnaporthe oryzae* develops a pressurized dome-shaped infection structure called an appressorium, which physically ruptures the rice leaf cuticle to gain entry to plant tissue. The cellular mechanism of plant infection is unknown. Here, we report that a toroidal F-actin network assembles in the appressorium at the point of plant infection by means of four septin GTPases. *M. oryzae* septins polymerize into a dynamic, hetero-oligomeric ring, which scaffolds F-actin, via the ezrin-radixin-moesin (ERM) protein, Tea1, and phosphatidylinositide interactions at the plasma membrane. The septin ring is essential for rice blast disease and assembles in a Cdc42 and Chm1-dependent manner. Septins also form a diffusion barrier to localize the Inverse-Bin-Amphiphysin-RVS (I-BAR)-domain protein, Rvs167, and Wiskott-Aldrich Syndrome protein (WASP), Las17 at the point of penetration. Septins thereby provide cortical rigidity and membrane curvature necessary for protrusion of a rigid penetration peg which breaches the leaf surface.

One Sentence Summary: A cellular mechanism is proposed by which the devastating rice blast fungus mechanically ruptures rice leaves and enters plant tissue.

Main Text:

The rice blast fungus *Magnaporthe oryzae* can cause disease in more than fifty grass species, including economically significant crops such as barley, wheat, millet and rice. Blast is the most devastating disease of cultivated rice and a constant threat to global food security. Each year up to 30% of the rice harvest is lost to blast disease– enough rice to feed 60 million people –and finding an effective way to control rice blast is therefore a priority. To infect rice leaves, *M. oryzae* develops a special infection structure called an appressorium (Fig. 1). The dome-shaped appressorium generates turgor of up to 8.0 MPa, equivalent to 40 times that of a car tyre, and translates this extreme pressure into physical force sufficient to break the leaf surface. Appressorium turgor is generated by rapid influx of water into the cell against a concentration gradient of glycerol, maintained in the appressorium by a specialized, melanin-rich cell wall (*1*). Turgor is translated into physical force, applied to the leaf surface by a narrow penetration peg that mechanically ruptures the tough leaf cuticle (*3*). The cellular mechanism by which an appressorium breaches the plant cuticle is not known.

In this study, we set out to investigate how an appressorium is able to cause plant infection. We first carried out live cell imaging of the actin cytoskeleton during appressorium maturation, by expressing the actin-binding protein gene fusion, LifeAct-RFP, (*4*) in *M. oryzae*. This revealed an extensive toroidal F-actin network at the base of the infection cell surrounding the appressorium pore (Fig. 1A). The appressorium pore is a circular region at the base of the appressorium, which marks the point where the penetration peg emerges to rupture the leaf cuticle. Ultrastructural studies have revealed that the appressorium pore initially lacks a cell wall and that the fungal plasma membrane makes direct contact with the rice leaf surface (*2*). As the appressorium inflates to full turgor (with a mean diameter of 8.0□m), a pore wall overlay develops in

this zone and the narrow (780 nm mean diameter) penetration peg emerges. Assembly of an F-actin network during appressorium turgor generation, just before plant infection, suggests that specific re-orientation of the F-actin cytoskeleton takes place at the base of the appressorium to facilitate plant infection (*2*). To investigate how the actin ring forms specifically at this location, we decided to investigate the septin gene family in *M. oryzae*. Septins are small morphogenetic GTPases, conserved from yeast to humans (*5, 6*), involved in cytokinesis, polarity determination and secretion (*7, 8*). Importantly, septins are thought to re-orient and re-organize the cytoskeleton to determine cell shape (*9-12*), and act as partitioning diffusion barriers to recruit and maintain specific proteins at discrete sub-cellular locations (*9, 10*). We identified a family of five septin genes in *M. oryzae*, four of which showed similarity to the core septins identified in the budding yeast *Saccharomyces cerevisiae* (Cdc3, Cdc10, Cd11, Cdc12) *(9)*. Sep3, for instance, showed 47% amino acid identity to Cdc3, Sep4 showed 55% identity to Cdc10, Sep5 showed 45% identity to Cdc11 and Sep6 showed 57% identity to Cdc12. We expressed the *M. oryzae* genes in temperature-sensitive *S. cerevisiae* septin mutants, that show defects in cell division and in all cases observed complementation of the cell separation defect, consistent with the *M. oryzae* proteins acting as functional septins (fig. S1). Next, we expressed Sep3-GFP, Sep4-GFP, Sep5-GFP and Sep6-GFP gene fusions in *M. oryzae* and observed that each septin formed a large 5 9m ring which co -localized with the F-actin toroidal network at the appressorium pore (Fig. 1A-D and Movie S1). In the case of Sep6-GFP, we also observed an additional bright punctate structure consistently associated with the appressorium septin ring (Fig. 1D). During vegetative or invasive growth of *M. oryzae*, septins formed a much wider range of structures, including long bars, gauzes, collars and rings (fig S2, figS3). As expected, septins also formed rings at sites of septation (*10*) including at the neck of nascent appressorium (fig S2). To understand the nature of the septin ring, we investigated fluorescence recovery

following partial photo-bleaching. We found 87% recovery of fluorescence after 15 minutes, consistent with the appressorium septin ring being a dynamic structure (Fig. 1F). We then carried out targeted gene deletions to produce isogenic mutants lacking *SEP3, SEP4, SEP5* or *SEP6* (fig. S4) and examined septin ring formation in each mutant. All septin null mutants showed mis-localisation of the remaining septin-GFPs, as shown in fig. S5. Core *M. oryzae* septins must therefore act co-operatively to form hetero-oligomers, which assemble into the large ring that surrounds the appressorium pore. Consistent with this idea, co-immuno-precipitation experiments using Sep5-GFP identified Sep3, Sep4 and Sep6 interactions as well as physical interaction with actin, tubulins and the Lte1 cell cycle control protein (*11*), as shown in Table S1. *M. oryzae* septin mutants showed a number of developmental phenotypes (fig. S6). Multiple rounds of nuclear division took place during appressorium development in septin mutants, for example, (fig. S7A and B) compared to a single round of mitosis and autophagy-associated cell death, which normally occurs in *M. oryzae* (*12, 13*). We also observed the expected role for septins in cytokinesis within somatic hyphae (*7-10*) and found that localization of myosin II and myosin light chain, for instance, to septum which separates the germ tube and appressorium (*10*) required the *M. oryzae* septins (fig. S7C and D).

Given the specific localization of the toroidal F-actin network and septin ring at the appressorium pore, we decided to investigate the effect of deleting *M. oryzae* septin genes on F-actin organization. We found that the appressorium F-actin network was disorganized in Δ*sep3*, Δ*sep4*, Δ*sep5*, or Δ*sep6* mutants (Fig. 2A). Organisation of the F-actin network which surrounds the site of plant infection is therefore septin-dependent. We reasoned that the F-actin network, scaffolded by septins, may provide cortical rigidity to the penetration peg in a manner analogous to a yeast bud in which assembly of F-actin cables requires the action of Cdc42 and the formins Bni1 and Bnr1

(*15*, *16*). To test this idea, we investigated F-actin and septin localization in a *M. oryzae* *Δcdc42* mutant and the F-actin network organisation and septin ring formation were both affected (Fig. 2). We observed, for instance, many aberrant ~0.5 diameter Sep3-GFP rings in a *Δcdc42* mutant but no central septin ring in the appressorium (Fig. 2B and C). Formation of the appressorium septin torus also required the Chm1 kinase (homologous to the *S. cerevisiae* Cla4 protein kinase), which is known to phosphorylate septins in yeast (*17*). Targeted deletion of *M. oryzae CHM1* (*18*) prevented formation of either the septin or F-actin networks within the appressorium (Fig. 2B and C). We also found that septin ring formation required the cell integrity pathway MAP kinase Mps1 (*19*) and the Mst12 transcription factor (*20*), which are both necessary for appressorium function (fig. S8). Furthermore, we discovered that septin ring formation depends on cell cycle progression, which is known to regulate appressorium development in *M. oryzae* (*12*) (fig. S9). Taken together, we conclude that septin ring assembly is necessary to scaffold F-actin as a toroidal network at the base of the appressorium, prior to plant infection.

To test whether septin-dependent assembly of the F-actin network is essential for rice blast disease, we inoculated each septin null mutant onto a susceptible rice cultivar and scored disease symptoms. Septin mutants were non-pathogenic, causing either no symptoms at all (*Δsep3*), or small necrotic flecks associated with abortive infection attempts that stimulate a rice defense response (Fig. 3). We also observed significant reductions in the ability of appressoria to form penetration pegs following deletion of *SEP3, SEP4, SEP5* or *SEP6* (Fig. 3A and B). Transmission electron microscopy and live cell imaging of rice leaf sheath infections in *Δsep3* mutants confirmed the inability of appressoria from septin mutants to rupture plant cuticles (Fig. 3C and D). Importantly, all the septin mutant phenotypes reported here were complemented by re-introduction of either a wild type allele, or the corresponding

septin-GFP fusion (fig. S10). We conclude that *M. oryzae* septins are necessary for rice blast disease.

To understand the precise nature of the cortical F-actin network in appressoria, we decided to investigate plasma membrane linkages at the appressorium base. It has been suggested that some F-actin-plasma membrane linkages may occur via ezrin, radixin, moesin (ERM) proteins, which contain a C-terminal actin-binding domain and an N-terminal ERM domain that binds transmembrane proteins, such as integrins (*21*). We identified a putative ERM protein-encoding gene in *M. oryzae*, *TEA1* (which showed 61% identity to *S. pombe* Tea1), and found that Tea1-GFP localized as a punctate ring in the appressorium, co-located with the F-actin and septin networks (Fig. 4A, fig. S11B). By contrast, in a *Δsep5* mutant Tea1-GFP was mis-localized and did not define the appressorium pore region (Fig. 4A, fig. S11E). Phosphorylation of ERM proteins is potentiated by phosphatidylinositol (PtdIns), 4,5-bisphosphate binding (*22*) and yeast septins, for example, associate with PtdIns-4-phosphate and PtdIns-4,5-bisphosphate via an N-terminal polybasic domain (*23*, *24*). We identified the *M. oryzae* PtdIns-4-kinase-encoding gene, *STT4* (showing 53% identity to *S. cerevisiae STT4*), and the PtdIns,4 phosphate-5-kinase-encoding gene *MSS4* (64% identity) and found that Stt4-GFP and Mss4-GFP localized to the appressorium pore, bounded by F-actin and the septin ring (Fig. 4B). To test whether *M. oryzae* septins associated with membrane domains enriched in phosphoinositides, we deleted the N-terminal polybasic domain of *M. oryzae* Sep5 and expressed the resulting Sep5Δpb-GFP fusion protein in a Δ*sep5* mutant. The Sep5Δpb-GFP formed normal septin rings at hyphal septa or the neck of the nascent appressorium, demonstrating that the stability of the septin was unaffected by deletion of the polybasic domain (Fig. 4C). Strikingly, however, the septin ring at the base of the appressorium could not form (Fig. 4C). We conclude that septin-PtdIns interactions and ERM protein-actin linkages occur at the appressorium pore.

Interestingly, *M. oryzae* Chm1-GFP also localized to the appressorium pore (Fig. 4D and fig. S11A and F), consistent with a role in septin phosphorylation (*25*).

We reasoned that in addition to scaffolding the F-actin network, the appressorium septin ring might also act as a diffusion barrier to constrain lateral diffusion of membrane-associated proteins involved in plant infection. Septin rings are known, for example, to act as diffusion barriers at the mother bud neck in *S. cerevisiae* (*26*, *27*). We decided to test whether *M. oryzae* septins affect distribution of proteins potentially involved in penetration peg development. Bin-Amphiphysin-Rvs (BAR) domain proteins have been shown to form oligomeric scaffold structures involved in membrane curvature (*28*). Whereas F-BAR proteins are well known to play roles in membrane invagination during endocytosis, the Inverse BAR (I-BAR) proteins are involved in negative membrane curvature leading to cellular protrusions (*28*). Because emergence of a penetration hypha from the appressorium requires extreme negative membrane curvature (*2*, *29*) we decided to ask whether septins play a role in I-BAR protein localisation. *M. oryzae* Rvs167 contains an I-BAR domain, showing 75 % identity to *S. cerevisiae* Rvs167p. We found that Rvs167-GFP localized to the centre of the appressorium pore, prior to penetration peg emergence. We found, however, that distribution of Rvs167-GFP was disrupted in a *Δsep5* mutant (Fig. 4E and fig. S11C and G). I-BAR proteins are proposed to link curved membrane structures to polymerization of cortical F-actin via non-specific electrostatic interactions (*30*) mediated by SH3 domains of I-BAR proteins and components of the WASP/WAVE complex (*31*). We isolated a WASP/Arp2/3 complex component, Las17 (*32*), homologous to Las17p of *S. cerevisiae*. *M. oryzae* Las17-GFP localized to the base of the appressorium, bounded by the septin ring (Fig. 4F), but in a *Δsep5* mutant Las17-GFP localization was disrupted with the protein distributed diffusely in the cytoplasm and to the plasma membrane (Fig. 4F and fig. S11D and H).

Based on the evidence presented in this report, we propose that appressoria of the rice blast fungus infect plants using a septin-dependent mechanism, summarized in Fig. 4G. In this model, isotropic expansion of the pressurized appressorium is directed into mechanical force generation at the base of the infection cell. This is dependent on assembly of an extensive toroidal F-actin network at the appressorium pore, which provides cortical rigidity at the initially wall-less region of the appressorium. Septins organize the cortical F-actin network, making direct phosphoinositide linkages to the plasma membrane and facilitating the action of ERM proteins, such as Tea1, which link cortical F-actin to the membrane. The septin ring also acts as a diffusion barrier to ensure precise localisation of proteins, such as the I-BAR protein, Rvs167, and the WASP/WAVE complex involved in membrane curvature at the tip of the emerging penetration peg and F-actin polymerization. In this way, the rice blast fungus extends a rigid penetration peg that ruptures the leaf cuticle and invades the host plant tissue.

References and Notes

1. J. C. de Jong, B. J. McCormack, N. Smirnoff, N. J. Talbot, *Nature* **389**, 244 (1997).
2. T. M. Bourett, R. J. Howard, *Canadian Journal of Botany* **68**, 329 (1990).
3. C. Bechinger *et al.*, *Science* **285**, 1896 (1999).
4. A. Berepiki, A. Lichius, J. Y. Shoji, J. Tilsner, N. D. Read, *Eukaryot Cell* **9**, 547 (2010).
5. A. S. Gladfelter, L. Kozubowski, T. R. Zyla, D. J. Lew, *Journal of Cell Science* **118**, 1617 (2005).
6. R. Lindsey, M. Momany, *Curr Opin Microbiol* **9**, 559 (2006).
7. L. M. Douglas, F. J. Alvarez, C. McCreary, J. B. Konopka, *Eukaryot Cell* **4**, 1503 (2005).
8. E. T. Spiliotis, W. J. Nelson, *Journal of Cell Science* **119**, 4 (2006).
9. L. H. Hartwell, *Experimental Cell Research* **69**, 265 (1971).
10. D. G. Saunders, Y. F. Dagdas, N. J. Talbot, *Plant Cell* **22**, 2417 (2010).
11. G. A. Castillon *et al.*, *Current Biology* **13**, 654 (2003).
12. D. G. Saunders, S. J. Aves, N. J. Talbot, *Plant Cell* **22**, 497 (2010).
13. C. Veneault-Fourrey, M. Barooah, M. Egan, G. Wakley, N. J. Talbot, *Science* **312**, 580 (2006).
14. E. Bi *et al.*, *Journal of Cell Biology* **142**, 1301 (1998).
15. A. E. Adams, D. I. Johnson, *et al.*, *Journal of Cell Biology* **111**, 131 (1990).
16. I. Sagot, S. K. Klee, D. Pellman, *Nature Cell Biology* **4**, 42 (2002).
17. M. Versele, J. Thorner, *Journal of Cell Biology* **164**, 701 (2004).
18. L. Li, C. Xue, K. Bruno, M. Nishimura, J. R. Xu, *Mol Plant Microbe Interact* **17**, 547 (2004).
19. J. R. Xu, C. J. Staiger, J. E. Hamer, *Proc Natl Acad Sci U S A* **95**, 12713 (1998).
20. G. Park, C. Xue, L. Zheng, S. Lam, J. R. Xu, *Mol Plant Microbe Interact* **15**, 183 (2002).
21. J. Gilden, M. F. Krummel, *Cytoskeleton (Hoboken)* **67**, 477 (2011).
22. B. T. Fievet *et al.*, *Journal of Cell Biology* **164**, 653 (2004).
23. A. Casamayor, M. Snyder, *Mol Cell Biol* **23**, 2762 (2003).
24. M. Onishi *et al.*, *Mol Cell Biol* **30**, 2057 (2010).
25. M. Iwase *et al.*, *Molecular Biology of the Cell* **17**, 1110 (2006).
26. Y. Barral, V. Mermall, M. S. Mooseker, M. Snyder, *Molecular Cell* **5**, 841 (2000).
27. P. A. Takizawa, J. L. DeRisi, J. E. Wilhelm, R. D. Vale, *Science* **290**, 341 (2000).
28. H. Zhao, A. Pykalainen, P. Lappalainen, *Current Opinion in Cell Biology* **23**, 14 (2011).
29. M. J. Egan, Z. Y. Wang, *et al.*, *Proc Natl Acad Sci U S A* **104**, 11772 (2007).
30. P. K. Mattila *et al.*, *Journal of Cell Biology* **176**, 953 (2007).
31. T. Takenawa, S. Suetsugu, *Nat Rev Mol Cell Biol* **8**, 37 (2007).
32. A. Madania *et al.*, *Molecular Biology of the Cell* **10**, 3521 (1999).
33. H. Leung *et al.*, *Curr Genet* **17**, 409 (May, 1990).
34. N. J. Talbot, D. J. Ebbole, J. E. Hamer, *Plant Cell* **5**, 1575 (1993).
35. J. Sambrook, E. F. Fritsch, T. Maniatis, *Cold Spring Harbour Laboratory press, New York, USA* (1989).
36. P. Kankanala, K. Czymmek, B. Valent, *Plant Cell* **19**, 706 (2007).
37. R. Lindsey, Y. Ha, M. Momany, *Plos One* **5** (2010).
38. M. J. Kershaw, N. J. Talbot, *Proc Natl Acad Sci U S A* **106**, 15967 (2009).

39. J. A. Sweigard, F. G. Chumley, B. Valent, *Mol Gen Genet* **232**, 183 (1992).
40. C. K. Raymond, T. A. Pownder, S. L. Sexson, *Biotechniques* **26**, 134 (1999).

Acknowledgments
We thank Prof. Jeremy Thorner (UC Berkeley) for providing yeast septin mutants. We acknowledge Dr. Hannah Florence from Exeter Mass Spectrometry facility and Dr. Martin Schuster from the Exeter Bio-imaging Centre. This work was funded by a Halpin Scholarship for rice blast research to YFD and grants to NJT from the BBSRC and the European Research Council. KY is funded by The Kyoto University Foundation. We thank Prof. Michelle Momany for critical reading of the manuscript and for valuable discussions.

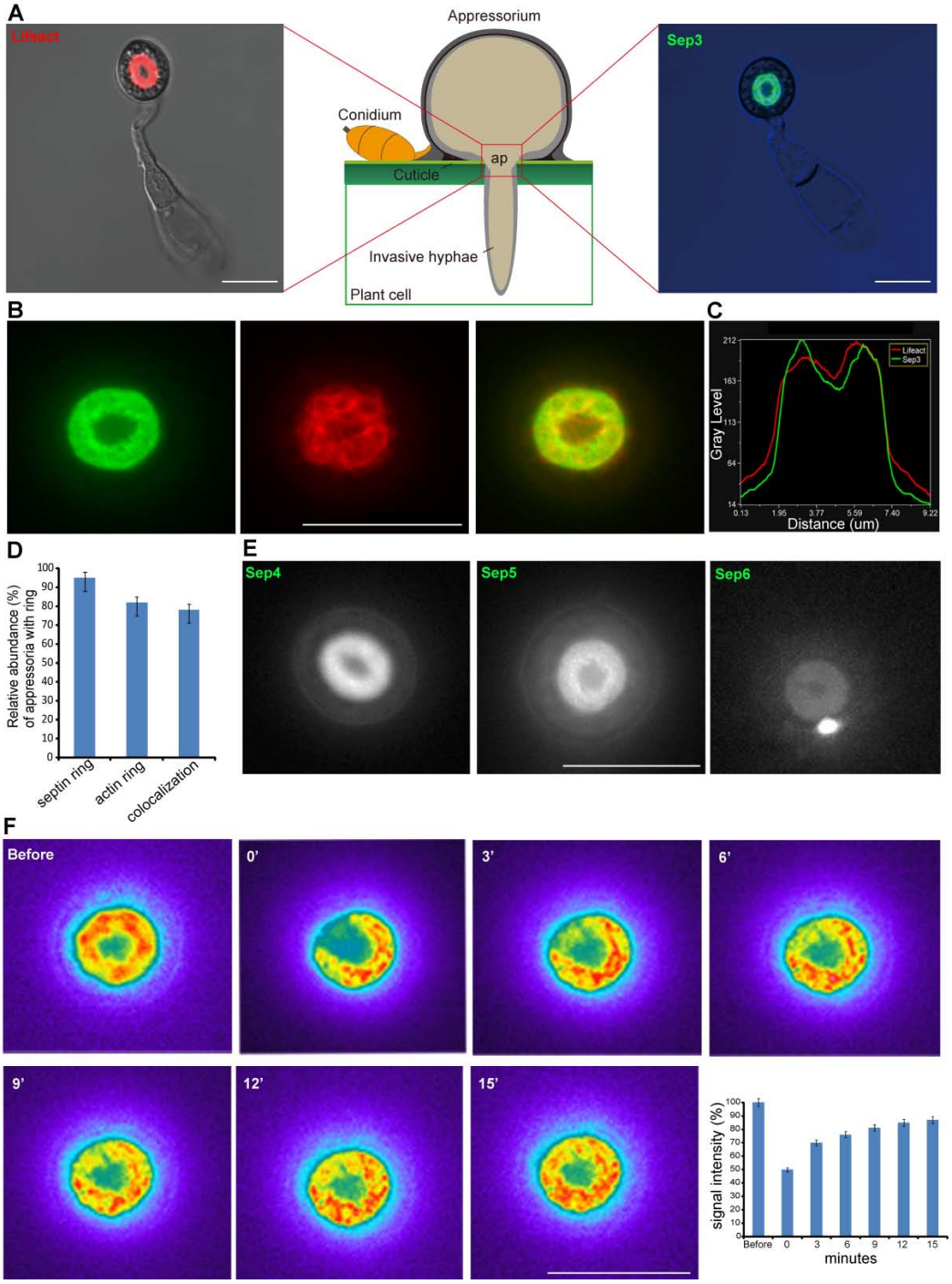
A
Lifeact
Appressorium
Conidium
ap
Cuticle
Invasive hyphae
Plant cell
Sep3
B
C
Gray Level
Distance (um)
Lifeact
Sep3
D
Relative abundance (%) of appressoria with ring
septin ring
actin ring
colocalization
E
Sep4
Sep5
Sep6
F
Before
0'
3'
6'
9'
12'
15'
signal intensity (%)
minutes

Fig.1. A toroidal-shaped F-actin network and large septin ring assemble at the appressorium pore in *M. oryzae*

(**A**) Cellular localization of LifeAct-RFP in the rice blast fungus *M. oryzae* in a mature appressorium visualized by laser confocal microscopy. Localisation of Sep3-GFP to a large 5.9□m diameter ring visualized by laser excitation epifluorescence microscopy. Conidia were germinated on hydrophobic glass slides for 24 h. ap = appressorium pore, the region that defines the position from which the penetration peg emerges (**B**) Photomicrographs showing that Sep3-GFP and Lifeact-RFP co-localize around the appressorium pore. (**C**) Linescan graph consistent with co-localization of the septin ring with the F-actin network. (**D**) Bar charts showing the percentage of appressoria which contained co-localizing septin and F-actin networks (n = 300). All cells in which an F-actin torus was observed contained a co-localizing septin ring (mean ± SD, of three independent experiments). (**E**) Core *M. oryzae* septins (Sep3, Sep4, Sep5 and Sep6) all form a ring around the appressorium pore (24 h). Sep6 also forms a distinct punctum in addition to localization to the septin ring. (**F**) Recovery of Sep3-GFP after partial photobleaching of the septin ring. Sep3-GFP showed 87% recovery in fluorescence 15 min after photobleaching (mean ± SD in three experiments). Scale bar = 10 μm

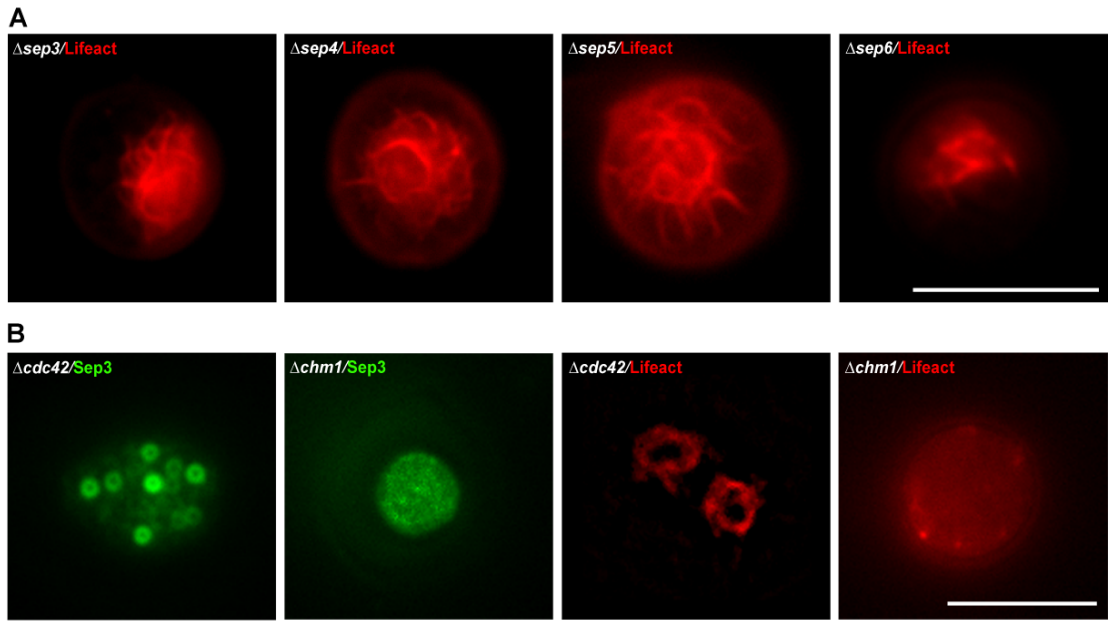
A
Δsep3/Lifeact
Δsep4/Lifeact
Δsep5/Lifeact
Δsep6/Lifeact
B
Δcdc42/Sep3
Δchm1/Sep3
Δcdc42/Lifeact
Δchm1/Lifeact

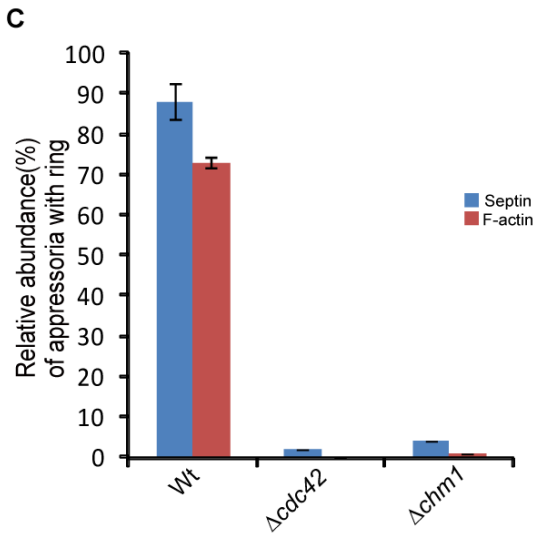
C
Relative abundance(%) of appressoria with ring
100
90
80
70
60
50
40
30
20
10
0
Septin
F-actin
Wt
Δcdc42
Δchm1

Fig.2. F-acting network organization is septin-dependent in *M. oryzae* appressoria. **(A)** Assembly of the toroidal F-actin network at the appressorium pore is dependent on septins. Micrographs showing localization of LifeAct-RFP in Δ*sep3*, Δ*sep4*, Δ*sep5*, and Δ*sep6* mutants revealed that the appressorium pore F-actin network cannot form correctly in septin mutants. (**B**) Live cell imaging to show cellular localization of Sep3-GFP and F-actin in Δ*cdc42* and Δ*chm1* mutants of *M. oryzae*. In a Δ*cdc42* mutant, Sep3-GFP localizes to small (0.5 μm diameter) rings. In a Δ*chm1* mutant the Sep3-GFP ring did not form at the appressorium pore. Δ*cdc42* and Δ*chm1* mutants do not form an F-actin network. (**C**) Bar charts showing the percentage of appressoria in which septin and F-actin network formation could be observed (n= 300, mean ±SD, three experiments). Scale bar = 10 μm.

Fig.3

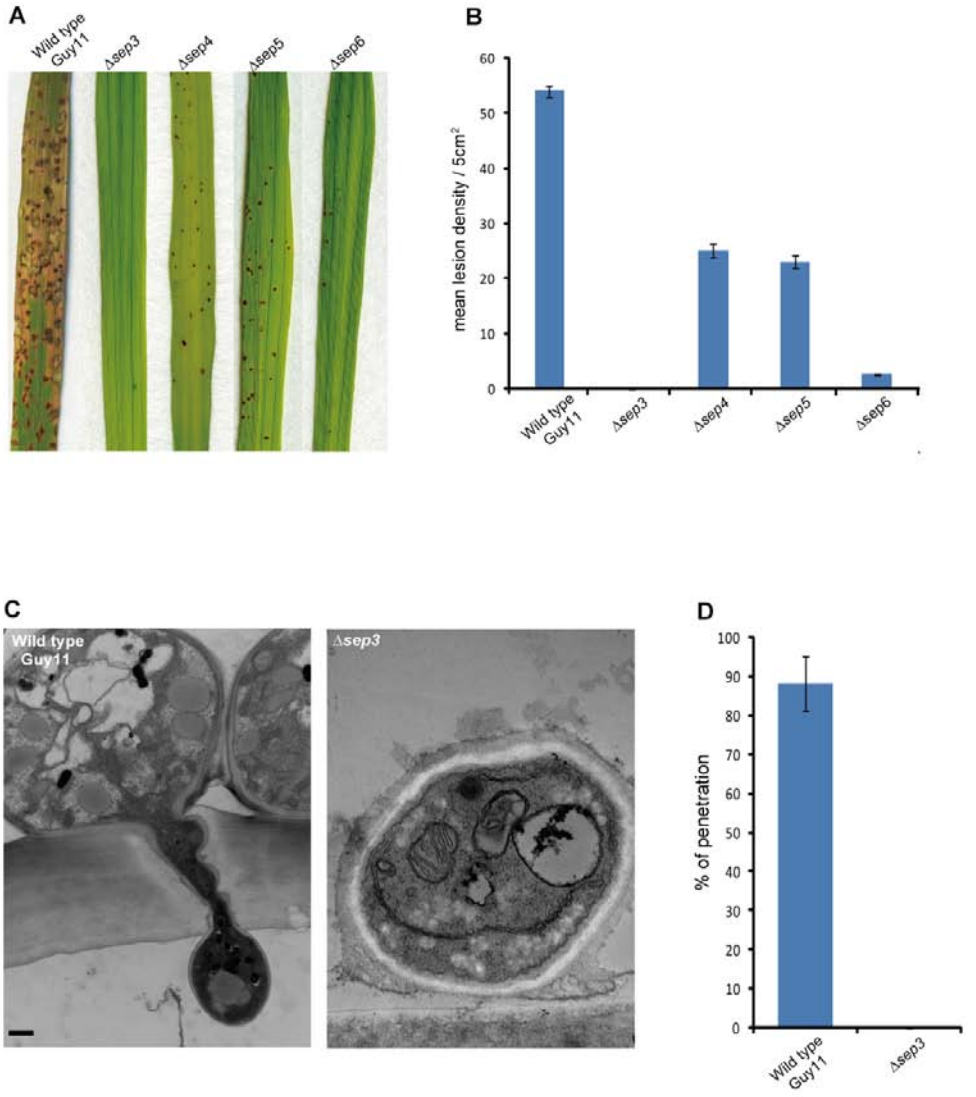
A
Wild type Guy11
Δsep3
Δsep4
Δsep5
Δsep6
B
mean lesion density / 5cm²
60
50
40
30
20
10
0
Wild type Guy11
Δsep3
Δsep4
Δsep5
Δsep6
C
Wild type Guy11
Δsep3
D
% of penetration
100
90
80
70
60
50
40
30
20
10
0
Wild type Guy11
Δsep3

Fig. 3 *M. oryzae* septin mutants are unable to cause rice blast disease. (**A**) Targeted deletion of each septin gene resulted in loss of pathogenicity on susceptible rice cultivar CO-39. The Δ*sep3* mutant caused no disease symptoms, Δ*sep4,* Δ*sep5,* and Δ*sep6* mutants elicited necrotic flecks due to abortive infection attempts. Septin mutants were unable to cause large spreading disease lesions observed in the isogenic wild type Guy11 (**B**) Bar charts showing frequency of disease lesions or necrotic flecks per 5 cm^2 of leaf surface (n=30 for each septin mutant) (mean ±SD, three experiments), reflecting frequency of penetration attempts. (**C**) Transmission electron micrographs of transverse section of wild type (24 h) and Δ*sep3* mutant appressoria (36 h) during leaf infection. No penetration pegs were observed in Δ*sep3* mutants. Scale bar = 2 μm. (**D**) Bar chart showing frequency of rice epidermal cell rupture at 400 infection sites, observed 36 h after conidial germination in wild type (Guy11) and Δ*sep3* mutant infections (mean ±SD, three experiments).

Fig.4

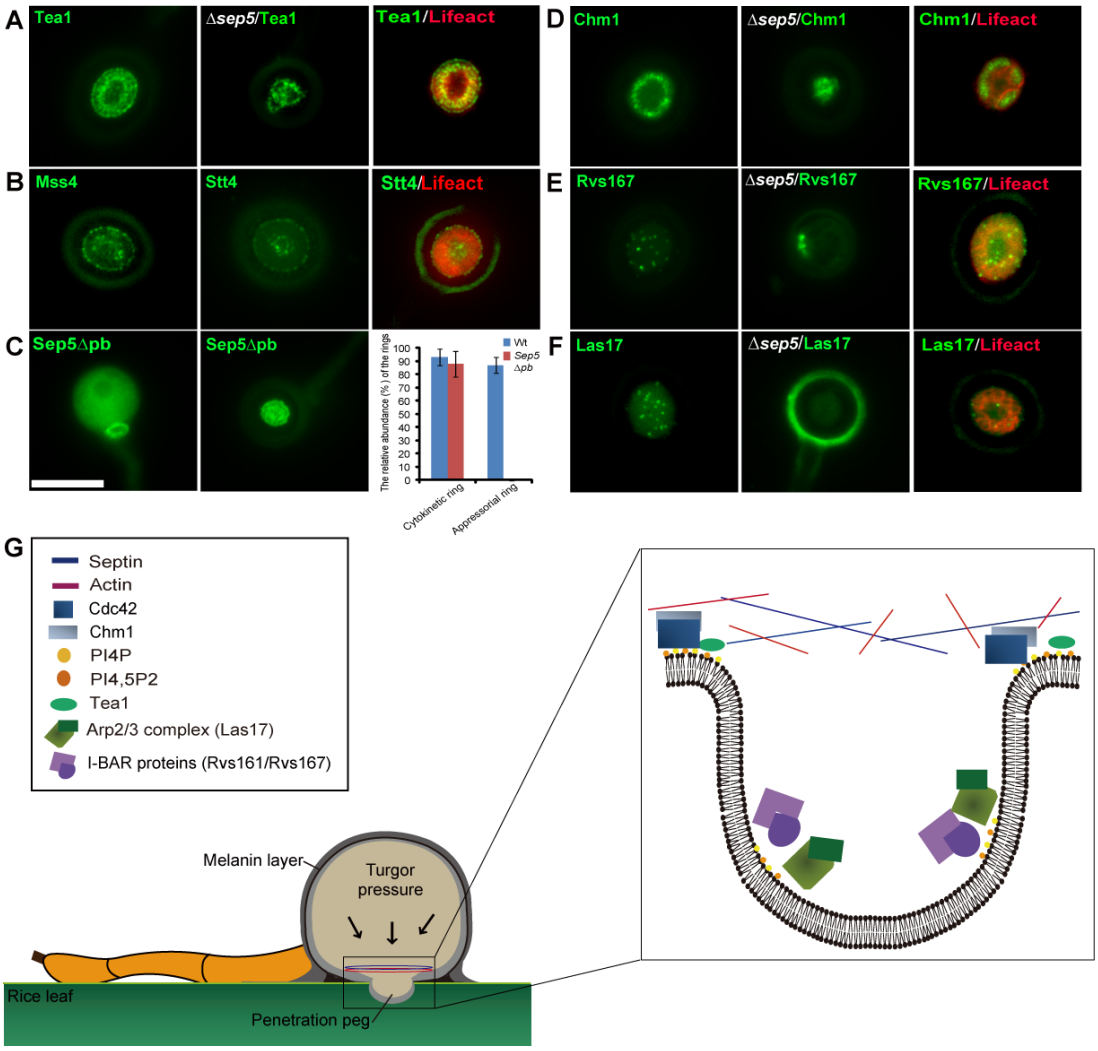
A
Tea1
Δsep5/Tea1
Tea1/Lifeact
B
Mss4
Stt4
Stt4/Lifeact
C
Sep5Δpb
Sep5Δpb
The relative abundance (%) of the rings
Wt
Sep5 Δpb
Cytokinetic ring
Appressorial ring
D
Chm1
Δsep5/Chm1
Chm1/Lifeact
E
Rvs167
Δsep5/Rvs167
Rvs167/Lifeact
F
Las17
Δsep5/Las17
Las17/Lifeact
G
Septin
Actin
Cdc42
Chm1
PI4P
PI4,5P2
Tea1
Arp2/3 complex (Las17)
I-BAR proteins (Rvs161/Rvs167)
Melanin layer
Turgor pressure
Rice leaf
Penetration peg

Fig. 4. Septin-dependent localization of specific proteins to the appressorium pore region in *M. oryzae* and model of septin-mediated plant infection.

(**A**) The ERM protein, Tea1-GFP localizes to the appressorium pore in a septin-dependent manner. Micrograph to show localization of Tea1-GFP to appressorium pore in Guy11, in a *Δsep5* mutant and co-localization with LifeactRFP (mean ±SD, three experiments, n = 300). **(B)** Micrograph to show localization of the phosphatidylinositol 4-kinase (Stt4-GFP) and phosphatidylinositol-4-phosphate 5-kinase (Mss4-GFP) to the centre and periphery of the appressorium pore and co-localization with LifeAct-RFP. **(C)** Micrograph and bar chart showing that the N-terminal polybasic rich domain (pb) of septin Sep5 is necessary for formation of the septin ring at the appressorium pore. (**D**) Chm1-GFP localizes to the appressorium pore where it co-localizes with LifeactRFP and this is impaired in a *Δsep5* mutant. (**E**) Micrograph to show localization of the I-BAR protein (Rvs167-GFP) to puncta within the centre of the appressorium pore, at the site of penetration peg emergence and impairment of this specific localization in a *Δsep5* mutant. (**F**) Localization of the N-WASP protein (Las17-GFP), a component of the actin polymerizing Arp2/3 complex, to the centre of the appressorium pore septin ring. Impairment of localization in a *Δsep5* mutant. Scale bar for all panels = 10 μm. (**G**) Model to show septin-mediated rice leaf infection by *M. oryzae*. In this model, septins scaffold an F-actin network necessary for cortical rigidity of the nascent penetration peg. Interactions of the cortical actin network with the plasma membrane are mediated by ERM proteins, such as Tea1. Hetero-oligomeric septin ring formation occurs at PtdIns-4-P and PtdIns-4,5-P-rich domains of the plasma membrane mediated by the polybasic rich domain of each septin. Septins act as a diffusion barrier to maintain distribution of I-BAR proteins at the appressorium pore where they play a role in membrane curvature and penetration peg emergence. Arp2/3 complex components within the peg emergence site induce polymerization of F-actin for further curvature of membrane and application of motive force during host cell penetration

Supplementary Materials:

Materials and Methods

Figures S1-S12

Tables S1-S2

Movie S1

References (*38-47*)

Materials and Methods:

Fungal Strains, Growth conditions, Pathogenicity and Infection related development assays and DNA Analysis

All the strains used in this study are derived from the Guy11 wild type strain of *Magnaporthe oryzae (33)*. Standard procedures for *M. oryzae* growth, maintenance, transformation, appressorium development assays, DNA extractions were done as described previously (*34*). All restriction digestions, DNA Gel blot analysis, Polymerase chain reaction and DNA sequencing analysis were performed using standard procedures (*35*).

Pathogenicity assays were performed as described previously (*12*). All experiments were carried out on the rice blast susceptible indica cultivar CO-39 rice cultivar (*34*) and repeated at least three times. Rice epidermis penetration assays were performed using leaf sheath assay as described previously (*36*). A suspension of 10^5 spores/mL was harvested in 0.2% gelatin and inoculated onto leaf sheaths of 3-4 week old rice plants. When ready for microscopy the sides of the leaf sheaths were trimmed to expose the transparent epidermal layer above the mid vein.

Complementation of Yeast Temperature Sensitive Septin Mutants

Temperature sensitive (ts) septin mutants of *S. cerevisiae* were kindly provided by Professor Michelle Momany from the University of Georgia and Professor Jeremy Thorner from the University of California, Berkeley. For complementation analysis, full length cDNAs of each *M. oryzae* septin were cloned into pYES2 plasmid (Invitrogen, Carlsbad, CA) and the resulting plasmids were transformed into corresponding mutants of *S. cerevisiae* septin mutants. *SEP3*-pYES2 plasmid was transformed into yeast strain DDY1453, *SEP4*-pYES 2 was transformed into yeast strain DDY1476, *SEP5*-pYES2 was transformed into yeast strain DDY1455, *SEP6*-pYES2 was transformed into yeast strain DDY1462. Empty pYES2 plasmid was transformed into yeast strains DDY1453, DDY1476, DDY1455, and DDY1462. Analysis of complementation were performed as described previously (*37*). *M. oryzae* septin genes have the following accession numbers; *SEP3* (MGG01521) *SEP4* (MGG06726) *SEP5* (MGG03087), *SEP6* (MGG07466).

Targeted deletion of septins and generation of GFP fused plasmids

Targeted gene deletions in *M. oryzae* were performed using the Split-Marker Method (*38*) using hygromycin resistance cassette *HPH (39)*. The resulting mutants were confirmed by DNA gel blot analysis and two independent transformants of Δ*sep3*, Δ*sep4*, Δ*sep5*, and Δ*sep6* were used for further analysis. The primers used to generate the deletion strains are listed in Supplementary Table 2.

For generation of translational GFP fusions the GAP Repair Cloning method, which is based on homologous recombination in *S. cerevisiae*, was used (*40*). Each fragment was amplified with primers, which have over-hangs complementary to the following fragment and transformed into URA3$^-$ yeast strain. The positive clones were identified with colony PCR and used for plasmid extraction. The primers used are listed in Supplementary Table2. All translational GFP fusions were done using native promoter and terminator (2 kb upstream of the start codon and 1 kb downstream of stop codon, respectively).

For complementation studies, Δ*sep3* was complemented with *SEP3-GFP*, Δ*sep4* was complemented with *SEP4-GFP*, Δ*sep5* was complemented with *SEP5-GFP, and* Δ*sep6* was complemented with *SEP6-GFP*, respectively. Full length genomic clones of each septin gene also complemented all phenotypes (data not shown).

Light and Epifluorescence Microscopy and Transmission Electron Microscopy

H1 (Histone1)-RFP inΔ *sep5* mutant was observed using a Zeiss LSM510 Meta confocal laser scanning microscope system. Argon (458, 477, 488, and 504 nm) and helium-neon (543 and 633 nm) lasers were used to excite the GFP and RFP fluorochromes and images were recorded under X63 oil objective. Image analysis was performed using the LSM Image browser (Zeiss). Appressorium development assays were performed on borosilicate glass coverslips as described previously (*12*). All other images were recorded using IX81 Inverted microscope (Olympus, Hamburg, Germany) and a UPlanSApo X100 or X60 oil objective. Images were captured using a charged coupled device (Visitron, System, Munich, Germany). Image analysis was performed using the MetaMorph 7.5 software (Molecular Devices, Dawnington, USA). Supplementary movie-1 was prepared after recording Z stacks of 200 nm step size with a Piezo drive (Piezosystem, Jena GmbH, Jena, Germany). Three-dimensional deconvolution of Z-stacks was obtained using AutoQuantX software (AutoQuant

Imaging, NY, USA). Ultra-thin sectioning and transmission electron microscopy was performed as described previously (*29*).

Identification of Septin interacting proteins

Proteins interacting with Sep5 were identified using the GFP-Trap method (Chromotek) followed by mass spectrometry. Lyophilized cell pellets were disrupted using a mixer mill (Retsch MM400) twice for 2.5 min at frequency 30/s using liquid nitrogen as a cooling agent. Depending on the volume of cell extracts, they were resuspended in 0.4 - 1 ml of extraction buffer (10 mM HEPES, 50 mM KCl, 1mM EGTA, 1mM $MgCl_2$ pH 7.0 containing protease inhibitors) and centrifuged for 30 min at 50.000*g* at 4°C. Total protein concentration for each soluble fraction of cell extract was calculated by Bradford and appropriate volumes of samples were mixed with 50µl of Chromotek beads at 4°C. After 2 h beads were washed three times with 500 µl of extraction buffer and analyzed by mass spectrometry. Samples were subjected to an in- solution trypsin digest. Analysis of samples was carried out using a QToF 6520 (Agilent) coupled to a 1200 series HPLC-Chip interface system. 1µl was loaded onto a micro C_{18} reverse phase analytical column (Agilent Protein Identification Chip, 75µm x 150mm). The enrichment column flow rate was 3 µl min^{-1} and the analytical column flow rate was 0.3 µl min^{-1}. Buffer A was 2% acetonitrile with 0.1% formic acid in water and buffer B was 95% acetonitrile with 0.1% formic acid in water. Complex digest solutions were separated using the following gradient, 0 min – 2 % B, 65 min – 30% B, 100 min – 60% B, 120 min – 100% B, 122 min – 2% B with a 7 min equilibration time. The desolvation gas temperature was 300°C and gas flow rate was 4 l min^{-1}. The capillary voltage was 1850 V with all analysis being carried out in positive ion mode. The fragmentor voltage was 175 V and skimmer 70 V. Scanning was performed using the autoMS/MS function at 4 scans sec^{-1} with a sloped collision energy of 3.7 V/100 Da with an offset of 5 V. Peak extraction and protein identification were carried out using Spectrum Mill MS Proteomics Workbench software (Agilent). M. oryzae protein database was obtained from NCBI. Precursor and fragment ion search tolerances were 20ppm and 50ppm respectively. The enzyme was specified as trypsin allowing for 2 missed cleavages. Carbamidomethylation was applied as a fixed modification on cysteines. Variable modifications included in the search were acetylation of lysines, oxidized methionines, pyroglutamic acid modification of N-terminal glutamines, and deamidation of asparagines. A hit was regarded as a probable identification when a minimum of 2

unique peptides achieved scores of >7 with matching forward-reverse values and percent score peak intensities (%SPI) >60%. Exceptions were made for identifications where a single peptide was used to identify a protein only when a score was >10 and the %SPI was >70%.

Generation of Sep5Δpb-GFP strain

The polybasic domain of Sep5 is localized at 8-12 amino acids. This region was deleted and the resulting protein was fused to GFP by using GAP repair cloning. Δ*sep5* mutant was transformed with *SEP5*Δ*pb*-GFP plasmid to obtain Sep5Δpb -GFP strain. The domain organization of Sep5 is summarized below.

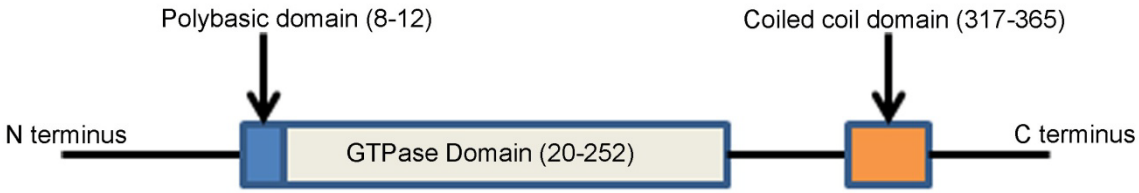

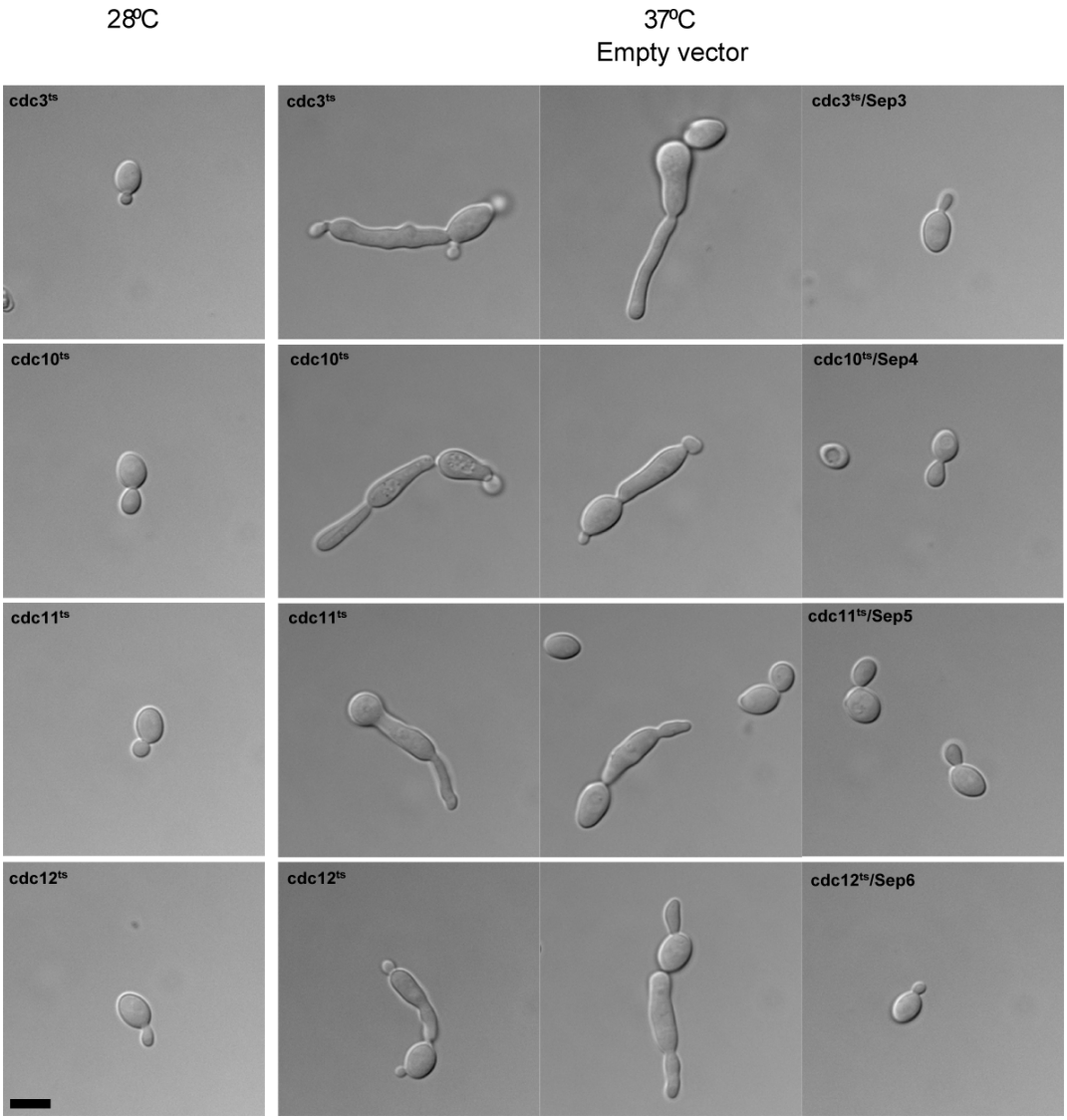
28ºC
37ºC
Empty vector
cdc3ts
cdc3ts
cdc3ts/Sep3
cdc10ts
cdc10ts
cdc10ts/Sep4
cdc11ts
cdc11ts
cdc11ts/Sep5
cdc12ts
cdc12ts
cdc12ts/Sep6

Fig. S1. *M. oryzae* core septins are functional homologues of *S. cerevisiae* septins.
Expression of the *M. oryzae* septins, *SEP3*, *SEP4*, *SEP5*, and *SEP6* complemented cell separation defects of *S. cerevisiae* temperature sensitive strains *cdc3-ts* (DDY1453), *cdc10-ts* (DDY1476), *cdc11-ts* (DDY1455), and *cdc12-6ts* (DDY1462), respectively. Full-length cDNAs of *M. oryzae* core septins (*SEP3*, *SEP4*, *SEP5* and *SEP6*) were cloned into the yeast expression vector pYES2 and transformed into corresponding temperature sensitive yeast strains. At the restrictive temperature, 37°C, expression of core septins from *M. oryzae* allowed complemented cells to grow as normal budded cells, whereas the empty vector containing strains still showed cell separation defects. Scale bar = 5 μm.

Fig.S2

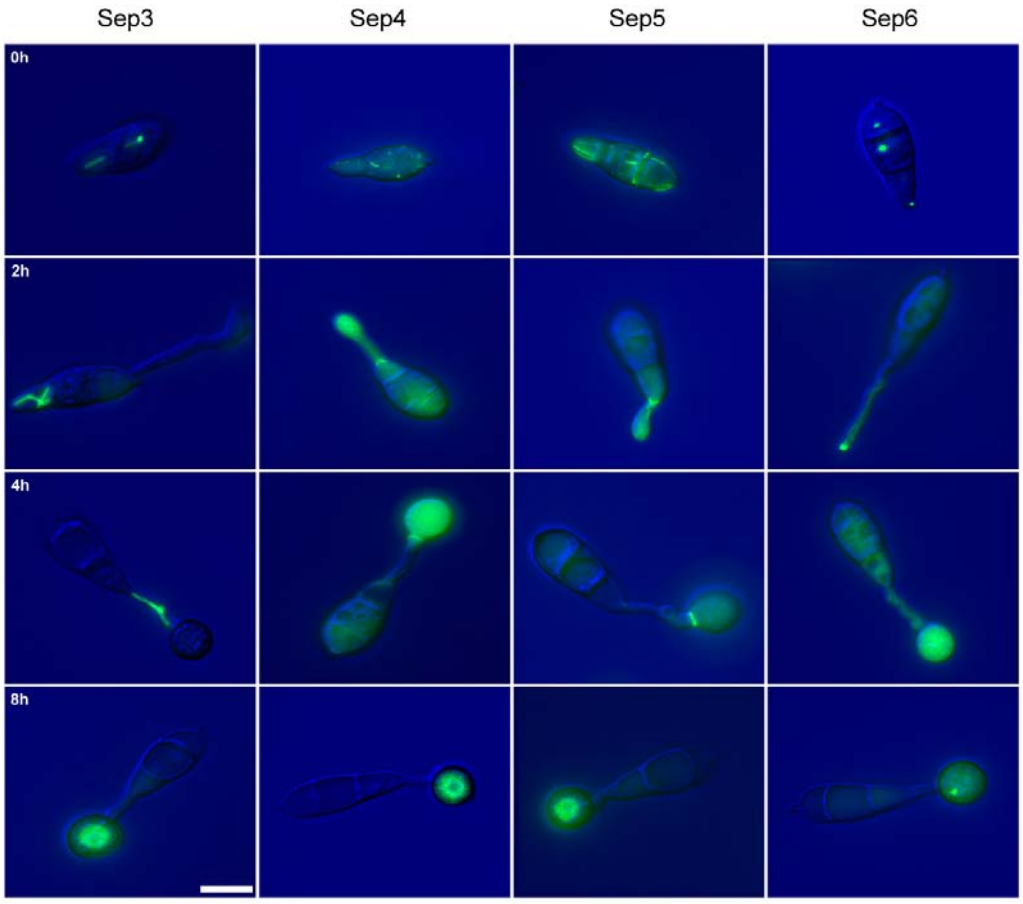

Fig. S2. Septins form diverse oligomeric structures during appressorium development of *Magnaporthe oryzae*

Time series of epifluorescence micrographs showing the localization of septins during different stages of appressorium development. Conidia were germinated on inductive artificial surface to observe the localization of septins in conidia (0 h), germlings (2 h), initial appressorium (4 h) and melanised appressorium (8 h). Septins formed various structures including bars (Sep3-GFP), rings (Sep4-GFP and Sep5-GFP), filaments (Sep4-GFP and Sep5-GFP), and puncta (Sep6-GFP). Scale bar = 10 μm

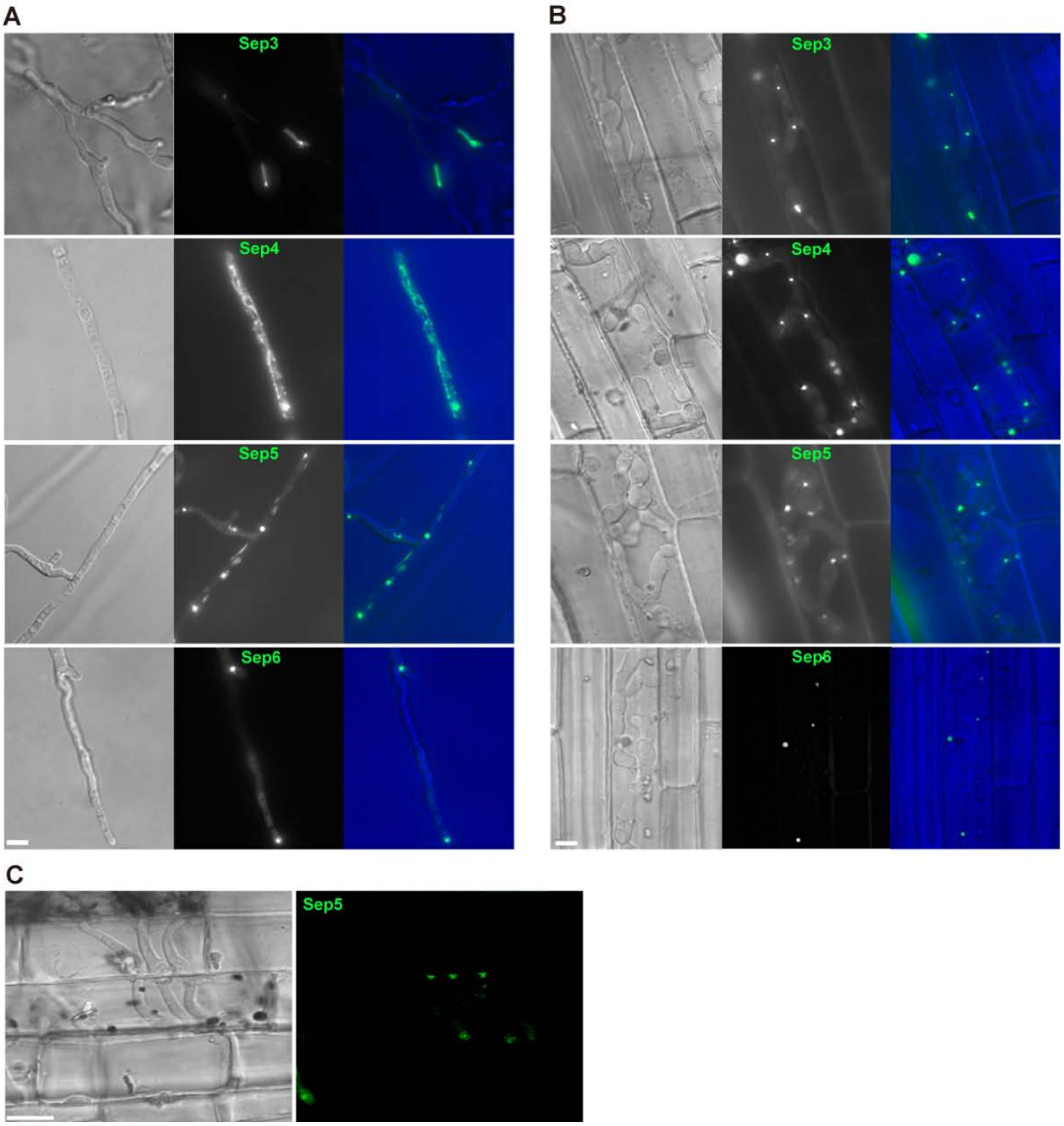
A
Sep3
Sep4
Sep5
Sep6
B
Sep3
Sep4
Sep5
Sep6
C
Sep5

Fig. S3. Localization of septins in vegetative hyphae and during invasive growth in rice leaf tissue.

(**A**) Live cell imaging to show septin localization in vegetative hyphae of *M. oryzae*. Septins form filaments of up to 200 μm length (Sep4-GFP, Sep5-GFP), bars of up to 100 nm in length (Sep3-GFP), and puncta (Sep6-GFP) in hyphae grown in complete medium. (**B**) and (**C**) Septins localized to invasive hyphal constrictions at rice cell junctions that mediate fungal cell-to-cell movement during *M. oryzae* invasive growth, as shown by live cell imaging of infected rice leaf sheaths. Scale bar = 10 μm.

Fig.S4

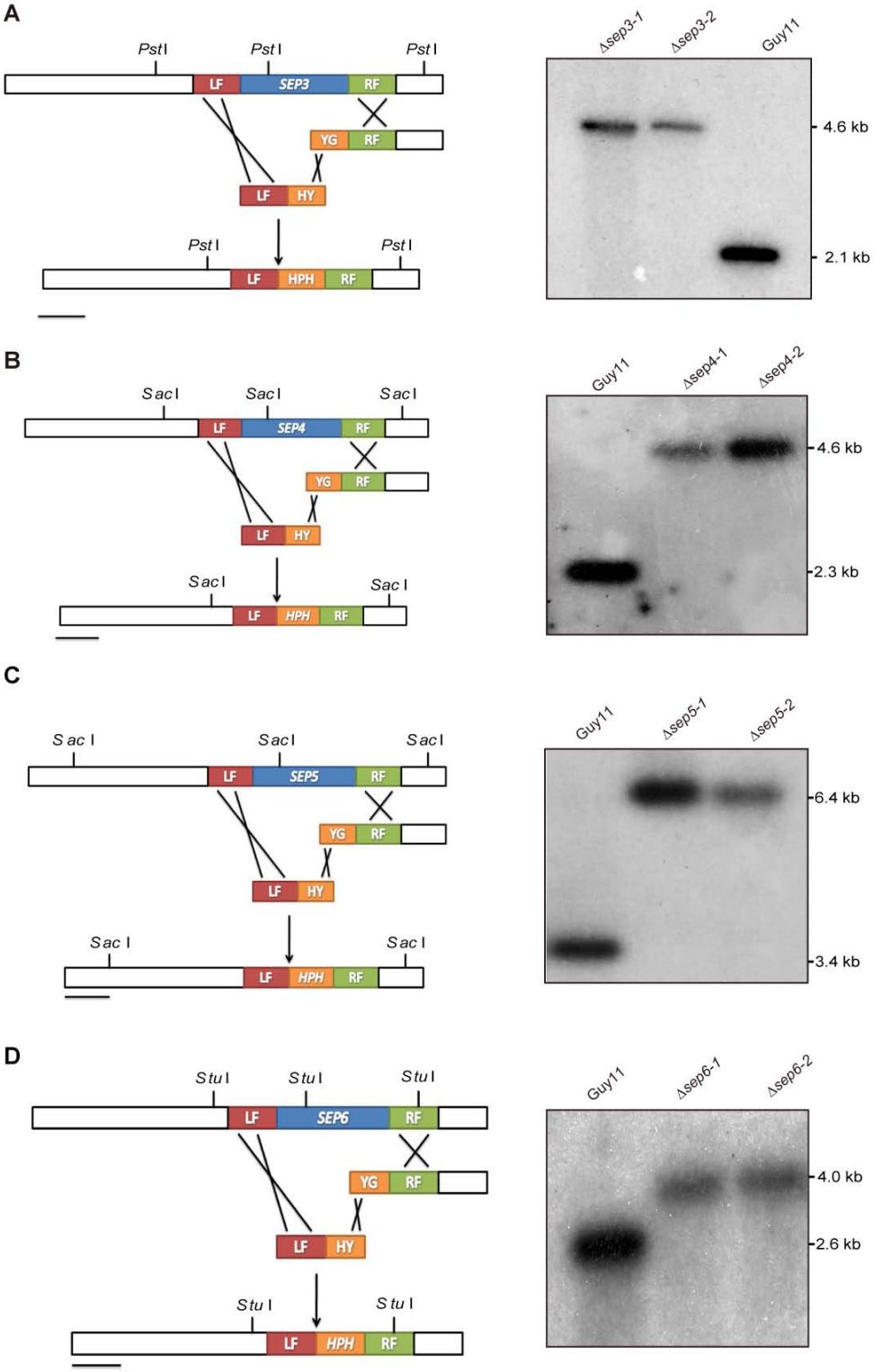
A
Pst I
Pst I
Pst I
LF
SEP3
RF
YG
RF
LF
HY
Pst I
Pst I
LF
HPH
RF
Δsep3-1
Δsep3-2
Guy11
4.6 kb
2.1 kb
B
Sac I
Sac I
Sac I
LF
SEP4
RF
YG
RF
LF
HY
Sac I
Sac I
LF
HPH
RF
Guy11
Δsep4-1
Δsep4-2
4.6 kb
2.3 kb
C
Sac I
Sac I
Sac I
LF
SEP5
RF
YG
RF
LF
HY
Sac I
Sac I
LF
HPH
RF
Guy11
Δsep5-1
Δsep5-2
6.4 kb
3.4 kb
D
Stu I
Stu I
Stu I
LF
SEP6
RF
YG
RF
LF
HY
Stu I
Stu I
LF
HPH
RF
Guy11
Δsep6-1
Δsep6-2
4.0 kb
2.6 kb

Fig. S4. Southern blot analysis of targeted gene deletion mutants.

Genomic DNA was extracted from each putative transformant and the wild type Guy11 strain and digested with the restriction enzymes indicated in the schematic diagrams on the left. Blots were probed with a restriction fragment comprising the Left Flank (LF) after fractionation by gel electrophoresis. The size difference in each blot is consistent with successful replacement of gene coding regions of each septin gene with the resistance cassette *HPH*. (**A**) Targeted gene deletion of *M. oryzae SEP3*. *Pst*I digested genomic DNA from Guy11 wild type strain and putative Δ*sep3* transformants were gel fractionated and probed with Left Flank (1.5 kb upstream of start codon). DNA gel blot analysis showed a 2.5 kb difference which is consistent with successful replacement of *SEP3* gene with the resistance cassette. (**B**) Targeted gene deletion of *M. oryzae SEP4*. *Sac*I digested genomic DNA from Guy11 wild type strain and putative Δ*sep4* transformants were gel fractionated and probed with Left Flank (1.5 kb upstream of start codon). DNA gel blot analysis showed a 2.2 kb difference which is consistent with successful replacement of *SEP4* gene with the resistance cassette. (**C**) Targeted gene deletion of *M. oryzae SEP5*. *Sac*I digested genomic DNA from Guy11 wild type strain and putative Δ*sep5* transformants were gel fractionated and probed with Left Flank (1.5 kb upstream of start codon). DNA gel blot analysis showed a 3.0 kb difference which is consistent with successful replacement of *SEP5* gene with the resistance cassette. (**D**) Targeted gene deletion of *M. oryzae SEP6*. *Stu*I digested genomic DNA from Guy11 wild type strain and putative Δ*sep6* transformants were gel fractionated and probed with Left Flank (1.5 kb upstream of start codon). DNA gel blot analysis showed a 1.4 kb difference which is consistent with successful replacement of *SEP6* gene with the resistance cassette.

Fig.S5

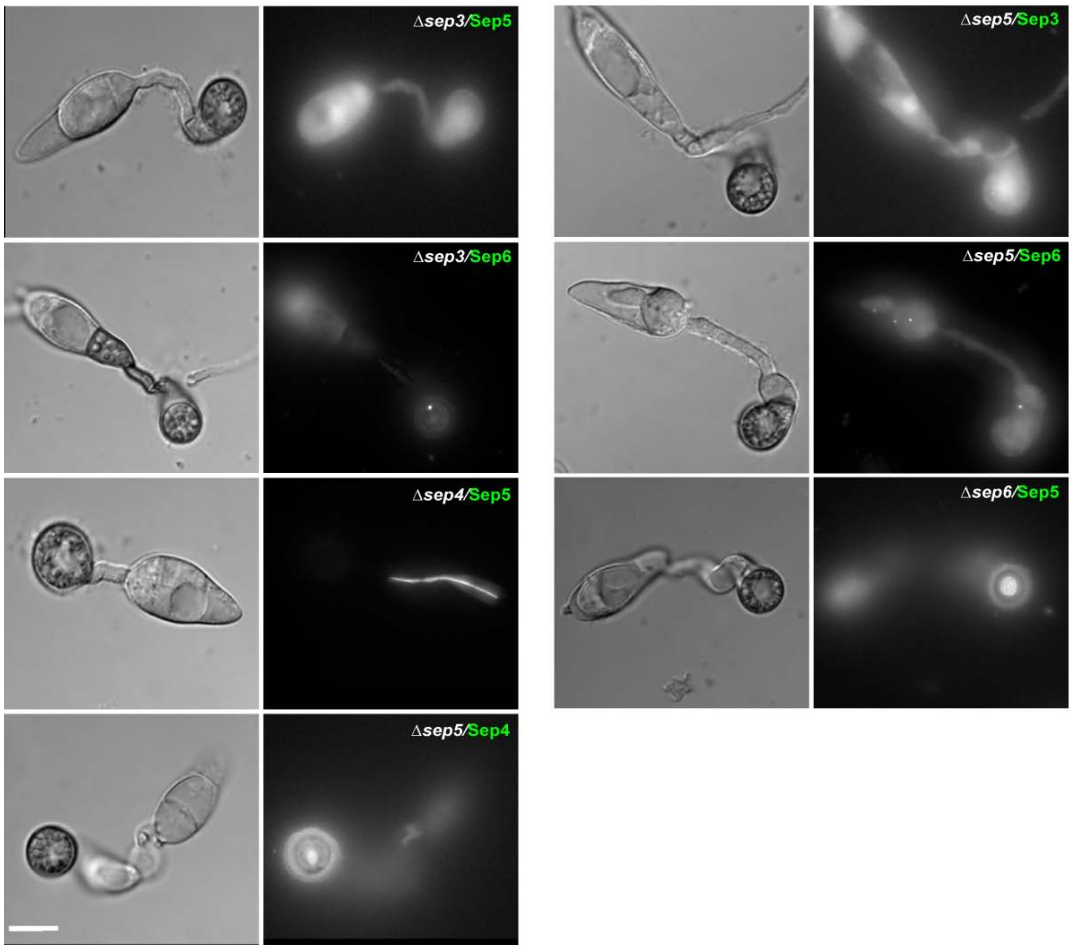
Δsep3/Sep5
Δsep5/Sep3
Δsep3/Sep6
Δsep5/Sep6
Δsep4/Sep5
Δsep6/Sep5
Δsep5/Sep4

Fig. S5. Appressorium pore septin ring formation requires all the core *M. oryzae* septins.

Epifluorescence micrographs to show localization of septins in each different septin mutant background. The *M. oryzae* Δ*sep3* mutant was transformed with *SEP5-GFP* and *SEP6-GFP* plasmids, The Δ*sep4* mutant was transformed with *SEP5-GFP*, Δ*sep5* was transformed with *SEP3-GFP, SEP4-GFP*, and *SEP6-GFP* and Δ*sep6* was transformed with *SEP5-GFP*. Single copy transformants were selected in each case and visualized by laser excitation epifluorescence microscopy. Septin ring formation was assessed 24h during appressorium development. Scale bar = 10 μm.

Fig.S6

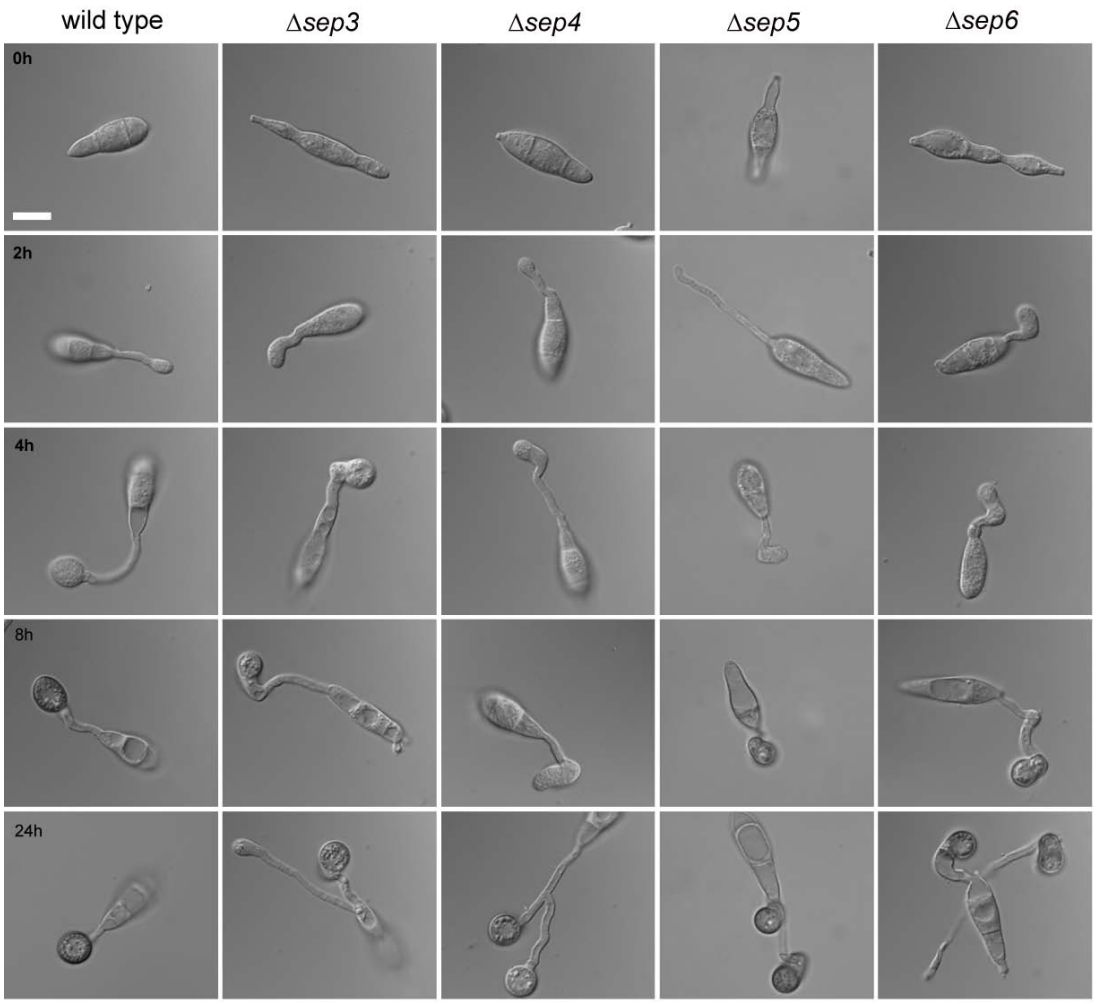

Fig. S6. Septin mutants of *M oryzae* show developmental effects on germ tube morphology and appressorium development in *Magnaporthe oryzae*

M. oryzae conidia were germinated on an inductive artificial surface to observe appressorium development in conidia (0 h), germlings (2 h), initial appressoria (4 h) melanised appressoria (8 h) and mature appressoria (24 h). Each septin mutant, Δ*sep3,* Δ*sep4,* Δ*sep5,* and Δ*sep6* mutants showed defects in germ tube formation, appressorium development and maturation. Conidial cell shape was aberrant being longer than the isogenic wild type strain, germ tubes were larger in diameter, and melanisation of appressorium was delayed. Strikingly, deletion of each septin often resulted in formation of two nascent appressoria at 24h. Scale bar = 10 μm.

Fig.S7

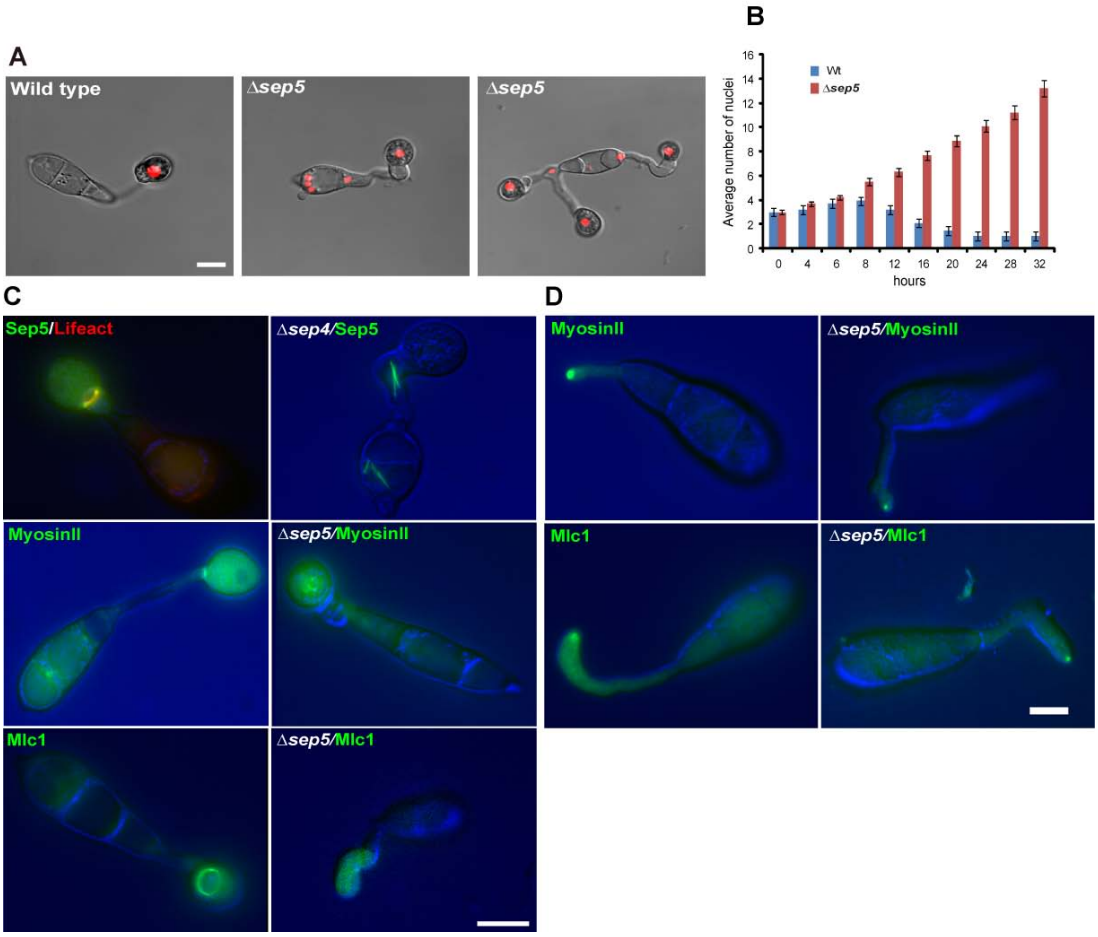
A
Wild type
Δsep5
Δsep5
B
Wt
Δsep5
Average number of nuclei
hours
C
Sep5/Lifeact
Δsep4/Sep5
MyosinII
Δsep5/MyosinII
Mlc1
Δsep5/Mlc1
D
MyosinII
Δsep5/MyosinII
Mlc1
Δsep5/Mlc1

Fig. S7. *M. oryzae* septin mutants show a cell cycle phenotype during appressorium development. (A). Micrographs of H1-RFP localization showing that septin mutants undergo unrestricted nuclear division during appressorium development. In wild type cells of *M. oryzae*, the mature appressorium contains a single nucleus whereas in septin mutants nuclei accumulate. Scale bar = 10 μm. (**B**) Bar chart showing the number of nuclei in Guy11 and septin mutants during appressorium development (mean ± SD, three experiments). (**C**) Sep4-GFP and Sep5-GFP form a cytokinetic ring at the neck of the appressorium, which colocalizes with an actomyosin ring, visualised with Lifeact-RFP. Myosin II and Myosin light chain 1 (Mlc1) are known components of actomyosin ring formation during cytokinesis. Expression of translational GFP fusions of Mlc1-GFP and MyoII-GFP in Guy11 and *sep5* mutant showed similar patterns of localization to the appressorium neck, prior to mitosis and their localization depend on septins. (**D**) Localization of Myosin II and Mlc1 to the germ tube tip in wild type and septin mutant germlings. Scale bar =10 μm.

Fig.S8

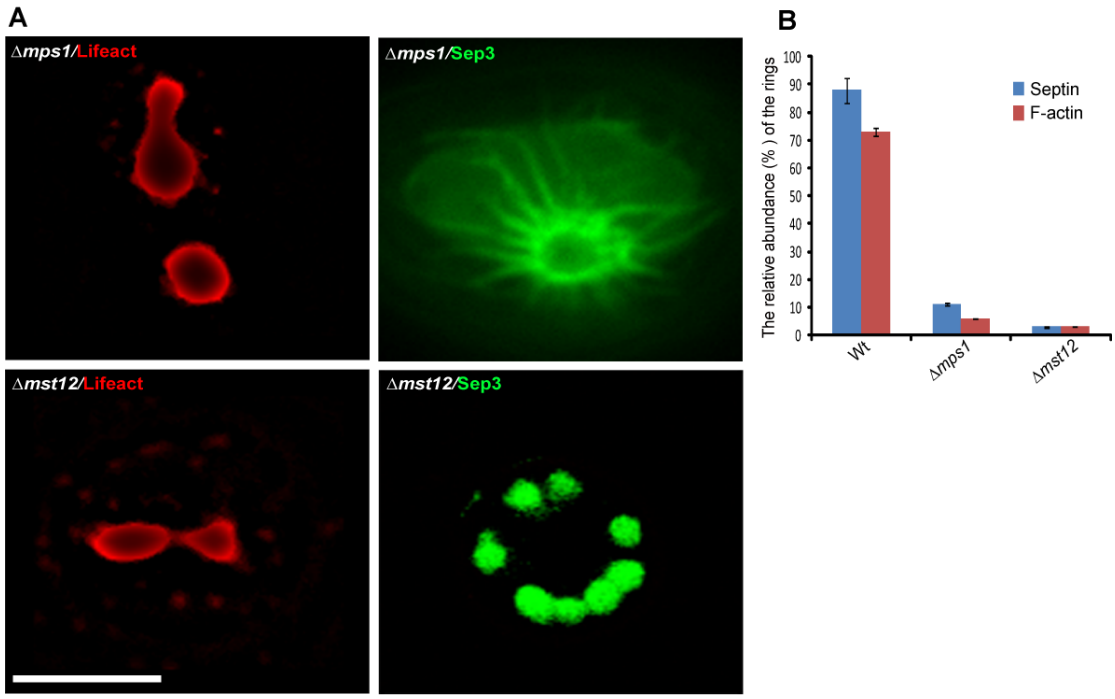
A
Δmps1/Lifeact
Δmps1/Sep3
Δmst12/Lifeact
Δmst12/Sep3
B
The relative abundance (%) of the rings
100
90
80
70
60
50
40
30
20
10
0
Septin
F-actin
Wt
Δmps1
Δmst12

Fig. S8. Appressorium pore septin and actin rings do not form in mutants defective in appressorium mediated plant infection.

(**A**) The Δ*mps1* MAP kinase mutant and Δ*mst12* transcription factor mutants are unable to undergo appressorium-mediated plant infection due to defects in penetration peg emergence. Expression of Sep3-GFP and LifeAct-RFP in Δ*mps1,* Δ*mst12* mutant revealed defects in septin and actin ring formation at the appressorium pore. (**B**) Bar charts showing the frequency of ring formation in appressoria of each mutant (mean ±SD, three experiments).

Fig.S9

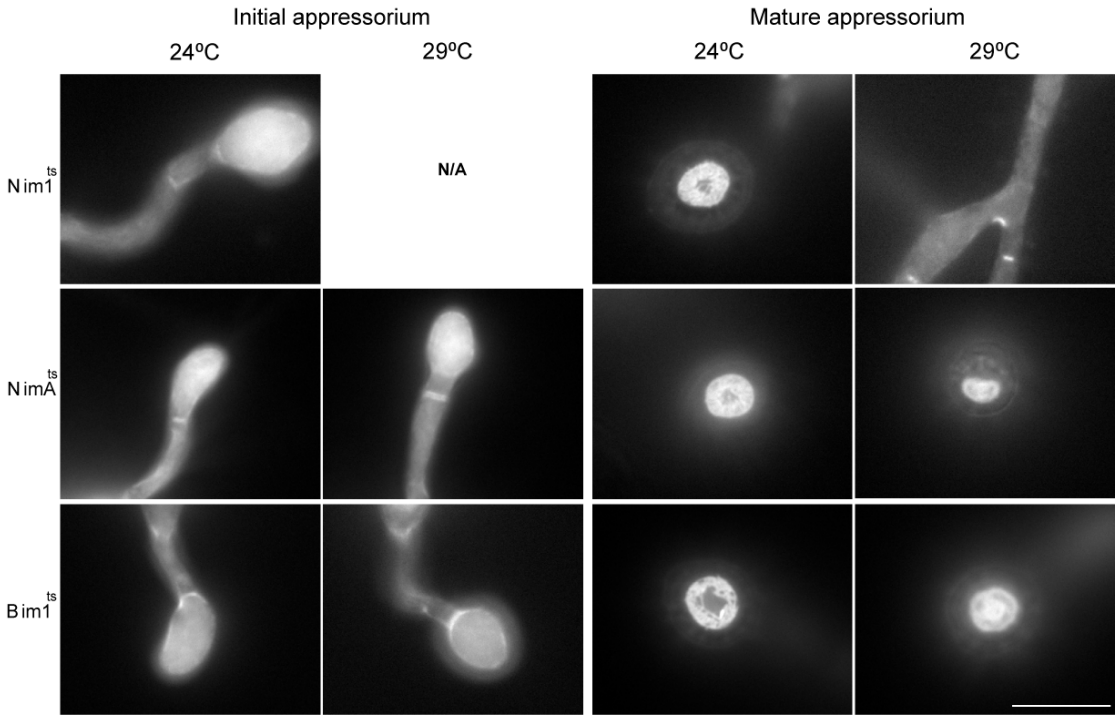
Initial appressorium
Mature appressorium
24ºC
29ºC
24ºC
29ºC
Nim1ts
N/A
NimAts
Bim1ts

Fig. S9. Assembly of the appressorium pore septin ring in *M. oryzae* is controlled by cell cycle checkpoints.

Septin ring formation was monitored by expression of Sep5-GFP in temperature-sensitive mutants of *M. oryzae* showing conditional blocks at distinct points in the cell cycle (*44*). The $Nim1^{ts}$ mutant is affected at the onset of S-phase undergoing aberrant mitoses in the absence of DNA replication at the semi-restrictive temperature (29 °C). Septin ring formation was blocked under these conditions as appressorium differentiation did not occur. NimA mutants show a temperature sensitive block at the G2-M transition and, as a consequence, cannot form mature, melanised appressoria. Cytokinetic septin ring formation occurred normally (*44*) but septin ring formation at appressorium pore was blocked, consistent with septin ring formation requiring maturation of the infection cell. Bim1 mutants are impaired in completion of mitosis, showing a temperature sensitive block prior to anaphase and mitotic exit. Such mutants are able to form melanised appressoria, but these are unable to penetrate rice cuticles and develop penetration hyphae (*44*). Expression of Sep5-GFP showed impairment of appressorium pore septin ring formation at the semi-permissive temperature. Scale bar = 10 μm.


A
Wt
Δsep3::SEP3-GFP
Δsep4::SEP4-GFP
Δsep5::SEP5-GFP
Δsep6::SEP6-GFP

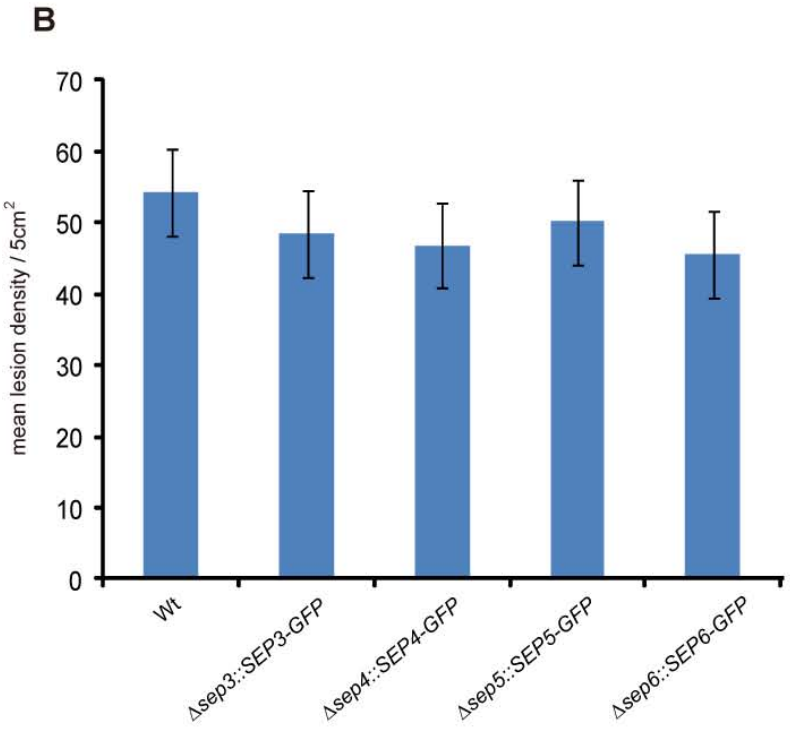
B
mean lesion density / 5cm2
70
60
50
40
30
20
10
0
Wt
Δsep3::SEP3-GFP
Δsep4::SEP4-GFP
Δsep5::SEP5-GFP
Δsep6::SEP6-GFP

Fig. S10. Complementation of septin mutants with Septin-GFP fusion proteins restores the ability to cause rice blast disease. (**A**) Expression of translational septin-GFP fusions restored virulence to each corresponding septin mutant on rice CO-39. Expression of *SEP3-GFP*, *SEP4-GFP*, *SEP5-GFP* and *SEP6-GFP* was carried out and single copy transformants selected by Southern blot analysis. Lesion density and size were identical to those following infection of rice seedlings with the wild type Guy11 strain. (**B**) Bar charts showing the number of lesions per 5 cm^2. (P values are 0.43 for Sep3, 0.31 for Sep4, 0.58 for Sep5 and 0.24 for Sep6) (n=30 for each septin mutant) (mean ±SD, three experiments).

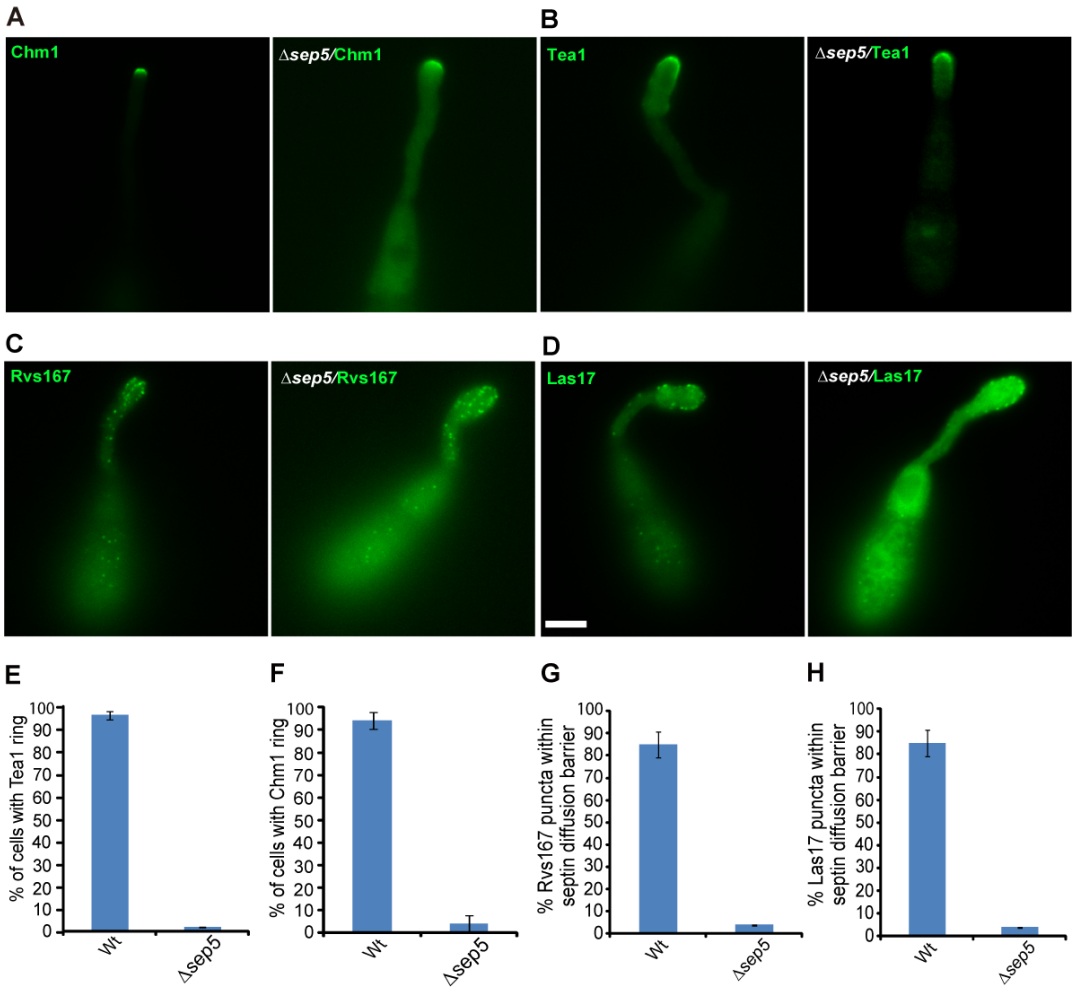
A
Chm1
Δsep5/Chm1
B
Tea1
Δsep5/Tea1
C
Rvs167
Δsep5/Rvs167
D
Las17
Δsep5/Las17
E
% of cells with Tea1 ring
F
% of cells with Chm1 ring
G
% Rvs167 puncta within septin diffusion barrier
H
% Las17 puncta within septin diffusion barrier
Wt
Δsep5

Fig. S11. Localization of Chm1, Tea1, I-BAR protein Rvs167 and N-WASP protein Las17 occurs normally in germlings of septin mutants of *M. oryzae*.

Micrographs to show that in a Δ*sep5* mutant, Chm1-GFP and Tea1-GFP localize as a crescent at the tip of the germ tube in the same way as in Guy11, (**A**) and (**B**) respectively. The I-BAR protein Rvs167-GFP and N-WASP protein Las17-GFP show punctate distribution predominantly at the tips of germ tubes in both Δ*sep5* and wild type strains, (**C**) and (**D**) respectively. Bar charts showing the localization of Tea1-GFP and Chm1-GFP in wild type and Δ*sep5* strains**, (E)** and **(F)** respectively. Bar charts to show the mislocalization of Rvs167-GFP and Las17-GFP in Δ*sep5* strain**, (G)** and **(H)** respectively. Scale bar = 10 μm. (mean ±SD, three experiments).

Table S1: Sep5 interacting proteins as identified by co-immunoprecipitation experiments[a].

	MS/MS Search Score	Spectral Intenstiy
Sep5	178.1 ± 10	5.03E+05
Sep3	160.9 ± 20	3.88E+05
Sep6	145.2 ± 20	6.28E+05
Sep4	107.2 ± 20	1.95E+05
Tubulin α 8 chain	40.77 ± 15	1.97E+05
Actin	31.1 ± 15	2.42E+05
Lte1[b]	11.7 ± 5	1.43E+06

[a] Values given are the mean of three independent experiments.
[b]Lte1 was pulled down only at the 4h time point during appressorium development, which coincides with the cytokinetic septin ring formation.

Table S2: Primers used in this study

Primer Name	DNA Sequence (5`-3`)
Sep350.1	CAAGGAATCAGGGGACTACAGTAT
Sep3M13F	GTCGTGACTGGGAAAACCCTGGCGATGAATGCGGACTTTGTCGTTACA
Sep3M13R	TCCTGTGTGAAATTGTTATCCGCTCAGAGTTGGAGGAGAAAAAGGCAC
Sep330.1	TTACCATCAGACCCCAACACCTAC
Sep450.1	TTTGCAGATGGCGGTTTGGTCCTT
Sep4m13f	GTCGTGACTGGGAAAACCCTGGCGGATGAAACTGGGGACGGACGTAGA
Sep4m13R	TCCTGTGTGAAATTGTTATCCGCTGCCGCAGCTCGCAAAGGATGACTA
Sep430.1	TGACATGACAACTCTCGGGCCAAC
Sep550.1	AGTATCAGTGGCAAAATTGACAAG
Sep5M13F	GTCGTGACTGGGAAAACCCTGGCGCTTGAAAGGAATTTGGTTGGTTAG
Sep5M13R	TCCTGTGTGAAATTGTTATCCGCTCCGCCTCACTATTATGTCTTCTTA
Sep530.1	AATTCTTGAGATCGTGTGCAATGC
Sep650.1	TCCACAGCCATACAAGAGAAAGAT
Sep6M13F	GTCGTGACTGGGAAAACCCTGGCGTAAAGGAATGACCGCAAGCAACTA
Sep6M13R	TCCTGTGTGAAATTGTTATCCGCTCGTTCAGGTCTGTTAAGCTGGATA
Sep630.1	TCAGCCACCTTGAGTACATAATCG
Sep3SUR	GATTATTGCACGGGAATTGCATGCTCTCACCCGATGTCAAAGACAGACCAGCCC
Sep3GFP	GGTGAACAGCTCCTCGCCCTTGCTCACCATACGGAGTGAGAAACCCTTCCTCTT
Sep4SUR	GATTATTGCACGGGAATTGCATGCTCTCACCTAGTTACTGGACTAGCCTAGACG
Sep4GFP	GGTGAACAGCTCCTCGCCCTTGCTCACCATGTAGCCATTCATAGTCATCCTTTG
Sep5SUR	GATTATTGCACGGGAATTGCATGCTCTCACCGGTCTGCGCACCAGCGTTACCAG
Sep5GFP	GGTGAACAGCTCCTCGCCCTTGCTCACCATGTTGCCGTCTTCCCCGTTTGCCTC
Sep6SUR	GATTATTGCACGGGAATTGCATGCTCTCACCAAATGCGACGGCAGAAACAGGGC
Sep6GFP	GGTGAACAGCTCCTCGCCCTTGCTCACCATGCGACGGCCATGCGAACGGGCAGC
Sep5BARF	ctccttgatgacgtcctcggaggaggccatGTTGCCGTCTTCCCCGTTTGCCTC
Sep511th Rev	CATCATCTTCTAACCGGTGGTAAA
Sep517th Forw	GTGACTTTTACCACCGGTTAGAAGATGATGGTGAAGAAGGGGATTCAGTTCTGT
Mlc1SUR	GATTATTGCACGGGAATTGCATGCTCTCACGTACCATTCGCAACGTGTTTGGAG
Mlc1GFP	GGTGAACAGCTCCTCGCCCTTGCTCACCATGTTGGCCAGAATGGTCCTAACAAG
Mss4SUR	GATTATTGCACGGGAATTGCATGCTCTCACCAGCAGCGTGCCATACGAGTGACG
Mss4GFP	GGTGAACAGCTCCTCGCCCTTGCTCACCATTGTCGGGAGCGGCGGGAGGGCTTT
Stt4PromF	tgcacgggaattgcatgctctcacgtcgacCATGGTCGATAGGCTTGTGCG
Stt4PromR	GATGTCGGGCTAGATCGAGGG
GFPStt4F	CGCTGTAAACCCTCGATCTAGCCCGACATCATGGTGAGCAAGGGCGAGGAGCTG
GFPR	CTTGTACAGCTCGTCCATGCCGTG
Stt4GFPF	ATCACTCACGGCATGGACGAGCTGTACAAGATGGCGACCAACATTCGCCAGAGGGCGCTT
Stt4R	TTCACACAGGAAACAGCTATGACCATGATTGAGCATTTCTCGCAACCCATAA
Chm1SUR	GATTATTGCACGGGAATTGCATGCTCTCACCCACGCAAAAGGTGAAGAAGC
Chm1GFP	GGTGAACAGCTCCTCGCCCTTGCTCACCATTTTGGCATGCTTCTTGAAGGC
SurF	AACTGTTGGGAAGGGCGATCGGTGCGGGCCGTCGACGTGCCAACGCCACAGTGC
SurR	GTCGACGTGAGAGCATGCAATTCC
Myo2PromF	tgcacgggaattgcatgctctcacgtcgacTGAATTTTGAGACGAAGGTCCCCA

Myo2PromR	GTTGATCTGCCCGTTGGGAGGCCG
GFPMyo2F	CTGATACGGCCTCCCAACGGGCAGATCAACATGGTGAGCAAGGGCGAGGAGCTG
GFPR	CTTGTACAGCTCGTCCATGCCGTG
Myo2GFPF	ATCACTCACGGCATGGACGAGCTGTACAAGATGGCGGAGACGTACGATGTCGGG
Myo2R	TTCACACAGGAAACAGCTATGACCATGATTGCCAGCGTCTCGCAGTGTGTCGTC
Las17SUR	GATTATTGCACGGGAATTGCATGCTCTCACACAAAATCCACCAAGACACCA
Las17GFP	GGTGAACAGCTCCTCGCCCTTGCTCACCATCCAATCATCATCTGAAGCTTC
Tea1SUR	GATTATTGCACGGGAATTGCATGCTCTCACAGTCTTTCACCTGCCCGTGGT
Tea1GFP	GGTGAACAGCTCCTCGCCCTTGCTCACCATTGCGTTGTCGAGCCTCTTCCT
Rvs167SUR	GATTATTGCACGGGAATTGCATGCTCTCACCACTGATGATGGGGTCAAGTCTGA
Rvs167-GFP	GGTGAACAGCTCCTCGCCCTTGCTCACCATTGATTGCAACTGCACATAGTTACC
CDC3F-EcoRI	GAATTCatgccgaaccagtggcatcgc
CDC3Rcomp-XbaI	TCTAGAttagcgcaggctaaagccttt
CDC10F-EcoRI	GAATTCATGGCGGCCATGCCTGCTGCC
CDC10RComp-XbaI	TCTAGACTAGTAGCCATTCATAGTCAT
CDC11F-EcoRI	GAATTCATGTCGTTTCCCGCCAAGATG
CDC11RComp-XbaI	TCTAGACTAGTTGCCGTCTTCCCCGTT
CDC12F-EcoRI	GAATTCATGGCTCCCGCTGCGACCGAG
CDC12RComp-XbaI	TCTAGATTAGCGACGGCCATGCGAACG

Movie S1: 3D reconstruction of the septin ring at the base of appressorium.
Visualized by laser excitation epifluorescence microscopy of Sep5-GFP in appressoria, 8h after inoculation.

References:

41. H. Leung *et al.*, *Curr Genet* **17**, 409 (1990).
42. N. J. Talbot, D. J. Ebbole, J. E. Hamer, *Plant Cell* **5**, 1575 (1993).
43. J. Sambrook, E. F. Fritsch, T. Maniatis, *CSHL press, New York, USA* (1989).
44. D. G. Saunders, S. J. Aves, N. J. Talbot, *Plant Cell* **22**, 497 (2010).
45. P. Kankanala, K. Czymmek, B. Valent, *Plant Cell* **19**, 706 (2007).
46. R. Lindsey, Y. Ha, M. Momany, *Plos One* **5** (2010).
47. M. J. Kershaw, N. J. Talbot, *Proc Natl Acad Sci U S A* **106**, 15967 (2009).
48. J. A. Sweigard, F. G. Chumley, B. Valent, *Mol Gen Genet* **232**, 183 (1992).
49. C. K. Raymond, T. A. Pownder, S. L. Sexson, *Biotechniques* **26**, 134 (1999).
50. M. J. Egan, Z. Y. Wang, *et al.*, *Proc Natl Acad Sci U S A* **104**, 11772 (2007).

Chapter4

NADPH oxidases regulate septin-mediated cytoskeletal re-modeling during plant infection by the rice blast fungus

Lauren S. Ryder[1], Yasin F. Dagdas[1], Thomas A. Mentlak[1], Michael J. Kershaw[1], Christopher R. Thornton[1], Martin Schuster[1], Jisheng Chen[2], Zonghua Wang[2] and Nicholas J. Talbot[1*]

[1]School of Biosciences, University of Exeter, Geoffrey Pope Building, Stocker Road, Exeter, England, EX4 4QD, United Kingdom

[2]The School of Life Sciences, Fujian Agriculture and Forestry University, Fuzhou, China

Corresponding author. E-mail: N.J.Talbot@exeter.ac.uk Tel: +44 (0)1392 725172; Fax: +44 (0)1392 263434.

Final Accepted Manuscript: Ryder, L.S. et al. NADPH oxidases regulate septin-mediated cytoskeletal remodeling during plant infection by the rice blast fungus. *Proceedings of the National Academy of Sciences of the United States of America* **110**, 3179-84 (2013)

The rice blast fungus *Magnaporthe* oryzae infects plants with a specialized cell called an appressorium, which uses turgor to drive a rigid penetration peg through the rice leaf cuticle. Here, we show that NADPH oxidases (Nox) are necessary for septin-mediated re-orientation of the F-actin cytoskeleton to facilitate cuticle rupture and plant cell invasion. We report that the Nox2-NoxR complex spatially organises a heteroligomeric septin ring at the appressorium pore, required for assembly of a toroidal F-actin network at the point of penetration peg emergence. Maintenance of the cortical F-actin network during plant infection independently requires Nox1, a second NADPH oxidase, which is necessary for penetration hypha elongation. Organisation of F-actin in appressoria is disrupted by application of anti-oxidants, while latrunculin-mediated depolymerisation of appressorial F-actin is competitively inhibited by reactive oxygen species (ROS), providing evidence that regulated synthesis of ROS by fungal NADPH oxidases directly controls septin and F-actin dynamics.

\body

Introduction

NADPH oxidases (Nox) are flavoenzymes that function by transferring electrons across biological membranes to catalyze reduction of molecular oxygen to superoxide (1, 2). In animal cells, Nox enzymes are implicated in cell proliferation, cell signalling and apoptosis (1-3), while in plants Nox are necessary for programmed cell death (4), the response to environmental stresses (4), pathogen infection (5), and polarised growth of root hairs (6). In filamentous fungi, Nox are necessary for cellular differentiation during sexual reproduction and for developmental processes that involve transitions from non-polarised to polarised cell growth, such as tissue invasion by mutualistic and pathogenic

fungi, and fungal virulence (7-9). The underlying function of Nox enzymes in these diverse developmental processes remains unclear.

In this study we set out to investigate the role of ROS synthesis by Nox during plant infection by the devastating rice blast pathogen *M. oryzae* (10). Rice blast disease is considered a major threat to global food security and remains difficult to control (11). Nox1 and Nox2 are necessary for an oxidative burst that is required for plant infection by the fungus (12), but why this is necessary for rice blast disease is not known. To infect rice plants, *M. oryzae* forms a specialized infection structure called an appressorium (10). This dome-shaped cell generates enormous turgor of up to 8.0MPa (12), which is translated into physical force at its base to rupture the rice leaf cuticle using a narrow, rigid, penetration peg which invades plant tissue. Recently, it has been reported that septin GTPases scaffold cortical F-actin in the appressorium at the site of plant infection, acting via the ezrin-radixin-moesin (ERM) protein, Tea1, and specific phosphatidylinoside interactions at the fungal plasma membrane (14). *M. oryzae* septins assemble into a hetero-oligomeric ring that surrounds the appressorium pore, a region at the base of the infection cell from which the penetration peg emerges. This acts to scaffold and re-organise the F-actin cytoskeleton and as a partitioning diffusion barrier to localize Bin-Amphiphysin-RVS (BAR)-domain proteins, implicated in membrane curvature and protrusion of the penetration peg through the rice leaf surface (13).

In this report, we show that NADPH oxidases play distinct, but essential, roles in F-actin re-modelling during plant infection. The Nox2 complex, which includes the $p67^{phox}$-like regulator NoxR, is necessary for assembly of septin GTPases at the appressorium pore, which is required for re-orientation of the F-actin cytoskeleton at the point of plant infection. Consistent with this, *Δnox2* mutants are unable to initiate penetration peg formation and cannot infect rice plants. We also show that Nox1 is required for correct organisation of the toroidal F-actin network, acting after septin

assembly. *Δnox1* mutants therefore initiate penetration peg development, but fail to elongate invasive hyphae to rupture the rice cuticle. These functions appear to require the regulated synthesis of reactive oxygen species and are likely to be a direct consequence of the enzymatic activity of NADPH oxidases. Our results provide evidence that Nox complexes play critical roles in both initiation and maintenance of polarised growth by the rice blast fungus during plant infection.

Results

***M. oryzae* NADPH oxidase mutants are impaired in F-actin organisation during appressorium development.**

To understand the role of NADPH oxidases during infection-associated-development, we identified *M. oryzae NOXR* (MGG_05280.6), which shares 38% amino acid sequence similarity with *Homo sapiens* $p67^{phox}$ (Fig. S1) and generated a Δ *noxR* null mutant (Fig. S2). We then introduced a LifeAct-RFP gene fusion (14) into isogenic *M. oryzae* Δ*nox1,* Δ*nox2*, Δ*nox1*Δ*nox2* (15) and Δ*noxR* mutants to observe organisation of F-actin by live cell imaging (13, 14). In the wild type *M. oryzae* strain, Guy11, a large toroidal-shaped F-actin network (~5.9μm in diameter) formed around the appressorium pore (13), which we visualised by live cell imaging and topologically characterized using transverse line scan analysis of LifeAct-RFP fluorescence intensity in the appressorium (Fig. 1*A*, see Movie S1). In Δ*nox1* mutants, the F-actin network was partially disorganised (Fig. 1, Fig. S3, Movie S2). Individual actin cables were not observed and a dense un-organized patch of actin instead accumulated at the appressorium pore (2.5μm ± 0.4μm in diameter, n=20). In the Δ*nox2* mutant, F-actin accumulated at the appressorium pore in a dense, unorganized patch (3.8μm in diameter ± 0.3 μm, n=20), shown in Fig. 1*A* and Movie S3. A similar pattern was observed in both the Δ*nox1*Δ*nox2* double mutant and in a Δ*noxR* mutant (4.2μm in diameter ± 0.4

μm, n=20), where a dense unorganized patch of actin was located at the appressorium pore (Fig. 1, Movies S4, S5, Fig. S3). To understand the nature of the F-actin network, we investigated fluorescence recovery of LifeAct-RFP after partial photobleaching. We found 75% recovery of fluorescence after 3.5 min, consistent with the appressorium F-actin toroidal network being highly dynamic (Fig.1*C*, see Movie S6). We conclude that F-actin organisation at the appressorium pore in *M. oryzae* requires Nox1, Nox2 and NoxR.

To investigate why Nox1 and Nox2/NoxR appear to play distinct roles in F-actin organisation during appressorium maturation, we decided to express Nox1-GFP, Nox2-RFP and GFP-NoxR gene fusions in *M. oryzae* (Fig. S4*A,B*). Nox1-GFP was predominantly localised at the plasma membrane during appressorium maturation (4-8 h) with evidence for subsequent endocytosis and internalisation apparent at later times. By contrast, Nox2-RFP was initially found at the appressorium cortex (4h), but was predominantly intracellular during appressorium maturation (8-12h) and during cuticle penetration (Fig. S4*B*). Nox2-RFP was observed in intracellular vesicles throughout appressorium maturation. NoxR-GFP also showed intracellular localisation with accumulation in the cytoplasm and vesicles. Transcriptional profile analysis showed distinct patterns of gene expression with *NOX2* and *NOXR* genes showing much higher relative levels of expression during appressorium maturation (Fig. S4*C*). We conclude that Nox1 and Nox2/NoxR act at different sub-cellular locations during appressorium morphogenesis.

Nox2 is essential for septin ring assembly at the appressorial pore.

We reasoned that Nox1 and Nox2 might act in distinct ways to regulate F-actin assembly and organisation and decided to test this idea. In *M. oryzae*, four septin GTPases (Sep3, Sep4, Sep5, and Sep6) are known to form a hetero-oligomeric ring at

the appressorium pore (~5.9µm in diameter) (13), which is necessary for F-actin organisation. We therefore expressed Sep5-GFP in Δ*nox1*, Δ*nox2* Δ*nox1*Δ*nox2* and Δ*noxR* mutants. In Guy11 and the Δ*nox1* mutant, a Sep5-GFP septin ring was present at the appressorium pore (Fig 2*A*). In the Δ*nox2* mutant, however, Sep5-GFP formed a dis-organised mass in the infection cell (3.2µm in diameter ± 0.3 µm, n=20; $P<0.05$ compared to wild type) (Fig. S5), which was also observed in a Δ*nox1*Δ*nox2* mutant (3.5µm in diameter ± 0.6 µm, n=20; $P<0.05$) (Fig. 2*A*). In Δ*noxR* mutants, aberrant septin rings formed, which were 19% smaller in diameter (mean = 4.76µm, n = 20) to Sep5-GFP rings in Guy11 (Fig. 2). We also expressed a Chm1-GFP fusion in each of the Nox mutants. Chm1 is a protein kinase that in yeast is known to phosphorylate septins (16) and in *M. oryzae* is distributed in a ring conformation around the appressorium pore (13) (Fig. 2*B*). A Chm1-GFP ring was present in Guy11 and Δ*nox1* mutants, but disorganised in Δ*nox2* and Δ*noxR* mutants, consistent with a role for Nox2 in the regulation of septin assembly and Chm1 kinase localisation (Fig. 2*B*). Quantitative analysis confirmed that Nox2 is essential for septin and Chm1 ring assembly, showing more severe disruption of septin ring assembly than Δ*nox1* or Δ*noxR* mutants (Fig. S6*A*,*B*). The N-WASP protein Las17, a component of the actin-polymerizing Arp2/3 complex, was observed by expression of a Las17-GFP fusion and localised as puncta in the appressorium pore in Guy11 (14) and the Δ*nox1* mutant, whereas in Δ*nox2* and Δ*noxR* mutants Las17-GFP localisation was disrupted, with the protein distributed diffusely in the cytoplasm and plasma membrane (Fig S7). The ERM domain fusion protein Tea1-GFP, which localises as a ring of puncta at the appressorium pore in both Guy11 (14) and Δ*nox1* mutants, also showed abnormal localisation in both Δ*nox2* and Δ*noxR* mutants. The localisation of Rvs167-GFP, a BAR domain protein (14), was also affected in Δ*nox2* and Δ*noxR* mutants, with puncta present in a misshapen appressorium pore (Fig. S7). We conclude that ERM-actin

interactions at the appressorium pore, which are essential for linking cortical F-actin to the membrane to facilitate penetration peg emergence, require the Nox2/NoxR complex. Furthermore, the role of septins in spatially localising the WASP/Arp2/3 complex component Las17 and BAR domain protein Rvs167 to the appressorium pore– which mediate penetration peg emergence –is compromised in the absence of Nox2/NoxR.

Given the distinct function of Nox2 in regulating septin-mediated F-actin re-organisation, we were interested to identify other potential components of the Nox2 complex, which might be involved in its recruitment to the appressorium pore. Studies in *M. oryzae*, *Podospora anserina* and *Botrytis cinerea* have highlighted a connection between Nox2 (NoxB) and the trans-membrane tetraspanin protein, Pls1(17-19). Mutants lacking *PLS1* in these fungi strongly resemble *nox2* (*noxB*) mutants and there is a very close phylogenetic association between fungi possessing both Nox2 and Pls1 homologues(20). It has been proposed that Pls1 might therefore be associated with Nox2 activity or specific recruitment to its site of action(21). To test this idea, we therefore expressed LifeAct-RFP, Sep5-GFP and Chm1-GFP in a *M. oryzae* Δ*pls1* mutant (Fig. 2*C*). Strikingly, we observed mis-localisation of F-actin, septin and Chm1 in the absence of the Pls1 tetraspanin in the same manner as Δ*nox2* mutants.

Reactive oxygen species-dependent organisation of the F-actin regulator, gelsolin in *M. oryzae*.

We were interested to determine whether Nox-dependent cytoskeletal re-modeling was due to regulated synthesis of ROS, or a more indirect role in cell signalling. In mammalian systems, an increasing body of evidence suggests that ROS generation may affect F-actin dynamics during cell shape changes, migration and cell motility (22), for example, in human sperm (23), low-density lipoprotein-induced stress fiber formation (24), endothelial cell mitogenesis and during apoptosis (25). Anti-oxidants have been

reported to exert a direct effect on F-actin cable elongation (26), while components of Nox complexes are also known to associate with F-actin (27) or actin-binding proteins (28). The actin-binding protein, gelsolin, which regulates F-actin dynamics by uncapping free barbed ends to promote actin polymerisation and by severing existing filaments (29) has, for example, been proposed as a likely target for regulation by ROS (22). We therefore expressed gelsolin-GFP in an *M. oryzae* Guy11 strain expressing LifeAct-RFP. We observed co-localization of gelsolin-GFP and LifeAct-RFP to the appressorium pore (Fig. 3*A*), consistent with gelsolin acting as an F-actin regulator. In a Δ*nox1* mutant, gelsolin-GFP still organised into a ring structure, but in Δ*nox2* or Δ*noxR* mutants Gelsolin-GFP formed a dis-organised patch at the appressorium base (Fig. 3*B*). To understand the nature of the gelsolin ring, we investigated fluorescence recovery after partial photobleaching. We found 83% recovery of fluorescence after 8 min, consistent with gelsolin turnover being associated with F-actin dynamics (Fig. 3*C*, see Movie S7). To determine whether F-actin and septin dynamics in appressoria were directly influenced by ROS synthesis, we applied the flavo-enzyme (Nox) inhibitor, diphenyleneiodonium chloride (DPI), (15) and the anti-oxidant ascorbate, both of which prevented formation of gelsolin-GFP and septin rings, resulting instead in aberrant smaller ring structures at the appressorium pore (Fig. 3*D*). This is consistent with ROS generation being required for both F-actin and septin ring assembly. We therefore applied the actin de-polymerising agent, Latrunculin A to *M. oryzae* appressoria which (as expected) led to disruption of gelsolin-GFP organisation. However, when we applied hydrogen peroxide (H_2O_2) in the presence of latrunculin A, this partially restored gelsolin-GFP ring formation (Fig. 3*E*, *F*). The de-polymerising activity of latrunculin A can therefore be partially prevented by the presence of high concentrations of ROS. Latrunculin A-treatment of mature appressoria (at 16 h) also inhibited appressorium-mediated cuticle penetration on rice epidermal strips (Fig. S8), but this was partially

remediated by simultaneous addition of H_2O_2 (Fig. S9). We conclude that regulated synthesis of ROS by *M. oryzae* Nox proteins can directly affect F-actin dynamics.

Nox1 and Nox2 play distinct roles during plant infection.

Given the distinct phenotypes of Δ*nox1* and Δ*nox2* mutants with respect to F-actin and septin dynamics, we were interested to see how they differed in their ability to cause rice blast disease. Previously, Δ*nox1* and Δ*nox2* mutants have been shown to be non-pathogenic (15) and we confirmed that Δ*noxR* and Δ*nox1*Δ*nox2* mutants were also unable to cause rice blast disease (Fig. 4*A*). Transmission electron microscopy of appressoria, however, showed that Δ*nox1* mutants still initiated penetration peg formation from the base of the infection cell (Fig. 4*C*). These short projections were unable to extend through the plant cell wall (Fig. 4*B*) and Δ*nox1* mutants were therefore unable to colonize rice tissue and cause disease. By contrast, appressoria of Δ*nox2*, Δ*nox1*Δ*nox2* and Δ*noxR* mutants were unable to re-polarise at the appressorium pore and could not form penetration pegs (Fig. 4*D-F*). We conclude that Nox2 and NoxR are necessary for septin-mediated initiation of polarised growth of the penetration peg at the appressorium base, while Nox1 is necessary for maintenance of penetration peg elongation.

Discussion

Regulated synthesis of ROS by NADPH oxidases is necessary for a wide variety of developmental processes in mammals, plants and fungi (1,3,6). In filamentous fungi, ROS generation has, for example, been associated with hyphal tip growth, spore formation, infection structure development, conidial anastomosis tube generation, fruiting body formation, fungal-plant mutualistic interactions and fungal virulence (1, 2). These diverse roles for ROS as signalling molecules in fungi are, however, still not

well understood. The best understood NADPH oxidase is the mammalian phagocytic leukocyte $gp91^{phox}$ (or Nox2), which is necessary for the defensive oxidative burst during microbial attack. The $gp91^{phox}$ protein is part of a membrane-spanning complex (flavocytochrome b_{558}) with the adaptor protein $p22^{phox}$, and interacts with the cytosolic regulatory proteins $p40^{phox}$, $p67^{phox}$, $p47^{phox}$ and Rac GTPase (3). In total there are five Nox enzymes in humans, which have been implicated in a variety of cellular processes, including cell proliferation, apoptosis and hormone responses. This has led to the suggestion that ROS production may be a ubiquitous signaling system controlling cellular differentiation in eukaryotes (3-6). Filamentous fungi possess up to three Nox enzymes. Nox 1 (or NoxA) and Nox2 (NoxB) are similar to $gp91^{phox}$, while Nox3 (NoxC) enzymes have EF-hand domains that putatively bind Ca^{2+} in the same way as plant respiratory burst oxidases (8, 9), and Human Nox5 (3). Fungal Nox complexes appear to involve interactions with cytosolic proteins, previously implicated in the regulation of polarity (1). A recent study of the plant-associated mutualistic fungus *Epichloë festucae*, for example, showed that NoxR interacts with homologs of the yeast polarity proteins Bem1 and Cdc24 (2) and that this requires the Phox and Bem1 (PB1) protein domain, which is also necessary for localisation of these proteins to actively growing hyphal tips. *E. festucae* mutants that lack Bem1 are defective in hyphal morphogenesis and growth in culture while Cdc24 appears to be essential for viability (2). The study therefore provided evidence for an important role for fungal NADPH oxidases in the establishment of polarity and the control of cellular differentiation. This is consistent with recent findings in plant pathogenic fungi, such as *Botrytis cinerea*, *Sclerotinia sclerotiorum* and *Claviceps purpurea* where Nox proteins have been shown to be necessary for fruit body formation and appressorium function (1, 25, 26), and experiments in *Podospora anserina* which have implicated Nox proteins in polarity establishment and invasive growth (27).

In this report, we have provided evidence that the role of fungal Nox in polarised fungal growth is likely to be based on re-modelling of the F-actin cytoskeleton. When considered together, our results are consistent with a model whereby the *M. oryzae* Nox2/NoxR complex is essential for septin-mediated F-actin assembly at the appressorium pore, which is a pre-requisite for penetration peg formation and rice infection. In *Saccharomyces cerevisiae*, a recently identified Nox-encoding gene, *YNO1*, has also been recently implicated in actin cable formation (30), suggesting that regulation of F-actin dynamics may be one of the key underlying mechanisms by which Nox exerts their diverse roles in cellular differentiation. In *M. oryzae*, Nox2 is regulated as part of a complex involving NoxR and is also known to interact with Rac1 (31), a small GTPase involved in polarised cell growth and also implicated in F-actin dynamics. Gelsolin is, for instance, a downstream effector of Rac1 (32). We also found evidence that the tetraspanin Pls1 may play a role in the Nox2 complex based on its effect on septin and F-actin organisation at the appressorium pore. Nox2 is therefore essential for initiation of polarised growth from the appressorium. Remediation of the effects of the actin depolymerising agent latrunculin A upon exposure to hydrogen peroxide, furthermore suggests that role of Nox2 and NoxR in polarity establishment may be a direct consequence of the regulated synthesis of ROS by NADPH oxidases, perhaps acting directly on actin regulatory proteins such as gelsolin. It has been suggested, for instance, that ROS may increase the actin severing ability of gelsolin, by disulfide bond formation in the protein, leading to greater exposure of barbed ends and increased actin polymerisation (22).

By contrast, we found that Nox1 is not required for septin ring assembly at the appressorium pore, but is necessary for correct organisation of the F-actin network which is scaffolded at this site. Furthermore, *nox1* mutants are able to initiate penetration peg formation (and therefore establish polarised growth) but cannot elongate

invasive hyphae, suggesting that the Nox1 complex may be required for maintenance of polarised growth, which is necessary for host cell entry and pathogenesis. Previously, it was shown that Δ *nox1* mutants display increased resistance to calcofluor white, indicating a defect in cell wall organisation, affecting chitin deposition. The lighter pigmentation of Δ *nox1* mutants also suggests a role in melanin biosynthesis or its polymerisation in the cell wall. These phenotypes are notably absent in the other Nox mutants, suggesting that Nox1 may supply ROS to the cell wall for oxidative cross-linking of proteins and this may be necessary for maintenance of polarised growth.

An important question that arises from this study is how two Nox complexes in the *M. oryzae* appressorium, which are likely to involve the same $p67^{phox}$ regulator, NoxR, can fulfil different functions. Our observations suggest that specificity may be due, at least in part, to their distinct sub-cellular locations. Nox1 occurs predominantly in the plasma membrane, resulting in extracellular ROS generation and consistent with its role in cell wall organisation. Conversely, Nox2 is present intracellularly and is differentially expressed during appressorium maturation. Localisation of Nox2 within membrane-bound vesicles is similar to localisation patterns of NoxA and NoxB to the endoplasmic reticulum (ER) observed in *B. cinerea* (21). Furthermore, Yno1 in yeast (30) and mammalian Nox4 also localise to the ER, suggesting that this may be an important site to ROS generation (21). Although we have not yet verified whether Nox2 acts within the ER, its intracellular location and association with the Pls1 tetraspanin suggests that it does act in a very different manner to Nox1, generating ROS within the appressorium to regulate F-actin organisation.

We conclude that infection of rice cells by *M. oryzae* therefore involves two separately operating Nox complexes that regulate the establishment of polarized growth by septin-mediated re-organisation of F-actin at the appressorium pore and then maintain polarized growth of the penetration hypha and organization of cortical F-actin. These

findings may offer a new potential target for rice blast disease control and, importantly, they may also provide new insight into the action of NADPH oxidases in diverse developmental processes in fungi, plants and animals.

Materials and Methods

Fungal Strains, Growth Conditions and DNA analysis.

The growth and maintenance of *M. oryzae* isolate, media composition, nucleic acid extraction, and fungal transformation were all as previously described (33). Gel electrophoresis, restriction enzyme digestion, gel blots, and sequencing were performed using standard procedures (34).

Plant Infection Assays.

Pathogenicity assays were performed by spraying seedlings of rice (*O. sativa*) cultivar CO-39 with a suspension of 10^5 conidia mL^{-1} by using an artist's airbrush (33). Infection-related development was observed by incubating conidia on hydrophobic glass coverslips and allowing appressoria to form after 24 h. Cuticle penetration was measured as described (35).

Generation of *M. oryzae* Δ*noxR* mutant and strains expressing GFP fusions.

Targeted gene replacement of the *NOXR* encoding gene was performed using the split marker strategy. Vectors were constructed using a Hygromycin B selectable marker, *hph*, for transformation of Guy11. The *hph* gene cassette was cloned into pBluescript (Strategene) as a 1.4 kb *Eco*RI-*Xba*I fragment. To amplify the split *hph* templates the primers used were M13 F with HY and M13 R with YG, as described previously (36). *M. oryzae NOXR* was amplified using primers designed to conserved DNA regions identified from an alignment of noxR sequences from *Magnaporthe oryzae*, *Epichloe*

festucae and *Homo sapiens* (see Table.S1). The noxR sequence was retrieved from the *M. oryzae* genome database at the Broad Institute (Massachussetts Institute of Technology, Cambridge, MA) (www.broad.mit.edu/annotation/fungi/magnaporthe). The wild type Guy11 was transformed with the *noxR:hph* deletion cassette. Transformants were selected in the presence of hygromycin B (200 $\mu g/mL^{-1}$) and assessed by Southern blot analysis. For generation of translational GFP fusions, GAP repair cloning based on homologous recombination in *S. cerevisiae* was used (37). Primers used are listed in Table S1. All translational GFP fusions were created using the native promoter and terminator sequences. Plasmids were transformed into Guy11, Δ*nox1*, Δ*nox2*, Δ*noxR* or Δ*pls1* strains and single copy transformants selected by Southern blot.

Analysis of gene expression using HT-SuperSAGE

A transcriptional profiling database (http://cogeme.ex.ac.uk/superSAGE/) (38) was interrogated to determine the expression of *NOX1*, *NOX2* and *NOXR* in Guy11 during appressorium development (4h, 6h, 8h, 14h, 16h after spore germination). Expression was plotted relative to gene expression in *M. oryzae* mycelium (38).

Light and Epifluorescence Microscopy and Transmission Electron Microscopy.

For epifluorescence microscopy conidia were incubated on coverslips/ leaf sheath and observed at each time point using an IX-81 Olympus inverted microscope connected to a CoolSNAP HQ2 camera. Photobleaching experiments were performed using a IX-81 Olympus inverted microscope with VS-LMS4 Laser-Merge-System and solid-state lasers (488 nm/70 mW and 561 nm/70 mW; Visitron Systems) and a PlanApo 100x/NA 1.45 Oil TIRF objective (Olympus). The 405-nm/60-mW diode laser, was modified by use of a ND 0.6 filter, resulting in 15 mW output power coupled into the light path by

an OSI-IX 71 adaptor (Visitron Systems) and controlled by a UGA-40 controller (Rapp OptoElectronic GmbH) and VisiFRAP 2D FRAP control software for Meta Series 7.5.x (Visitron Systems). For recovery curves, part of the Lifeact-RFP or Gelsolin-GFP ring was photobleached and the average intensity of the region measured and normalised with a unbleached region of the ring. Three-D projections were captured using a Zeiss LSM510 Meta confocal laser scanning microscope system. HeNe 543 nm lasers were used for excitation, and all images were recorded following examination under the 363 x oil objective. LSM image browser (Zeiss) or Metamorph 7.5 (molecular devices) were used for image analysis. Ultra-thin sectioning and transmission electron microscopy was performed as described previously (15).

Acknowledgements

This work was supported by a grant to NJT and CRT from the Biotechnology and Biological Sciences Research Council (BB/G013896/), a grant to JC and ZW from National Natural Science Foundation of China (31030004), a Halpin Scholarship to YFD and a European Research Council Advanced Investigator award, GENBLAST, to NJT.

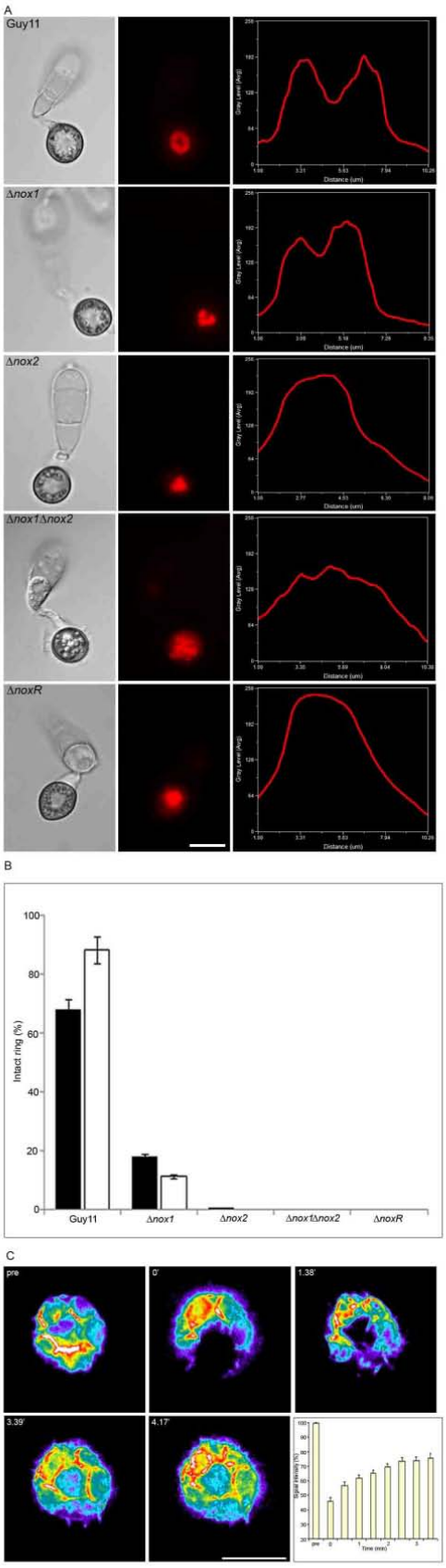
A
Guy11
Δnox1
Δnox2
Δnox1Δnox2
ΔnoxR
Distance (um)
B
Intact ring (%)
100
80
60
40
20
0
Guy11
Δnox1
Δnox2
Δnox1Δnox2
ΔnoxR
C
pre
0'
1.38'
3.39'
4.17'

Fig. 1. *M. oryzae* NADPH oxidase mutants show aberrant F-actin organisation during appressorium development. (*A*) Micrographs of F-actin organisation visualised by expression of LifeAct-RFP in Guy11Δ *nox1*, Δ*nox2*, Δ*nox1*Δ*nox2* and Δ*noxR* mutants. Conidial suspensions at 5 x 10^4 mL^{-1} were inoculated onto glass coverslips for 24 h. Linescan graphs show LifeAct-RFP fluorescence in a transverse section of individual appressoria. Scale bar=10 μm (*B*) Bar chart to show percentage of appressoria containing intact F-actin rings after 16 h (black bars) and 24 h (white bars). Values are mean ± 2SE for three repetitions of the experiment, n=100. (*C*) Recovery of LifeAct-RFP ring after partial photobleaching, with 75 % recovery in fluorescence after 3.5 min. Values are means ± 2SE, n=24). Scale bar = 5μm.

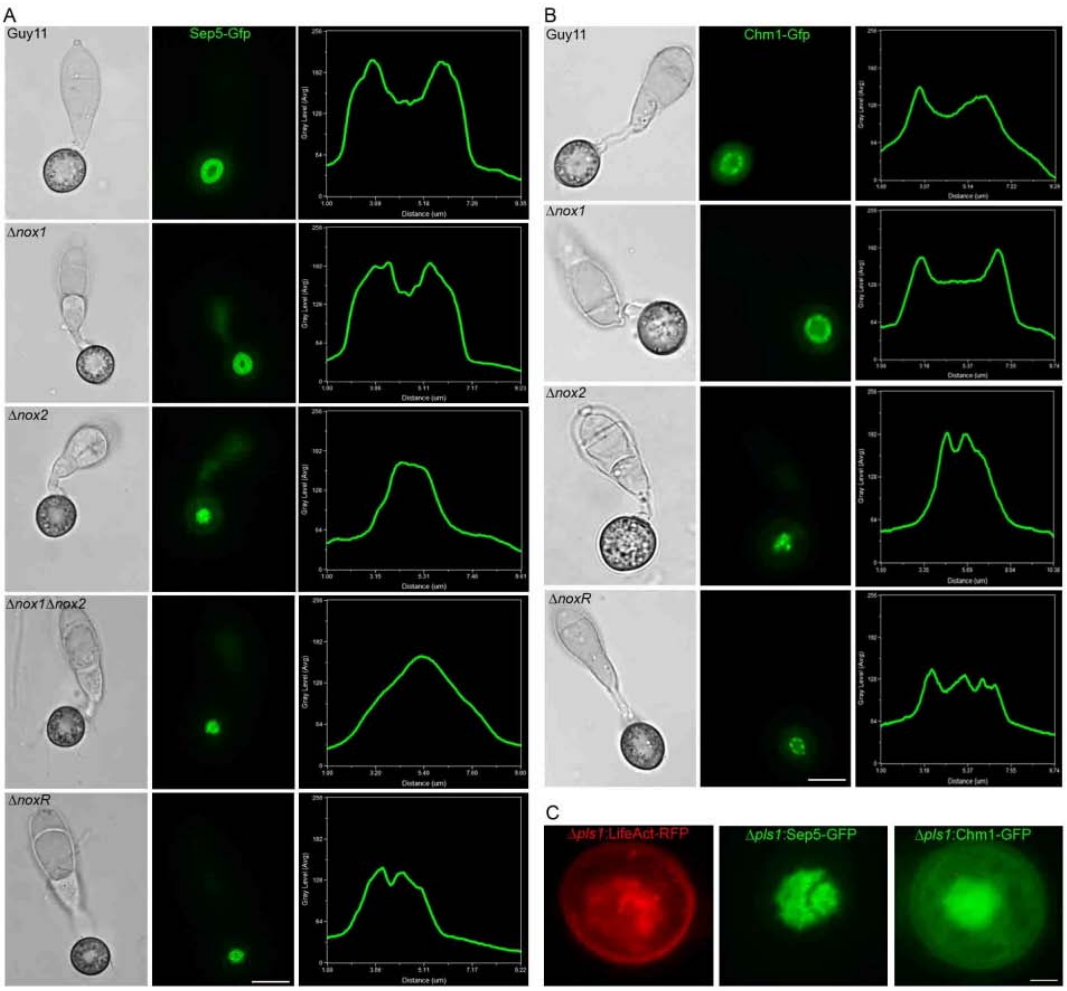
A
Guy11
Sep5-Gfp
Δnox1
Δnox2
Δnox1Δnox2
ΔnoxR
B
Guy11
Chm1-Gfp
Δnox1
Δnox2
ΔnoxR
C
Δpls1:LifeAct-RFP
Δpls1:Sep5-GFP
Δpls1:Chm1-GFP

Fig. 2. *M. oryzae* Nox2 is essential for septin ring formation at the appressorium pore. (*A*) Micrographs to show cellular localisation of Sep5-GFP in Guy11Δ *nox1*, Δ*nox2*, Δ*nox1*Δ*nox2* and Δ*noxR* during appressorium development after 24 h. Linescan graphs represent Sep5-GFP fluorescence in a transverse section of individual appressoria. (*B*) Micrographs to show localisation of the Chm1 septin kinase in appressoria. Chm1-GFP was expressed in Guy11, Δ*nox1*, Δ*nox2* and Δ*noxR* mutants. Linescan graphs showing Chm1-GFP fluorescence. (*C*) Micrographs to show localisation of LifeAct-RFP, Sep5-GFP and Chm1-GFP in the tetraspanin mutant Δ*pls1*. Scale bars = 10μm.

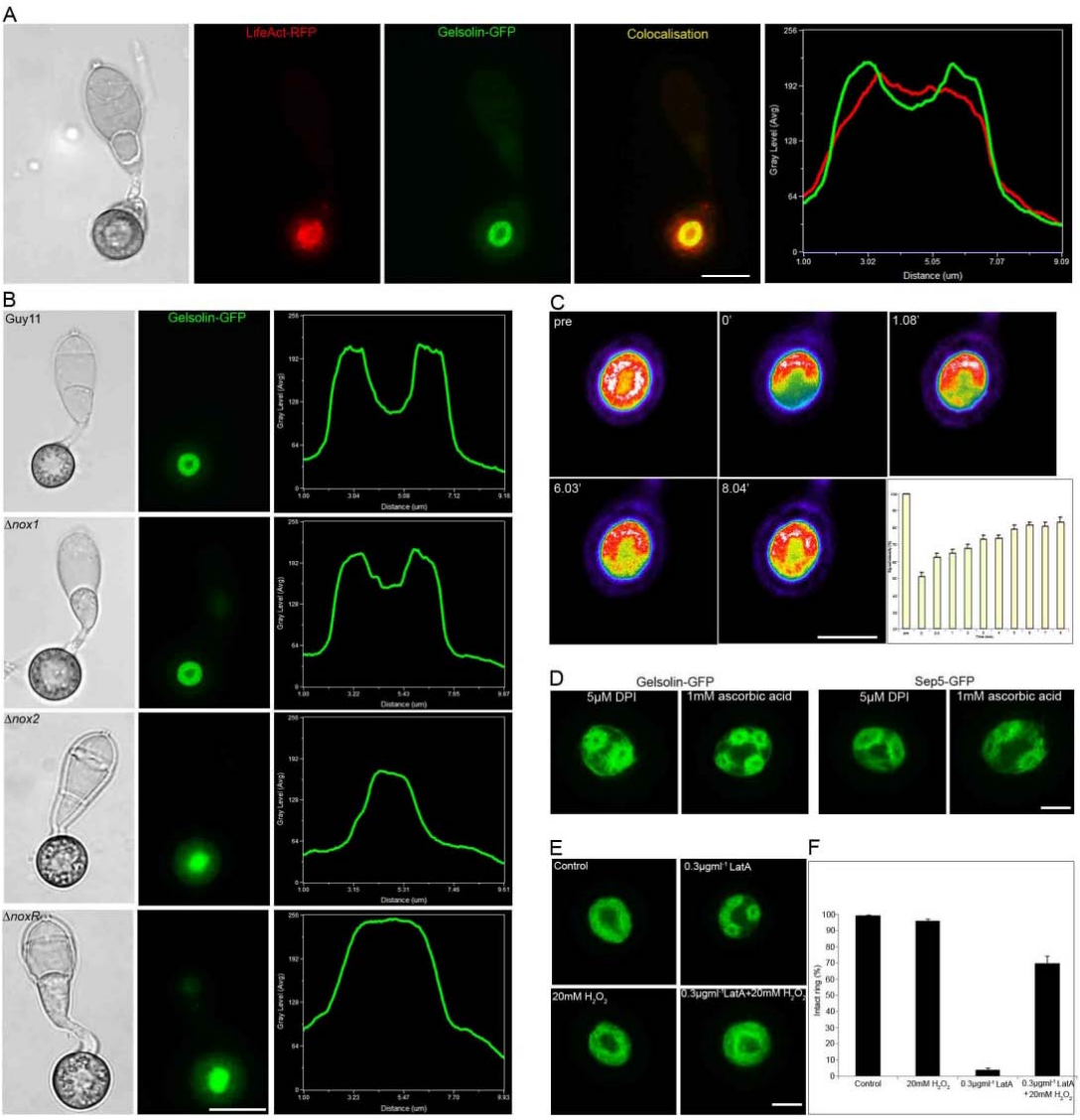
A
LifeAct-RFP
Gelsolin-GFP
Colocalisation
Gray Level (Avg)
Distance (um)
B
Guy11
Gelsolin-GFP
Δnox1
Δnox2
ΔnoxR
C
pre
0'
1.08'
6.03'
8.04'
D
Gelsolin-GFP
Sep5-GFP
5μM DPI
1mM ascorbic acid
E
Control
0.3μgml-1 LatA
20mM H2O2
0.3μgml-1 LatA+20mM H2O2
F
Intact mg (%)
Control
20mM H2O2
0.3μgml-1 LatA
0.3μgml-1 LatA +20mM H2O2

Fig. 3. Reactive oxygen species-dependent organisation of the F-actin regulator, gelsolin, in *M. oryzae*. (*A*) Micrographs and linescan graph showing co-localization of LifeAct-RFP and Gelsolin-GFP in the appressorium of the *M. oryzae* wild type strain Guy11. (*B*) Micrographs and corresponding linescan graphs to show organisation of Gelsolin-GFP expressed in appressoria of Guy11, Δ*nox1*, Δ*nox2*, and Δ *noxR* mutants after 24 h. (*C*) Recovery of gelsolin-GFP ring after partial photobleaching, with 83% recovery after 8 min. Values are means ± 2SE, n=23. Scale bar= 5µm. (*D*) Micrographs to show effect of exposure to the NADPH oxidase inhibitor diphenylene iodonium (DPI) or anti-oxidant ascorbate on Gelsolin-GFP and Sep5-GFP organisation. Conidia expressing Gelsolin-GFP and Sep5-GFP were independently exposed to 5µM DPI or 1mM ascorbic acid after 16h and observed by epifluorescence microscopy after 24 h. (*E*) Micrographs to show effect of latrunculin A treatment on gelsolin-GFP organisation in the presence or absence of ROS. Gelsolin-GFP was organised as a ring in *M. oryzae* in the presence or absence of 20 mM H_2O_2. Treatment with 0.3 µgmL-1 latrunculin A led to dis-organisation of Gelsolin-GFP, which was partially remediated by simultaneous addition of 20 mM H_2O_2. (*F*) Barchart showing percentage of appressoria containing intact gelsolin-GFP rings after 24 h. Values are means ± 2SE for three repetitions of the experiment, n=50. Scale bars = 10µm.

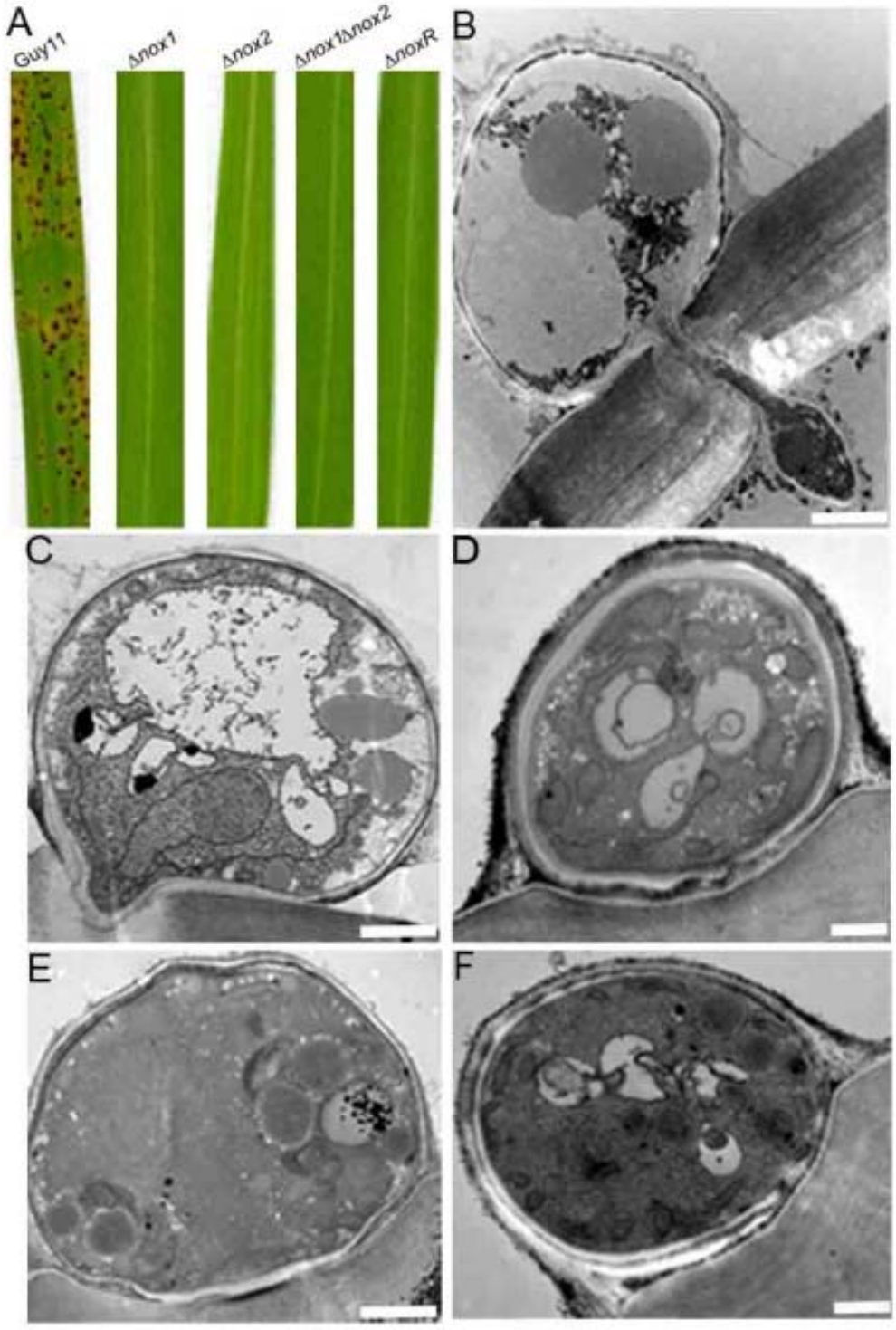
A
Guy11
Δnox1
Δnox2
Δnox1Δnox2
ΔnoxR
B
C
D
E
F

Fig. 4. *M. oryzae* NADPH oxidase mutants do not cause rice blast disease. (*A*) Seedlings of rice cultivar CO-39 were inoculated with *M. oryzae* conidial suspensions of equal concentration (1 x 10^5 conidia per ml^{-1}) of wild type Guy11, and isogenic Δ*nox1*, Δ*nox2*, Δ*nox1*Δ*nox2* and Δ*noxR* mutants. Seedlings were incubated for 5 days to allow development of blast disease symptoms. *B-F*, Transmission electron micrographs showing transverse sections of appressoria undergoing development on onion epidermis after 24h. (*B*) Guy11 appressorium showing penetration hypha development. (*C*) Δ*nox1* mutant appressorium showing re-polarisation to form an aberrant penetration peg. (*D*) Δ*nox2* mutant appressorium impaired in penetration peg development. (*E*) Δ*nox1*Δ*nox2* mutant. (*F*) Δ*noxR* mutant. Scale bars = 2.0 μm.

References:

1. Sumimoto H (2008) Structure, regulation and evolution of Nox-family NADPH oxidases that produce reactive oxygen species. *The FEBS Journal* 275:3249-3277.
2. Lambeth JD (2004) NOX enzymes and the biology of reactive oxygen. *Nature Rev. Immunol.* 4:181-189.
3. Brown DI & Griendling KK (2009) Nox proteins in signal transduction. *Free Radic Biol Med* 47:1239-1253.
4. Suzuki N, *et al.* (2011) Respiratory burst oxidases: the engines of ROS signaling. *Curr Opin Plant Biol* 14:691-699.
5. Torres MA, Dangl JL, & Jones JD (2002) Arabidopsis gp91phox homologues AtrbohD and AtrbohF are required for accumulation of reactive oxygen intermediates in the plant defense response. *Proc Natl Acad Sci U S A* 99:517-522.
6. Foreman J, *et al.* (2003) Reactive oxygen species produced by NADPH oxidase regulate plant cell growth. *Nature* 422:442-446.
7. Heller J & Tudzynski P (2011) Reactive oxygen species in phytopathogenic fungi: signaling, development, and disease. *Annu Rev Phytopathol* 49:369-390.
8. Takemoto D, *et al.* (2011) Polarity proteins Bem1 and Cdc24 are components of the filamentous fungal NADPH oxidase complex. *Proc Natl Acad Sci U S A* 108:2861-2866.
9. Takemoto D, Tanaka A, & Scott B (2007) NADPH oxidases in fungi: diverse roles of reactive oxygen species in fungal cellular differentiation. *Fungal Genet. Biol* 44:1065-1076.
10. Wilson RA & Talbot NJ (2009) Under pressure: investigating the biology of plant infection by Magnaporthe oryzae. *Nat Rev Microbiol* 7:185-195.
11. Fisher MC, *et al.* (2012) Emerging fungal threats to animal, plant and ecosystem health. *Nature* 484:186-194.
12. de Jong JC, McCormack BJ, Smirnoff N, & Talbot NJ (1997) Glycerol generates turgor in rice blast. *Nature* 389:244-244.
13. Dagdas YF, *et al.* (2012) Septin-mediated plant cell invasion by the rice blast fungus, Magnaporthe oryzae. *Science* 336:1590-1595.
14. Berepiki A, Lichius A, & Read ND (2011) Actin organization and dynamics in filamentous fungi. *Nature Rev. Microbiol.* 9:876-887.
15. Egan MJ, Wang ZY, Jones MA, Smirnoff N, & Talbot NJ (2007) Generation of reactive oxygen species by fungal NADPH oxidases is required for rice blast disease. *Proc Natl Acad Sci U S A* 104:11772-11777.
16. Versele M & Thorner J (2004) Septin collar formation in budding yeast requires GTP binding and direct phosphorylation by the PAK, Cla4. *J. Cell Biol.* 164:701-715.
17. Clergeot PH, *et al.* (2001) PLS1, a gene encoding a tetraspanin-like protein, is required for penetration of rice leaf by the fungal pathogen Magnaporthe grisea. *Proc Natl Acad Sci U S A* 98:6963-6968.
18. Gourgues M, Brunet-Simon A, Lebrun MH, & Levis C (2004) The tetraspanin BcPls1 is required for appressorium-mediated penetration of Botrytis cinerea into host plant leaves. *Mol Microbiol* 51:619-629.
19. Lambou K, *et al.* (2008) The crucial role of the Pls1 tetraspanin during ascospore germination in Podospora anserina provides an example of the

convergent evolution of morphogenetic processes in fungal plant pathogens and saprobes. *Eukaryot Cell* 7:1809-1818.
20. Malagnac F, *et al.* (2008) Convergent evolution of morphogenetic processes in fungi: Role of tetraspanins and NADPH oxidases 2 in plant pathogens and saprobes. *Commun Integr Biol* 1:180-181.
21. Tudzynski P, Heller J, & Siegmund U (2012) Reactive oxygen species generation in fungal development and pathogenesis. *Curr. Opin. Microbiol.* 15:653-659.
22. Moldovan L, Mythreye K, Goldschmidt-Clermont PJ, & Satterwhite LL (2006) Reactive oxygen species in vascular endothelial cell motility. Roles of NAD(P)H oxidase and Rac1. *Cardiovasc Res* 71:236-246.
23. de Lamirande E, Tsai C, Harakat A, & Gagnon C (1998) Involvement of reactive oxygen species in human sperm arcosome reaction induced by A23187, lysophosphatidylcholine, and biological fluid ultrafiltrates. *Journal of Andrology* 19:585-594.
24. Holland JA, *et al.* (2001) Low-density lipoprotein induced actin cytoskeleton reorganization in endothelial cells: mechanisms of action. *Endothelium : J. Endothelial Cell Res.* 8:117-135.
25. Irani K (2000) Oxidant signaling in vascular cell growth, death, and survival : a review of the roles of reactive oxygen species in smooth muscle and endothelial cell mitogenic and apoptotic signaling. *Circ Res* 87:179-183.
26. Pardee JD, Simpson PA, Stryer L, & Spudich JA (1982) Actin filaments undergo limited subunit exchange in physiological salt conditions. *J. Cell Biol.* 94:316-324.
27. Tamura M, Kai T, Tsunawaki S, Lambeth JD, & Kameda K (2000) Direct interaction of actin with p47(phox) of neutrophil NADPH oxidase. *Biochem.Biophys. Res Comm.* 276:1186-1190.
28. Wientjes FB, Reeves EP, Soskic V, Furthmayr H, & Segal AW (2001) The NADPH oxidase components p47(phox) and p40(phox) bind to moesin through their PX domain. *Biochem.Biophys. Res Comm* 89:382-388.
29. Kwiatkowski DJ (1999) Functions of gelsolin: motility, signaling, apoptosis, cancer. *Current Opin. Cell Biol.* 11:103-108.
30. Rinnerthaler M, *et al.* (2012) Yno1p/Aim14p, a NADPH-oxidase ortholog, controls extramitochondrial reactive oxygen species generation, apoptosis, and actin cable formation in yeast. *Proc Natl Acad Sci U S A* 109:8658-8663.
31. Chen J, *et al.* (2008) Rac1 is required for pathogenicity and Chm1-dependent conidiogenesis in rice fungal pathogen Magnaporthe grisea. *PLoS Pathog* 4:e1000202.
32. Arcaro A (1998) The small GTP-binding protein Rac promotes the dissociation of gelsolin from actin filaments in neutrophils. *J. Biol. Chem.* 273:805-813.
33. Talbot NJ, Ebbole DJ, & Hamer JE (1993) Identification and characterization of MPG1, a gene involved in pathogenicity from the rice blast fungus Magnaporthe grisea. *Plant Cell* 5:1575-1590.
34. Sambrook J, Fritsch EF, & Maniatis T (1989) Molecular cloning - a laboratory manual, second edition. *Cold Spring Harbour Laboratory Press, New York, USA*
35. Thines E, Weber RW, & Talbot NJ (2000) MAP kinase and protein kinase A-dependent mobilization of triacylglycerol and glycogen during appressorium turgor generation by Magnaporthe grisea. *Plant Cell* 12:1703-1718.
36. Kershaw MJ & Talbot NJ (2009) Genome-wide functional analysis reveals that infection-associated fungal autophagy is necessary for rice blast disease. *Proc Natl Acad Sci U S A* 106:15967-15972.

37. Oldenburg KR, Vo KT, Michaelis S, & Paddon C (1997) Recombination-mediated PCR-directed plasmid construction in vivo in yeast. *Nucleic Acids Res* 25:451-452
38. Soanes DM, Chakrabarti A, Paszkiewicz KH, Dawe AL, Talbot NJ (2012) Genome-wide Transcriptional Profiling of Appressorium Development by the Rice Blast Fungus *Magnaporthe oryzae*. *PLoS Pathog* 8: e1002514.

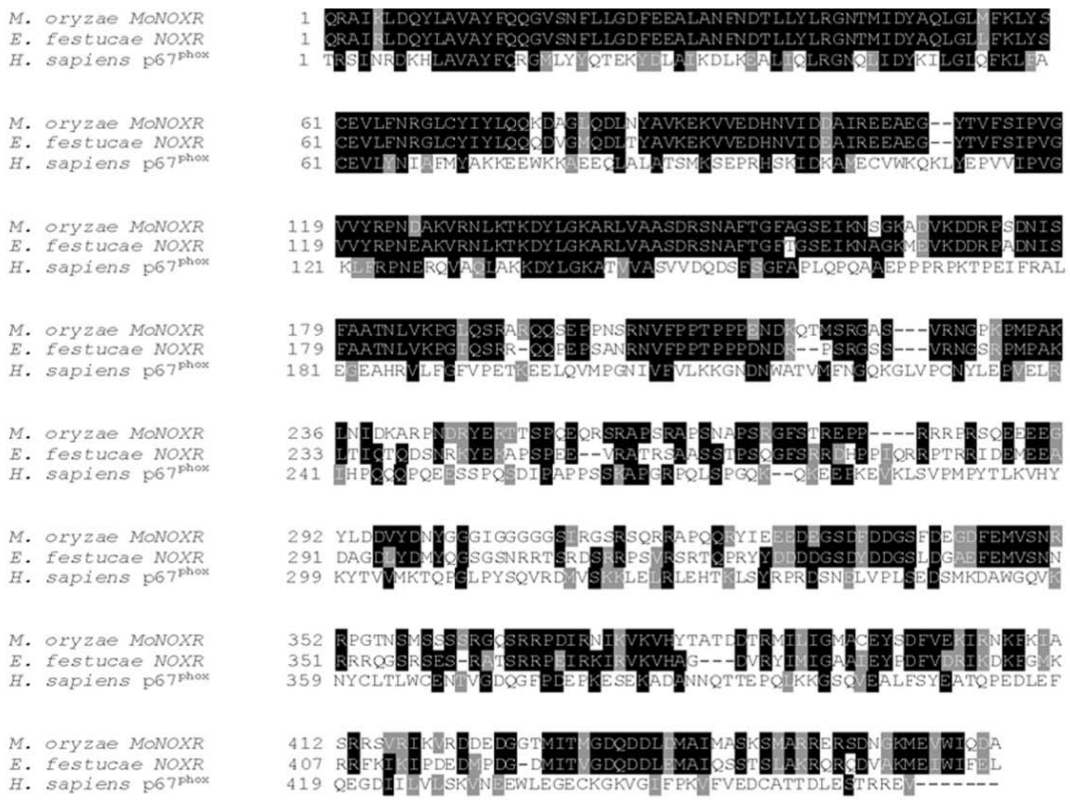
M. oryzae MoNOXR
E. festucae NOXR
H. sapiens p67phox

Fig. S1. Amino acid sequence alignment of *M. oryzae* NADPH oxidase isoform R protein. The amino acid sequence of NoxR was aligned with human $p67^{phox}$ and *E. festucae* NoxR. Sequences were aligned using ClustalW and shaded using GeneDoc version 2.6.02. Amino acid residues within a black background were identical among all listed proteins, dark grey residues were identical in two out of three of the listed proteins and those shown on a white background do not show any similarity.

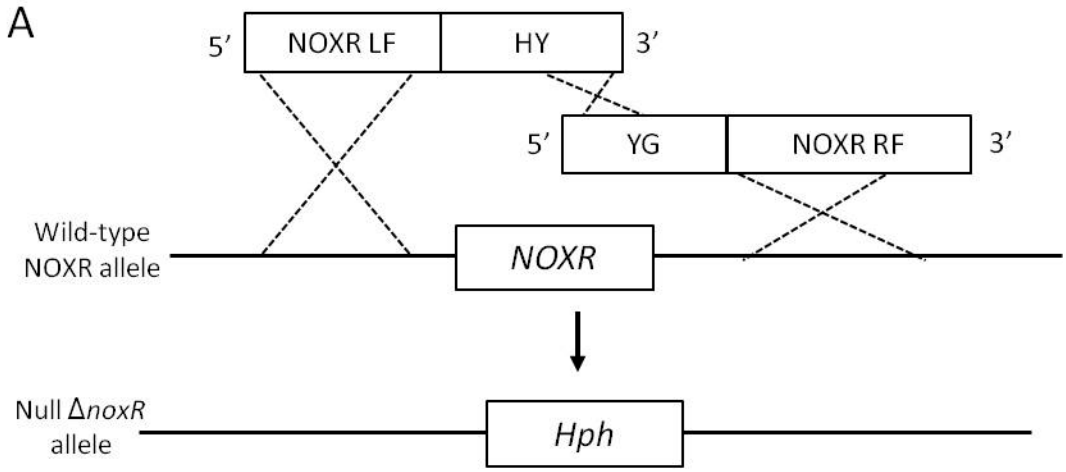
A
5′
NOXR LF
HY
3′
5′
YG
NOXR RF
3′
Wild-type
NOXR allele
NOXR
Null ΔnoxR
allele
Hph

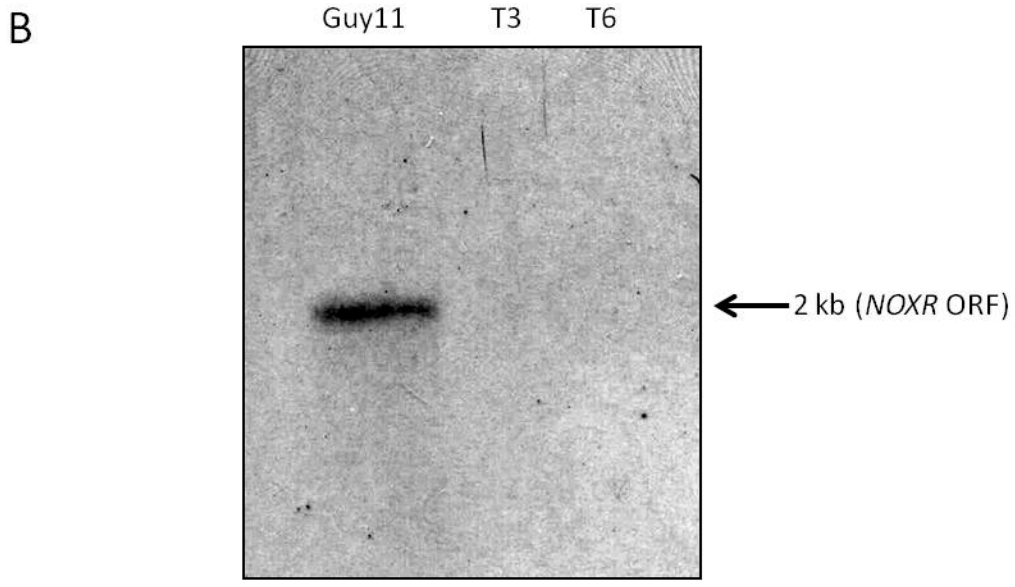
B
Guy11
T3
T6
2 kb (NOXR ORF)

Fig. S2. One step targeted gene replacement of the *M. oryzae NOXR* gene. (*A*) A 1.4 kb hygromycin B resistance gene cassette was introduced into the NOXR coding sequence using the split marker method. (*B*) Second round PCR fragments were introduced into *M. oryzae* Guy11 and targeted deletion mutants selected on hygromycin B and identified by probing with a deleted 500 bp region of the *NOXR* coding sequence. Southern blot analysis was carried out and two putative gene replacement mutants, T3 and T6 were identified.

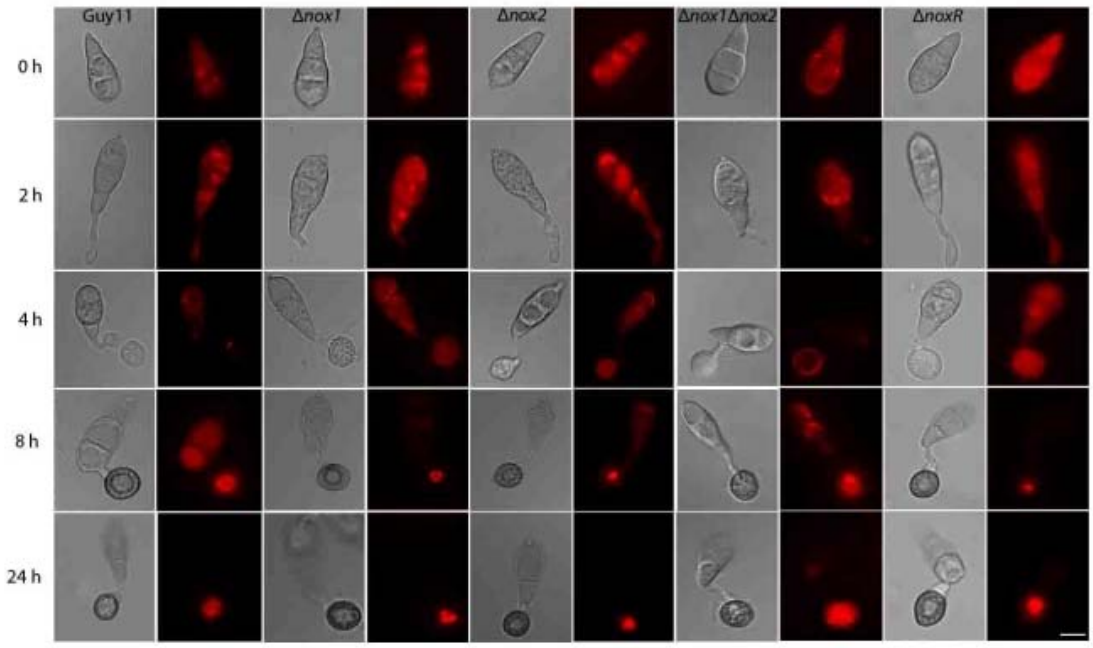
Guy11
Δnox1
Δnox2
Δnox1Δnox2
ΔnoxR
0 h
2 h
4 h
8 h
24 h

Fig. S3. LifeAct-RFP localisation in NADPH oxidase mutants of *M. oryzae*. Micrographs showing expression of LifeAct-RFP in NADPH oxidase mutants during a timecourse of appressorium development by *M. oryzae*. Conidia were harvested from Guy11, Δ*nox1,* Δ *nox2*, Δ *nox1*Δ*nox2* and Δ*noxR* mutants expressing LifeAct-RFP, inoculated onto hydrophobic glass coverslips and observed by epifluorescence microscopy. A toroidal F-actin network was observed in wild type (Guy11) infection cells at the appressorium pore after 8 h. At 24 h the F-actin network was fully formed and individual actin cables could be distinguished. In Δ*nox1* mutants the F-actin network was distorted and by 24 h the ring-shaped structure at the appressorium pore was no longer intact. In Δ*nox2,* Δ*noxR* and Δ*nox1* Δ*nox2* mutants the F-actin network was not observed. Instead a disorganised accumulation of actin was detected in the centre of the appressorium. Scale bar, 10μm.

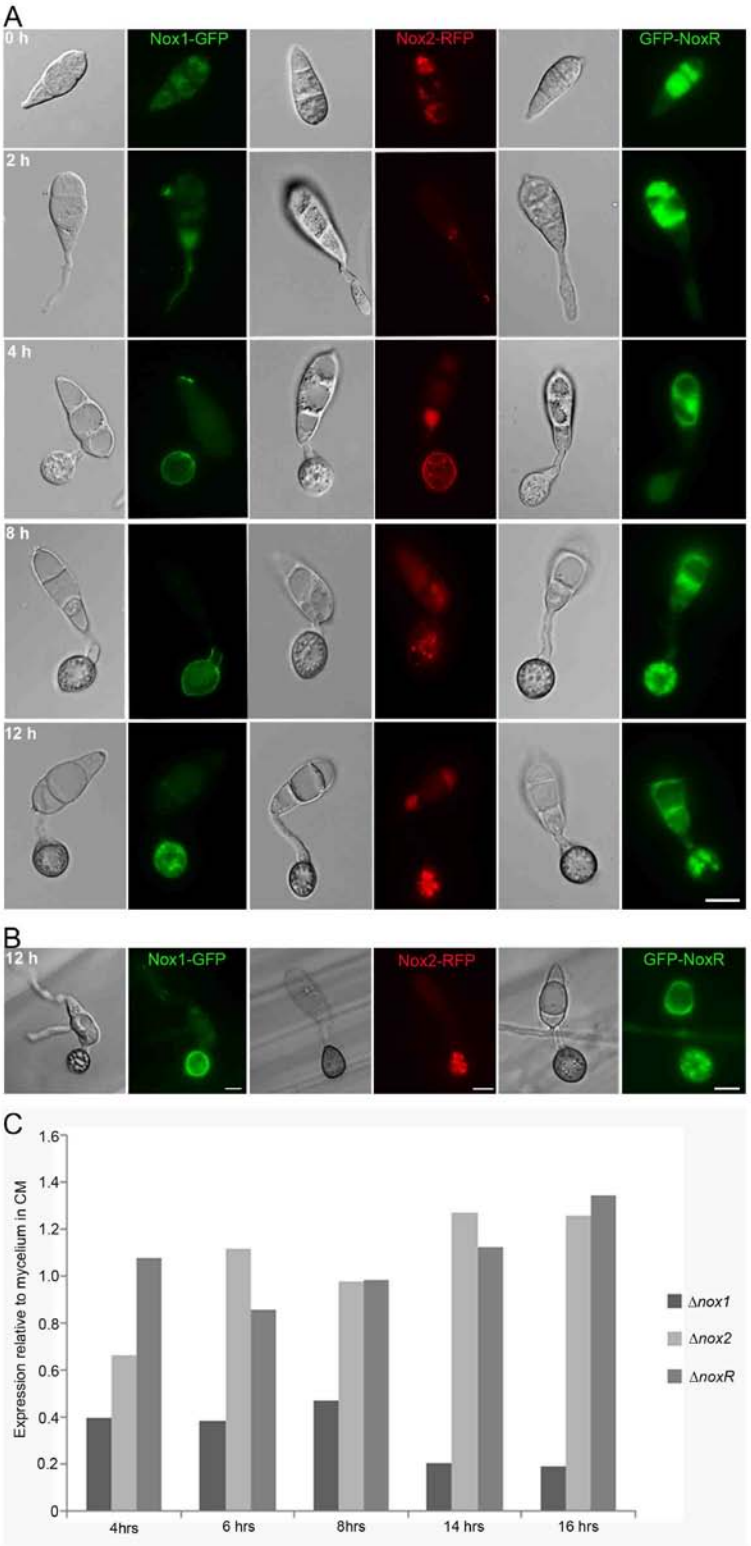
A
0 h
Nox1-GFP
Nox2-RFP
GFP-NoxR
2 h
4 h
8 h
12 h
B
12 h
Nox1-GFP
Nox2-RFP
GFP-NoxR
C
Expression relative to mycelium in CM
1.6
1.4
1.2
1.0
0.8
0.6
0.4
0.2
0
4hrs
6 hrs
8hrs
14 hrs
16 hrs
Δnox1
Δnox2
ΔnoxR

Fig. S4. Live cell imaging of Nox1-GFP, Nox2-RFP and GFP-NoxR expressed during appressorium development by *M. oryzae*. Independent transformants were generated expressing *NOX1-GFP, NOX2-RFP* and *GFP-NOXR* translational gene fusions expressed under control of their native promoters. Strains were inoculated onto hydrophobic glass coverslips and observed by epifluorescence microscopy. (*A*) Nox1-GFP was initially observed at the appressorium cortex from 4h. After 12 h Nox1-GFP was also observed in the central appressorium vacuole. Nox2-RFP was initially observed at the periphery of the appressorium from 4h. After 12 h, Nox2-RFP expression increased, forming punctate structures throughout the appressorium. GFP-NoxR expression was observed in the cytoplasm of both ungerminated condia and appressoria. Scale bars, 10 μm. (*B)* On a yielding surface that could be ruptured by *M. oryzae* appressoria, similar localisation patterns were observed. Conidial suspensions were inoculated onto sterile onion epidermis and observed for a 12h period. Scale bars, 10 μm. (*C*) SuperSAGE analysis showing the expression of Nox genes in Guy11. Bar graphs show abundance of transcripts encoding each Nox gene in a Guy11 timecourse during appressorium development (4h, 6h, 8h, 14h, 16h).

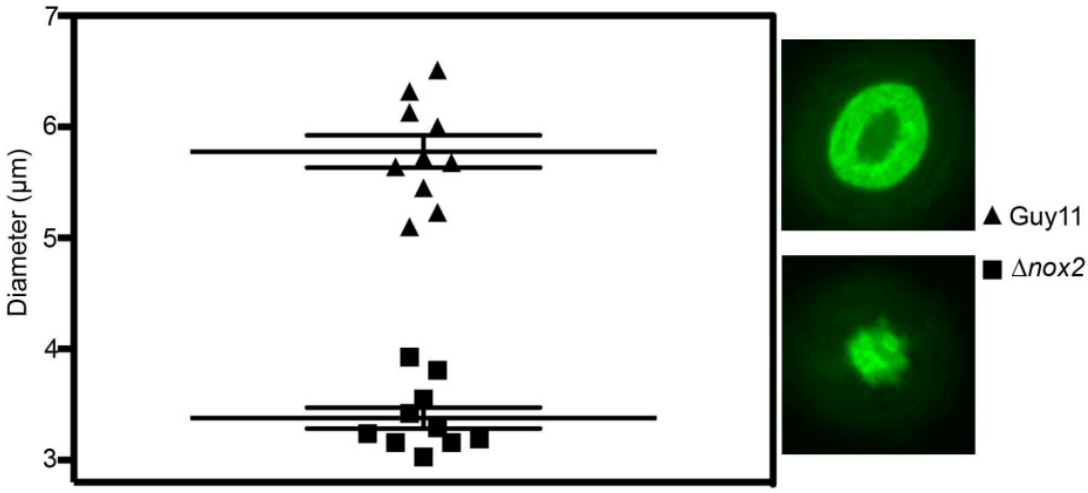
7
6
5
4
3
Diameter (µm)
▲ Guy11
■ Δnox2

Fig.S5. Graph to show the range of Sep5-GFP ring sizes observed in wild type and Δ*nox2* mutants of *M. oryzae* during appressorium development.

Live cell imaging experiments were carried out by expression of *SEP5-GFP* in Guy11 or Δ*nox2* mutant. Triangles represent the diameter values of septin rings observed in Guy11. Black square represent the diameter values of aberrant septin accumulations observed in theΔ *nox2* mutant. Long horizontal lines represent the mean diameter and short horizontal lines are the standard error of the mean.. The y-axis show diameter in micrometers.

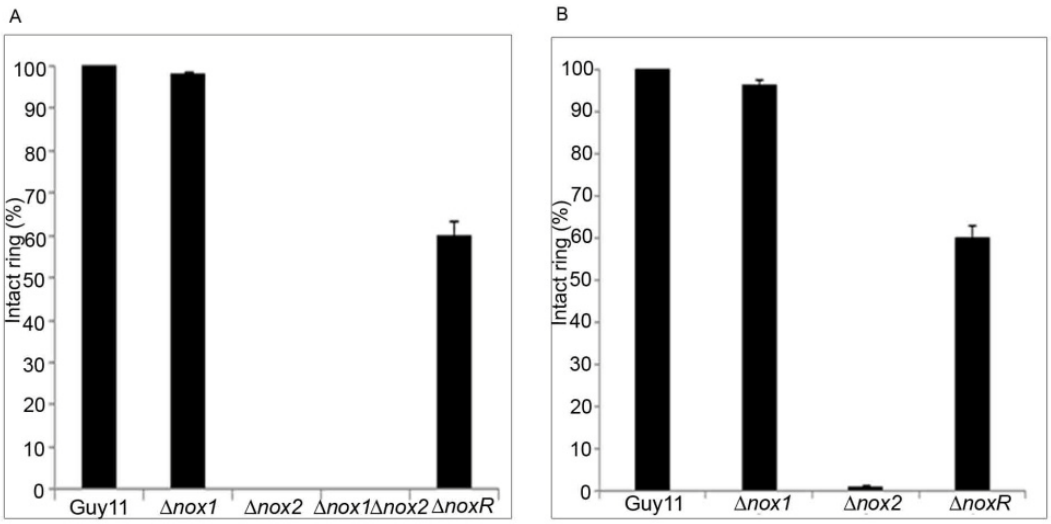
A
Intact ring (%)
100
90
80
70
60
50
40
30
20
10
0
Guy11
Δnox1
Δnox2
Δnox1Δnox2
ΔnoxR
B
Intact ring (%)
100
90
80
70
60
50
40
30
20
10
0
Guy11
Δnox1
Δnox2
ΔnoxR

Fig.S6. Live cell imaging of Sep5-GFP and Chm1-GFP in Δ*nox2* and Δ*noxR* mutants. (*A*) Bar chart showing the percentage of appressoria with intact Sep5-GFP rings after 24 h. Values are mean ± 2SE for three repetitions of the experiment, n=100.. (*B*) Bar chart to show the percentage of appressoria containing intact Chm1-GFP rings after 24 h. Values are mean ± 2SE for three repetitions of the experiment, n=100..

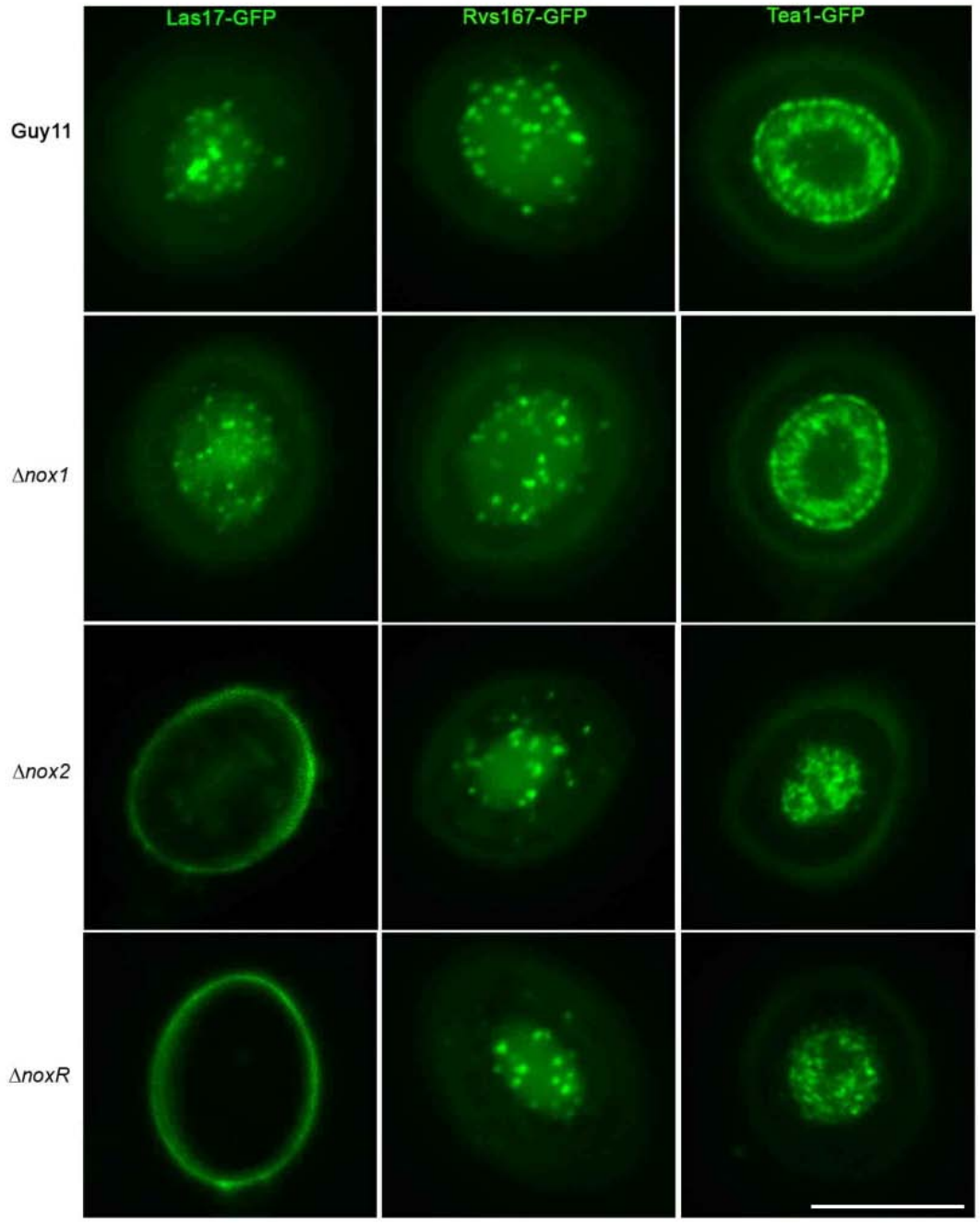
Las17-GFP
Rvs167-GFP
Tea1-GFP
Guy11
Δnox1
Δnox2
ΔnoxR

Fig. S7. Expression and localisation of Las17-GFP, Tea1-GFP and Rvs167-GFP in Δ*nox2* and Δ*noxR* mutants of *M. oryzae*. Δ*nox1,* Δ*nox2* and Δ*noxR* mutants were independently transformed with *LAS17-GFP, TEA1-GFP* and *RVS167-GFP* gene fusions, inoculated onto glass coverslips and observed by epifluorescence microscopy. In Δ*nox1* mutants, *Las17-GFP, Tea1-GFP* and *Rvs167-GFP* localised in the same pattern as Guy11. In Δ*nox2* and Δ*noxR* mutants, *Las17-GFP, Tea1-GFP* and *Rvs167-GFP* were mislocalised. Therefore, ERM-actin interactions at the appressorium pore, which are essential for linking cortical F-actin to the membrane to facilitate penetration peg emergence, require the Nox2/NoxR complex. Scale bars, 10 μm.

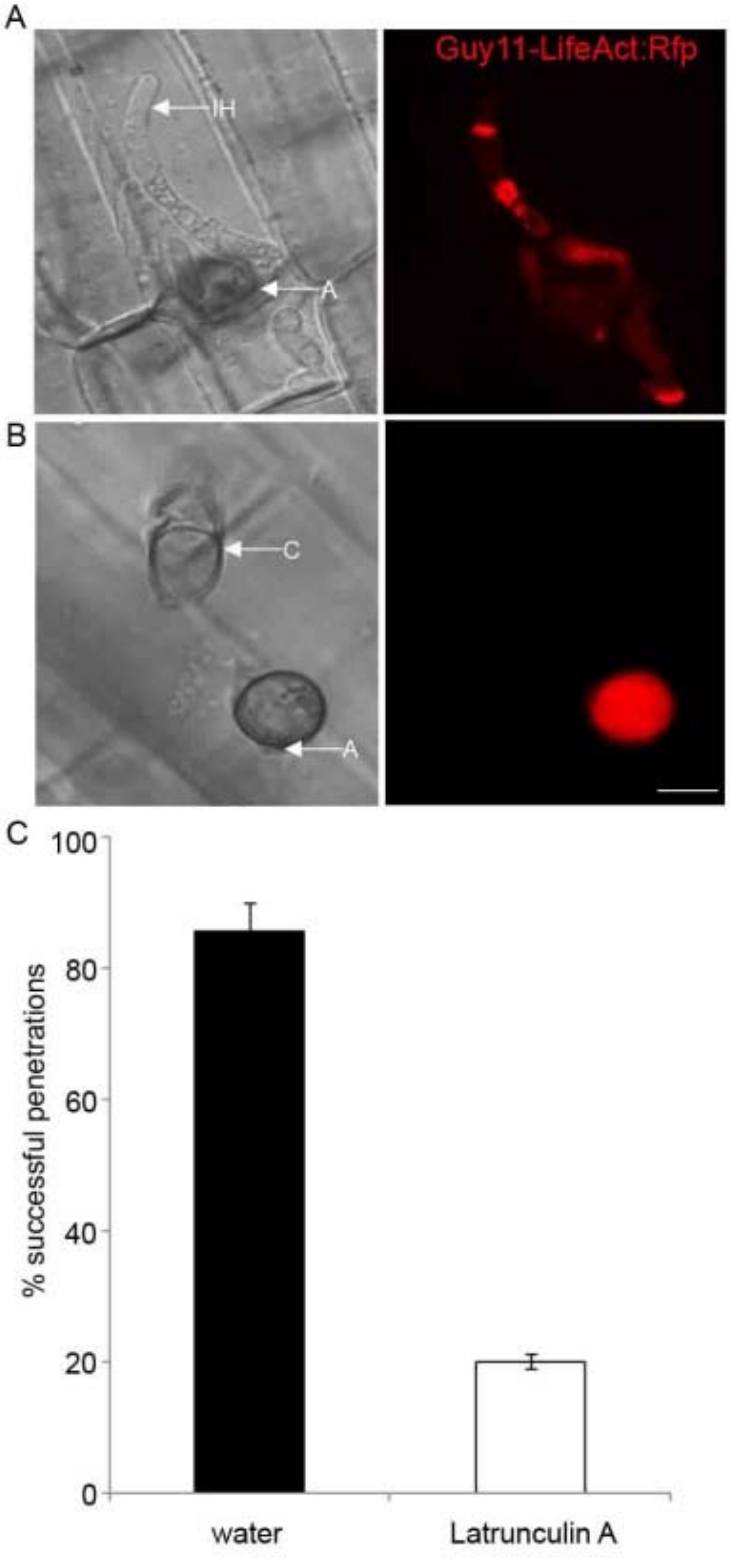
A
IH
A
Guy11-LifeAct:Rfp
B
C
A
C
100
80
60
40
20
0
% successful penetrations
water
Latrunculin A

Fig. S8. Exposure to Latrunculin A prevents appressorium-mediated rice infection by *M. oryzae.* Micrographs of LifeAct-RFP localisation in the presence or absence of LatrunculinA. A conidial suspension of the Guy11 expressing LifeAct:RFP at $5x10^4$ mL^{-1} was inoculated onto the surface of rice leaf sheath and incubated in a moist chamber at 24^oC. (*A*) De-ionised water or (*B*) 3 μg mL^{-1} Latrunculin A was added to the conidial suspension after 16 h. Representative images were recorded using an IX-81 Olympus inverted microscope, A= appressorium, C= conidium and IH= invasive hypha. (*C*) Bar charts to show percentage of appressoria forming penetration pegs after 24 h (n = 100). The percentage of appressoria forming penetration hyphae following Latrunculin A treatment was significantly reduced ($P<0.001$) compared to water treatment. Values in **c** are means ± 2SE for three repetitions of the experiment. Scale bar, 10μm.

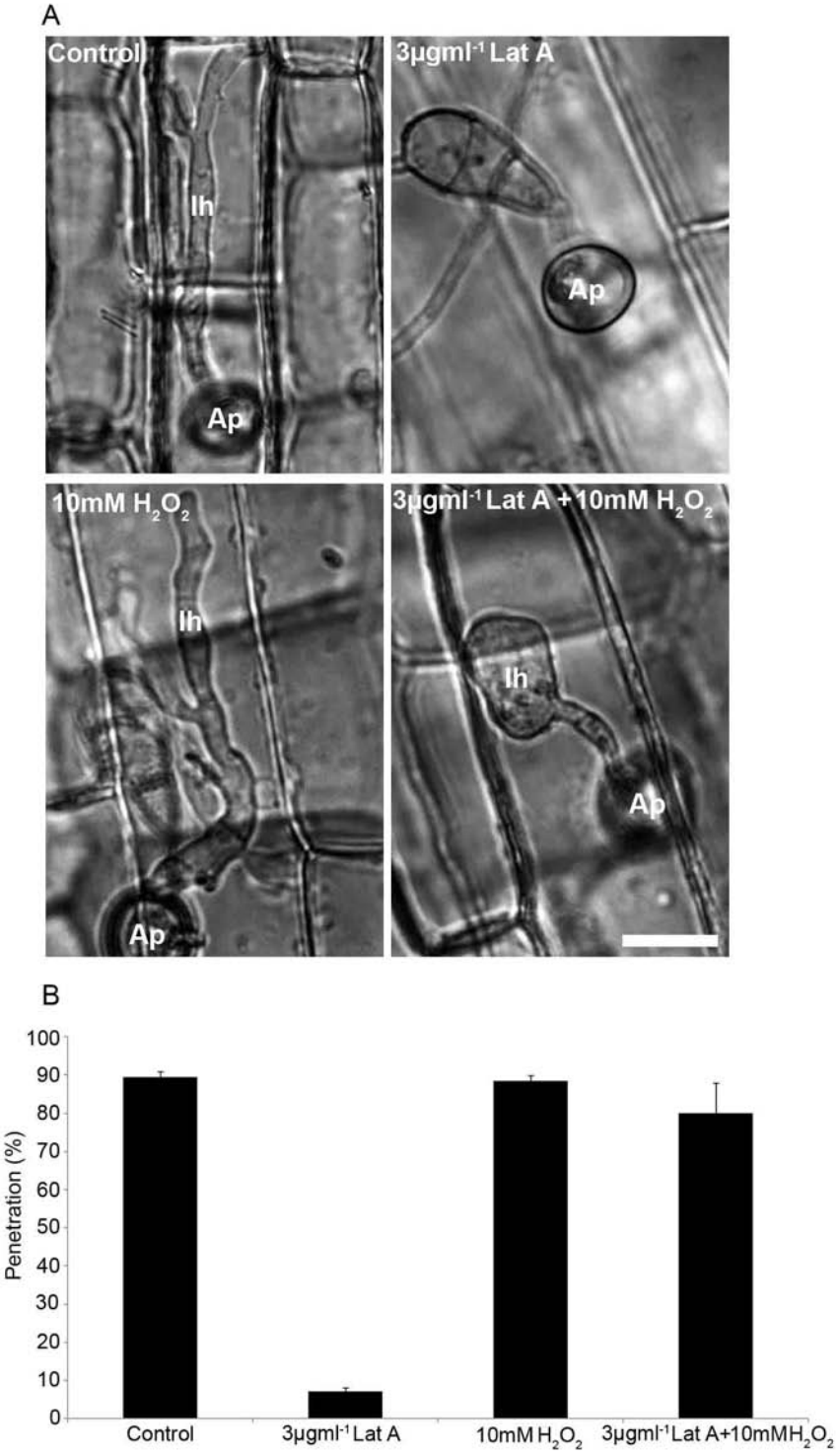
A
Control
3µgml-1 Lat A
10mM H2O2
3µgml-1 Lat A +10mM H2O2
Ih
Ap
B
Penetration (%)
100
90
80
70
60
50
40
30
20
10
0
Control
3µgml-1 Lat A
10mM H2O2
3µgml-1 Lat A+10mMH2O2

Fig. S9. Addition of H_2O_2 partially remediates the effects of Latrunculin A on appressorium-mediated plant infection by *M. oryzae*. A conidial suspension of wild type Guy11 at $5x10^4$ mL^{-1} was inoculated onto the surface of rice leaf sheath and incubated in a moist chamber at 24^oC to form appressoria. At 16h, de-ionised water, 3 μg mL^{-1} Latrunculin A, 10mM H_2O_2, or 3 μg mL^{-1} Latrunculin A and 10mM H_2O_2 was added to the developing appressoria, respectively. (*A*) Bright field micrographs were recorded using an IX-81 Olympus inverted microscope, A= appressorium, C= conidium and IH= invasive hypha. * = aberrant swollen penetration hypha. (*B)* Bar charts to show percentage of appressoria forming penetration pegs after 24 h (n = 100). A significant reduction in penetration peg formation was observed following latrunculin A treatment ($P<0.001$) but simultaneous addition of 10mM H_2O_2 restored the frequency of peg formation to almost wild type levels. Pegs ruptured the leaf cuticle but did not develop into extensive invasion hyphae. Values are means ± 2 SE. Scale bar, 10μm.

Movie S1. Three dimensional rotational movie to show toroidal F-actin network at the appressorium pore in the wild type *M. oryzae* strain Guy11.

Movie S2. Three dimensional rotational movie to show misshapen F-actin network at the appressorium pore of the *M. oryzae* Δ*nox1* mutant.

Movie S3. Three dimensional rotational movie to show distorted F-actin network in the appressorium of the *M. oryzae* Δ*nox2* mutant.

Movie S4. Three dimensional rotational movie to show distorted F-actin network in the appressorium of the *M. oryzae* Δ*nox1*Δ*nox2* mutant.

Movie S5. Three dimensional rotational movie to show distorted F-actin network at the centre of the appressorium of the *M. oryzae* Δ*noxR* mutant.

Movie S6. Live-cell imaging to show recovery of LifeAct-RFP after partial photobleaching.

Movie S7. Live-cell imaging to show recovery of Gelsolin-GFP after partial photobleaching.

Two distinct secretion systems facilitate tissue invasion by the rice blast fungus *Magnaporthe oryzae*

Martha C. Giraldo[1,*], Yasin F. Dagdas[2,*], Yogesh K. Gupta[2] , Thomas A. Mentlak[2,4] , Mihwa Yi[1], Ana Lilia Martinez-Rocha[2,5], Hiromasa Saitoh[3], Ryohei Terauchi[3], Nicholas J. Talbot[2], Barbara Valent[1]

[1]Department of Plant Pathology, Kansas State University, Manhattan, Kansas 66506, USA. [2]School of Biosciences, University of Exeter, EX4 4QD, UK. [3]Iwate Biotechnology Research Center, Kitakami, Iwate, 024-0003 Japan. [4]Current Address: Cambridge Consultants Ltd, Cambridge, CB4 0DW, U.K. [5]Current Address: University of Hamburg ([*]Contributed equally)

To cause plant diseases, pathogenic micro-organisms secrete effector proteins into host tissue to suppress immunity and support pathogen growth. Bacterial pathogens have evolved several distinct secretion systems to target effector proteins, but whether fungi, which cause the major diseases of most crop species, also require different secretory mechanisms is not known. Here, we report that the rice blast fungus *Magnaporthe oryzae* possesses two distinct secretion systems to target effectors during plant infection. Cytoplasmic effectors, which are delivered into host cells, preferentially accumulate in the biotrophic interfacial complex (BIC), a novel plant membrane-rich structure associated with invasive hyphae. We show that the BIC is associated with a novel form of secretion involving exocyst components and the Sso1 t-SNARE. By contrast, effectors that are secreted from invasive hyphae into the extracellular compartment follow the conventional secretory pathway. We conclude that the blast fungus has evolved distinct secretion systems to facilitate tissue invasion.

Biotrophic pathogens grow in intimate contact with living host cells and deliver effector proteins into and around these host cells[1-4]. In pathogenic bacteria, effectors serve a variety of functions including induction of host cell entry by intracellular pathogens, modulating host cell signaling and suppressing immune responses. These distinct functions are associated with specific forms of secretion that operate during pathogenesis[5,6]. Eukaryotic microbial pathogens, such as fungi and oomycetes, possess even larger numbers of effector proteins that are secreted during host infection[3,4,7,8]. They serve to suppress immunity[9-11], modulate metabolism[12], and prevent recognition of the invading microbe[13,14]. Although the functions of most of these effectors are still unknown, it is increasingly clear that fungal effectors are delivered both to the inside of host cells, as well as to the host-pathogen interface during infection.

The ascomycete fungus *Magnaporthe oryzae* causes rice blast, the most serious disease of cultivated rice and a major threat to global food security[15-17]. Additionally, a wheat-adapted population of *M. oryzae* has recently emerged to cause wheat blast disease in South America, and this fungus now also poses a threat to global wheat production[18,19]. To cause disease, the fungus uses a special infection cell called an appressorium, which ruptures the rice cuticle and allows the fungus entry to epidermal cells[16,20,21]. *M. oryzae* then invades rice tissue using specialized filamentous invasive hyphae (IH), which successively occupy living rice cells[22] and colonize tissue extensively before the appearance of disease symptoms. Host cells are initially invaded by narrow tubular primary hyphae that subsequently develop into enlarged, bulbous IH (Fig. 1a)[22]. Morphologically, bulbous IH are constricted at septal junctions, resembling pseudohyphae produced by the human fungal pathogen *Candida albicans*[23,24]. Differentiation of specialized IH recurrs for each hypha entering a living host cell (Fig. 1a), and this differentiation process appears critical for disease development.

During biotrophic invasion, *M. oryzae* expresses many low molecular weight effector proteins that possess classical signal peptides which facilitate delivery into the endoplasmic reticulum (ER)[8,25,26]. The ER chaperone Lhs1 is furthermore required for secretion of effectors[27]. Previous *in planta* analyses have involved live cell imaging of *M. oryzae* strains secreting chimeric effector proteins labeled with C-terminal green fluorescent protein (GFP), monomeric red fluorescent protein (mRFP), or monomeric Cherry (mCherry). Secreted effectors show distinct patterns of accumulation within the Extra-Invasive Hyphal Membrane (EIHM) compartment enclosing IH growing in rice cells[14,25,28]. Apoplastic effectors, for example, are generally dispersed and retained within the EIHM compartment, where they outline the entire IH. By contrast, cytoplasmic effectors preferentially accumulate in the biotrophic interfacial complex (BIC)[28], a membrane-rich structure that initially appears adjacent to primary hyphal tips, but is later positioned subapically as IH develop within rice cells (Fig. 1a). Fluorescent effector proteins that accumulate in BICs appear to be translocated across the EIHM into the cytoplasm of living rice cells[28]. Translocation of effectors into rice cells has been most clearly visualized by expression of fluorescent effector fusion proteins that possess an additional C-terminal nuclear localization signal (NLS). The NLS serves to enhance the sensitivity of effector detection in host cells by concentrating them in the rice nucleus. Using this sensitive assay, it has been shown that some translocated cytoplasmic effectors move ahead of the invading pathogen, into 3 to 4 layers of surrounding rice cells, presumably to prepare these cells for fungal colonization[28].

The distinct localization patterns of cytoplasmic and apoplastic effectors within the EIHM compartment raises questions regarding the mechanism by which effectors are secreted by IH within living plant cells. Protein secretion associated with apical tip growth in filamentous fungi involves the Spitzenkörper, the vesicle supply centre feeding vesicles to growing hyphal tips[29-32]. The 3-component polarisome complex

nucleates actin cables for transporting vesicles to the growth point. Near the polarized secretion site, vesicles dock with the exocyst, a complex of 8 proteins that has been implicated in tethering vesicles to the target membrane before fusion. However, it is becoming clear that the exocyst plays a role at many sites in a cell as a spatio-temporal regulator of membrane trafficking in response to diverse signals[33]. Fusion of secretory vesicles to the plasma membrane is then directed by SNAREs (soluble N-ethylmaleimide-sensitive factor attachment protein receptors), with the v-SNARE on the vesicle, and cognate t-SNARE on the membrane. Hyphal growth and secretion in filamentous fungi was thought to occur exclusively at the hyphal tips, but this no longer appears to be the case[29]. In *Trichoderma reesei* and *Aspergillus oryzae*, exocytosis mediated by SNARE proteins can also occur in subapical hyphal compartments[34,35].

In this study, we have focused on investigating how IH secrete effectors during host cell invasion. We were specifically interested in determining whether effectors destined for translocation to host cells follow the same secretory route as those that accumulate in the apoplast. Here, we present evidence for two distinct secretory pathways in *M. oryzae*. We show that BICs are plant-derived, membrane-rich interfacial structures associated with accumulation of effectors that ultimately enter host cells, and that subapical, BIC-associated IH cells are enriched in secretion machinery components. Using a combination of pharmacological and gene functional analyses, we show that the conventional fungal ER-Golgi secretion pathway is involved in secretion of apoplastic effectors, but not cytoplasm effectors and conversely, that cytoplasmic, effectors, require exocyst components Exo70 and Sec5 for efficient secretion. Taken together, our results are consistent with operation of two distinct secretory pathways for effector delivery during plant infection by the rice blast fungus.

Results

The Biotrophic Interfacial Complex (BIC) is a plant-derived structure. To define the location and structure of the BIC, we first generated fungal transformants expressing fluorescently-labeled plasma membrane and cytoplasmic markers, together with BIC-localized cytoplasmic effectors (Fig. 1b; Supplementary Fig. 1). Red fluorescence of cytoplasmic effector Pwl2:mRFP in the BIC was consistently located outside the fungal plasma membrane, which was visualized by expression of the *M. oryzae* membrane ATPase Pma1 as a translational fusion to GFP (Fig. 1b). These results confirmed that the BIC lies outside the fungal plasma membrane. We then generated transgenic rice lines expressing the fluorescently-labeled plasma membrane marker Lti6B-GFP and the ER marker, HDEL-GFP, which provided evidence that BICs are associated with concentrated regions of plant plasma membrane and ER (Fig. 1c,d). When considered together, these results demonstrate that the BIC is a plant-derived interfacial structure and that effectors must be secreted by the invading fungus in order to be observed so specifically at the BIC.

Organisation of secretory complexes within invasive hyphae of *M. oryzae*. To investigate mechanisms of effector secretion by IH inside rice cells, we identified *M. oryzae* orthologs of genes implicated in polarized growth and secretion (see Supplementary Fig. 2, and Supplementary Table 1)[23,30,32,33]. These genes encoded the myosin motor regulatory component Mlc1 (MGG_09470.6) (associated with the Spitzenkörper in *C. albicans*[23]), polarisome component Spa2 (MGG_03703.6), and exocyst component Exo70 (MGG_01760.6). Additional genes encoded v-SNARE Snc1 (MGG_12614.6) and t-SNARE Sso1 (MGG_04090.6), which together mediate docking and fusion of vesicles with the plasma membrane target site[35]. All genes were expressed in *M. oryzae* under control of their native promoters and with C-terminal translational

fusions of GFP. Each putative secretion component localized as expected, showing concentrated fluorescence at the tips of vegetative hyphae growing on agar medium (Supplementary Fig. 3). Spitzenkörper localization of Mlc1:GFP was confirmed by co-localization with the Styryl dye FM4-64, the endocytotic tracer dye that is a generally-accepted Spitzenkörper marker (Supplementary Fig. 3a)[23,36-38]. All five secretory components also concentrated at the growing tips of primary hyphae adjacent to BICs (visualised by cytoplasmic effector Pwl2:mRFP[28]) (Fig. 2a and Supplementary Fig. 3). Therefore, secretory machineries of vegetative and primary invasive hyphae appear similarly organised.

After primary hyphae differentiated into bulbous IH, Mlc1:GFP no longer identified a Spitzenkörper at invasive hyphal tips, which is consistent with results after differentiation of *C. albicans* hyphae into pseudohyphae[23]. Instead, Mlc1:GFP showed significant focal fluorescence in the subapical BIC-associated cells, which were no longer growing (Fig. 2b). Polarisome marker Spa2:GFP remained localized at hyphal growth points (Fig. 2c), and was not observed in the BIC-associated IH cell. Similar to Mlc1:GFP, Snc1:GFP, Exo70:GFP and Sso1:GFP each showed significant focal fluorescence in the subapical BIC-associated cells (Fig. 2d-f). In subsequently invaded cells, all markers first showed significant fluorescence at tips of the initially tubular IH that entered the cell. After differentiation of bulbous IH, all markers except Spa2:GFP localized to the BIC-associated IH cell. This is shown for Sso1:GFP fluorescence in the 7 visible hyphae growing in a second-invaded cell (Fig. 2g). We conclude that primary hyphae and bulbous IH are distinct morphological cell types and switching between tubular and bulbous IH *in planta* may involve a spatio-temporal reorientation of secretory machinery. Additionally, after differentiation and further growth, we conclude that subapical bulbous IH cells associated with BICs are capable of active secretion.

Brefeldin A treatment identifies distinct effector secretion pathways. To test the nature of fungal secretion, we first exposed *M. oryzae* IH to Brefeldin A (BFA), which inhibits conventional ER-to-Golgi secretion in fungi[39]. For these experiments, we used a *M. oryzae* strain expressing both apoplastic effector Bas4:GFP and cytoplasmic effector Pwl2:mCherry:NLS (Fig. 3a). We found that the apoplastic effector Bas4:GFP was retained in the hyphal ER within 3 hours of exposure of infected rice tissue to BFA, but cytoplasmic effector Pwl2:mCherry:NLS still exhibited BIC-accumulation with no observable fluorescence inside the hyphal ER (Fig. 3b). The distinct BFA localization patterns for Pwl2 and Bas4 were independent of the fluorescent proteins used and the added NLS (Supplementary Fig. 4a). To determine whether these effects were general, we tested additional cytoplasmic effectors AVR-Pita (Fig. 3c), Bas1 (Fig. 3c) and Bas107 (Supplementary Fig. 4b). Secretion and BIC localization of all three continued in the presence of BFA with no accumulation of fluorescence inside IH. By contrast, secretion of additional apoplastic effectors Slp1:GFP[14] and Bas113:mRFP was blocked by BFA treatment (Supplementary Fig. 4c).

To confirm that secretion of Pwl2:GFP into BICs continued in the presence of BFA, we performed fluorescence recovery after photobleaching (FRAP) analysis. Using transformants expressing both Pwl2:GFP and Bas4:mRFP, we photobleached Pwl2:GFP in subapical BICs and then monitored fluorescence recovery over time in the presence or absence of BFA. For BFA-treated tissues, retention of Bas4:mRFP in the hyphal ER confirmed that the treatment was effective before fluorescence in the BICs was photobleached. As expected from previous results[28], full recovery of fluorescence in BICs occurred within 3 hours, and identical recovery rates were observed in the presence or absence of BFA (Fig. 3d). Recovery of fluorescence therefore indicates that the fungus continues to secrete cytoplasmic effector protein into BICs in the presence of

BFA. During fungal invasion of rice cells, BFA therefore reproducibly blocked secretion of apoplastic effectors, but not BIC accumulation of cytoplasmic effectors.

We tested whether the fungal cytoskeleton is important for effector secretion using the microtubule inhibitor Methyl 1-(butylcarbamoyl)-2-benzimidazolecarbamate (MBC) and the actin inhibitor latrunculin A (LatA). Secretion of Bas4:mRFP was visibly impaired when infected rice tissues were treated with MBC or LatA, but secretion of Pwl2:GFP did not appear to be impaired (Supplementary Fig. 5). FRAP experiments again confirmed that Pwl2:GFP continued to accumulate in BICs in the presence of MBC or LatA, further supporting the operation of distinct effector secretion mechanisms.

Efficient secretion of cytoplasmic effectors requires the exocyst complex. We next investigated protein secretion components necessary for effector secretion. In yeast, Exo70 and Sec5 are subunits of the octameric exocyst complex implicated in spatiotemporal regulation of membrane trafficking[33]. We produced a series of targeted gene replacement mutants for the *M. oryzae EXO70* and *SEC5* genes in strains expressing fluorescent effectors (Supplementary Fig. 6). These mutants formed normal-appearing IH in first-invaded rice cells. Compared to isogenic wild type strains imaged in the same experiment (Fig. 4a), all Δ*exo70* and Δ*sec5* mutants showed significant accumulation of cytoplasmic effectors Pwl2:mCherry:NLS and Bas1:mRFP inside BIC-associated cells, indicating impaired secretion (Fig. 4). Secretion of Pwl2:mCherry:NLS was impaired in 60 of 65 random infection sites for Δ*exo70* mutants (Fig. 4b) and in 37 of 40 randomly selected infection sites for Δ*sec5* mutants (Fig. 4c). Effector fluorescence inside the IH occurred in the form of small vesicles or vacuole-like puncta. Fluorescence intensity distribution scans confirmed significant retention of cytoplasmic effectors inside IH cells. Importantly, the internal cytoplasmic effector fluorescence was

generally restricted to the BIC-associated IH cells under these imaging conditions rather than at hyphal tips, although in 20% of imaged sites, low levels of Pwl2 fluorescence were observed in vacuoles in subsequently-formed IH. Similar results were obtained for independent transformants expressing a different cytoplasmic effector, Bas1:mRFP (Fig. 4d-f). Conversely, secretion of the apoplastic effector Bas4 was not impaired (Fig. 4b,c).

Partial retention of these cytoplasmic effectors inside BIC-associated IH cells contrasts to results of extensive imaging of BIC-accumulated effectors in wild type strains[14,25,28], in which effector fluorescence was never observed inside the BIC-associated cells. Additionally, Δ*exo70* and Δ*sec5* mutants showed significant pathogenicity defects (Fig. 5a,b). We conclude that the exocyst is critical both for efficient secretion into BICs and for fungal pathogenicity.

A t-SNARE Sso1 is required for normal BIC development. Targeted gene replacement of the *M. oryzae* t-SNARE *SSO1* (Supplementary Fig. 6) produced mutants with both a BIC developmental defect (Figure 5c-e) and reduced pathogenicity (Fig. 5a,b). In contrast to wild type strains, independent Δ*sso1* mutants showed 2 points of focal accumulation of cytoplasmic effectors. One appeared to be a normal BIC adjacent to the first-differentiated IH cell and the second was a focal fluorescent region adjacent to the primary hypha before the point of differentiation. This 'double BIC' phenotype was observed in 32 of 40 IH expressing Pwl2:mCherry:NLS and in 25 of 30 IH expressing Bas1:mRFP. Double BICs were not observed with any wild type strains or mutants defective in other secretion pathway genes. When considered together with the localization pattern of Sso1:GFP (Fig. 2f,d), these results implicate the t-SNARE Sso1 in accumulation of effectors at the BIC.

Discussion

In this report we have provided evidence that *M. oryzae* possesses two distinct routes by which it secretes effector proteins during biotrophic invasion of rice (Fig. 6). Apoplastic effectors accumulate at the host-pathogen interface and are actively secreted via the conventional secretory process previously defined in filamentous fungi. As expected, this process is inhibited by BFA, implicating Golgi-dependent secretion. By contrast, cytoplasmic effectors destined for delivery into rice cells are secreted by a different pathway involving the exocyst complex and insensitive to BFA treatment.

Previous studies have highlighted the presence of a membrane-rich complex, the BIC, at the host pathogen interface in rice blast infection. We have now clearly shown that the BIC is a plant-derived interfacial structure that lies outside of the fungal plasma membrane and cell wall in a region rich in plant plasma membrane and ER. We have also shown that the exocyst components Exo70 and Sec5 play roles in an unconventional secretory mechanism for blast effectors, which leads to their accumulation at the BIC. Both Δ*exo70* and Δ*sec5* mutants show inefficient cytoplasmic effector secretion but are still viable, suggesting that there is functional redundancy in the system. Indeed, yeast Exo70 and Sec3 are both exocyst subunits identified as playing a role in docking secretory vesicles to active sites of exocytosis[33]. Perhaps Exo70 function can be at least partially fulfilled by Sec3 or some unknown component. The exocyst component Sec5 appears to function by interacting with Exo70 and Sec3 to mediate polarized targeting of secretory vesicles to the plasma membrane. Additionally, both mutant analysis andlocalization results indicate that the t-SNARE Sso1 plays a role in IH of *M. oryzae*. The Δ*sso1* mutant consistently produces second BIC-like regions of focal effector accumulation midway through relatively long primary hyphae (Fig. 5). This Sso1:GFP localization pattern is consistent with specialized exocytotic pathways employing different surface SNAREs at different hyphal sites for cytoplasmic effector

secretion and for hyphal growth. There is precedent for involvement of SNARE proteins in secretion from subapical regions of hyphae from the industrially-important cellulolytic filamentous fungus *T. reesei*[35], in which there is more than one pathway for exocytosis which employs different t-SNARE proteins at distinct sites in hyphae. That is, a complex of the v-SNARE SncI and t-SNARE SsoI localizes to subapical plasma membrane regions and a different complex localizes to growing hyphal tips.

Secretion of cytoplasmic effectors by a distinct pathway that is predominantly localized to BIC-associated cells is consistent with the BIC being important in effector delivery or sequestration by the host. BICs have been hypothesized as the site of translocation of cytoplasmic effectors into the rice cytoplasm based on a strong correlation between preferential BIC localization of effectors such as PWL2, Avr-Pita, AvrPit-z, Avr-Pia and Avr-Pii and translocation to the rice cytoplasm ([11,28] and Yi and Valent, unpublished data). Several aspects of this study are consistent with the idea that BIC-associated bulbous IH cells actively secrete cytoplasmic effectors. First, BIC-associated bulbous IH cells contain concentrated fluorescent foci of GFP-labeled secretory pathway components, the myosin regulatory light chain Mlc1, exocyst component Exo70, v-SNARE Snc1 and t-SNARE Sso1. The only exception to this was the polarisome component Spa2, which still localized to the IH growth points, similarly to Spa2 accumulation at pseudohyphal growth points in *C. albicans*[18]. Secondly, fluorescent cytoplasmic effectors rapidly accumulate at BICs following photobleaching and this process is BFA-insensitive. Thirdly, cytoplasmic effector proteins accumulate predominantly inside the BIC-associated cells of Δ*exo70* and Δ*sec5* mutants rather than at hyphal tips, suggesting that exocytosis may occur predominantly from BIC-associated cell. Our results are also consistent with new evidence that expression of cytoplasmic effectors is highly upregulated in BIC-associated cells compared to lower basal levels of expression throughout the IH at later infection stages (C.H. Khang and B.

Valent, unpublished results). We also found that the t-SNARE Sso1 not only localized adjacent to the BIC, but that mutants lacking this gene showed defects in normal BIC development. When considered together these observations support a central role for the BIC as a destination for secretion of effectors that are ultimately taken up by rice cells.

In summary, our results provide evidence that targeting fungal effectors to distinct host compartments may require separate, specialised secretory processes in the rice blast fungus, *M. oryzae*. Identifying how these processes function will prove pivotal in controlling rice blast disease and also determining the nature and evolution of exocyst processes in fungal pathogens.

Methods

Assays for live cell imaging of *M. oryzae* vegetative hyphae and invasive hyphae in rice sheath epidermal cells. Fungal transformants were stored in dried filter papers at -20°C, and cultured on oatmeal agar plates at 24°C under continuous light[40]. From fresh fungal cultures, a small plug cut from the hyphal growth zone was placed on the edge of a sterile water agar slide and incubated in a humid chamber for 16 to 18 hours. Vegetative hyphae continued to grow on the water agar surface facilitating observation of filamentous vegetative hyphae during active growth. First, new fungal transformants were evaluated at 16 to 18 hours post inoculation (hpi) using vegetative hyphae to confirm fluorescence expression. Active growth was documented by time-lapse imaging using AxioVisionLE software, version 4.8. Independent transformants were selected for use based on the highest intensity of the fluorescent marker. These transformants were evaluated during infection *in planta* by rice sheath inoculations. Rice sheath inoculations were performed as described[17] using the susceptible rice line YT-16. Briefly, five cm-long sheath pieces from 3 week-old plants were placed in a glass container under high humidity conditions. Sheaths were placed on acrylic stands to

avoid contact with wet paper and to hold epidermal cells directly above the mid-vein horizontally flat for uniform inoculum distribution in the trimmed sheath pieces. A spore suspension (~200 µl of a suspension of 1 X 10^5 spores/ml in 0.25% gelatin, Cat. # G-6650, Sigma Aldrich) was injected in one end of the sheath using a 200 µl pipette. Each segment was trimmed at 22 to 36 hpi and imaged immediately. Conventional epifluorescence and differential interference contrast microscopy (DIC) were performed with a Zeiss Axioplan 2 IE MOT microscope, using a 63X/1.2 NA (numerical aperture) C-Apochromat water immersion objective lens. Images were acquired using a Zeiss AxioCam HRc camera and analyzed with Zeiss Axiovision digital image-processing software, version 4.8. Fluorescence was observed with an X-Cite®120 (EXFO Life Sciences) mercury lamp source. Filter sets used were: GFP (excitation 480 ± 10 nm, emission 510 ± 10 nm, filter set 41020, Chroma Tech. Corp., Rockingham, VT); and mRFP, mCherry or FM4-64 (excitation 535 ± 25 nm, emission 610 ± 32 1/2 nm, Zeiss). Confocal imaging was performed with a Zeiss Axiovert 200M microscope equipped with a Zeiss LSM 510 META system using two water immersion objectives, 40X/1.2 NA and 63X/1.2 NA C-Apochromat. Excitation/emission wavelengths were 488 nm/505-550 nm for EGFP, and 543 nm/560-615 nm for mRFP, mCherry and FM4-64. Images were acquired and processed using LSM510 AIM version 4.2 SP1 software.

Identification of *M. oryzae* secretory pathway genes. Sequence data was accessed from the *Saccharomyces* Genome Database (SGD) (http://www.yeastgenome.org/sitemap.html) under the following accession numbers MLC1/YGL106W, SNC1/YAL030W, SPA2/YLL021W, SEC5/YDR166C, SSO1/YPL232 and EXO70/YJL085W. Analysis of the predicted protein sequences was performed using BLASTP[41] from NCBI GeneBank (http://www.ncbi.nlm.nih.gov/genbank/), Broad Institute's *Magnaporthe grisea*

Genome Database (http://www.broadinstitute.org/annotation/genome/magnaporthe_grisea/MultiHome.html, MGOS (http://www.mgosdb.org/), SGD (http://www.yeastgenome.org/sitemap.html), and the Biological General Repository for Interaction Datasets (BioGRID) database (http://www.thebiogrid.org). Multiple protein sequence alignments were used to find diagnostic patterns to characterize protein families and to detect homology between *M. oryzae* ortholog sequences and existing families of sequences. These protein sequence alignments were performed using CLUSTALW2 from EMBL-EBI (http://www.ebi.ac.uk/Tools/clustalw2/index.html. In ClustalW2, the guide trees, used to guide the multiple alignment, were calculated by a distance matrix method using the Neighbour Joining tree_BLOSUM62[42]. *M. oryzae* genes selected were *MLC1* (MGG_09470), *SNC1* (MGG_12614), *SPA2* (MGG_03703), *EXO70* (MGG_01760), *SEC5* (MGG_07150), and *SSO1* (MGG_04090). Further details are listed in Supplementary Table 1.

FM4-64 staining and treatment with pharmacological inhibitors. Fungal transformants expressing secretion machinery components were treated with FM4-64 (4 µg/ml in water). An aqueous 17 mM stock solution of FM4-64 (Cat # 13320, Invitrogen, Carlsbad, CA) was made and stored at -20ºC as described in Bolte et al[43]. Vegetative hyphae at ~16 to 18 hpi on a water agar slide were incubated for 5 to 30 min in a 10 µM aqueous solution of FM4-64 for uniform staining. In planta, inoculated trimmed leaf sheaths, ~24 hpi, were incubated in a 10 µM aqueous working solution for 1 to 5 hours. To examine the effects of brefeldin A (BFA) (Sigma) on IH secretion of effectors in planta, we prepared stock solutions of BFA, 10 mg/ml, in dimethyl sulfoxide (DMSO, Sigma) according to Bourett and Howard[44]. We incubated the leaf sheath tissue at 27 - 28 hpi (2 x 10^4 spores/ml in 0.25% gelatin solution) in 50 µg/ml

BFA (0.1% DMSO). Treatments with the microtubule inhibitor Methyl 1-(butylcarbamoyl)-2-benzimidazolecarbamate (MBC, the active ingredient in the fungicide benomyl) and the actin inhibitor latrunculin A (LatA) were performed on infected sheath tissue to examine the effects of hyphal cytoskeletal organization. Stock solutions of 10mg/ml MBC (Sigma) and 100µg/ml latrunculin A (Sigma) were prepared according to Czymmek et al[45]. For in planta experiments with both drugs, we prepared working solutions of 50µg/ml in 0.1% DMSO and treated inoculated tissue as described for BFA.

Fluorescence recovery after photobleaching (FRAP). Experiments were performed using a Zeiss LSM 510 confocal microscope with a 488nm argon laser and a C-Apochromat 40x/1.2 NA water immersion objective at 2x optical zoom. For FRAP analyses, the specific region of interest (ROI) covering the entire fluorescence in the BIC was selected for bleaching. We used twenty bleaching iterations at 100% laser power for a BIC containing cytoplasmic effector Pwl2:GFP fusion protein. Image scans were taken with the acousto-optic tunable filter attenuated to 5% laser power immediately before and after bleaching. Images were recorded up to 3 hours after bleaching of the BIC region. During these time periods, the ROI showed from 70% to complete recovery. For quantitative analyses, the GFP fluorescence recovery curves were measured as the mean intensity of ROI pixels using the LSM software (version 4.2 SP1), normalized, and graphed using Microsoft Excel.

Vector construction and Agrobacterium-mediated transformation of M. oryzae. Unless noted otherwise, transformation cassettes to observe M. oryzae fluorescently-labeled cellular components and effector proteins were constructed containing the entire protein coding sequence with its native promoter (~1 kb) in a translational fusion with

GFP, mRFP or mCherry. The GFP gene used was the EGFP gene from Clontech. The mRFP gene was obtained from Campbell et al[46]. The mCherry gene from Shaner et al[47] was isolated from pAN583. The plasmid containing the PWL2 promoter and coding sequence fused to a nuclear targeting mCherry:NLS sequence was obtained from Khang et al[28]. Each cassette was cloned into the pBHt2 binary vector for fungal transformation by A. tumefaciens[48] and for selection of positive transformants using resistance to hygromycin or geneticin (G418). Details of plasmid construction and corresponding fungal transformants used in this study are listed in Supplementary Tables 2 and 3, respectively. M. oryzae field isolates O-137[49] and Guy11[50], and laboratory strain CP987[49] were used as recipients. Fungal transformants were purified by isolation of single spores and 7 to 10 independent transformants were analyzed per gene.

Targeted gene replacements in *M. oryzae*. Targeted gene replacements for *EXO70*, *SEC5* and *SSO1* were carried out using the split marker method[51]. A 1.4 kb hygromycin resistance cassette or a 2.8 kb sulphonylurea resistance cassette replaced the coding sequence of each gene. Approximately 1.0 kb of flanking sequences were used for homologous recombination, and positive transformants were confirmed by DNA gel blot analysis (Supplementary Fig. 6). At least two positive transformants were used for further analysis of every gene in each background.

Generation of transgenic rice plants. Gene fusions for expressing the plant plasma membrane marker low temperature inducible protein 6B, LTi6B:GFP[52], and the Endoplasmic Reticulum marker GFP:HDEL[53] were transformed into rice cultivar *Oryza sativa* cv Sasanishiki[54] using standard rice transformation. Putative transformants of rice were selected on 100 μg mL^{-1} hygromycin, confirmed by DNA gel blot, and expression checked by qRT-PCR, immunoblotting, and epifluorescence microscopy.

Accession Numbers. In GenBank, the sequence data for the genes used in this study are under U26313 for PWL2, FJ807764 for Bas1, AF207841 for AVR-Pita1, MGG_10020.6 for Bas107, FJ807767 for Bas4, MGG_05785.6 for Bas113 and MGG_10097.6 for Slp1.

Supplementary Information

Supplementary Figures

Supplementary Figure 1. The BIC is a plant-derived interfacial structure.

Supplementary Figure 2. Alignment of the predicted amino acid sequences for protein markers of secretory components in *M. oryzae* and other fungi.

Supplementary Figure 3. Secretion in primary invasive hyphae inside plant cells resembles secretion by vegetative hyphae *in vitro*.

Supplementary Figure 4. Cytoplasmic effector sequences and not the fluorescent protein or nuclear localization sequences determine BFA-insensitive secretion.

Supplementary Figure 5. Secretion of apoplastic effectors is more dependent on cytoskeletal function than is secretion of cytoplasmic effectors.

Supplementary Figure 6. Southern blot analysis of targeted gene deletion mutants.

Supplementary Tables

Supplementary Table 1. Cellular markers targeted for identification of protein secretion components in fungi.

Supplementary Table 2. Plasmids used.

Supplementary Table 3. Fungal and rice transformants.

Acknowledgements We thank Melinda Dalby for technical support at KSU. This work was supported by a grant from the Biotechnology and Biological Sciences Research Council to NJT, a Halpin Scholarship to YFD and YKG, a Sainsbury studentship from Gatsby Charitable Foundation to TAM, and a European Research Council Advanced Investigator award to NJT; by grants from the National Research Initiative Competitive Grants Program (Grants 2008-35600-18809 and 2010-65108-20538) from the USDA National Institute of Food and Agriculture to BV; and a Grant-in-Aid by MAFF (Genomics for Agricultural Innovation PMI-0010), PROBRAIN and MEXT, Japan (Grant-in-Aid for Scientific Research on Innovative Areas 23113009) to RT and HS. We acknowledge support from the COBRE Confocal Microfluorometry and Microscopy Core at KSU, funded by NIH Grant P20 RR-017686. This is contribution # 13-140-J from the Agricultural Experiment Station at KSU.

Author Contributions

B.V. and N.T. developed the research plan and experimental strategy. M.C.G. helped to design experiments, constructed fluorescently-tagged *M. oryzae* strains and carried out live cell imaging experiments using laser confocal microscopy, FRAP and inhibitor analysis. Y.F.D. helped to design experiments, constructed fluorescently-tagged *M. oryzae* strains and a range of targeted deletion mutants. Y.K.G. generated *M. oryzae* exocyst mutants, fluorescently-tagged strains to define exocyst components and carried out pathogenicity assays. T.A.M. designed and constructed transgenic rice and *M. oryzae* lines expressing fluorescent membrane markers to define the BIC using laser enhanced epifluorescence microscopy. M.Y. generated and characterized *M. oryzae* strains. H.S. and R.T. generated transgenic rice lines. All authors analysed data and contributed to writing the paper, led by B.V. and N.T.

Author Information

These authors contributed equally to this work:

Martha C. Giraldo and Yasin F. Dagdas

Yogesh K. Gupta and Thomas A. Mentlak

Author Affiliations

Department of Plant Pathology, 4024 Throckmorton Plant Sciences Center, Kansas State University, Manhattan, KS 66506-5502, USA

Martha C. Giraldo, Mihwa Yi and Barbara Valent

School of Biosciences, Geoffrey Pope Building, University of Exeter, Exeter, EX4 4QD, U.K.

Yasin F. Dagdas, Yogesh K. Gupta, Thomas A. Mentlak and Nicholas J. Talbot

Iwate Biotechnology Research Center, Narita 22-174-4, Kitakami, Iwate 024-0003, Japan

Hiromasa Saitoh and Ryohei Terauchi

Present address: Cambridge Consultants Ltd, Science Park, Milton Road, Cambridge

CB4 0DW, U.K.

Thomas A. Mentlak

Competing financial interests

The authors declare no competing financial interests.

Corresponding authors

Correspondence to: Barbara Valent and Nicholas J. Talbot, who contributed equally.

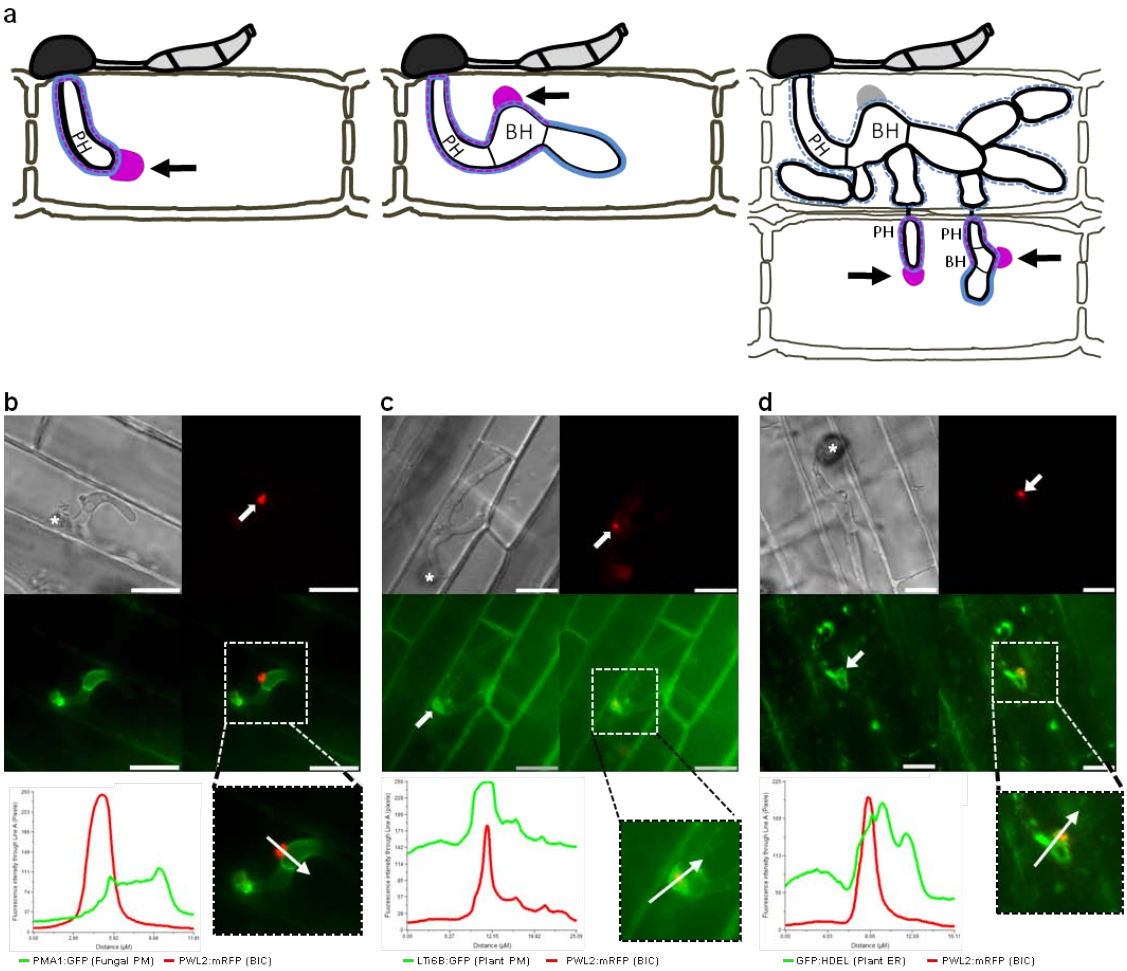
a
PH
BH
b
c
d
PMA1:GFP (Fungal PM)
PWL2:mRFP (BIC)
LTi6B:GFP (Plant PM)
PWL2:mRFP (BIC)
GFP:HDEL (Plant ER)
PWL2:mRFP (BIC)

Figure 1. The biotrophic interfacial complex (BIC) is a plant-derived membrane-rich structure. (a) Schematic representation of the differentiation of a filamentous primary hypha (left, ~22-25 hours post inoculation, hpi) into a bulbous invasive hypha (middle, ~26-30 hpi), in a first-invaded rice cell. This differentiation process is repeated for each new hypha that invades a living neighbor cell (right, ~36-40 hpi). Cytoplasmic effectors show preferential accumulation in the BIC (black arrows), which is first located in front of growing primary hyphal tips, and then remains behind beside the first differentiated bulbous IH cell. Typical accumulation patterns for cytoplasmic (magenta) and apoplastic (blue) effectors are shown. (**b-d**) Live cell imaging of *M. oryzae* infection of rice epidermis with the BIC (Red) visualized by accumulation of IH-secreted Pwl2:mRFP. (**b**) The BIC (Red) is located outside the fungal plasma membrane (Green), which was visualised by expression of *M. oryzae* ATPase Pma1:GFP, imaged at 23 hpi. Lack of co-localisation between Pwl2:mRFP and Pma1:GFP, indicated by fluorescence intensity distribution, confirms that the BIC does not contain fungal plasma membrane. (**c**) The BIC (Red) co-localized with intense fluorescence from a rice plasma membrane marker LTi6B:GFP (Green), visualized in transgenic rice at 24 hpi. Note that the plant plasma membrane marker also outlined the entire IH, consistent with invagination around the fungus during cell invasion. Co-localisation indicated by fluorescence intensity distribution indicates that the BIC contains material derived from plant plasma membrane. **(d**) The BIC (Red) co-localized with fluorescence from rice ER marker GFP:HDEL (Green) expressed in transgenic plants and imaged at 24 hpi. Fluorescence intensity distribution demonstrates co-localisation of the BIC and plant ER. White asterisks in DIC images indicate appressoria. Scale bars, 10µm.

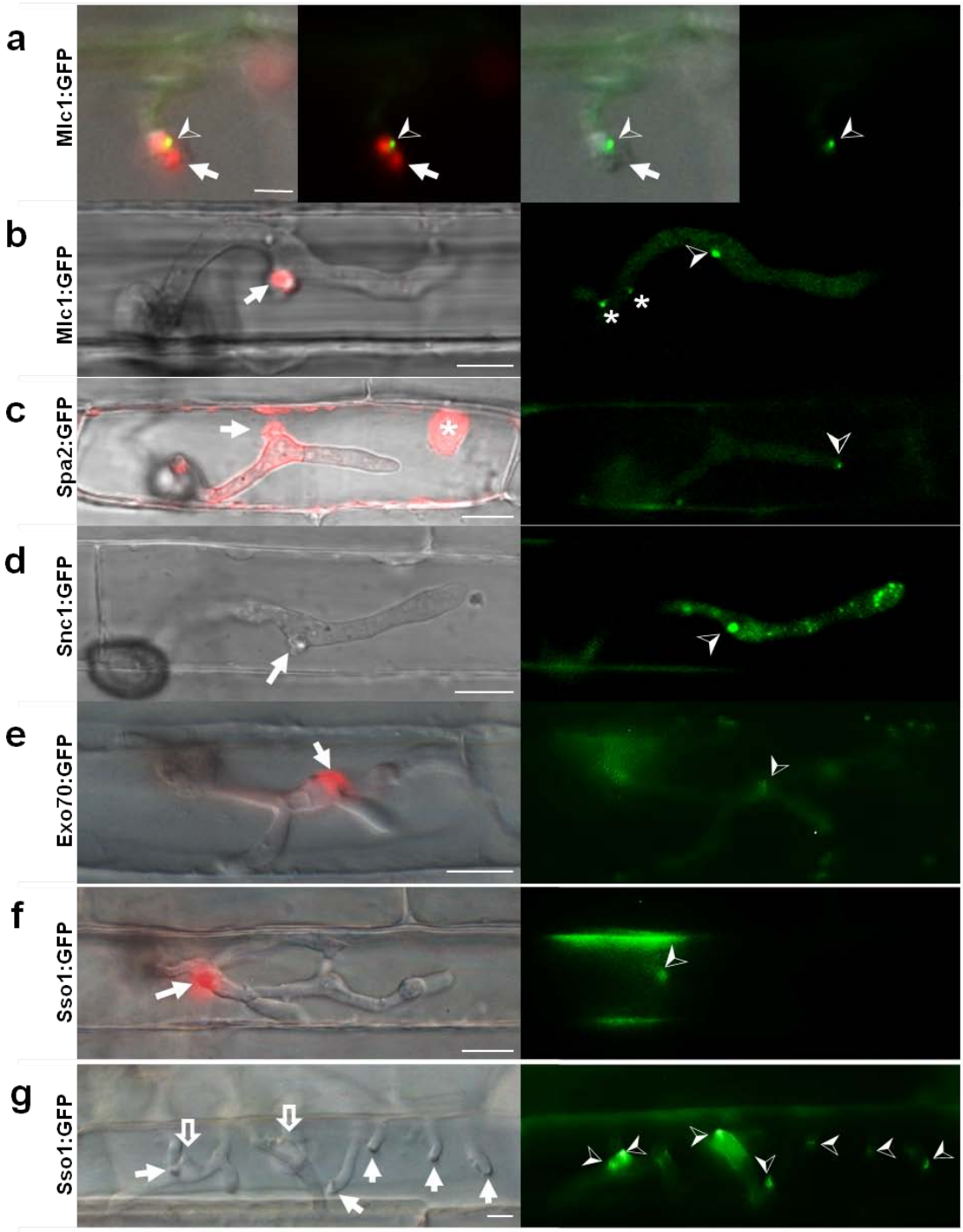
a
Mlc1:GFP
b
Mlc1:GFP
c
Spa2:GFP
d
Snc1:GFP
e
Exo70:GFP
f
Sso1:GFP
g
Sso1:GFP

Figure 2. BIC-associated IH cells contain components of the secretory machinery. All live cell images are representative of at least 5 biological replicates with >50 images each. BICs are labeled by arrows in all panels and by cytoplasmic effector Pwl2:mRFP in all panels except d and g. **(a)** The myosin regulatory light chain Mlc1:GFP (➢) labels the Spitzenkörper at the primary hyphal tip before hyphal differentiation at 24 hpi. Images left to right: merged GFP, mRFP and bright-field; merged GFP and mRFP; merged GFP and bright-field; and GFP alone. Scale bar, 5µm. **(b)** After differentiation of bulbous IH at 27 hpi, Mlc1:GFP accumulates in a single large fluorescent punctum in the BIC-associated bulbous IH cell (➢) and near septa (*). Spitzenkörper-like fluorescence was not observed in the growing hyphal tips. Images left to right: merged mRFP and bright-field; and GFP alone. **(c)** Polarisome component Spa2:GFP localizes as a distinct punctum at the tip of growing IH (➢) at 27 hpi. Spa2 fluorescence is not observed in the subapical BIC-associated IH cell. In this image, saturated fluorescence from Pwl2:mRFP labels the rice cytoplasm and nucleus (*). Here, saturated Pwl2:mRFP fluorescence is seen is the EIHM compartment surrounding the BIC-associated cells as previously reported[28]. Images left to right: merged mRFP and bright-field; and GFP alone. (**d**) v-SNARE Snc1:GFP localizes to a large fluorescent point (➢) in the BIC-associated IH cell and to smaller vesicles in growing IH at 27 hpi. Images left to right: bright-field; and GFP alone. (**e**) Faint fluorescence from exocyst component Exo70:GFP localizes to the subapical BIC-associated cell at 28 hpi. Images left to right: merged bright-field and mRFP; and GFP alone. **(f)** t-SNARE Sso1:GFP (➢) localizes in the BIC-associated IH cell near the BIC, shown in a first-invaded rice cell at 27 hpi. Images left to right: merged bright-field and mRFP; and GFP alone. **(g)** t-SNARE Sso1:GFP (➢) in a second-invaded cell accumulated near BICs, as a crescent at the tips of 5 undifferentiated primary IH, and as puncta in 2 BIC-associated IH cells after

differentiation, at 40 hpi (as described in Fig. 1a, right panel). Images left to right: bright-field; and GFP alone. Scale bars, 10μm unless stated otherwise.

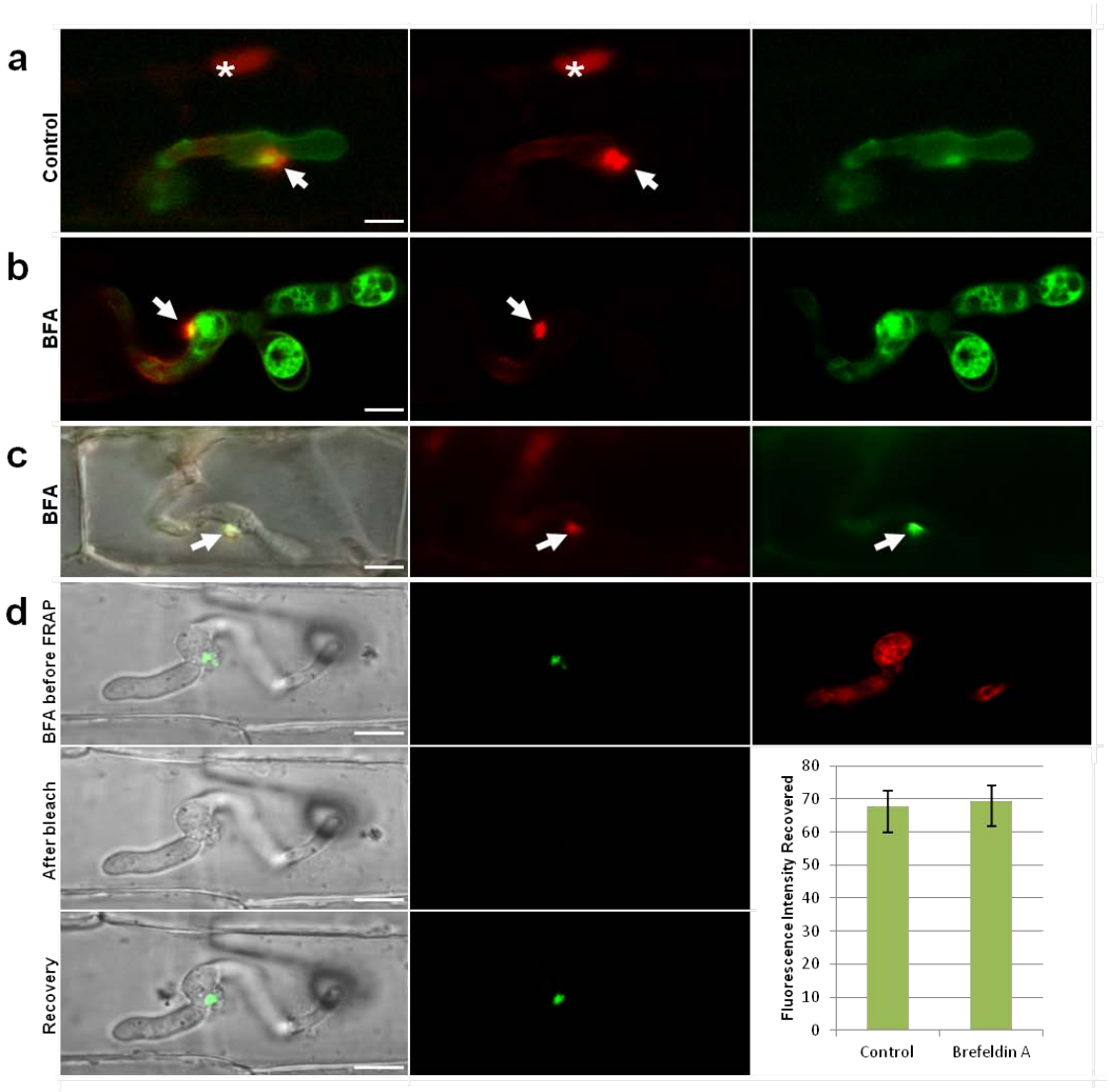
a
Control
b
BFA
c
BFA
d
BFA before FRAP
After bleach
Recovery
Fluorescence Intensity Recovered
80
70
60
50
40
30
20
10
0
Control
Brefeldin A

Figure 3. Brefeldin A blocks secretion of apoplastic effectors but not secretion of cytoplasmic effectors. (**a-c**) Images left to right: merged mCherry and GFP; mCherry alone; and GFP alone. **(a**) After secretion, cytoplasmic effector Pwl2:mCherry:NLS (red) shows preferential BIC localization (arrow) and translocation into the rice cell where it accumulates in the rice nucleus (*). Bas4:GFP shows apoplastic localization outlining the IH. **(b**) In the presence of BFA, Pwl2:mCherry:NLS remains BIC-localized (arrow), but Bas4:GFP (green) is retained in the fungal ER, imaged with the same transformant in (**a**) 10 hrs after exposure of infected rice tissue to BFA. **(c**) Cytoplasmic effectors Bas1:mRFP (red, middle) and AVRPita:GFP (green, right) still co-localized in the BIC (arrow) after 5 h exposure to BFA. **(d**) Fluorescence Recovery After Photobleaching (FRAP) demonstrates continuous secretion of Pwl2:GFP into the BIC in the presence of BFA. *M. oryzae* strains expressing Pwl2:GFP and Bas4:mRFP were incubated in BFA for 3 h before photobleaching of Pwl2:GFP in the BIC. Retention of Bas4:mRFP in the ER demonstrated that the BFA treatment was effective. Recovery of pre-bleach levels of Pwl2:GFP fluorescence was observed after 3 h in the presence of BFA, consistent with the recovery timeline for previous FRAP analysis[28]. Images left to right before photobleaching: merged bright-field and GFP; GFP alone; and mRFP alone. Images left to right after photobleaching and recovery: merged bright-field and GFP; and GFP alone. FRAP results were identical in the presence or absence of BFA ($p=0.019$). Bars show mean fluorescence intensity recovery after bleaching (mean$\pm$SD, four FRAP experiments). Scale bars, 10µm.

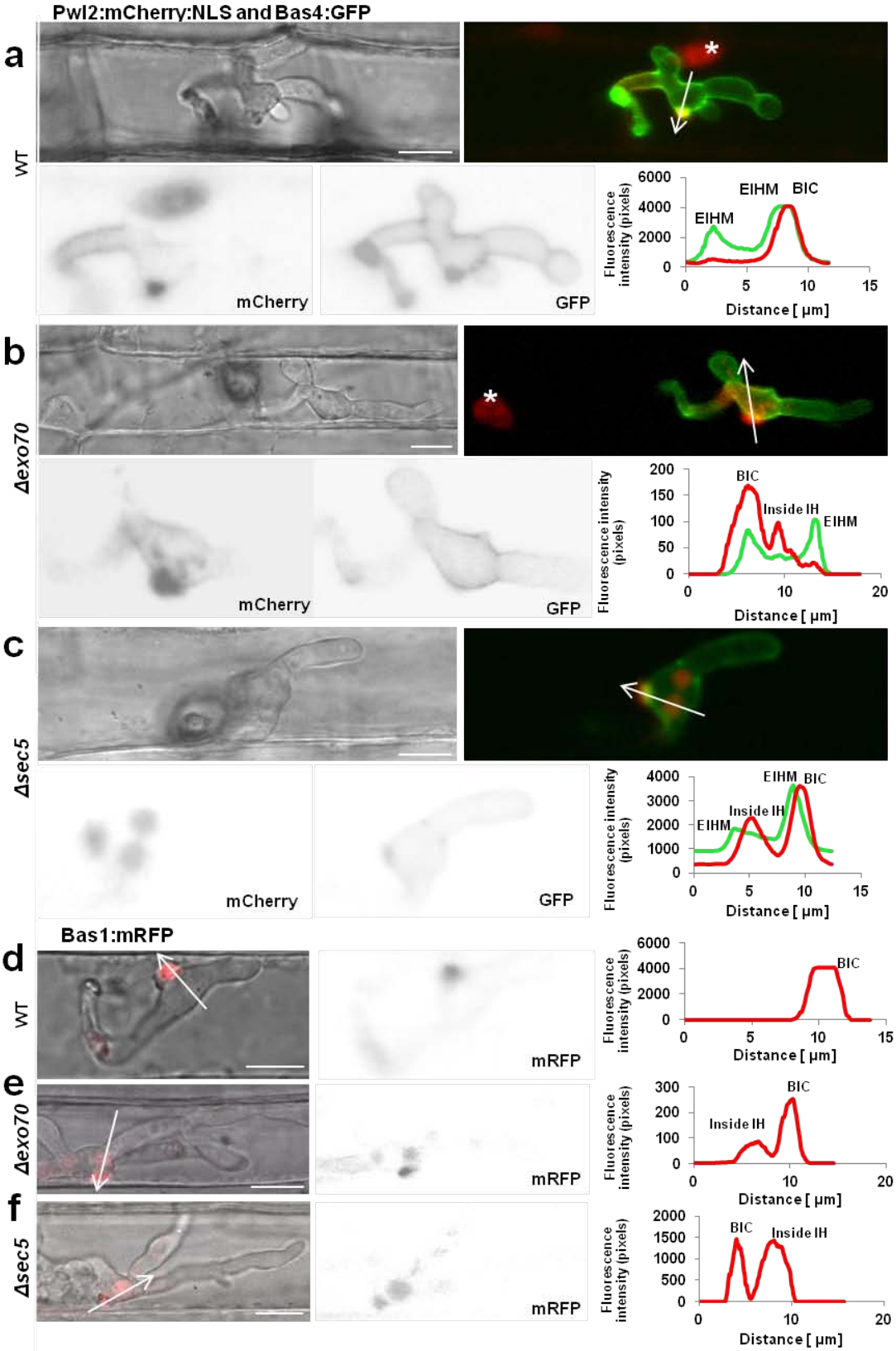
Pwl2:mCherry:NLS and Bas4:GFP
a
WT
mCherry
GFP
Fluorescence intensity (pixels)
EIHM
BIC
Distance [µm]
b
Δexo70
Inside IH
c
Δsec5
Bas1:mRFP
d
e
f
mRFP

Figure 4. Secretion of cytoplasmic effectors by *M. oryzae* involves exocyst components Exo70 and Sec5. (**a-c)**, Wild type strain Guy11 and corresponding mutants expressed Pwl2:mCherry:NLS and Bas4:GFP. Images clockwise from the upper left: bright field (BF); merged mCherry (red) and GFP (green); fluorescence intensity linescans for mCherry (red) and GFP (green) along the path indicated by the white arrow; GFP fluorescence alone in black and white inverse image; and mCherry fluorescence alone in black and white inverse image. **(a**) Pwl2:mCherry:NLS in wild type shows preferential BIC localization, translocation and accumulation in the rice nucleus (white asterisk). Bas4:GFP localizes to the EIHM compartment. (**b**) *Δexo70* mutant shows partial retention of Pwl2:mCherry:NLS, predominantly in the BIC-associated IH cell. Bas4:GFP secretion appears normal. Internal red fluorescence in the BIC-associated IH cell is further visualized by black and white inverse image (lower left) and confirmed by the fluorescence intensity scans, which show red fluorescence between the peaks of green fluorescence marking the EIHM. The red fluorescence in the rice nucleus is consistent with partial blockage of effector secretion. (**c**) *Δsec5* mutant showing partial retention of Pwl2:mCherry:NLS inside the BIC-associated IH cell, but no retention of Bas4:GFP, as further visualized by black and white inverse images and fluorescence intensity scans. (**d-f**) Images left to right: merged bright-field and mRFP; mRFP shown in inverse black and white; and corresponding fluorescence intensity scans. (**d**) Wild type strain Guy11 expressing Bas1:mRFP, which localizes to BICs and is translocated into the rice cytoplasm. Internal Bas1:mRFP fluorescence is not observed inside wild type IH cells. (**e**) Bas1:mRFP expressed by an *Δexo70* mutant shows significant retention inside the IH, predominantly in the BIC-associated cells. The Δ*exo70* mutants displayed impaired secretion of Bas1:mRFP in 22 of 28 imaged infection sites. (**f**) Bas1:mRFP expressed by an *Δsec5* mutant strain shows significant retention of Bas1:mRFP inside the IH. The Δ*sec5* mutants showed impaired Bas1

secretion of in 23 of 27 infection sites. Line scans shown are representative of wild type (n=20) and knock-out mutants (n=20 for each). Scale bars, 10µm.

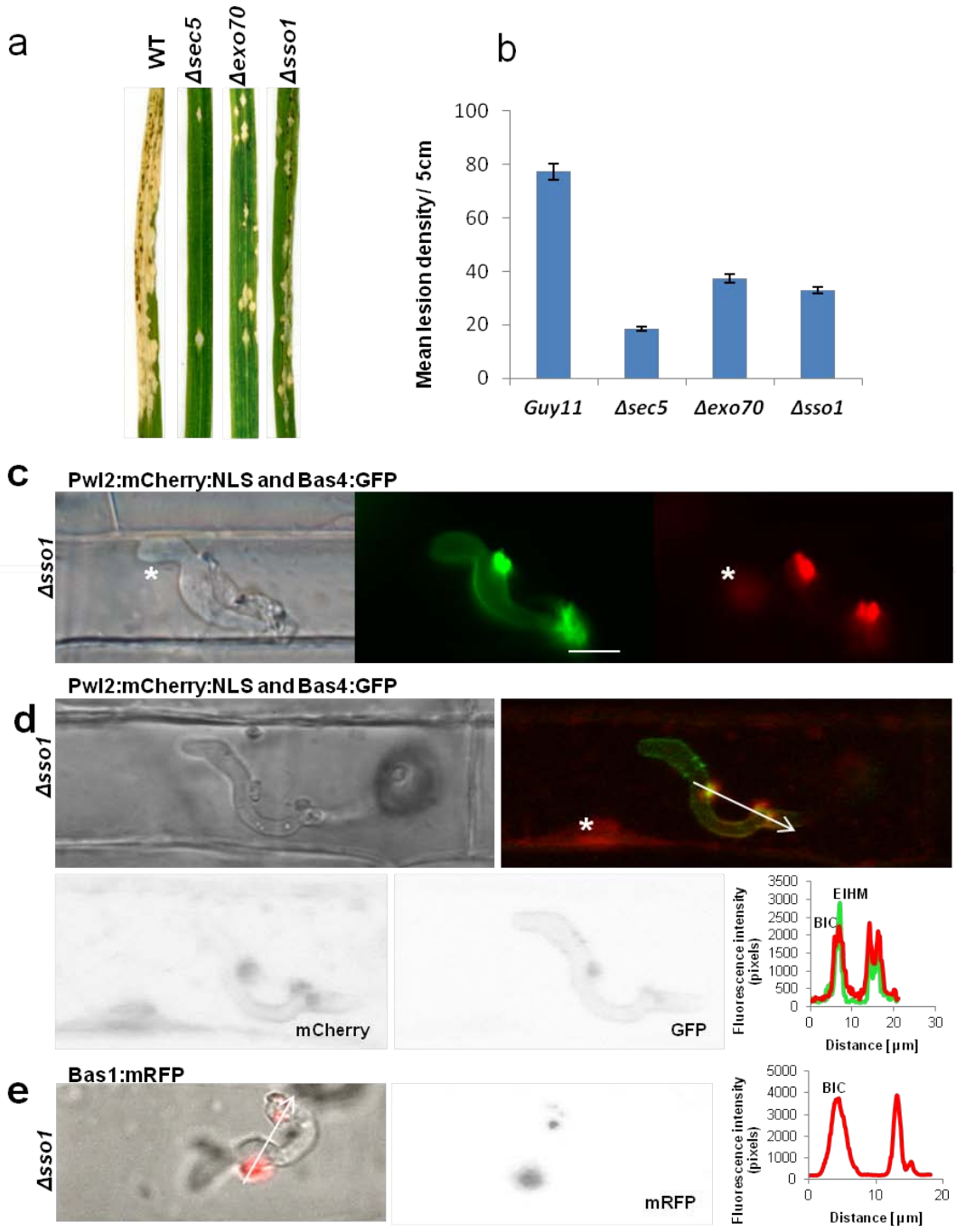
a
WT
Δsec5
Δexo70
Δsso1
b
Mean lesion density/ 5cm
100
80
60
40
20
0
Guy11
Δsec5
Δexo70
Δsso1
c
Pwl2:mCherry:NLS and Bas4:GFP
Δsso1
d
Pwl2:mCherry:NLS and Bas4:GFP
Δsso1
mCherry
GFP
Fluorescence intensity (pixels)
EIHM
BIC
Distance [µm]
e
Bas1:mRFP
Δsso1
mRFP
BIC

Figure 5. Pathogenicity impacts and *M. oryzae* t-SNARE Sso1 plays a role in BIC development.

(a) Targeted deletion of each of the *SEC5, EXO70* and *SSO1* genes in the aggressive Chinese field isolate O-137 resulted in a significant reduction in pathogenicity on a fully susceptible rice cultivar YT-16 in whole plant spray inoculation assays at Kansas State University. (**b)** Similar pathogenicity defects for each Guy11 mutant strain were observed on rice cultivar CO-39 at the University of Exeter. Bar chart showing frequency of lesions formed per 5 cm of CO-39 leaf surface ($P<0.05$ for all mutants; n=30 for each mutant; mean ±SD, three experiments). (**c**) *Δsso1* mutant showing inappropriate secretion of Pwl2:mCherry:NLS during plant infection. Expression of Pwl2:mCherry:NLS consistently identifies a second BIC-like structure before the first differentiated cell forms. (**d**) Another infection site in which Pwl2:mCherry:NLS expressed by an *Δsso1* mutant strain shows inappropriate secretion. The second BIC-like structure consistently occurs midway along the primary hypha before the first-differentiated IH cell forms. (**e**) Bas1:mRFP expressed by an *Δsso1* mutant shows the same double BIC pattern observed for Pwl2:mCherry:NLS (Fig. 6). Line scans shown are representative of wild type (n=20) and knock-out mutants (n=20 for each). Left to right: all images except (**a**) are merged bright-field and mRFP, and mRFP alone. Scale bars, 10µm.

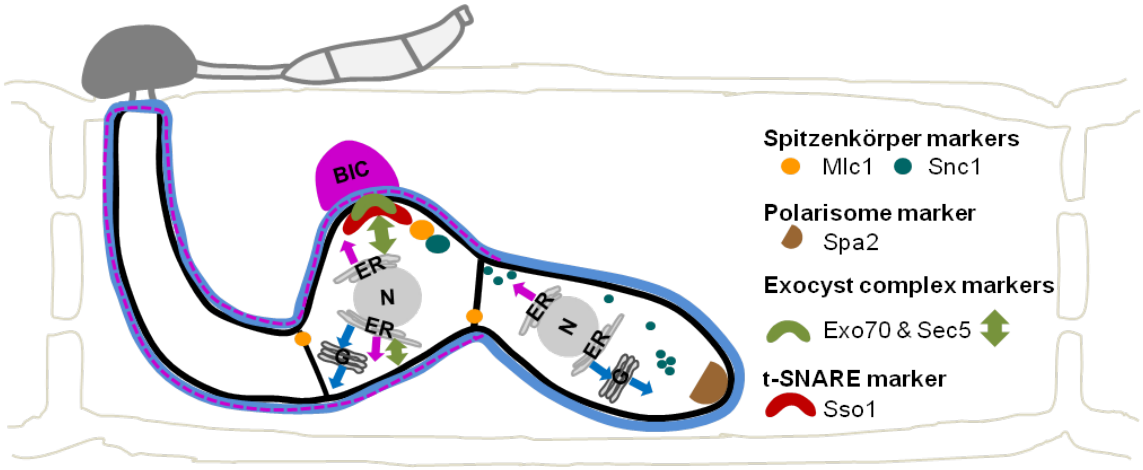
BIC
ER
N
ER
G
ER
N
ER
G
Spitzenkörper markers
Mlc1
Snc1
Polarisome marker
Spa2
Exocyst complex markers
Exo70 & Sec5
t-SNARE marker
Sso1

Figure 6. Model for effector secretion by *M. oryzae*. Apoplastic effectors Bas4, Bas113 and Slp1 (blue) follow the conventional, BFA-sensitive, Golgi-dependent secretion pathway. Cytoplasmic, BIC-localized effectors Pwl2, Bas1, Bas107, and AVR-Pita (magenta) follow a nonconventional, BFA-insensitive secretion pathway that depends on exocyst and SNARE proteins.

1 Goldberg, D. E. & Cowman, A. F. Moving in and renovating: exporting proteins from Plasmodium into host erythrocytes. *Nat. Rev. Microbiol.* **8**, 617-621 (2010).

2 Koeck, M., Hardham, A. R. & Dodds, P. N. The role of effectors of biotrophic and hemibiotrophic fungi in infection. *Cell Microbiol.* **13**, 1849-1857 (2011).

3 Bozkurt, T. O., Schornack, S., Banfield, M. J. & Kamoun, S. Oomycetes, effectors, and all that jazz. *Curr Opin Plant Biol* **15**, 483-492 (2012).

4 Rafiqi, M., Ellis, J. G., Ludowici, V. A., Hardham, A. R. & Dodds, P. N. Challenges and progress towards understanding the role of effectors in plant-fungal interactions. *Curr Opin Plant Biol* **15**, 477-482 (2012).

5 Alfano, J. R. & Collmer, A. Type III secretion system effector proteins: double agents in bacterial disease and plant defense. *Annu. Rev. Phytopathol.* **42**, 385-414 (2004).

6 Galan, J. E. & Collmer, A. Type III secretion machines: bacterial devices for protein delivery into host cells. *Science* **284**, 1322-1328 (1999).

7 Schirawski, J. *et al.* Pathogenicity determinants in smut fungi revealed by genome comparison. *Science* **330**, 1546-1548 (2010).

8 Valent, B. & Khang, C. H. Recent advances in rice blast effector research. *Current Opinion in Plant Biology* **13**, 434-441 (2010).

9 Birch, P. R. *et al.* Towards understanding the virulence functions of RXLR effectors of the oomycete plant pathogen *Phytophthora infestans*. *J Exp Bot* **60**, 1133-1140 (2009).

10 Hogenhout, S. A., Van der Hoorn, R. A., Terauchi, R. & Kamoun, S. Emerging concepts in effector biology of plant-associated organisms. *Mol. Plant Microbe Interact.* **22**, 115-122 (2009).

11 Park, C. H. *et al.* The *Magnaporthe oryzae* effector AvrPiz-t targets the RING E3 ubiquitin ligase APIP6 to suppress pathogen-associated molecular pattern-triggered immunity in rice. *The Plant cell* **24**, 4748-4762 (2012).

12 Djamei, A. *et al.* Metabolic priming by a secreted fungal effector. *Nature* **478**, 395-398 (2011).

13 de Jonge, R. *et al.* Conserved fungal LysM effector Ecp6 prevents chitin-triggered immunity in plants. *Science* **329**, 953-955 (2010).

14 Mentlak, T. A. *et al.* Effector-mediated suppression of chitin-triggered immunity by *Magnaporthe oryzae* is necessary for rice blast disease. *Plant Cell* **24**, 322-335 (2012).

15 Fisher, M. C. *et al.* Emerging fungal threats to animal, plant and ecosystem health. *Nature* **484**, 186-194 (2012).

16 Wilson, R. A. & Talbot, N. J. Under pressure: investigating the biology of plant infection by *Magnaporthe oryzae*. *Nat. Rev. Microbiol.* **7**, 185-195 (2009).

17 Wang, G.-L. & Valent, B. 464 (Springer Science and Business Media, New York, New York, 2009).
18 Cruz, C. D. *et al.* Preliminary assessment of resistance among U.S. wheat cultivars to the *Triticum* pathotype of *Magnaporthe oryzae*. *Plant Dis.* **96**, 1501-1505, doi:10.1094/pdis-11-11-0944-re (2012).
19 Urashima, A. S., Lavorent, N. A., Goulart, A. C. P. & Mehta, Y. R. Resistance spectra of wheat cultivars and virulence diversity of *Magnaporthe grisea* isolates in Brazil. *Fitopathologia Brasileira* **29**, 511-518 (2004).
20 Dagdas, Y. F. *et al.* Septin-mediated plant cell invasion by the rice blast fungus, *Magnaporthe oryzae*. *Science* **336**, 1590-1595 (2012).
21 Fernandez, J. & Wilson, R. A. Why no feeding frenzy? Mechanisms of nutrient acquisition and utilization during infection by the rice blast fungus *Magnaporthe oryzae*. *Mol. Plant-Microbe Interact.* **25**, 1286-1293, doi:10.1094/mpmi-12-11-0326 (2012).
22 Kankanala, P., Czymmek, K. & Valent, B. Roles for rice membrane dynamics and plasmodesmata during biotrophic invasion by the blast fungus. *Plant Cell* **19**, 706-724 (2007).
23 Crampin, H. *et al. Candida albicans* hyphae have a Spitzenkorper that is distinct from the polarisome found in yeast and pseudohyphae. *Journal of Cell Science* **118**, 2935-2947 (2005).
24 Sudbery, P., Gow, N. & Berman, J. The distinct morphogenic states of *Candida albicans*. *Trends Microbiol.* **12**, 317-324 (2004).
25 Mosquera, G., Giraldo, M. C., Khang, C. H., Coughlan, S. & Valent, B. Interaction transcriptome analysis identifies *Magnaporthe oryzae* BAS1-4 as biotrophy-associated secreted proteins in rice blast disease. *Plant Cell* **21**, 1273-1290 (2009).
26 Saitoh, H. *et al.* Large-scale gene disruption in *Magnaporthe oryzae* identifies MC69, a secreted protein required for infection by monocot and dicot fungal pathogens. *PLoS Pathog.* **8**, e1002711 (2012).
27 Yi, M. *et al.* The ER chaperone LHS1 is involved in asexual development and rice infection by the blast fungus *Magnaporthe oryzae*. *Plant Cell* **21**, 681-695 (2009).
28 Khang, C. H. *et al.* Translocation of *Magnaporthe oryzae* effectors into rice cells and their subsequent cell-to-cell movement. *Plant Cell* **22**, 1388-1403 (2010).
29 Read, N. D. Exocytosis and growth do not occur only at hyphal tips. *Mol. Microbiol.* **81**, 4-7 (2011).
30 Steinberg, G. Hyphal growth: a tale of motors, lipids, and the spitzenkörper. *Eukaryotic Cell* **6**, 351-360 (2007).
31 Sudbery, P. Fluorescent proteins illuminate the structure and function of the hyphal tip apparatus. *Fungal Genet. Biol.* **48**, 849-857 (2011).
32 Riquelme, M. *et al.* Architecture and development of the *Neurospora crassa* hypha - a model cell for polarized growth. *Fungal Biol.* **115**, 446-474 (2011).
33 Heider, M. R. & Munson, M. Exorcising the exocyst complex. *Traffic* **13**, 898-907 (2012).
34 Hayakawa, Y., Ishikawa, E., Shoji, J.-y., Nakano, H. & Kitamoto, K. Septum-directed secretion in the filamentous fungus *Aspergillus oryzae*. *Molecular Microbiology* **81**, 40-55, doi:10.1111/j.1365-2958.2011.07700.x (2011).
35 Valkonen, M. *et al.* Spatially segregated SNARE protein interactions in living fungal cells. *J. Biol. Chem.* **282**, 22775-22785 (2007).

36 Atkinson, H. A., Daniels, A. & Read, N. D. Live-cell imaging of endocytosis during conidial germination in the rice blast fungus, *Magnaporthe grisea*. *Fungal Genet. Biol.* **37**, 233-244 (2002).
37 Fischer, R., Zekert, N. & Takeshita, N. Polarized growth in fungi; interplay between the cytoskeleton, positional markers and membrane domains. *Mol. Microbiol.* **68**, 813-826 (2008).
38 Fischer-Parton, S. *et al.* Confocal microscopy of FM4-64 as a tool for analysing endocytosis and vesicle trafficking in living fungal hyphae. *Journal of Microscopy* **198**, 246-259 (2000).
39 Chardin, P. & McCormick, F. Brefeldin A: the advantage of being uncompetitive. *Cell* **97**, 153-155 (1999).
40 Valent, B., Farrall, L. & Chumley, F. G. *Magnaporthe grisea* genes for pathogenicity and virulence identified through a series of backcrosses. *Genetics* **127**, 87-101 (1991).
41 Altschul, S. F. *et al.* Gapped BLAST and PSI-BLAST: a new generation of protein database search programs. *Nucleic Acids Research* **25**, 3389-3402 (1997).
42 Saitou, N. & Nei, M. The neighbor-joining method: a new method for reconstructing phylogenetic trees *Molecular Biology and Evolution* **4**, 406-425 (1987).
43 Bolte, S. *et al.* FM-dyes as experimental probes for dissecting vesicle trafficking in living plant cells. *Journal of Microscopy* **214**, 159-173 (2004).
44 Bourett, T. M. & Howard, R. J. Brefeldin A-induced structural changes in the endomembrane system of a filamentous fungus, *Magnaporthe grisea*. *Protoplasma* **190**, 151-163 (1996).
45 Czymmek, K. J. *et al.* Live-cell imaging of tubulin in the filamentous fungus Magnaporthe grisea treated with anti-microtubule and anti-microfilament agents. *Protoplasma* **225**, 23-32 (2005).
46 Campbell, R. E. *et al.* A monomeric red fluorescent protein. *Proc. Natl Acad. Sci. USA* **99**, 7877-7882 (2002).
47 Shaner, N. C. *et al.* Improving the photostability of bright monomeric orange and red fluorescent proteins. *Nature Methods* **5**, 545(547) (2008).
48 Khang, C. H., Park, S.-Y., Lee, Y.-H. & Kang, S. A dual selection based, targeted gene replacement tool for *Magnaporthe grisea* and *Fusarium oxysporum*. *Fungal Genetics and Biology* **42**, 483-492 (2005).
49 Orbach, M. J., Farrall, L., Sweigard, J. A., Chumley, F. G. & Valent, B. A telomeric avirulence gene *AVR-Pita* determines efficacy for the rice blast resistance gene *Pi-ta*. *Plant Cell* **12**, 2019-2032 (2000).
50 Leung, H., Borromeo, E. S., Bernardo, M. A. & Notteghem, J. L. Genetic analysis of virulence in the rice blast fungus *Magnaporthe grisea*. *Phytopathology* **78**, 1227-1233 (1988).
51 Kershaw, M. J. & Talbot, N. J. Genome-wide functional analysis reveals that infection-associated fungal autophagy is necessary for rice blast disease. *Proc. Natl Acad. Sci. USA* **106**, 15967-15972 (2009).
52 Kurup, S. *et al.* Marking cell lineages in living tissues. *Plant Journal* **42**, 444-453 (2005).
53 Runions, J., Brach, T., Kuhner, S. & Hawes, C. Photoactivation of GFP reveals protein dynamics within the endoplasmic reticulum membrane. *J Exp Bot* **57**, 43-50 (2006).

54 Yoshida, K. *et al.* Association genetics reveals three novel avirulence genes from the rice blast fungal pathogen *Magnaporthe oryzae*. *Plant Cell* **21**, 1573-1591 (2009).

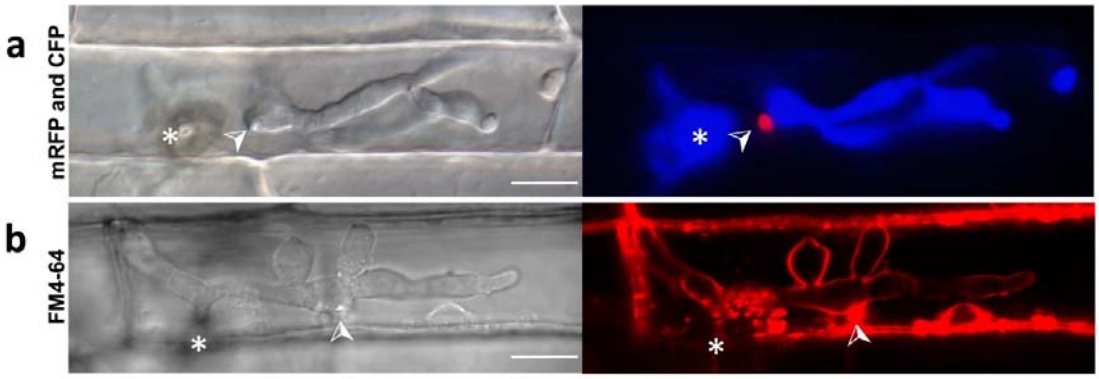
a
mRFP and CFP
b
FM4-64

Supplementary Figure 1. BICs are interfacial structures outside the fungus.

(**a**) BICs are spatially separated from the fungal cytoplasm. Imaging was performed with fungal transformants expressing a constitutive, cytoplasmic fluorescent protein, in this case the cyan fluorescent protein (blue) under control of the constitutive ribosomal protein P27 promoter from *M. oryzae*. The BIC (➢), labeled with Bas1:mRFP, does not co-localize with the fluorescent marker in the fungal cytoplasm. Images left to right are bright-field; and merged mRFP and CFP channels. (**b**) The BIC region (➢) is heavily stained by the lipophilic styryl dye FM4-64[1,2], which is internalized by endocytosis in infected rice cells. FM4-64 is excluded from fungal membranes by the surrounding plant-derived EIHM. In this case, infected rice sheath cells were exposed to FM4-64 for 4 h before imaging. The lack of staining in the fungal membranes is clearly observed by the absence of dye in the hyphal septa, which would have become stained by lateral diffusion of dye that had inserted in the fungal plasma membrane. Additionally, there is no late-stage staining of fungal vacuolar membranes. Images left to right are bright-field alone; and red channel alone. Appressorium penetration sites are labeled with a white asterisk. Scale bars, 10μm.

(a) Mlc1 protein sequence alignment

(b) Snc1 protein sequence alignment

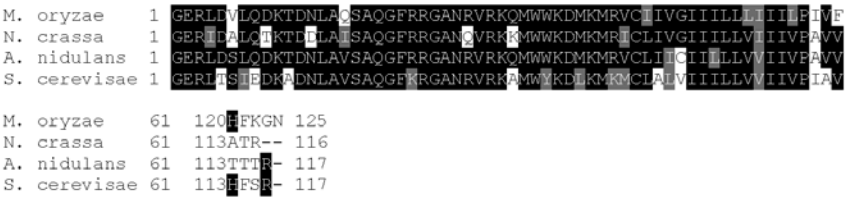

(c) Spa2 protein sequence alignment

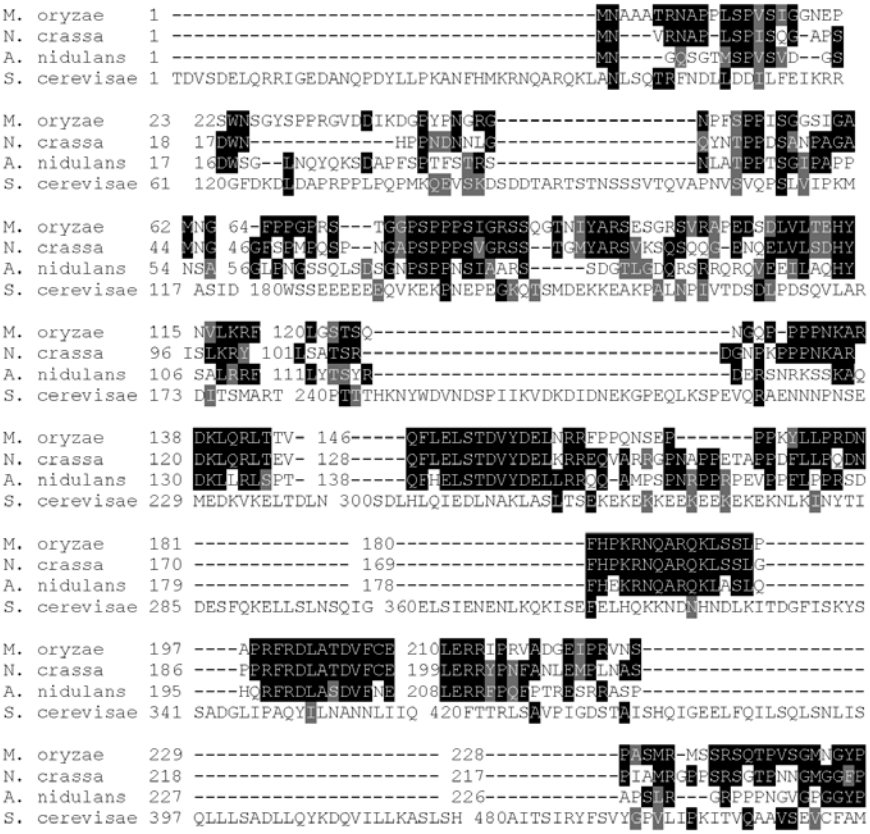

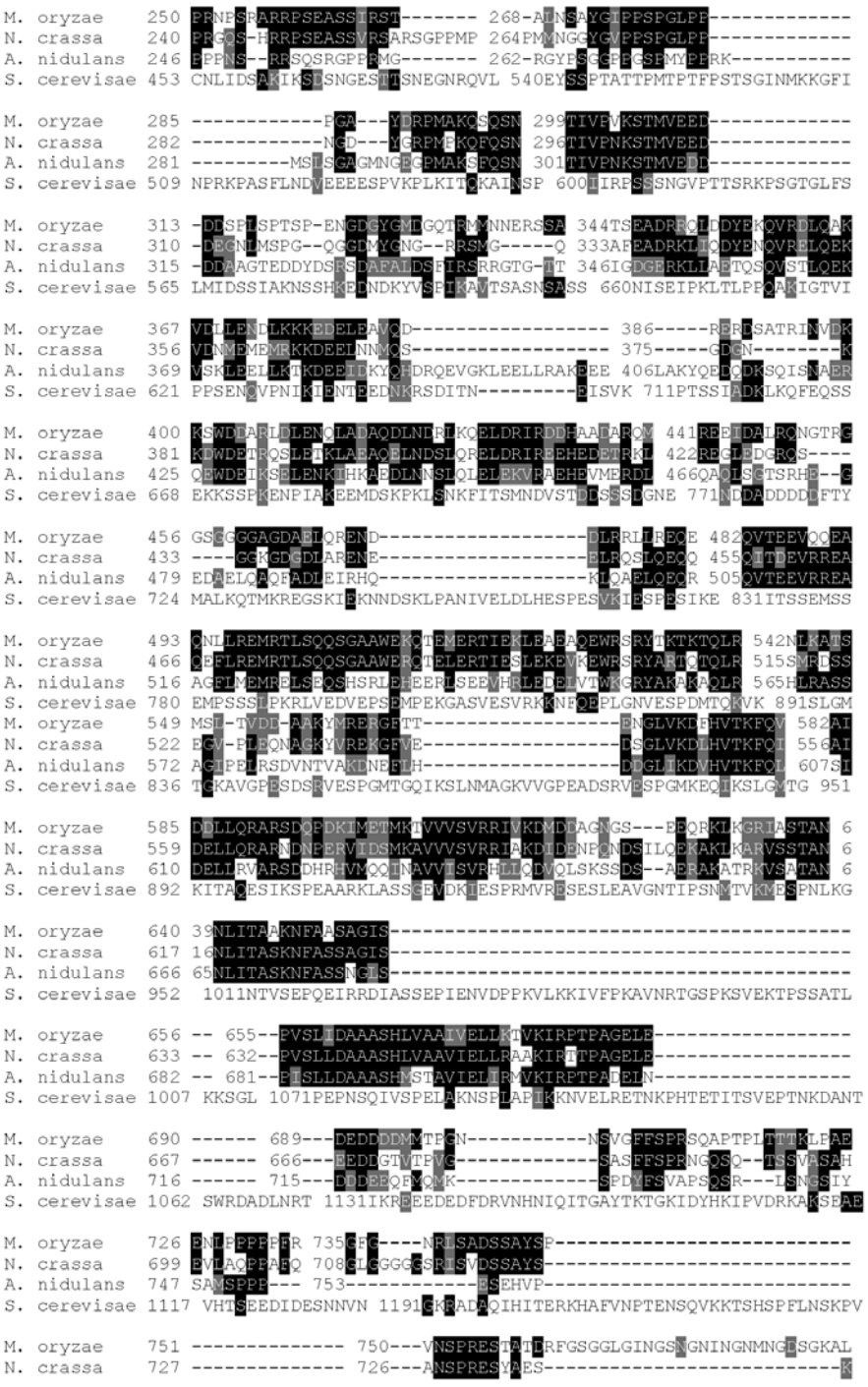

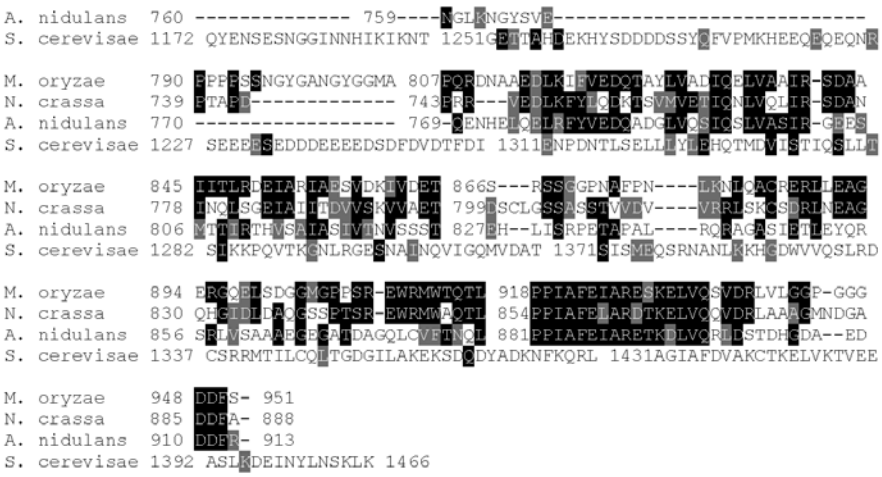

(d) Sec5 protein sequence alignment

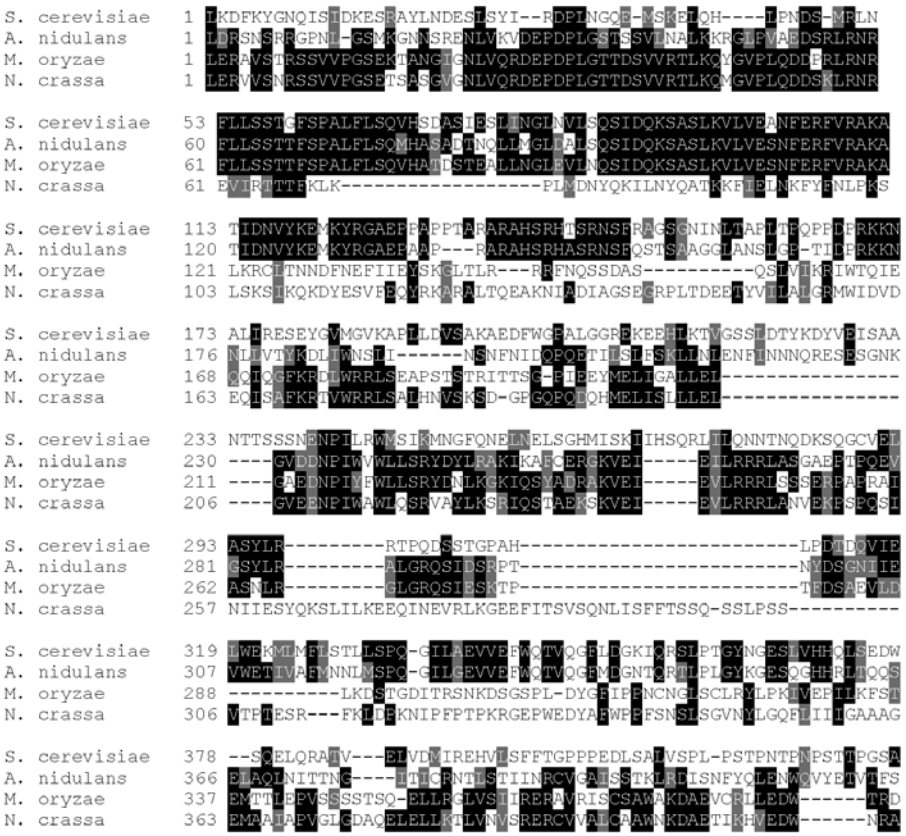

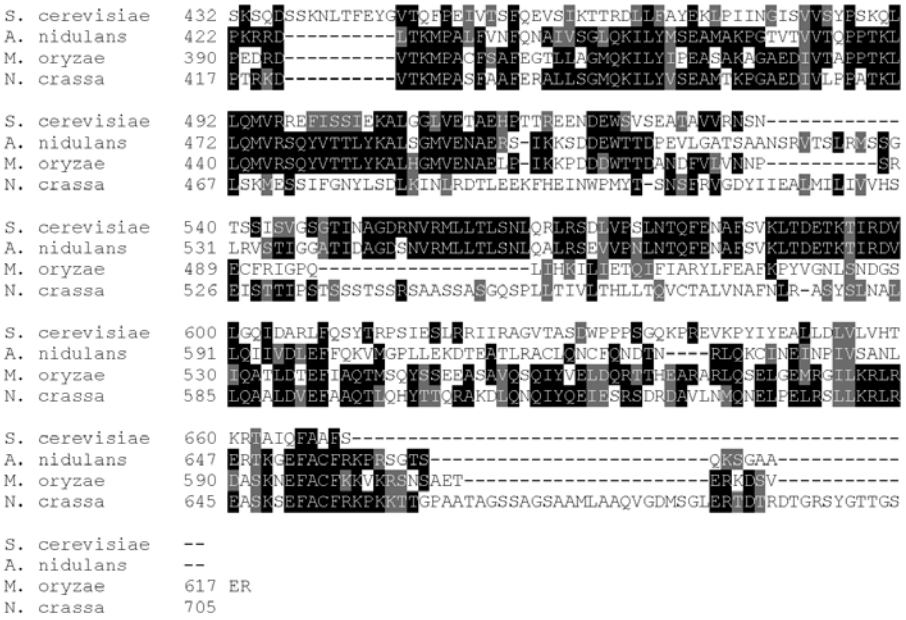

(e) Exo70 protein sequence alignment

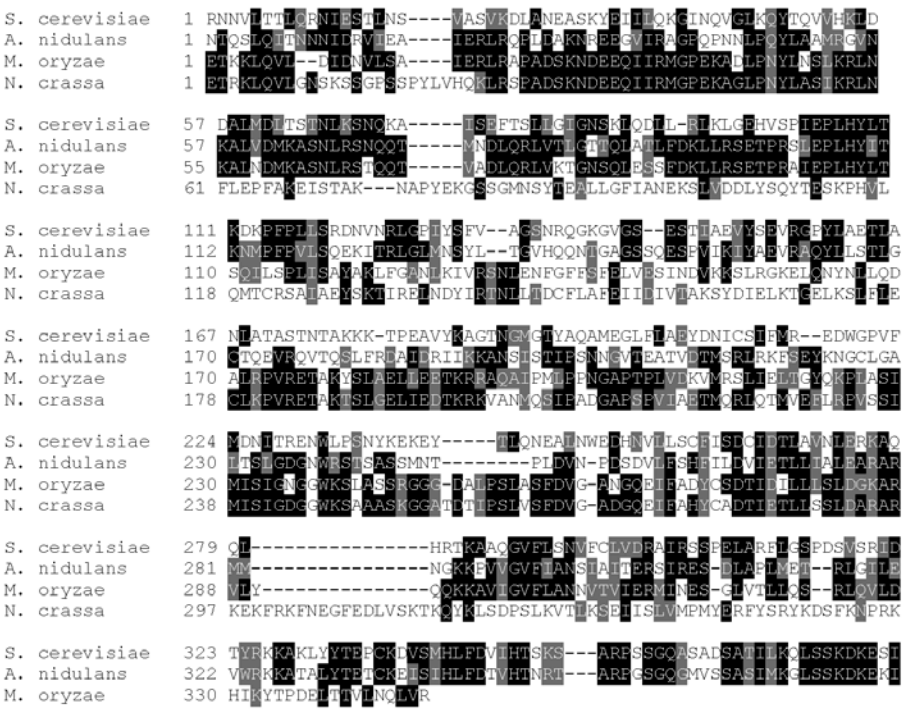

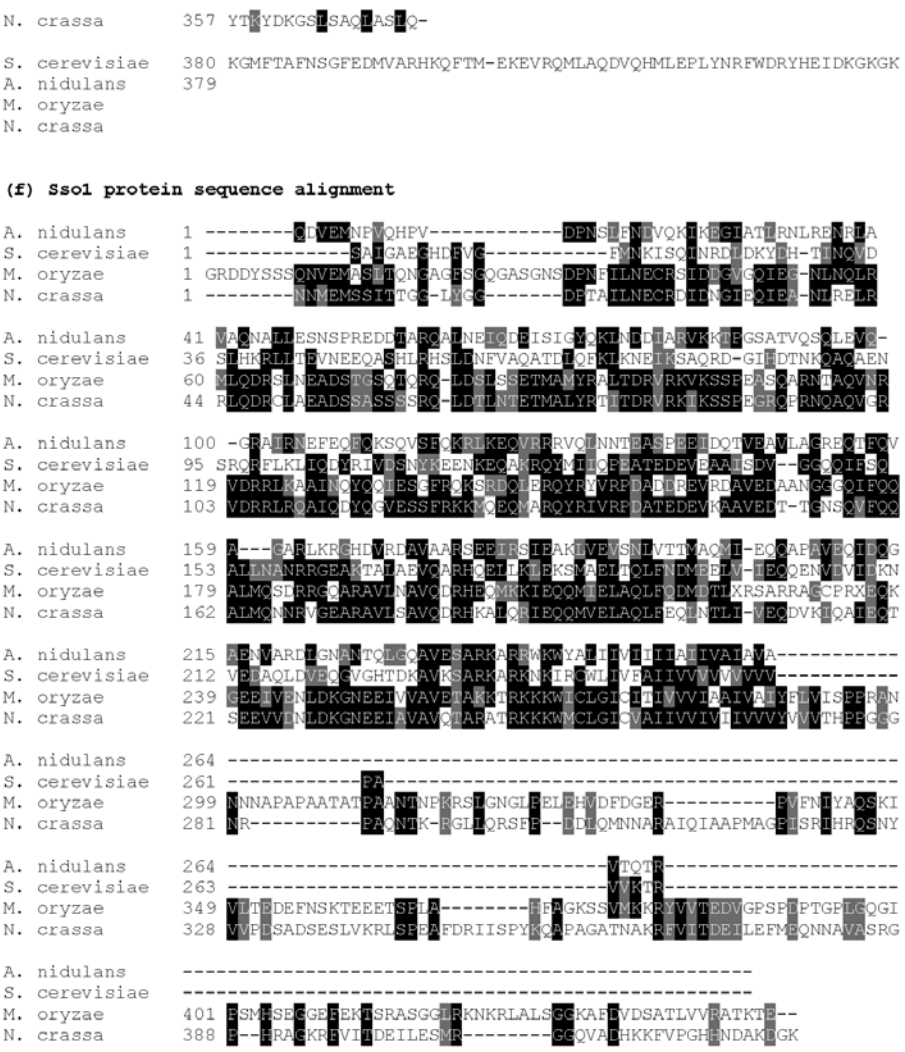

(f) Sso1 protein sequence alignment

Supplementary Figure 2. Alignment of the predicted amino acid sequences for protein markers of secretory components in *M. oryzae* and other fungi.

Sequences were aligned using ClustalW[3] and shaded by BoxShade 3.2. Identical amino acids are highlighted on a black background and similar amino acids on a light grey background. The *M. oryzae* amino acid sequence is aligned with the sequences of the putative homologs in *S. cerevisiae*, *A. nidulans* and *N. crassa* respectively. (**a**) Mlc1 (MGG_09470.6) is aligned with YGL106W, AN6732 and NCU06617. (**b**) Snc1 (MGG_12614.6) is aligned with YAL030W, AN8769 and NCU00566. (**c**) Spa2 (MGG_03703.6) is aligned with YLL021W, AN3815 and NCU03115. (**d**) Sec5 (MGG_07150.6) is aligned with YDR166C, AN1002 and NCU07698. (**e**) Exo70 (MGG_01760.6) is aligned with YJL085W, AN6210 and NCU08012. (**f**) Sso1 (MGG_04090.6) is aligned with YPL232W, AN3416 and NCU02460.

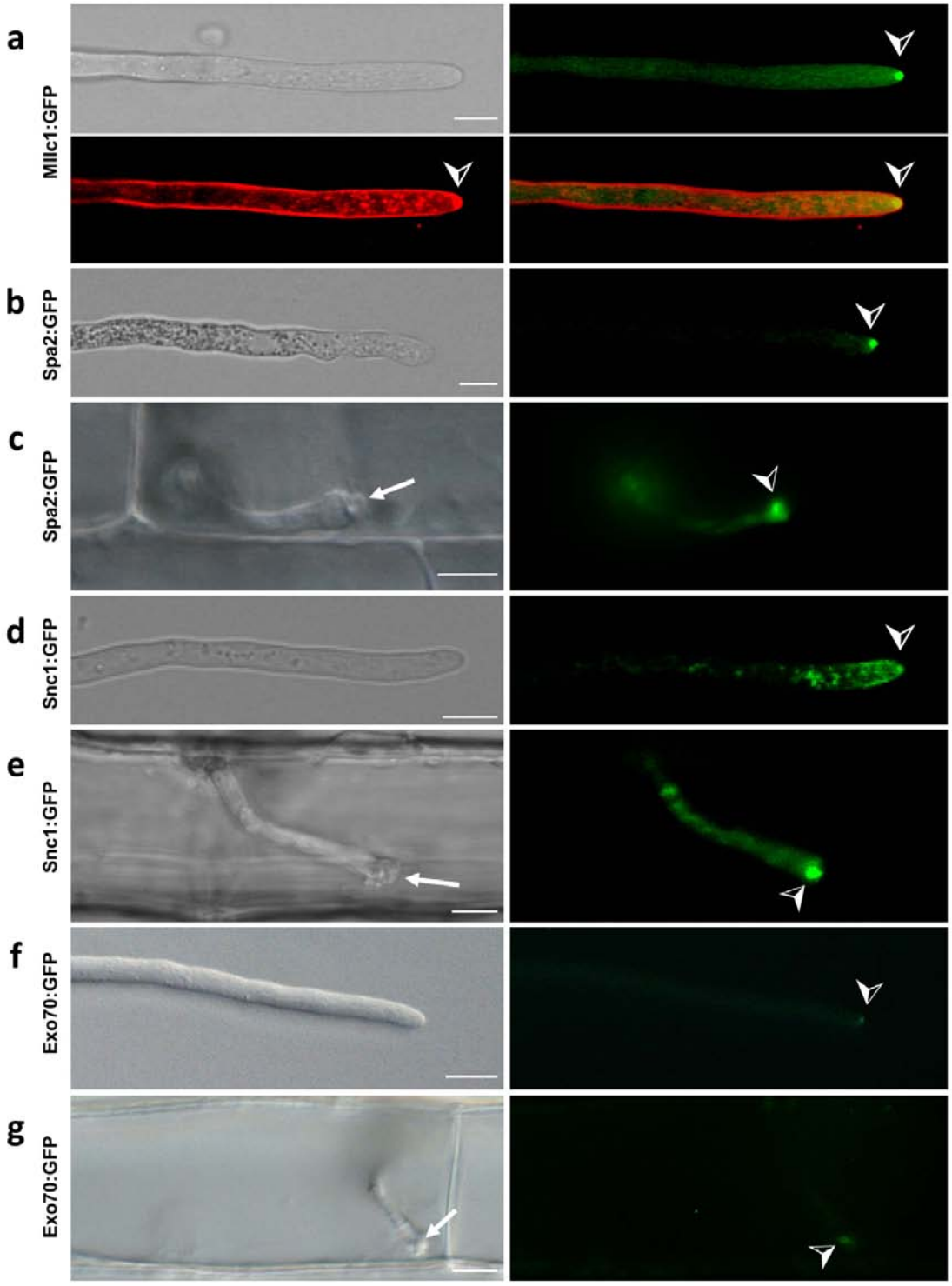
a
Mlc1:GFP
b
Spa2:GFP
c
Spa2:GFP
d
Snc1:GFP
e
Snc1:GFP
f
Exo70:GFP
g
Exo70:GFP

Supplementary Figure 3. Secretion in primary invasive hyphae inside plant cells resembles secretion by vegetative hyphae *in vitro*.

We identified putative *M. oryzae* secretory components[4], confirmed that they localize as expected in vegetative hyphae *in vitro*, and determined how they localize in the tubular primary hyphae growing in rice cells. BICs (labeled with an arrow in c, e, and g) are only associated with invasive hyphae *in planta*. (**a**) Mlc1:GFP (MGG_09470.6), the myosin light chain 1 regulatory subunit, localizes to Spitzenkörper at the tips of *M. oryzae* vegetative filamentous hyphae (➢), as shown for true hyphae of the human fungal pathogen *Candida albicans*[5]. The Mlc1 fluorescence co-localises (yellow) with the endocytic tracker dye FM4-64 (red), which is generally known to label Spitzenkörper in filamentous fungi[5,6]. For these experiments, the *M. oryzae* vegetative hyphae (➢) were imaged while growing at a rate of 5 to 10 μm per minute on water agar-coated microscope slides. This confocal image was acquired 10 minutes after addition of the dye. Images clockwise from upper left are bright-field; GFP; merged GFP and FM4-64 channels; and FM4-64 alone. Similarly, Mlc1:GFP identifies Spitzenkörper in filamentous primary hyphae inside rice cells (Fig. 2a). Note that FM4-64 is not useful for identifying Spitzenkörper in invasive hyphae inside rice cells, since this dye is excluded from these hyphae by the surrounding EHIM (Supplementary Figure 1b). (**b**) *SPA2* (MGG_03703.6) encodes one of three components of the polarisome, involved in nucleating actin microfilaments for targeting vesicles to hyphal growth points. *M. oryzae* Spa2:GFP localizes to the tip of a vegetative hypha (➢) growing as described in (a). (**c**) Polarisome component Spa2:GFP concentrates at the primary hyphal tip (➢) behind the BIC (arrow) in a rice cell at 22 hpi. (**d**) *SNC1* (MGG_12614.6) encodes a v-SNARE vesicle membrane receptor involved in the fusion of secretory vesicles and target membrane. Snc1:GFP localizes at the vegetative hyphal tip (➢) as expected. (**e**) v-SNARE Snc1:GFP accumulates in a bright fluorescent punctum near the primary hyphal tip (➢) in a rice cell at 24 hpi. (**f**) *EXO70* (MGG_01760.6) encodes one of eight components of the exocyst[7], an eight subunit complex implicated in tethering secretory vesicles to the plasma membrane before SNARE-mediated fusion. Exo70:GFP localizes at the vegetative hyphal tip (➢) as expected. (**g**) Exocyst component Exo70:GFP accumulates as a bright fluorescent punctum near the primary hyphal tip (➢) in a rice cell at 24 hpi. Except in (a), all images from left to right are bright-field; and GFP alone. Scale bars, 5μm.

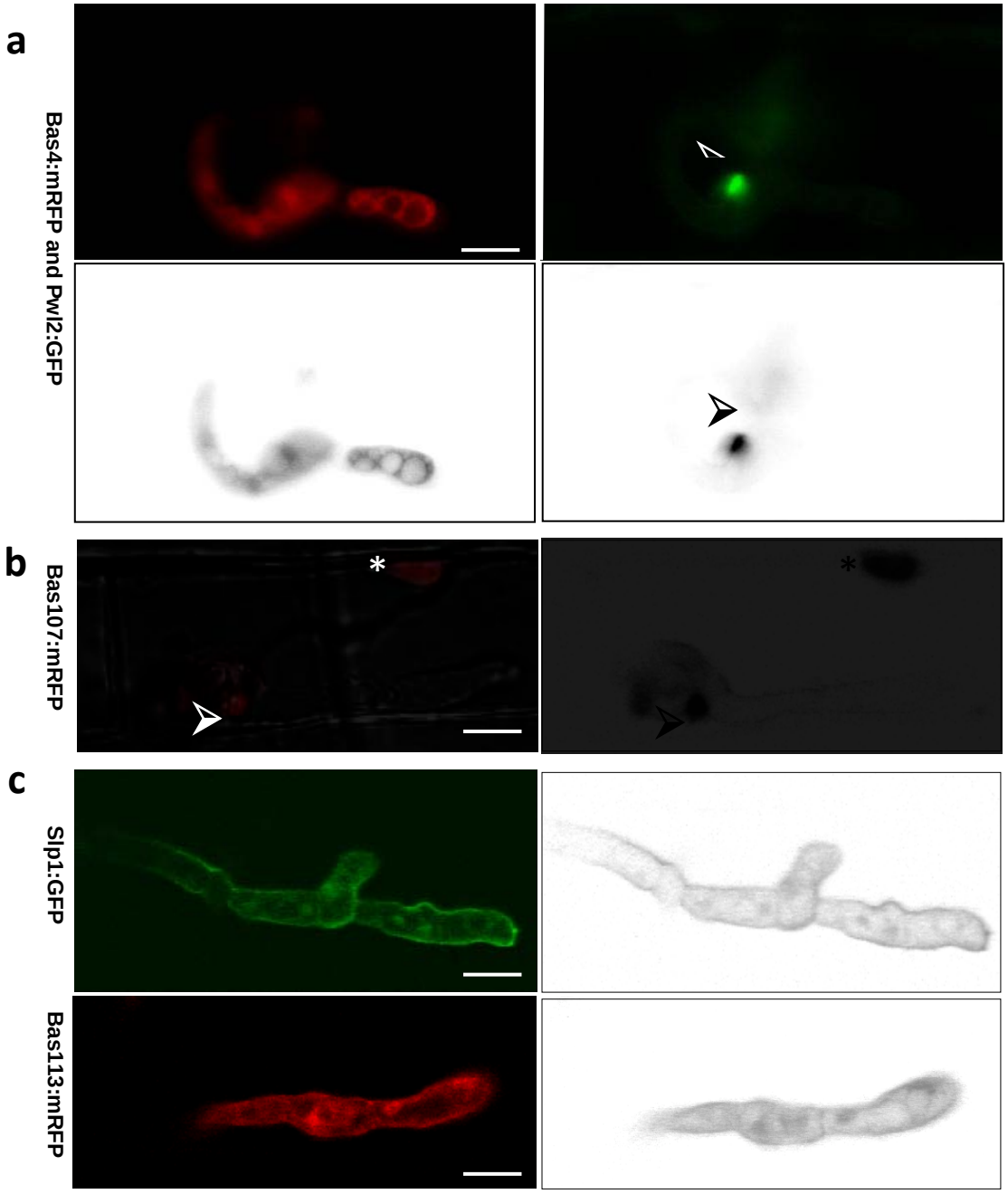
a
Bas4:mRFP and Pwl2:GFP
b
Bas107:mRFP
c
Slp1:GFP
Bas113:mRFP

Supplementary Figure 4. Cytoplasmic effector sequences and not the fluorescent protein or nuclear localization sequences determine BFA-insensitive secretion.

In fungi, a hallmark of Golgi-dependent secretion is sensitivity to the fungal metabolite Brefeldin A (BFA)[8], which blocks ER-to-Golgi transport by blocking the recruitment of the ADP-ribosylation factor Arf1 to the Golgi. We tested multiple fluorescent versions of effectors, with and without artificially-added nuclear localization signals, to confirm that BFA-insensitive secretion is characteristic of BIC-localized cytoplasmic effectors and is independent of the fluorescent protein or added nuclear localization signal. Fluorescent BICs are labeled with an arrowhead (➢). (**a**) Secretion of cytoplasmic effector Pwl2:GFP, with a C-terminal fusion to GFP instead of mRFP, continues in the presence of BFA. Notice that in this case the Pwl2:GFP fusion protein does not contain an NLS signal. Even after 6 hrs and 50 minutes, the fluorescent protein is not retained in the fungal cytoplasm. At the same time, secretion of apoplastic effector Bas4:mRFP is blocked by the BFA treatment. The red or green channel in each image in the top panel is shown as a black and white inverse image below, in order to highlight the fluorescence patterns associated with apoplastic and cytoplasmic effectors, respectively, after BFA treatment. (**b)** Secretion of putative effector Bas107 is not impaired by BFA treatment. In this image, Bas107:mRFP, which accumulates in the BIC and is translocated to the rice cytoplasm (Mihwa Yi and Barbara Valent, unpublished), shows its normal localization pattern 5 hrs after exposure to BFA. Note that Bas107 fusion proteins naturally accumulate in the rice nucleus (white asterisk) after translocation, without an artificially-added nuclear localization signal. Images from left to right are merged bright-field and mRFP; and mRFP as a black and white inverse image. (**c**) Additional apoplastic effectors Slp1:GFP[9] and Bas113:mRFP (Mihwa Yi and Barbara Valent, unpublished) show retention in the fungal ER similarly to Bas4:GFP and Bas4:mRFP. Both infection sites shown here were imaged 5 hrs after exposure to BFA. Images from left to right: GFP or mRFP alone with their corresponding black and white inverse image. Scale bars, 10µm.

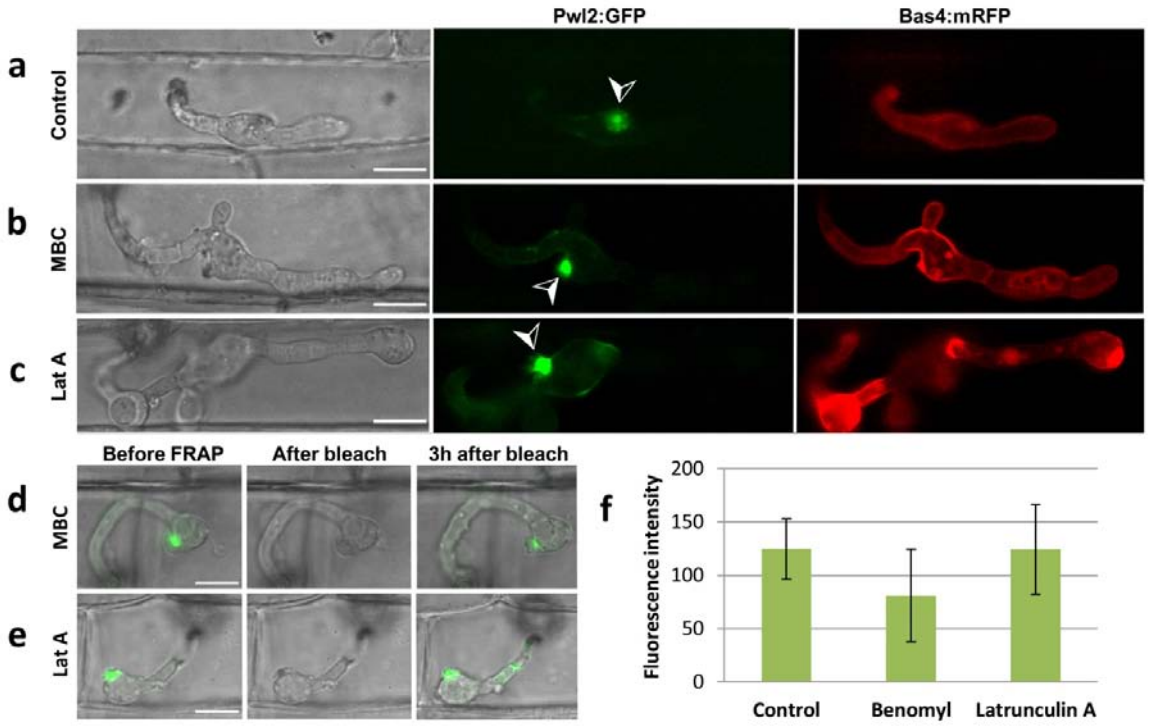
Pwl2:GFP
Bas4:mRFP
a
Control
b
MBC
c
Lat A
Before FRAP
After bleach
3h after bleach
d
MBC
e
Lat A
f
Fluorescence intensity
200
150
100
50
0
Control
Benomyl
Latrunculin A

Supplementary Figure 5. Secretion of apoplastic effectors is more dependent on cytoskeletal function than is secretion of cytoplasmic effectors.

(a) Cytoplasmic effector Pwl2:GFP is secreted and localized in the BIC (➢) and apoplastic Bas4:mRFP outlines the IH in the normal localization pattern in the absence of chemical treatments. (**b**) Rice sheath tissue invaded by the same fungal transformant in (a) was exposed to MBC (active ingredient in the fungicide benomyl), which inhibits microtubule formation in ascomycetous fungi but not in plants. Three hours after addition of MBC to infected tissue, secretion of apoplastic Bas4:mRFP is impaired, as indicated by retention of this fluorescent protein in the hyphae. No effect was observed on secretion of Pwl2:GFP into the BIC (➢), suggesting that Pwl2 secretion and accumulation in BICs is less dependent on microtubules than Bas4 secretion to the apoplast. (**c**) Rice sheath tissue invaded by the same fungal transformant in (a) was exposed to Latrunculin A (LatA), which inhibits polymerization of actin in fungi and in plants. By 3 hrs after exposure of infected tissue to LatA, invasive hyphal depolarization occurs and secretion of apoplastic Bas4:GFP is impaired. No effect was observed on secretion and accumulation of Pwl2:GFP in the BIC (➢), which indicates that Pwl2 secretion is less dependent on actin microfilaments than Bas4 secretion is. (**d**) FRAP analysis demonstrates continuous secretion of Pwl2:GFP into the BIC in the presence of MBC. Transformants expressing both Pwl2:GFP and Bas4:mRFP were incubated in MBC for 3 hrs, or until impaired secretion of Bas4:mRFP was observed, before photobleaching the BIC. Recovery of pre-bleach Pwl2:GFP fluorescence was seen after 3 additional hrs in the presence of MBC, comparable to controls without MBC. (**e**) FRAP demonstrates continuous secretion of Pwl2:GFP into the BIC in the presence of LatA. Transformants expressing both Pwl2:GFP and Bas4:mRFP were incubated in LatA for 3 hrs before photobleaching the BIC. Recovery of Pwl2:GFP fluorescence was seen in the BIC after 3 additional hrs in the presence of LatA, comparable to controls without LatA. (**f**) FRAP results were identical in the presence or absence of MBC ($p=0.014$) and in the presence or absence of LatA ($p=0.015$). Bars show mean fluorescence intensity recovery after bleaching (mean$\pm$SD, four FRAP experiments). Images (a-c) from left to right are bright-field; GFP alone; and mRFP alone; and all images (d-e) are merged bright-field and GFP. Scale bars, 10µm.

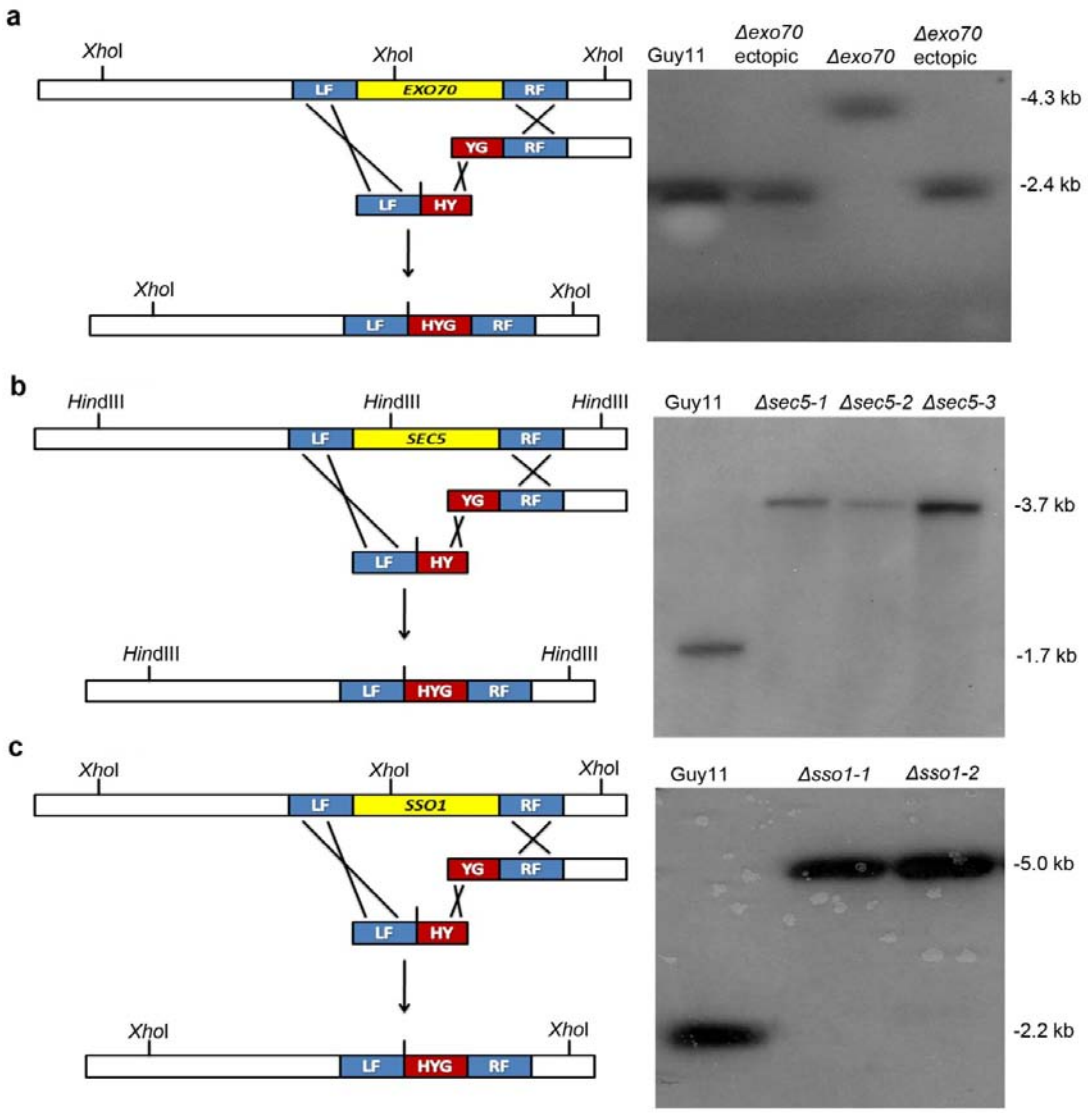
a
XhoI
XhoI
XhoI
LF
EXO70
RF
YG
RF
LF
HY
XhoI
XhoI
LF
HYG
RF
Guy11
Δexo70 ectopic
Δexo70
Δexo70 ectopic
-4.3 kb
-2.4 kb
b
HindIII
HindIII
HindIII
LF
SEC5
RF
YG
RF
LF
HY
HindIII
HindIII
LF
HYG
RF
Guy11
Δsec5-1
Δsec5-2
Δsec5-3
-3.7 kb
-1.7 kb
c
XhoI
XhoI
XhoI
LF
SSO1
RF
YG
RF
LF
HY
XhoI
XhoI
LF
HYG
RF
Guy11
Δsso1-1
Δsso1-2
-5.0 kb
-2.2 kb

Supplementary Figure 6. Southern blot analyses of targeted gene deletion mutants.

Genomic DNA was extracted from each putative transformant and wild type strain Guy11 and digested with the restriction enzymes indicated in the schematic diagrams on the left. Blots were probed with a restriction fragment comprising the Left Flank (LF) after fractionation by gel electrophoresis. The size difference in each blot is consistent with successful replacement of gene coding regions of each target gene with the hygromycin resistance cassette *HPH*. (**a**) Targeted gene deletion of *M. oryzae EXO70*. *Xho*I digested genomic DNA from the wild type strain Guy11 and putative Δ*exo70* transformants were gel fractionated and probed with Left Flank (1.5 kb upstream of start codon). DNA gel blot analysis showed a 1.9 kb difference which is consistent with successful replacement of *EXO70* gene with the resistance cassette. (**b**) Targeted gene deletion of *M. oryzae SEC5*. *Hin*dIII digested genomic DNA from Guy11 and putative Δ*sec5* transformants were gel fractionated and probed with Left Flank (1.5 kb upstream of start codon). DNA gel blot analysis showed a 2.0 kb difference which is consistent with successful replacement of *SEC5* gene with the resistance cassette. (**c**) Targeted gene deletion of *M. oryzae SSO1*. *Xho*I digested genomic DNA from Guy11 and putative Δ*sso1* transformants were gel fractionated and probed with Left Flank (1.5 kb upstream of start codon). DNA gel blot analysis showed a 2.8 kb difference which is consistent with successful replacement of *SSO1* gene with the resistance cassette. Similar analyses confirmed targeted gene replacement mutants in a second wild type strain, O-137 (data not shown).

Supplementary Table 1. Cellular markers targeted for identification of protein secretion components in fungi.

Name	SGD ID	Broad Inst. Version 6	Size nt (aa)	Function	Localization	Protein Family	Blastp % e-value
Mlc1	YGL106W	MGG_09470	1018 (147)	Myosin regulatory light chain	Apical body, Spitzenkörper marker	EF-hand superfamily	60% 3.1e-24
Snc1	YAL030W	MGG_12614	1295 (125)	v-SNARE, mediate endocytosis and exocytosis	Transport vesicle membrane	Synaptobrevin/VAMP family of R-type v-SNARE proteins	68% 3.6e-25
Spa2	YLL021W	MGG_03703	3006 (951)	Polarisome component	Polarisome, hyphal tip	GIT_SHD family of ADP-ribos	55% 3.5e-22
Exo70	YJL085W	MGG_01760	1977 (630)	Exocyst complex subunit	Sites of the exocyst in the plasma membrane	Exo7-like	43% 7.9e-23
Sec5	YDR166C	MGG_07150	3227 (1055)	Exocyst complex subunit	Vesicle tethering in exocytosis	Sec5-like	52% 1e-22
Sso1	YPL232W	MGG_04090	1900 (500)	t-SNARE, determine the site of vesicle fusion	Plasma membrane	Syntaxin-related	52% 2.8e-28

Supplementary Table 2. Plasmids used.

Clone	Description
pBV14	RP27:ECFP expression binary vector derived from pSM324. Ampicillin and Bialaphos resistance.
pBV176	EGFP expression binary vector derived from pBHt2. Kanamycin and Hygromycin resistance.
pBV317	Pwl2:mRFP:β-tubulin-terminator cloned in *Eco*RI -*Hind*III sites of pBHt2. Kanamycin and Hygromycin resistance.
pBV367	mRFP expression binary vector derived from pBGt (Seogchan Kang, unpublished results), consisting of three modules: P27 (*Eco*RI-*Bam*HI fragment), mRFP (*Bam*HI-*Sph*I fragment), and *N.crassa* β-tubulin terminator (*Sph*I-*Hind*III fragment) that were cloned in *Eco*RI-*Hind*III sites of pBGt. Kanamycin and Geneticin (G418) resistance.
pBV403	EGFP expression binary vector derived from pBGt (Seogchan Kang,unpublished results), consisting of 2 kb P27*AVR-Pita* SP:GFP (*Eco*RI-*Bam*HI fragment), and *N.crassa* β-tubulin terminator (*Sph*I-*Hind*III fragment) cloned in *Eco*RI-*Hind*III sites of pBGt. Kanamycin and Geneticin (G418) resistance.
pBV435	For expression of Pwl2:EGFP:Ter and Bas4:mRFP:Ter, cloned in *Eco*RI-*Bam*HI sites of pBV367. Kanamycin and Geneticin (G418) resistance.
pBV591	For expression of Pwl2:mCherry:NLS:Tnos and Bas4:EGFP:Ter, cloned in *Eco*RI-*Hind*III sites of pBHt2. Kanamycin and Hygromycin resistance.
pBV912	BAS107:mRFP expression binary vector derived from pFLR. Kanamycin and Hygromycin resistance.
pBV915	BAS113:mRFP expression binary vector derived from pFLR. Kanamycin and Hygromycin resistance.
pBV946	For expression of Mlc1:GFP, 1.76 kb of *Mlc1* gene, including 1 kb promoter and coding sequence, cloned in *Eco*RI-*Bam*HI sites of pBV403. Kanamycin and G418 resistance.
pBV947	For expression of Exo70:GFP, 2.97 kb of *Exo70* gene, including 1 kb promoter and coding sequence, cloned in *Eco*RI-*Bam*HI sites of pBV403. Kanamycin and G418 resistance.
pNJT1	For expression of Sso1:GFP, 1.5 kb of *Sso1* gene promoter and coding sequence, cloned in PYC1 vector carrying Sulphonylurea resistance.
pNJT2	For expression of Snc1:GFP, 1.5 kb of *Snc1* gene promoter and coding sequence, cloned in PYC1 vector carrying Sulphonylurea resistance.
pNJT3	For expression of Spa2:GFP, 2 kb of *Spa2* gene promoter and coding sequence, cloned in PYC1 vector carrying Sulphonylurea resistance.
pNJT4	For expression of Slp1:GFP, 2 kb of *Slp1* gene promoter and coding sequence, cloned in PYC1 vector carrying Sulphonylurea resistance.

Clone	Description
pNJT5	For expression of Pma1:GFP, 2 kb of *Slp1* gene promoter and coding sequence, cloned in PYC1 vector carrying Sulphonylurea resistance.
pNJT6	Lti6B:GFP, obtained from Kurup et. al., 2005[10].
pNJT7	GFP:HDEL, obtained from Zheng et. al., 2005[11].

Supplementary Table 3. Fungal and rice transformants.

Name	Description [background strain; plasmid used]
KV9	Transformant expressing constitutive cyan fluorescent protein [strain O-391; pBV14]. Bialaphos resistance.
KV96	Transformant expressing Bas1 promoter and coding sequence (115 aa) with mRFP reporter gene into KV9 [strain O-391; pBV367]. Bialaphos resistance.
KV105	Transformant expressing both a fusion of the Pwl2 promoter and entire coding sequence with the EGFP reporter gene, and a fusion of the Bas4 promoter and entire coding sequence with the mRFP reporter gene [strain O-137; pBV435]. Hygromycin resistance.
KV112	Transformant expressing Bas1 promoter and coding sequence (115 aa) with mRFP reporter gene [strain O-137; pBV367]. G418 resistance.
KV118	Transformant expressing Pwl2 promoter and coding sequence (145 aa) with mRFP reporter gene [strain O-137; pBV317]. Hygromycin resistance.
KV121	Transformant expressing both a fusion of the Pwl2 promoter and entire coding sequence with the mCherry:NLS reporter gene, and a fusion of the Bas4 promoter and entire coding sequence with the EGFP reporter gene [strain O-137; pBV591]. Hygromycin resistance.
KV125	Transformant expressing Mlc1, promoter and coding sequence with GFP reporter gene [strain CP987; pBV403]. G418 resistance.
KV126	Transformant expressing Mlc1, promoter and coding sequence with GFP reporter gene [strain KV118; pBV403]. G418 resistance.
KV130	Transformant expressing Exo70, promoter and coding sequence with GFP reporter gene [strain CP987; pBV403]. G418 resistance.
KV131	Transformant expressing Exo70, promoter and coding sequence with GFP reporter gene [strain KV118; pBV403]. G418 resistance.
KV132	Transformants expressing BAS107:mRFP [strain O-137; pBV912]. Hygromycin resistance.
KV133	Transformants expressing BAS113:mRFP [strain O-137; pBV915]. Hygromycin resistance.
Ex0149	Transformant expressing Snc1 (2kb promoter and entire coding sequence) fused to GFP [strain Guy11]. Sulfonylurea resistance.
Ex0150	Transformant expressing Spa2 (2kb promoter and entire coding sequence) fused to GFP [strain Guy11]. Sulfonylurea resistance.
Ex0151	Δ*exo70*, KO mutant into KV121 [strain O-137; pBV591]. Sulfonylurea resistance.
Ex0152	Δ*sec5*, KO mutant into KV121 [strain O-137; pBV591]. Sulfonylurea resistance.
Ex0153	Δ*sso1*, KO mutant into KV121 [strain O-137; pBV591]. Sulfonylurea resistance.
Ex0158	Δ*exo70*, KO mutant into KV112 [strain O-137; pBV367]. Hygromycin resistance.
Ex0159	Δ*sec5*, KO mutant into KV112 [strain O-137; pBV367]. Hygromycin resistance.
Ex0160	Δ*sso1*, KO mutant into KV112 [strain O-137; pBV367]. Hygromycin resistance.
Ex0166	Transformant expressing Slp1 (2kb promoter and entire coding sequence) fused to GFP

Name	Description [background strain; plasmid used]
	[strain Guy11]. Sulfonylurea resistance.
Ex0174	Transformant expressing Spa2 (2kb promoter and entire coding sequence) fused to GFP [strain KV118; pBV317]. Sulfonylurea resistance.
Ex0175	Δexo70, KO mutant into the strain Guy11. Hygromycin resistance.
Ex0176	Δsec5, KO mutant into the strain Guy11. Hygromycin resistance.
Ex0177	Δsso1, KO mutant into the strain Guy11. Hygromycin resistance.
Ex0178	Transformant expressing Pma1 (2kb promoter and entire coding sequence) fused to GFP, into KV118 [strain O-137; pBV317]. Sulfonylurea resistance.
Ex0179	Transformant expressing Sso1 (2kb promoter and entire coding sequence) fused to GFP, into KV118 [strain O-137; pBV317]. Sulfonylurea resistance.
EXR1	*Oryza sativa* cv. *sasanishiki* rice line containing Lti6B:GFP vector, Lti6B gene expressed under 35S promoter. [pNJT6].
EXR2	*Oryza sativa* cv. *sasanishiki* rice line containing GFP:HDEL vector, HDEL sequence expressed under 35S promoter. [pNJT7].

References

1 Atkinson, H. A., Daniels, A. & Read, N. D. Live-cell imaging of endocytosis during conidial germination in the rice blast fungus, *Magnaporthe grisea*. *Fungal Genet. Biol.* **37**, 233-244 (2002).

2 Bolte, S. *et al.* FM-dyes as experimental probes for dissecting vesicle trafficking in living plant cells. *J. Microscopy* **214**, 159-173 (2004).

3 Thompson, J. D., Higgins, D. G. & Gibson, T. J. CLUSTAL W: improving the sensitivity of progressive multiple sequence alignment through sequence weighting, position-specific gap penalties and weight matrix choice. *Nucleic Acids Research* **22**, 4673 - 4680 (1994).

4 Sudbery, P. Fluorescent proteins illuminate the structure and function of the hyphal tip apparatus. *Fungal Genet. Biol.* **48**, 849-857 (2011).

5 Crampin, H. *et al. Candida albicans* hyphae have a Spitzenkorper that is distinct from the polarisome found in yeast and pseudohyphae. *J. Cell Science* **118**, 2935-2947 (2005).

6 Fischer-Parton, S. *et al.* Confocal microscopy of FM4-64 as a tool for analysing endocytosis and vesicle trafficking in living fungal hyphae. *J. Microscopy* **198**, 246-259 (2000).

7 Heider, M. R. & Munson, M. Exorcising the exocyst complex. *Traffic* **13**, 898-907 (2012).

8 Chardin, P. & McCormick, F. Brefeldin A: the advantage of being uncompetitive. *Cell* **97**, 153-155 (1999).

9 Mentlak, T. A. *et al.* Effector-mediated suppression of chitin-triggered immunity by *Magnaporthe oryzae* is necessary for rice blast disease. *Plant Cell* **24**, 322-335 (2012).

10 Kurup, S. *et al.* Marking cell lineages in living tissues. *Plant Journal* **42**, 444-453 (2005).

11 Zheng, H. *et al.* A Rab-E GTPase mutant acts downstream of the Rab-D subclass in biosynthetic membrane traffic to the plasma membrane in tobacco leaf epidermis. *Plant Cell* **17**, 2020-2036, doi:10.1105/tpc.105.031112. (2005).

Chapter 6

Discussion and Future Directions

Morphological changes are a common strategy employed by both animal and plant fungal pathogens in order to survive under stressful host conditions. For animal pathogens, such as *Cryptococcus neoformans* and *Histoplasma capsulatum*, pathogenicity is, for example, tightly linked to a switch from a filamentous hyphal growth form to yeast-like growth (1, 2). By contrast, another animal pathogen, *Candida albicans*, predominantly utilizes its filamentous form to cause systemic disease. This suggests that fungal dimorphism has provided a selective advantage in the evolution of pathogenicity (3).

Plant pathogens can be classified as biotrophs, hemibiotrophs and necrotrophs. Biotrophs strictly depend on living host tissue to support growth and are obligate parasites (4). Necrotrophs kill their hosts and proliferate by feeding on dead cells (5). Hemibiotrophs initialy have a biotrophic phase and subsequently kill host cells upon induction of necrotrophy (6). Pathogens classified under these categories have a completely different genome organization, host range and possess distinct infection strategies(6-8). However, a common pathogenicity associated morphotype used by fungi exhibiting each of these types of lifestyles is the formation of a special infection cell called the appressorium (9). Appressorium development involves a series of morphological changes that are triggered by exposure to the host. Identification of the genes that control these shape changes is therefore key to understanding infection-related development of a broad range of the most devastating plant pathogens, including wheat stem rust, powdery mildew and rice blast.

Appressorium development in the rice blast fungus *M. oryzae* has been used as a model to understand appressorium-mediated plant infection. When cultured on rich growth medium *M. oryzae* spores germinate and the fungus grows filamentously. However, when these spores land on an inductive plant surface two symmetry-breaking events mark the development of a functional appressorium. First, the polarized germ tube hooks at its tip and starts to swell. Isotropic growth is followed by melanisation and maturation of appressorium, which involves formation of a septum at the base of the cell and generation of a pore where no cell wall or melanin layer is initially present.

This is followed by a repolarization event when the narrow penetration peg emerges from the appressorium pore, breaches the cuticle and starts to colonize the underlying plant tissue (10). Within the plant, *M. oryzae* grows as bulbous invasive hyphae with similar properties to pseudohyphae formed by fungi such as *C. albicans* (11).

Appressorium development has many distinct parallels with yeast budding and mating

Asymmetric growth during germ tube formation of the appressorium is in many ways similar to the well-studied mating response of budding yeast to peptide pheromones. Pheromones from opposing mating types bind to and activate the G protein coupled receptor Ste2/Ste3 (12). Activation of the receptor causes Gβγ subunits to dissociate from the inhibitory Gα subunit. Dissociated Gβγ subunits bind to the scaffold protein Ste5 which makes an active kinase complex at the plasma membrane with Ste11, Ste7 and Fus3 MAPK (reviewed in (13)). Active Fus3 MAPK then phosphorylates downstream proteins such as Ste12 which is necessary for mating and also induces a G_1 cell cycle arrest by activation of Far1. Far1 binds to the Cln/Cdc28 complex and inhibits its catalytic activity (14). Active Gβγ and Far1 also recruit the "master regulator" of polarity, the Cdc42 GTPase, to the plasma membrane in clusters at the shmoo tip (15). Active Cdc42 generates a polarized actin cytoskeleton which carries vesicles, proteins and mRNA required for sustained polar growth at the tip. Polarized actin cables also carry activated Gβγ subunits to the apex of the shmoo, which ensures high levels of Cdc42 at the shmoo tip required for prolonged apical growth during mating. Initial polarized localization of Cdc42 is amplified by recruitment of the guanine exchange factor Cdc24, the scaffold protein Bem1 and the p21-activated kinase Ste20. This constitutes an active signalling complex at the shmoo tip for establishment of polarity (reviewed in (16)).

A very similar signalling cascade is activated during yeast filamentous growth, which is a nutrient-foraging starvation response. Upon perception of sucrose/glucose, a G-protein coupled receptor activates Gβγ subunits (17). Together with Ras2, Gβγ subunit activates adenylate cyclase required for cAMP generation. Binding of cAMP to the regulatory subunit of protein kinase A (PKA) releases active PKA holoenzyme, which eventually induces expression of Flo11 (18). A similar Ste5-Ste11-Ste7 kinase complex and

Cdc42-Ste20 signalling module is involved in activation of filamentous growth (reviewed in (19)). Continuous clustering of the Cdc42-Cdc24 complex relies on scaffolds made of polarisome components and septins (20, 21). The polarisome consists of the formin Bni1, Spa2, Bud6 and Pea2 and is required for F-actin organization at the apical tip (reviewed in (22)). Septins are localized to the mother-bud neck or the shmoo neck. Here, they recruit proteins required for actomyosin ring formation such as Myosin II, the IQ-GAP protein Iqg1 or polarity establishment proteins such as Spa2 (23, 24). Although septins are not localized at growth points in yeast, they are essential for organization of polarized plasma membrane domains and cell compartmentalization. By acting as diffusion barriers at the plasma membrane, ER and nuclear envelope, they maintain the asymmetry essential for mating or budding (25, 26).

There are distinct parallels with the observations I have made in the rice blast fungus *M. oryzae* with yeast budding and mating. Within two hours of landing on the plant leaf surface, the polarized germ tube switches to isotropic growth during initiation of appressorium development. Changes in polarity are similar to the isotropic growth transition during budding. Another p21-activated kinase, Cla4, mediates the apical-isotropic growth switch in budding yeast. Cells lacking Cla4 or carrying the $cdc42^{V44A}$ allele which binds Cla4 poorly, generate very long buds (27, 28). The switch is tightly linked to cell cycle progression and requires activation of Clb/Cdc28 complex. At the beginning of the cell cycle, the Cdc42-Cla4 complex establishes a septin scaffold at the mother-bud neck. Septins act as scaffolds for Nim1-related kinases which activate Hsl17, which degrades Swe1, a part of the morphogenesis checkpoint (29). Swe1 monitors the septin scaffold and inhibits Cdc28/Clb complex if there is any problem with septin ring formation. When it is degraded by Hsl7, the apical to isotropic growth switch occurs (30). Consistent with this, septin mutants or *nim1* deletions cause elongated cells, which can be corrected with an additional *swe1* deletion (31).

The repolarization event that happens during penetration peg emergence in *M. oryzae* is in many ways similar to emergence of a new bud, but leads to formation of a polarized penetration peg which eventually differentiates into bulbous invasive hyphae.

Many of the proteins that play roles in polarized growth have been functionally characterized in *M. oryzae*. Appressorium development is a nutrient starvation response

as in yeast filamentous growth. Deletion of the Gα subunit MagB, the adenylate cyclase Mac1 or Gβ subunit Mgb1 prevent appressorium formation (32, 33). Consistently, increased Mgb1 levels, a dominant active MagB, overexpression of Ras2 or deletion of the phosphodiesterase PdeH leads to appressorium formation on non-inductive surfaces (34-36). Moreover, deletion of a negative regulator of G protein signalling, Rgs1, also results in appressorium formation on non-inductive surfaces, consistent with a role for a G protein induced cAMP increase during initial appressorium morphogenesis (37). Similar to Ste5/Ste11/Ste7/Fus3 MAPK scaffold, *M. oryzae* possesses a Mst50/Mst11/Mst7/Pmk1 module. Deletion of any of these genes prevents appressorium formation (35, 38, 39). In contrast to yeast, however, Cdc42 does not seem to be the master regulator of polarity in *M. oryzae*. Although deletion of Cdc42 results in loss of pathogenicity, the mutant is still able to form appressorium (40). This may be due to the fact that unlike yeast, *M. oryzae* has another small GTPase called Rac1 that is involved in regulation of polarity. Rac1 interacts with the Cdc42 effector Cla4 (named Chm1 in *M. oryzae*) and deletion of Rac1 prevents appressorium formation (41). Cdc24 functions as a guanine exchange factor for Rac1 as well (42). Interestingly, in *U. maydis* Cla4 was shown to induce degradation of Cdc24 during filament formation (43). A similar negative feedback loop may integrate Cdc42 and Rac1 signalling during appressorium development. Although Cdc42 is not the master regulator, Cdc42 mutants are unable to penetrate rice leaves, which mean that Cdc42 has a role in the second polarization event. Rather than Ste20, Cla4 is more important for appressorium development and deletion of Cla4 leads to loss of pathogenicity and mislocalization of septins (44, 45). Consistent with the role of Cla4 in appressorium repolarization, Cla4 forms a ring at the appressorium pore region which co-localizes with the septin/actin rings (45). Rac1 may therefore be the main regulator of polarity, because Cla4 mutants are able to make an appressorium but unable to produce penetration pegs (44).

This study has revealed that septins form two scaffolds during appressorium development. The first scaffold forms at the appressorium neck which mediates actomyosin ring formation during cytokinesis and differentiation of the infection cell. The septin ring forms prior to nuclear division and defines the subsequent septation site (46). The actomyosin ring components actin, myosin light chain kinase, myosin II and tropomyosin are localized at the neck and their localization depends on septin oligomers

(45). The second ring forms around the appressorium pore where repolarization takes place for plant infection. Here, septins recruit a 5.9 μm toroidal F-actin network. The rings around the appressorium pore are essential for two reasons. Since the pore region does not have a strengthening cell wall or melanin layer, and there is turgor within the maturing appressorium, the rings provide essential cortical rigidity at the plasma membrane. Secondly, septins act as diffusion barriers to maintain the position of curvature inducing proteins such as Las17 and Rvs167. Initial negative membrane curvature is essential for protrusion of penetration pegs (45).

The Cdc42-Cla4 complex appears to control organisation of septins as a ring around the appressorium pore. Deletion of Cdc42, for example, results in formation of several small septin rings which can also be observed on LatA treated cells. Deletion of Cla4 also causes formation of unorganized septin/actin rings (45). The role of Rac1 in septin/actin organization is not known but because Rac1 seems to be more important for polarity establishment in *M. oryzae*, it would be interesting to observe the re-organization of the F- actin cytoskeleton in a *Δrac1* mutant.

The Nox complex controls septin-mediated F-actin remodelling

NADPH oxidases Nox1 and Nox2, which interact with Rac1 in a yeast two hybrid assay, were recently shown to control cytoskeleton remodelling during appressorium repolarization (41, 47). NADPH oxidases are flavoenzymes that generate superoxide by electron transfer through biological membranes. Previously, it was shown that deletion of Nox enzymes in *M. oryzae* caused a penetration defect and loss of virulence (48). We have now shown that the p67 phox regulatory subunit, NoxR is essential for penetration and that Nox controls F-actin cytoskeleton remodelling prior to penetration. Nox1 appears to control actin organization and deletion of *NOX1* prevents actin ring formation, but not septin accumulation. Septins and Chm1 are normally distributed in *Δnox1* mutants. Nox2/NoxR controls septin, actin and Chm1 rings and deletion of either gene results in formation of unorganized cytoskeletal structures in appressoria. The actin binding protein gelsolin, which has been shown in mammalian systems to be directly regulated by ROS (49), also forms a dynamic ring around the appressorium pore. The gelsolin ring is mislocalized by treating the cells with Nox inhibitor DPI or ROS scavenger ascorbate (47). In the mutualistic, endophytic fungus *Epichloë festucae*,

NoxR was shown to interact with Cdc24 and Bem1 and a Δbem1 mutant was defective in hyphal morphogenesis (50). An essential question is therefore whether Bem1 is part of the Nox complex in *M. oryzae*? Since Bem1 has been shown to interact with MAPK scaffolding protein Ste5 in yeast (51), is it involved in integration of GTPase signalling with MAPK cascade in *M. oryzae*? Mst50 expression is very high in the mature appressorium and the protein is known to interact with Cdc42 (35). It would therefore be interesting to see whether Mst50 interacts with Rac1 and/or the Nox complex. We have also shown that the tetraspanin homolog Pls1 is involved in cytoskeleton remodelling during appressorium development. Both septin and F-actin rings fail to form in the absence of tetraspanin (47). Tetraspanins are highly conserved proteins with four membrane spanning domains (52), which interact with each other and other membrane proteins to induce formation of tetraspanin enriched microdomains (TEM) (53). Tetraspanins have been extensively studied in human cells. Known protein interactors of tetraspanins include Gα, Gβ subunits, PI4K and PKC. They also interact with the cortical actin cytoskeleton via ERM proteins (53). Strikingly, both the PI4K homolog Mss4 and the ERM protein Tea1 localize as punctate rings around the appressorium pore (45). This suggests that Pls1 may be involved in polarization of the appressorium pore membrane. A striking phylogenetic feature of the tetraspanin gene family in filamentous fungi is the co-occurrence of tetraspanins with possession of a Nox2 (54). This suggests that Pls1-enriched microdomains in the appressorium may contain the Nox2 complex, necessary for appressorium repolarization. The requirement of Nox2 for Tea1 localization is also consistent with this idea (47). Since TEMs contain G-protein signalling components in humans, further characterization of fungal TEMs may provide a link between surface signalling and organisation of the cortical F-actin cytoskeleton.

The presence of a Nox/Tetraspanin complex to induce cytoskeleton remodelling prior to penetration, serves to focus motive force at the pore and bring about plant infection. However, we still do not know the nature of the inducing factor that initiates appressorium repolarization. We can explain the first switch to isotropic growth which initiates appressorium swelling as a consequence of the fungus response to surface hydrophobicity and surface hardness, analogous to the induction of pseudohyphal growth in *S. cerevisiae*, but there is no report to explain the induction of repolarization which leads to penetration peg emergence by a pathogenic fungus. One potential

candidate may be the extreme levels of turgor within the mature appressorium itself. A hypothesis could be proposed in which the sensing of turgor is required for initiation of repolarization at the base of the infection cell. Turgor pressure-driven repolarization suggests a checkpoint which is irreversibly activated once a certain pressure threshold has been breached. It also requires the timing of turgor generation to match the timing of septin/actin ring repolarization. Although we do not have tools such as nano-indentation used in plants to measure turgor pressure (55), an indirect measurement of turgor pressure is to measure the amount of glycerol within the appressorium. It has been shown in by de Jong and co-workers that glycerol accumulation peaks around 10 hours after inoculation (56). This corresponds to the timing of cytoskeleton remodelling. An easy way to test this hypothesis would be to check septin/actin ring formation when the turgor pressure is artificially lowered, for example, by addition of glycerol. It can also be tested genetically by observing appressorium repolarization in melanin-deficient mutants such as *buf1*, *rsy1* or *alb1*. Melanin has been shown to be required for accumulation of glycerol necessary for turgor generation(56). Initial observations under both conditions have, in fact, shown that septin rings do not form (Dagdas et. al., unpublished). To investigate the likely molecular mechanism that mediates the pressure checkpoint a variety of sensors should be explored in future. These sensors include Sho1, Sln1, and Wsc1. Deletion of Sho1 has a minor effect on appressorium formation (57) and septins can still form a ring in *Δsln1* mutants (Dagdas et. al., unpublished). Wsc1 therefore seems to be the best potential candidate for an appressorium turgor pressure sensor. Wsc1 is a glycoyslated membrane protein that has been shown to act as a nanospring, which measures turgor pressure changes in yeast cells (58). We have recently generated a *Δwsc1* mutant (Dagdas et. al., unpublished). Currently, we are investigating septin-mediated F-actin re-organization during appressorium development in the *Δwsc1* mutant. Wsc1 has been shown to act upstream of Pkc1 (59) which in yeast is the main component of the protein kinase C-mediated cell integrity pathway. Initial yeast two hybrid analysis has shown that Pkc1 in *M. oryzae* interacts with the Nox complex (Dagdas et. al., unpublished). Previous studies in human neutrophil cells showed phosphorylation of Nox2 or the NoxR homolog P67phox by Pkc1 (60). Presence of Pkc1 in TEMs also supports this hypothesis (61) (Figure 1).

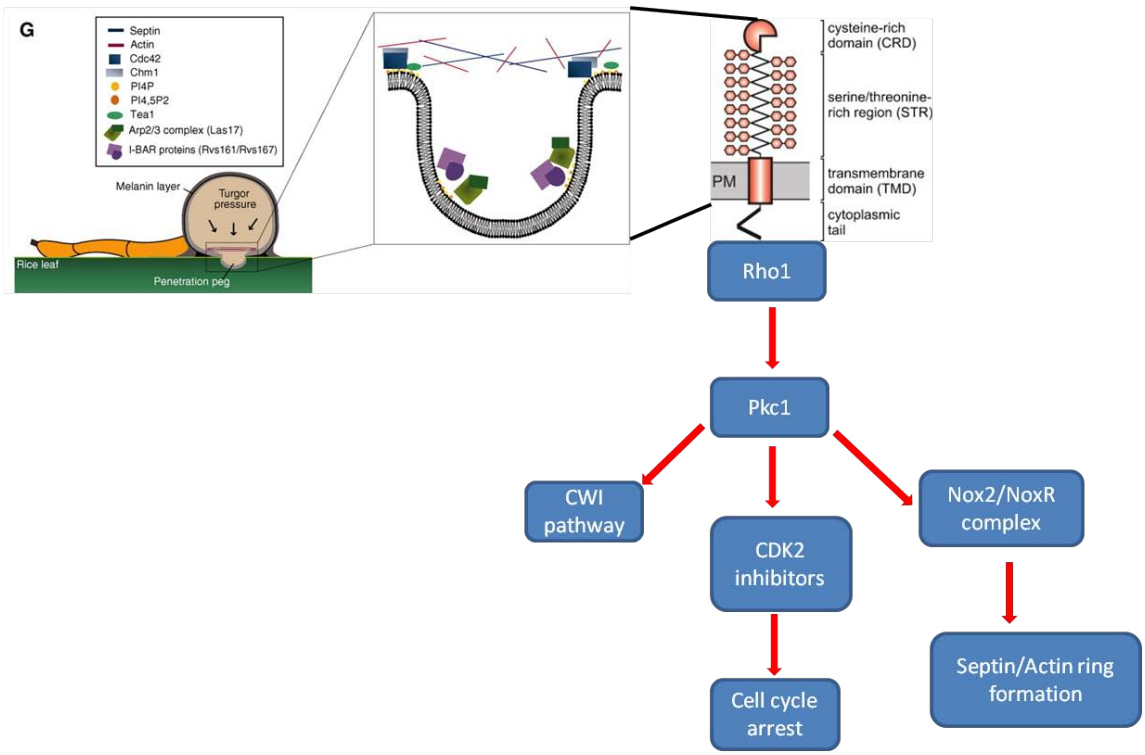

Figure 1: A turgor pressure driven checkpoint controls appressorium repolarization. (Modified from Dagdas, et al., 2012 and Jendretzki et al., 2011).

Appressorium development is controlled by cell-cycle checkpoints

As in yeast, polarity switches during appressorium development are tightly linked to cell cycle checkpoints. The G1-S transition is known to be the commitment step for appressorium morphogenesis. Completion of S-phase induces appressorium swelling. Functional perturbation of the Nim1 kinase results in hyperpolarized germ tubes, which are unable to swell and form appressoria. However the G2-M transition and mitotic exit are necessary for appressorium function. Blocking the G2-M transition by generating a temperature sensitive nimA^{E37G} allele allows formation of melanised appressoria but these cells are unable to cause disease. Similarly, preventing mitotic exit by disturbing the anaphase promoting complex also resulted in melanised appressorium which are unable to produce penetration pegs (62). Consistent with these observations, septin ring formation at the appressorium neck was mislocalized when G1-S transition was prevented. However, it was normal in following G2-M and mitotic exit arrest

experiments. The septin ring at the appressorium pore was mislocalized in all cell cycle mutants, explaining why morphologically normal appressoria are unable to cause disease (45). As in yeast, B type cyclins are responsible for mitotic exit and expression of stabilized B cyclins prevented mitotic exit (62). Currently there is no report on dissection of Cdc28-cycin complexes. It would therefore be interesting to see the dynamic changes in Cdc28 interacting partners and their roles in appressorium morphogenesis. Also it seems that there is a cell cycle arrest in mature appressoria. Nuclear division does not happen until penetration peg emergence. Since the cell cycle machinery is highly conserved in both yeast and *M. oryzae*, an analogous protein to Far1 in yeast might, for example, be responsible for the G1 arrest seen in mature appressorium. Another possibility is a morphogenesis checkpoint overseeing the integrity of septin rings at the appressorium pore. When the penetration peg emerges, the rings depolymerise and septins localize to the hyphal tip. Depolymerisation of the septin ring, for instance, might induce degradation of an inhibitor such as Swe1 in yeast to activate cell division. Also there is no current information on the role of the cell cycle controlling differentiation of bulbous hyphae formation during plant infection. It is tempting to speculate that differentiation of bulbous invasive hyphae during *in planta* growth may be regulated by a further cell-cycle checkpoint.

Another question waiting to be answered is when does the germ tube start swelling? What determines the length of germ tube? One possibility is a morphogen gradient linking cell size to cell division and when cells reach a certain size, mitosis is then induced. In *S. pombe* a gradient of Pom1 kinase links cell size control with cell cycle progression. Pom1 exerts its effect on the Cdr2-Cdr1-Wee1 node which is localized at interphase nodes in the middle of the cell. Phosphorylation of Cdr2 by Pom1 leads to activation of Wee1, which inhibits Cdk2 and causes a cell division delay. When the cell size increases, the concentration of Pom1 at the interphase node decreases, allowing Cdk2 to remain active and induce cell division (63, 64). Similar to *S. pombe*, a *Δpom1* mutant in *M. oryzae* shows a restricted colonial growth phenotype (Dagdas et. al., unpublished). Further characterization of this mutant might explain why only one of the three nuclei in the conidium undergoes nuclear division. Because *M. oryzae* septa are not complete, the three-celled conidium can be seen as one unit. High concentrations of Pom1 might therefore inhibit nuclear division in non-germ tube forming cells. Formation of the germ tube would cause a decrease in the local concentration of Pom1

that allow nuclear division. Septins are known to generate diffusion barriers and in *M. oryzae* septin mutants, nuclei in all cells can divide and there are several nuclei in mature appressorium (45). This supports the idea that the morphogen gradient that controls nuclear division dynamics during appressorium development is maintained by septin diffusion barriers. This idea could be directly tested by detailed analysis of a *Δpom1* mutant.

Two distinct secretion pathways mediate effector secretion in *M. oryzae*

Although there is some information about the role of signalling pathways during appressorium morphogenesis, we know almost nothing about the morphogenetic machinery that controls plant tissue invasion by *M. oryzae*. We do not know, for example, whether the switch from primary invasive hyphae to bulbous hyphae is controlled by cell cycle progression. We also do not know whether there is a morphogenetic switch that controls transition from the biotrophic stage of infection to the necrotrophic stage. To gain insight into the secondary bulbous hyphae differentiation, we need mutants which are unable to switch from primary invasive hyphae to secondary invasive hyphae. Currently there are two mutants which are shown to be arrested in the primary hyphae stage. One of them is a mutation in a MADS-box transcription factor, *Δmig1*, which was shown to interact with Mps1 (65). Identification of the genes controlled by Mig1 transcription factors might shed some light on development of secondary invasive hyphae. The other mutant is a histone deacetylase mutant called *Δtig1(66)*. Tig1 is a component of conserved histone deacetylase transcriptional corepressor complex which was shown to be required for infectious growth. The phenotype of a *Δtig1* mutant suggests the switch from primary invasive hyphae to secondary invasive hyphae may involve a change in histone acetylation patterns, which might induce activation of a set of genes responsible for bulbous hyphae formation. It would be interesting to see the expression level of Mig1 transcription factor in a *Δtig1* mutant.

Plant pathogenic fungi produce large amounts of secreted proteins called effectors, which suppress host defence responses and facilitate plant tissue invasion (11, 67-70). What we know about effector delivery in *M. oryzae* is limited to microscopic studies showing accumulation of effector proteins at a unique sub-apical structure named

biotrophic interfacial complex (71). Fluorescently tagged effector proteins localize to hyphal tips in the primary invasive hyphae. When primary invasive hyphae differentiate into bulbous hyphae, effectors accumulate at BICs, which we have shown to be rich in plant membrane (72, 73). Secretion in fungi happens through the hyphal tip and septum, so this is a rather unexpected place for active secretion to occur. However photobleaching experiments have confirmed that BICs do appear to be active sites of secretion (71). This suggests that reorientation of secretion to the subapex occurs during differentiation of the BIC, which was confirmed by localizing Mlc1 and Snc1 during bulbous hyphae differentiation (Giraldo, Dagdas et. al., unpublished). Since the polarisome is still localized at hyphal tips, this suggests the presence of an effector-specific secretion system. This idea was supported by differential sensitivity of apoplastic and symplastic effector secretion to BrefeldinA (Giraldo and Dagdas et. al., unpublished). Apoplastic effectors, such as Slp1 and Bas4 outline hyphae (74, 75) whereas symplastic effectors such as Pwl2 and Bas1, are translocated into the rice cytoplasm and they are thought to be involved in suppression of host immunity and facilitation of fungal colonization and localize to the BICs. Upon BrefeldinA treatment, apoplastic effectors accumulate in intracellular fungal compartments that resemble ER, but symplastic effectors still actively accumulate at BICs. Since BrefeldinA blocks ER to Golgi transport, symplastic effectors could be translocated via an unconventional secretion system. BrefeldinA-insensitive secretion has been demonstrated for many plasma membrane and extracellular proteins, which do not have a signal peptide. Unconventional secretion seems to depend on the autophagy machinery or GRASP proteins (76). However, known effectors of *M. oryzae* do have a signal peptide and deletion of the GRASP homolog *GRH1* does not affect symplastic effector secretion (Dagdas et. al., unpublished). Another possibility may be that effectors are translocated as mRNAs and therefore do not need a conventional secretion system. Such a secretion system, which bypasses the Golgi network for transport has been shown for Ist2p transport in yeast. Ist2p is translated from a localized transcript and plasma membrane localization of Ist2 does not require the common SEC pathway. A protein sorting signal has been defined in Ist2, which mediates interaction of the protein with membrane lipids. This enables direct transfer of the protein from the cortical ER to the plasma membrane (77-79). Very close association of ER with BIC-associated plasma membrane supports such a hypothesis (Dagdas et. al., unpublished). Furthermore deletion of an ER chaperone Lhs1 blocks effector secretion (80). However no common

sorting signal similar to Ist2 has been identified in *M. oryzae* effector proteins and amino acid sequences of known effectors are quite diverse. One way to test this hypothesis may be to block motor proteins that have been shown to carry mRNA. In yeast an actin-based mRNA transport is present and the responsible motor protein is Myosin. However in fungi, studies carried out to date in *Ustilago maydis* showed that mRNA transport happens on microtubules and the main motors are dynein and kinesin3 (81). Since these motor proteins are also responsible for long-range protein transport, functional characterization could lead us to the identification of a potential effector secretion system in *M. oryzae.* This would be significant in defining the pathway necessary for delivering this key proteins to rice cells during plant infection.

Science is built up of facts, as a house is built of stones; but an accumulation of facts is no more science than a heap of stones is a house.

Jules-Henri Poincare

References

1. Lin X (2009) Cryptococcus neoformans: morphogenesis, infection, and evolution. *Infect Genet Evol* 9(4):401-416 .
2. Maresca B & Kobayashi GS (1989) Dimorphism in Histoplasma capsulatum: a model for the study of cell differentiation in pathogenic fungi. *Microbiol Rev* 53(2):186-209 .
3. Klein BS & Tebbets B (2007) Dimorphism and virulence in fungi. *Curr Opin Microbiol* 10(4):314-319 .
4. Genre A & Bonfante P (2007) Check-in procedures for plant cell entry by biotrophic microbes. *Mol Plant Microbe Interact* 20(9):1023-1030 .
5. van Kan JA (2006) Licensed to kill: the lifestyle of a necrotrophic plant pathogen. *Trends Plant Sci* 11(5):247-253 .
6. Oliver RP & Ipcho SV (2004) Arabidopsis pathology breathes new life into the necrotrophs-vs.-biotrophs classification of fungal pathogens. *Mol Plant Pathol* 5(4):347-352 .
7. Spanu PD, *et al.* (2010) Genome expansion and gene loss in powdery mildew fungi reveal tradeoffs in extreme parasitism. *Science* 330(6010):1543-1546 .
8. Amselem J, *et al.* (2011) Genomic analysis of the necrotrophic fungal pathogens Sclerotinia sclerotiorum and Botrytis cinerea. *PLoS Genet* 7(8):e1002230 .
9. Lee N, D'Souza CA, & Kronstad JW (2003) Of smuts, blasts, mildews, and blights: cAMP signaling in phytopathogenic fungi. *Annu Rev Phytopathol* 41:399-427 .
10. Caracuel-Rios Z & Talbot NJ (2007) Cellular differentiation and host invasion by the rice blast fungus Magnaporthe grisea. *Curr Opin Microbiol* 10(4):339-345 .
11. Valent B & Khang CH (2010) Recent advances in rice blast effector research. *Curr Opin Plant Biol* 13(4):434-441 .

12. Hartwell LH (1980) Mutants of Saccharomyces cerevisiae unresponsive to cell division control by polypeptide mating hormone. *J Cell Biol* 85(3):811-822 .
13. Schwartz MA & Madhani HD (2004) Principles of MAP kinase signaling specificity in Saccharomyces cerevisiae. *Annu Rev Genet* 38:725-748 .
14. Peter M, Gartner A, Horecka J, Ammerer G, & Herskowitz I (1993) FAR1 links the signal transduction pathway to the cell cycle machinery in yeast. *Cell* 73(4):747-760 .
15. Butty AC, Pryciak PM, Huang LS, Herskowitz I, & Peter M (1998) The role of Far1p in linking the heterotrimeric G protein to polarity establishment proteins during yeast mating. *Science* 282(5393):1511-1516 .
16. Pruyne D & Bretscher A (2000) Polarization of cell growth in yeast I. Establishment and maintenance of polarity states. *J Cell Sci* 113(3):365-375.
17. Mosch HU, Roberts RL, & Fink GR (1996) Ras2 signals via the Cdc42/Ste20/mitogen-activated protein kinase module to induce filamentous growth in Saccharomyces cerevisiae. *Proc Natl Acad Sci U S A* 93(11):5352-5356 .
18. Rupp S, Summers E, Lo HJ, Madhani H, & Fink G (1999) MAP kinase and cAMP filamentation signaling pathways converge on the unusually large promoter of the yeast FLO11 gene. *Embo J* 18(5):1257-1269 .
19. Cullen PJ & Sprague GF, Jr. (2012) The regulation of filamentous growth in yeast. *Genetics* 190(1):23-49 .
20. Jaquenoud M & Peter M (2000) Gic2p may link activated Cdc42p to components involved in actin polarization, including Bni1p and Bud6p (Aip3p). *Mol Cell Biol* 20(17):6244-6258 .
21. Kadota J, Yamamoto T, Yoshiuchi S, Bi EF, & Tanaka K (2004) Septin ring assembly requires concerted action of polarisome components, a PAK kinase Cla4p, and the actin cytoskeleton in Saccharomyces cerevisiae. *Mol Biol Cell* 15(12):5329-5345.
22. Harris SD, *et al.* (2005) Polarisome meets spitzenkorper: microscopy, genetics, and genomics converge. *Eukaryot Cell* 4(2):225-229 .
23. Longtine MS & Bi EF (2003) Regulation of septin organization and function in yeast. *Trends Cell Biol* 13(8):403-409 .
24. Jimenez J, *et al.* (1998) Morphogenesis beyond cytokinetic arrest in Saccharomyces cerevisiae. *Journal of Cell Biology* 143(6):1617-1634 .
25. Barral Y, Mermall V, Mooseker MS, & Snyder M (2000) Compartmentalization of the cell cortex by septins is required for maintenance of cell polarity in yeast. *Mol Cell* 5(5):841-851 .
26. Dobbelaere J & Barral Y (2004) Spatial coordination of cytokinetic events by compartmentalization of the cell cortex. *Science* 305(5682):393-396 .
27. Cvrckova F, De Virgilio C, Manser E, Pringle JR, & Nasmyth K (1995) Ste20-like protein kinases are required for normal localization of cell growth and for cytokinesis in budding yeast. *Genes Dev* 9(15):1817-1830 .
28. Richman TJ, Sawyer MM, & Johnson DI (1999) The Cdc42p GTPase is involved in a G(2)/M morphogenetic checkpoint regulating the apical-isotropic switch and nuclear division in yeast. *Journal of Biological Chemistry* 274(24):16861-16870 .
29. McMillan JN, Sia RA, Bardes ES, & Lew DJ (1999) Phosphorylation-independent inhibition of Cdc28p by the tyrosine kinase Swe1p in the morphogenesis checkpoint. *Mol Cell Biol* 19(9):5981-5990 .
30. Shulewitz MJ, Inouye CJ, & Thorner J (1999) Hsl7 localizes to a septin ring and serves as an adapter in a regulatory pathway that relieves tyrosine

phosphorylation of Cdc28 protein kinase in Saccharomyces cerevisiae. *Mol Cell Biol* 19(10):7123-7137 .
31. Longtine MS, *et al.* (2000) Septin-dependent assembly of a cell cycle-regulatory module in Saccharomyces cerevisiae. *Mol Cell Biol* 20(11):4049-4061 .
32. Liu S & Dean RA (1997) G protein alpha subunit genes control growth, development, and pathogenicity of Magnaporthe grisea. *Mol Plant Microbe Interact* 10(9):1075-1086 .
33. Choi W & Dean RA (1997) The adenylate cyclase gene MAC1 of Magnaporthe grisea controls appressorium formation and other aspects of growth and development. *Plant Cell* 9(11):1973-1983 .
34. Nishimura M, Park G, & Xu JR (2003) The G-beta subunit MGB1 is involved in regulating multiple steps of infection-related morphogenesis in Magnaporthe grisea. *Mol Microbiol* 50(1):231-243 .
35. Park G, *et al.* (2006) Multiple upstream signals converge on the adaptor protein Mst50 in Magnaporthe grisea. *Plant Cell* 18(10):2822-2835 .
36. Zhang H, *et al.* (2011) Two phosphodiesterase genes, PDEL and PDEH, regulate development and pathogenicity by modulating intracellular cyclic AMP levels in Magnaporthe oryzae. *PLoS One* 6(2):e17241 .
37. Liu H, *et al.* (2007) Rgs1 regulates multiple Galpha subunits in Magnaporthe pathogenesis, asexual growth and thigmotropism. *Embo J* 26(3):690-700 .
38. Xu JR & Hamer JE (1996) MAP kinase and cAMP signaling regulate infection structure formation and pathogenic growth in the rice blast fungus Magnaporthe grisea. *Genes Dev* 10(21):2696-2706 .
39. Zhao X, Kim Y, Park G, & Xu JR (2005) A mitogen-activated protein kinase cascade regulating infection-related morphogenesis in Magnaporthe grisea. *Plant Cell* 17(4):1317-1329 .
40. Zheng W, *et al.* (2009) A Cdc42 ortholog is required for penetration and virulence of Magnaporthe grisea. *Fungal Genet Biol* 46(6-7):450-460 .
41. Chen J, *et al.* (2008) Rac1 is required for pathogenicity and Chm1-dependent conidiogenesis in rice fungal pathogen Magnaporthe grisea. *PLoS Pathog* 4(11):e1000202 .
42. Leveleki L, Mahlert M, Sandrock B, & Bolker M (2004) The PAK family kinase Cla4 is required for budding and morphogenesis in Ustilago maydis. *Mol Microbiol* 54(2):396-406 .
43. Frieser SH, Hlubek A, Sandrock B, & Bolker M (2011) Cla4 kinase triggers destruction of the Rac1-GEF Cdc24 during polarized growth in Ustilago maydis. *Mol Biol Cell* 22(17):3253-3262 .
44. Li L, Xue C, Bruno K, Nishimura M, & Xu JR (2004) Two PAK kinase genes, CHM1 and MST20, have distinct functions in Magnaporthe grisea. *Mol Plant Microbe Interact* 17(5):547-556 .
45. Dagdas YF, *et al.* (2012) Septin-mediated plant cell invasion by the rice blast fungus, Magnaporthe oryzae. *Science* 336(6088):1590-1595 .
46. Saunders DG, Dagdas YF, & Talbot NJ (Spatial uncoupling of mitosis and cytokinesis during appressorium-mediated plant infection by the rice blast fungus Magnaporthe oryzae. *Plant Cell* 22(7):2417-2428 .
47. Ryder LS, *et al.* (2013) NADPH oxidases regulate septin-mediated cytoskeletal remodeling during plant infection by the rice blast fungus. *Proc Natl Acad Sci U S A* 110(8):3179-3184 .
48. Egan MJ, Wang ZY, Jones MA, Smirnoff N, & Talbot NJ (2007) Generation of reactive oxygen species by fungal NADPH oxidases is required for rice blast disease. *Proc Natl Acad Sci U S A* 104(28):11772-11777 .

49. Moldovan L, Mythreye K, Goldschmidt-Clermont PJ, & Satterwhite LL (2006) Reactive oxygen species in vascular endothelial cell motility. Roles of NAD(P)H oxidase and Rac1. *Cardiovasc Res* 71(2):236-246 .
50. Takemoto D, *et al.* (2011) Polarity proteins Bem1 and Cdc24 are components of the filamentous fungal NADPH oxidase complex. *Proc Natl Acad Sci U S A* 108(7):2861-2866 .
51. Leeuw T, *et al.* (1995) Pheromone response in yeast: association of Bem1p with proteins of the MAP kinase cascade and actin. *Science* 270(5239):1210-1213 .
52. Boucheix C & Rubinstein E (2001) Tetraspanins. *Cell Mol Life Sci* 58(9):1189-1205 .
53. Yanez-Mo M, Barreiro O, Gordon-Alonso M, Sala-Valdes M, & Sanchez-Madrid F (2009) Tetraspanin-enriched microdomains: a functional unit in cell plasma membranes. *Trends Cell Biol* 19(9):434-446 .
54. Malagnac F, *et al.* (2008) Convergent evolution of morphogenetic processes in fungi: Role of tetraspanins and NADPH oxidases 2 in plant pathogens and saprobes. *Commun Integr Biol* 1(2):180-181 .
55. Forouzesh E, Goel A, Mackenzie SA, & Turner JA (2012) In vivo extraction of Arabidopsis cell turgor pressure using nanoindentation in conjunction with finite element modeling. *Plant J* .
56. de Jong JC, McCormack BJ, Smirnoff N, & Talbot NJ (1997) Glycerol generates turgor in rice blast. *Nature* 389(6648):244-244.
57. Liu W, *et al.* (2011) Multiple plant surface signals are sensed by different mechanisms in the rice blast fungus for appressorium formation. *PLoS Pathog* 7(1):e1001261 .
58. Dupres V, *et al.* (2009) The yeast Wsc1 cell surface sensor behaves like a nanospring in vivo. *Nat Chem Biol* 5(11):857-862 .
59. Philip B & Levin DE (2001) Wsc1 and Mid2 are cell surface sensors for cell wall integrity signaling that act through Rom2, a guanine nucleotide exchange factor for Rho1. *Mol Cell Biol* 21(1):271-280 .
60. Reeves EP, *et al.* (1999) Direct interaction between p47phox and protein kinase C: evidence for targeting of protein kinase C by p47phox in neutrophils. *Biochem J* 344 Pt 3:859-866 .
61. Zhang XA, Bontrager AL, & Hemler ME (2001) Transmembrane-4 superfamily proteins associate with activated protein kinase C (PKC) and link PKC to specific beta(1) integrins. *J Biol Chem* 276(27):25005-25013 .
62. Saunders DG, Aves SJ, & Talbot NJ (Cell cycle-mediated regulation of plant infection by the rice blast fungus. *Plant Cell* 22(2):497-507 .
63. Martin SG & Berthelot-Grosjean M (2009) Polar gradients of the DYRK-family kinase Pom1 couple cell length with the cell cycle. *Nature* 459(7248):852-856 .
64. Moseley JB, Mayeux A, Paoletti A, & Nurse P (2009) A spatial gradient coordinates cell size and mitotic entry in fission yeast. *Nature* 459(7248):857-860 .
65. Mehrabi R, Ding S, & Xu JR (2008) MADS-box transcription factor mig1 is required for infectious growth in Magnaporthe grisea. *Eukaryot Cell* 7(5):791-799 .
66. Ding SL, *et al.* (2010) The tig1 histone deacetylase complex regulates infectious growth in the rice blast fungus Magnaporthe oryzae. *Plant Cell* 22(7):2495-2508 .
67. Bozkurt TO, Schornack S, Banfield MJ, & Kamoun S (2012) Oomycetes, effectors, and all that jazz. *Curr Opin Plant Biol* 15(4):483-492 .

68. Hogenhout SA, Van der Hoorn RA, Terauchi R, & Kamoun S (2009) Emerging concepts in effector biology of plant-associated organisms. *Mol Plant Microbe Interact* 22(2):115-122 .
69. Ellis JG, Rafiqi M, Gan P, Chakrabarti A, & Dodds PN (2009) Recent progress in discovery and functional analysis of effector proteins of fungal and oomycete plant pathogens. *Curr Opin Plant Biol* 12(4):399-405 .
70. De Wit PJ, Mehrabi R, Van den Burg HA, & Stergiopoulos I (2009) Fungal effector proteins: past, present and future. *Mol Plant Pathol* 10(6):735-747 .
71. Khang CH, *et al.* (2010) Translocation of Magnaporthe oryzae effectors into rice cells and their subsequent cell-to-cell movement. *Plant Cell* 22(4):1388-1403 .
72. Kankanala P, Czymmek K, & Valent B (2007) Roles for rice membrane dynamics and plasmodesmata during biotrophic invasion by the blast fungus. *Plant Cell* 19(2):706-724 .
73. Mosquera G, Giraldo MC, Khang CH, Coughlan S, & Valent B (2009) Interaction transcriptome analysis identifies Magnaporthe oryzae BAS1-4 as Biotrophy-associated secreted proteins in rice blast disease. *Plant Cell* 21(4):1273-1290 .
74. Mentlak TA, *et al.* (2012) Effector-mediated suppression of chitin-triggered immunity by magnaporthe oryzae is necessary for rice blast disease. *Plant Cell* 24(1):322-335 .
75. Mosquera G, Giraldo MC, Khang CH, Coughlan S, & Valent B (2009) Interaction transcriptome analysis identifies Magnaporthe oryzae BAS1-4 as Biotrophy-associated secreted proteins in rice blast disease. *Plant Cell* 21(4):1273-1290 .
76. Nickel W & Rabouille C (2009) Mechanisms of regulated unconventional protein secretion. *Nat Rev Mol Cell Biol* 10(2):148-155 .
77. Ercan E, *et al.* (2009) A conserved, lipid-mediated sorting mechanism of yeast Ist2 and mammalian STIM proteins to the peripheral ER. *Traffic* 10(12):1802-1818 .
78. Franz A, Maass K, & Seedorf M (2007) A complex peptide-sorting signal, but no mRNA signal, is required for the Sec-independent transport of Ist2 from the yeast ER to the plasma membrane. *FEBS Lett* 581(3):401-405 .
79. Juschke C, Wachter A, Schwappach B, & Seedorf M (2005) SEC18/NSF-independent, protein-sorting pathway from the yeast cortical ER to the plasma membrane. *J Cell Biol* 169(4):613-622 .
80. Yi M, *et al.* (2009) The ER chaperone LHS1 is involved in asexual development and rice infection by the blast fungus Magnaporthe oryzae. *Plant Cell* 21(2):681-695 .
81. Vollmeister E, Schipper K, & Feldbrugge M (2012) Microtubule-dependent mRNA transport in the model microorganism Ustilago maydis. *RNA Biol* 9(3):261-268 .